Technische Universität München

Fakultät für Maschinenwesen

Lehrstuhl für Nukleartechnik

Core Design and Optimization of the High Conversion Small Modular Reactor

Denis Janin

Vollständiger Abdruck der von der Fakultät für Maschinenwesen der Technischen Universität München zur Erlangung des akademischen Grades eines

Doktor-Ingenieurs (Dr.-Ing.)

genehmigten Dissertation.

Vorsitzender:	Prof. Phaedon-Stelios Koutsourelakis, PhD
Prüfer der Dissertation:	1. Prof. Rafael Macián-Juan, PhD
	2. Prof. Dr. Jean-Baptiste Thomas

Die Dissertation wurde am 08.05.2018 bei der Technischen Universität München eingereicht und durch die Fakultät für Maschinenwesen am 01.11.2018 angenommen.

ABSTRACT

This research work investigates the design and optimization of the high conversion small modular reactor (HCSMR) core. The HCSMR has a thermal output of 600 MW for 200 MW electrical. It is an integrated PWR with a tightened fuel assembly lattice. The rod-to-rod pitch is 1.15 cm in a hexagonal fuel assembly geometry. As a result the moderation ratio (1.0) is reduced compared to large PWRs (around 2.0) and the HCSMR has an improved ability to convert ^{238}U into ^{239}Pu and use plutonium isotopes more efficiently. The core is loaded with MOX fuel.

The HCSMR concept finds its roots both in large high conversion light water reactors and small modular reactor (SMR) concepts. The reduced core size results in an increased neutron leakage rate compared to large cores. This intrinsically supports the core behavior in voided situations. The necessity to introduce fertile fuel materials in the core to keep negative void coefficients is reduced, contributing to the HCSMR safety and limited core heterogeneity.

The fuel of light-water reactors (LWRs) is mostly low-enriched uranium. Considering current industrial practices, close to 20 tons of natural uranium are needed to generate one TWhe. LWR natural uranium needs could be reduced by increasing the conversion of ^{238}U into ^{239}Pu. This can be achieved by tightening the fuel assembly lattice, which reduces the moderation ratio and hence hardens the neutron spectrum. Such cores loaded with MOX fuel in a closed fuel cycle can reach conversion factors above 0.8 compared to LWR conversion factors close to 0.5. It also enables a better plutonium utilization and limits the production of minor actinides.

A renewed interest in small modular reactors (SMRs) can be seen worldwide. The intention to reach long cycle lengths influenced SMR designers to adopt fuel management strategies resulting in low fuel discharge burnup. This leads to a substantial increase in natural uranium needs compared to today's LWRs. For such SMR designs close to 40 tons of natural uranium are needed to generate one TWhe.

The HCSMR core is designed using multi-objective optimization methods. This aims at addressing the multiple parameters influencing the core design by exploring all possible trade-offs between core performances and safety requirements. The objectives are not weighted in a global optimization function: Pareto optimum HCSMR cores are designed.

The neutron-physics computations are performed with the deterministic code APOLLO2, CRONOS2 and APOLLO3®. For comparison the Monte-Carlo code TRIPOLI-4® is employed. The URANIE platform is used to perform the optimization: to set-up design of experiment, create surrogate model functions and implement genetic algorithms optimization.

The outcome is a population of Pareto optimal HCSMR cores. This population makes it possible to reach cycle lengths up to 1200 EFPD, conversion ratios above 0.9 with negative void coefficients and maximum linear power below 400 W/cm. The associated natural uranium needs are significantly reduced, under seven tons of natural uranium are needed to generate one TWhe.

Keywords: LWR, High Conversion, Under-moderated, SMR, Multi-objective Optimization, Neural Network, Core design

RESUME

Ce travail a pour objectif la conception et l'optimisation d'un petit réacteur à haut facteur de conversion (HCSMR : High Conversion Small Modular Reactor). Le HCSMR a une puissance thermique de 600 MW pour 200 MW électrique. Le concept HCSMR est un petit cœur de type REP intégré, utilisant des assemblages combustibles MOX hexagonaux à pas resserré. Le rapport de modération du HCSMR (1.0) est réduit comparé aux REP standards (2.0). Ceci permet une meilleure conversion des isotopes ^{238}U en ^{239}Pu ainsi qu'une utilisation améliorée du plutonium.

Les racines du concept HCSMR se trouvent à la fois dans les cœurs à hauts facteurs de conversion de puissance, et dans les cœurs de petits réacteurs (SMR : Small Modular Reactor). Comparé à un cœur de forte puissance un petit cœur a un taux de fuite neutronique plus élevé. Ceci améliore naturellement le comportement du cœur en situation vidangée. La nécessité d'introduire des éléments combustibles dits fertiles pour limiter l'effet de vidange est alors réduite, contribuant à la sureté du HCSMR et permettant de limiter les hétérogénéités du cœur.

Le combustible des Réacteurs à Eau Légère (REL) est principalement composé d'uranium enrichi. En considérant les pratiques industrielles actuelles, près de 20 tonnes d'uranium naturel sont nécessaires pour produire un TWhe. En améliorant la conversion d'^{238}U en ^{239}Pu, les besoins d'uranium naturel peuvent être réduits. Ceci peut être obtenu lorsque le spectre neutronique est durcit. Des cœurs de ce type chargés avec du combustible MOX dans un cycle combustible fermé conduisent à des facteurs de conversion supérieurs à 0,8. Les RELs actuels ont un facteur de conversion proche de 0,5. Les concepts sous-modérés permettent également une meilleure utilisation du plutonium et limite la production d'actinides mineurs.

Un regain d'intérêt est observé pour les projets SMR. Le souhait des concepteurs d'obtenir de longues durées de cycle conduit à des taux de combustion du combustible relativement faibles. En conséquence, les besoins d'uranium naturel pour ce type de cœur sont élevés : près de 40 tonnes d'uranium naturel sont nécessaires pour produire un TWhe pour un SMR.

La conception du cœur HCSMR utilise des méthodes d'optimisation multicritères. L'objectif est d'explorer l'ensemble des meilleures combinaisons parmi les critères de conception. Plutôt que définir une fonction globale d'optimisation, ce travail s'articule autour de la recherche de surface de Pareto. Les études neutroniques sont réalisées avec les codes déterministes APOLLO2, CRONOS2 et APOLLO3®. Les résultats sont comparés avec ceux obtenus via le code Monte-Carlo TRIPOLI-4®. La plateforme URANIE est utilisée pour les étapes d'optimisation : la création de plan d'expérience, la formation de méta-modèle et l'utilisation d'algorithme génétique.

Le résultat de ce travail est une population de cœurs HCSMR optimisés. Parmi ces concepts il est possible d'obtenir des durées de cycle supérieures à 1200 JEPP, des facteurs de conversion au-delà de 0,9 tout en maintenant les taux de vidanges négatifs et des puissances linéiques maximales inférieures à 400 W/Cm. Les besoins d'uranium naturel associés sont réduits à environ sept tonnes pour produire un TWhe.

Mots clés: REL, Haut facteurs de conversion, réacteurs sous-modérés, SMR, Optimisation multi-objectifs, Réseaux de neurones, conception réacteurs.

ZUSAMMENFASSUNG

Diese Forschungsarbeit untersucht die Auslegung und Optimierung eines kleinen modularen Reaktors mit erhöhten Brutraten (HCSMR: High Conversion Small Modular Reactor). Der HCSMR hat eine thermische Leistung von 600 MW und erzeugt 200 MW elektrisch. Es ist ein integrierter DWR (Druckwasserreaktor) mit kompaktem Reaktorgitter. Der Abstand zwischen zwei Brennstäben beträgt 1,15 cm in einem hexagonalen Gitter. Damit ist das Moderator-zu-Brennstoffverhältnis (1,0) im Vergleich zu einem großen DWR (2,0) reduziert, und daher hat der HCSMR eine verbesserte Fähigkeit zur Konversion von ^{238}U nach ^{239}Pu und kann Plutonium Isotope effizienter spalten. Im Kern des HCSMR sind MOX Brennelemente eingesetzt.

Das HCSMR Konzept leitet sich vom großen DWR mit erhöhten Konversionsraten und von kleinen modularen Reaktoren (SMR) ab. Eine reduzierte Kernhöhe und -breite führten zu einer größeren Neutronenleckage im Vergleich zu einem Standard DWR. Dies wirkt sich positiv auf das Sicherheitsverhalten bei Kühlmittelverluststörfällen aus. Der Bedarf an Brutmaterial zur Minimierung des Kühlmitteldichtekoeffizienten wird damit ebenso reduziert, so dass die gesamte Sicherheit des HCSMR aufgrund verringerter Heterogenität profitiert.

DWR Brennstoff besteht heutzutage hauptsächlich aus schwach angereichertem Uran. Moderne DWR benötigen ca. 20 Tonnen natürliches Uran (U-nat), um eine TWhe zu erzeugen. Der Verbrauch an Uran könnte reduziert werden, wenn sich die interne Konversion von ^{238}U auf ^{239}Pu erhöhen ließe. Ein kompakteres Brennstoffgitter ermöglicht dies, und das reduzierte Moderationsverhältnis macht das Neutronenspektrum härter. Solche Kerne ermöglichen Konversionsraten über 0,8 in einem geschlossenen Brennstoffkreislauf. Im Vergleich dazu haben aktuelle DWR-Konversionsraten von ca. 0,5. Dadurch wird auch eine bessere Nutzung von Plutonium möglich bei gleichzeitig verringertem Aufbau der minoren Aktinoide.

International wird ein erneutes Interesse an kleinen Reaktoren (SMR) beobachtet. Der Wunsch nach großer Zykluslänge führt bei SMR zwangsläufig auf niedrige Entlade-Abbrände. Das bedeutet einen Anstieg des Bedarfs an natürlichem Uran im Vergleich zu heutigen DWR. Solche SMR haben einen Bedarf von ca. 40 Tonnen natürlichem Uran für die Erzeugung einer TWhe.

Der HCSMR Kern wurde mit einer multi-Parameter Optimierungsmethode ausgelegt. Damit sind die verschiedenen Parameter, die die Kernauslegung betreffen, als Gesamtheit berücksichtigt. Die Optimierungsziele werden dabei als Pareto-Optimum erreicht.

Die neutronenphysikalischen Berechnungen wurden mit den deterministischen Programmen APOLLO2, CRONOS2 und APOLLO3® und mit dem Monte-Carlo-Programm TRIPOLI-4® durchgeführt. Das Programm URANIE wurde für die Optimierung verwendet: Eingabe-Erstellung, Bildung von Ersatz-Funktionen und die Anwendung der Optimierungs-Algorithmen.

Als Ergebnis wurde eine Population von optimierten HCSMR-Kernen erzeugt. Diese Pareto-optimalen Kerne ermöglichen Zyklen über 1200 VLT, Konversionsraten über 0,9 mit negativem Kühlmitteldichtekoeffizienten und eine maximale lineare Leistung unter 400 W/cm. Der U-nat Bedarf des HCSMR ist damit reduziert auf sieben Tonnen U-nat für die Erzeugung einer TWhe.

Keywords: LWR, Erhöhte Konversionsraten, Unter-moderiert, SMR, Multi-Parameter, Optimierung, Neuronal Netzwerke, Kernauslegung.

TABLE OF CONTENTS

List of Tables

List of Figures

LIST OF ABBREVIATIONS

BOC	Beginning of Cycle
CF	Conversion Factor
CRDM	Control Rod Drive Mechanism
DHRS	Decay Heat Removal System
DoE	Design of Experiment
ECDS	Emergency Cool-Down System
EFPD	Equivalent Full Power Day
EOC	End of Cycle
EPZ	Emergency Planning Zone
EUR	European Utility Requirements
FA	Fuel Assembly
GA	Genetic Algorithm
GDA	Generic Design Assessment
GIF	Generation IV International Forum
HCBWR	High Conversion Boiling Water Reactor
HCLWR	High Conversion Light Water Reactor
HCPWR	High Conversion Pressurized Water Reactor
HCSMR	High Conversion Small Modular Reactor
IAEA	International Atomic Energy Agency
ICFM	In-Core Fuel Management
LOCA	Loss-Of Coolant Accident
LOO	Leave One Out
MC	Monte-Carlo
MOC	Methods of Characteristics
MOO	Multi-Objectives Optimization
MW	Mega Watt
MWe	Mega Watt electric
MWt	Mega Watt thermic
NPP	Nuclear Power Plant
NRC	Nuclear Regulatory Commission
NSSS	Nuclear Steam Supply System
OAT	One at a Time
PWR	Pressurize Water Reactor
RMSE	Root Mean Square Error
RP	Research Plan
RPV	Reactor Pressure Vessel
RRV	reactor recirculation valves
SG	Steam Generator
SMR	Small and Modular Reactor or Small and Medium Reactor.
Unat	Natural Uranium

Introduction

INTRODUCTION

Martin Heinrich Klaproth, a German chemist, discovered uranium in 1789 together with Zirconium. Uranium was later used by Henri Becquerel, a French physicist, to provide the first evidence of radioactivity. Marie Curie, French physicist and chemist, then studied the characteristics of radioactivity and explored the properties of radium.

Curie's work paved the way for peaceful use of nuclear energy and nuclear medicine. Those discoveries, together with the first fission chained reaction obtained in 1942 by Enrico Fermi, an Italian physicist, led to the revolutionary technical development of nuclear fission that is continuing to have an impact on our daily lives.

Commercial nuclear power plants (NPPs) began operation in the 1950s. Several reactor technologies have been developed since then. Light-water reactors (LWRs) are the most commonly constructed and have now been in operation for more than 60 years. In 2017, 82 % of the 448 nuclear power reactors operated worldwide are LWRs. They benefit from a lot of positive experience.

LWRs utilize mostly low-enriched uranium fuel. Uranium is a natural element found in rock, soil and water. Resources of uranium are proven large enough to continue supporting NPP operations for several decades. Uranium remains, however, a finite resource. To increase the sustainability of nuclear fission, nuclear engineers have developed several reactor concepts beyond LWRs.

In particular, LWRs could become more sustainable with an enhanced ability to convert ^{238}U isotopes into ^{239}Pu. Such reactor designs are referred to as high conversion cores and have been studied for many years. High conversion light water reactors (HCLWR) can either use boiling or pressurized technologies. High conversion is obtained for design with a conversion factor above 0.8.

The conversion factor characterizes the ability of a nuclear core to convert fertile fuel into fissile fuel. It is defined as the ratio of fissile material mass at the end of irradiation compared to the fissile material mass at the beginning of irradiation. LWRs currently in operation have conversion factors between 0.4 and 0.6. A high conversion ratio leads to a better utilization of natural resources and reduces requirements in natural uranium. Yet none of the HCLWR concepts have been industrially developed so far.

The low prices for natural uranium observed in past years do not encourage substantial efforts to reduce the uranium consumption in LWRs. However, this situation is likely to evolve in the future and tension on uranium markets could arise. This would reinforce the necessity to reduce uranium needs for LWR technologies.

An alternative to reducing uranium consumption is to switch from LWR technologies to fast reactors and the so-called Generation IV of reactors. Those innovative designs also have high conversion factors, even above 1.0. However they are based on different reactor technologies, often using liquid metal as coolant. Generation IV reactors are expected to become commercially

available in just a few decades. In the meantime there is more opportunities for LWR technologies with an increased conversion factor.

A high conversion factor in LWR design can be obtained by reducing the moderation ratio. The moderation ratio characterizes the proportion of neutron moderator volume to the volume of fuel. In a standard PWR the moderation ratio is close to two, whereas it is only around one only in under-moderated cores.

A tighter fuel lattice enables the increase of the ratio of fuel to water volume, hence reducing the moderation ratio. As a consequence the neutrons have fewer chances to be slowed-down to thermal energies. The neutron spectrum is shifted to higher energies, becoming an epithermal spectrum. With an epithermal spectrum the conversion of ^{238}U isotopes into ^{239}Pu is increased.

The use of mixed oxide (MOX) fuel, often considered in under-moderated cores, also contributes to harden the neutron spectrum and increase fuel conversion. Moreover MOX fuel, obtained after LWR fuel reprocessing, is an important contributor to a reduction of uranium needs in LWR technologies and an increase of nuclear power sustainability. However, MOX fuel loaded in under-moderated designs should contain a high content of plutonium isotopes, often above 10%, due to the epithermal neutron spectrum. This is required to obtain a critical core.

The studies of LWR with reduced moderation ratio started in the 70's. Several projects were developed up until the 90's, mostly in the USA, Japan, France, Germany and Israel. Most of the designs developed use pressurized water as a coolant and moderator. The designs studied in the 20^{th} century did not lead to commercial developments.

In the year 2000's a renewed interest for under-moderated cores was observed in some countries. France, Japan and the USA were working on advanced concepts. The improvement of core design tools and safety analysis techniques enabled more accurate assessments. However, none of the concepts studied have reached advanced development stages so far. The lack of economic interest is certainly the first reason. The technical challenges associated with high conversion cores are also an explanation.

The main technical challenge lies in the reactivity management in case of loss of coolant. For safety reasons, the reactivity should decrease when the moderator is voided. The behavior in case of loss of coolant is characterized by the void coefficient, quantifying the reactivity variation between nominal and voided situations. The void coefficient must be negative. This is a limiting parameter for the design of high-conversion cores.

Under-moderated cores tend to have positive void coefficients mainly for two reasons. In case of a loss of coolant the neutron spectrum becomes a fast neutron spectrum. As a result, with MOX fuel containing a high content of plutonium isotopes, the ratio of capture over fission reaction rates decreases. This increases the reactivity. Secondly, fast fissions increase in such voided situations, also contributing to an increase of the reactivity.

Several design options exist to limit the void coefficient. The most studied is the introduction of fertile fuel in the core together with the MOX fissile fuel. Fertile fuel contains only depleted

uranium. The absence of plutonium isotopes enables the limitation of the reactivity increase in case of a loss of coolant. The fertile material enables neutron 'sterile' capture without fission.

The fertile fuel can be introduced either radially or axially in the core. Fuel assemblies containing only fertile fuel rods can be loaded within or around the core. Alternatively fuel rods can be inserted in MOX fuel assemblies in the core design. Axially, layers of fertile materials can be added at the bottom, top or even within the core active zone.

As a consequence, under-moderated core designs containing fertile materials become rather heterogeneous. This tends to create local power peaks due to neutron spectrum variation at the interface between fissile and fertile medium. It also adds complexity to safety analysis, fuel manufacturing and even the operation of the core.

In a small under-moderated core an intrinsic mechanism related to the core size and geometry is limiting the void coefficient. A large core has by design less neutron leakage than a small core. In normal operations this tends to decrease the neutron-physics performances of small cores compared to large ones. But in voided situations this would help to keep a negative void coefficient. Small under-moderated cores require therefore less fertile materials and their design is simpler compared to large under-moderated designs. This characteristic is the primary motivation to design a small under-moderated core.

The second main motivation to design an under-moderated core of small size is linked to the limited fuel efficiency of Small Modular Reactors (SMRs). The aim to reach long cycle lengths often led designers to adopt fuel management strategies resulting in low fuel discharge burnup. This is motivated by the new paradigm SMRs bring to nuclear.

Small cores are not new to the nuclear industry but a renewed interest in SMRs has been observed around the world over the last ten years. Currently more than 70 innovative SMR designs are in development with various levels of maturity and chances for deployment. The benefits of installing innovative SMR technologies are multiple and diverse.

From an investment perspective, SMRs require less capital compared to large reactors. SMR construction times are shorter than large units. Hence their financing and associated costs are smaller than for large units. This also applies in case of project delay and cost over-run: damages from projects of limited size and associated extra costs are reduced compared to a similar situation with large reactors. In other words, from an investment perspective the risks are smaller with SMRs compared to large units.

With regards to the industrial aspect, SMRs are anticipated to be simpler and easier to build than large units. The reduced power of small core makes it possible to limit the number of systems in the plant. In some designs the core, steam generators and the pressurizer are integrated into one vessel, limiting the number of pipes, valves and pumps, as well as the related maintenance and safety demonstration needs. Moreover, SMRs' limited power enables implementing passive safety features, such as natural circulation, and hence limits the number of active safety systems.

Furthermore, designers envisage small plants to be modular. This has two meanings: modularity in the construction process and modularity in deployment. For the first aspect, pre-fabricated

modules prepared in factories are expected to be delivered to the construction site. This approach, already implemented for some large NPP projects, aims at reducing onsite erecting time as well as the associated costs and risks.

Secondly the modularity in deployment refers to the construction of several small modules in one SMR plant. Each module has its own nuclear core and turbine with some balance of plant equipment possibly shared. It is a shift from an economy of scale to an economy of the multiple. The concept of economy of scale has been the driven mechanism in NPP design for many years. The larger the power unit can be, the more economically viable it would be since several systems must be erected independently of the design size, and a larger power output means more financial revenues.

The economy of multiple requires high design standardization combined with the approaches mentioned above. Nevertheless, the overall SMR costs for a given installed power are likely to be higher compared to large units. This remains the main challenge for SMRs, for which the competitiveness has not been proven so far.

The business case of SMRs is challenging but further aspects support it. SMRs can fit into small power grids, increasing the deployment opportunities compared to large units. This is particularly relevant for countries with limited grid size. The modularity features of SMRs can also help to accommodate power demand increase, with modules built in an incremental manner as energy demand rises. This approach enables the revenues of a module to finance the construction of the next one and limit the associated financial costs.

Last but not least, the reduced footprint of SMRs can also facilitate finding more construction sites suitable to building SMRs, as well as the deployment in remote areas where limited power is needed. Those niche markets also include innovative deployment approaches such as under-water or barge-mounted designs.

Innovative SMRs also create challenges. The willingness to limit maintenance outage time to maximize power generation and revenues encourages designers to plan long fuel cycle lengths for SMRs: from two to over ten years. As a consequence, fuel management strategies are often far from optimum with regards to the use of natural resources.

This latter aspect supports designing a small core with a high conversion ratio: the scope for improvement in uranium utilization is more important for SMRs compared to large reactors. Moreover, in case uranium prices would substantially increase, the economic relevance of SMRs – not proven yet – would be further challenged. The option to limit uranium needs could hence support SMRs' economical robustness.

The previous observations led to the introduction of the high conversion small modular reactor (HCSMR) design, the focus of this research work. This project aims at designing and optimizing the HCSMR core design. The HCSMR should benefit of the extensive knowledge existing within the nuclear engineering community.

This research work is performed at the initiative of PreussenElektra GmbH (formerly E.ON Kernkraft GmbH) with the support of the Technical University of Munich (TUM) and the French

Atomic Energy Commission (Commissariat à l'Energie Atomique et aux énergies alternatives, CEA). This joint-work also results from the 2010 cooperation agreement signed between E.ON Kernkraft and the CEA ambitioning at fostering joint research work in the field of nuclear power between both organizations.

The HCSMR concept aims at improving the use of natural resources. A few boundary conditions are imposed to the HCSMR core. The design is rated at 600 MW thermal for an electrical output of 200 MW. It uses standard oxide fuel material in a tight hexagonal lattice, resulting in a reduced moderation ratio around unity. The fuel can include MOX, enriched uranium or a mixture of both. Thorium fuel is excluded from this study's scope.

The HCSMR conversion factor should be higher than 0.8 to reach improved efficiency with regard to natural resources utilization. Moreover the HCSMR should not use soluble boron in the primary coolant to control the reactivity. The use of MOX fuel and the under-moderated characteristics limits the reactivity swing over the cycle. This supports a soluble boron-free reactivity management concept.

This research work focuses on core design and neutron-physics studies of the HCSMR concept. Analysis of unexpected transients' and detailed thermo-hydraulic studies are not performed in this work. A large part of this research project is dedicated to the optimization of the core design. For example, the core active height, its fuel management approach, the reflector type or fuel type and plutonium content are parameters to be optimized. To perform the optimization of the HCSMR design, multi-objective optimization techniques are implemented.

Optimizing a design is a classic exercise in engineering. Several methods are available to optimize systems. A classic approach combines parametric analysis and engineering judgment. As systems become more complex, the ability of engineers to consider all horizons and optimize using intuition and "common sense" is questionable, particularly as many optimization objectives and constraints must be considered together.

The design of the HCSMR core is complex since several parameters are considered and some core configurations have a rather heterogeneous aspect. The rapid development of computer science and high performance computing (HPC) techniques enable the implementation of robust optimization methods.

The multi-objective optimization approach implemented in this work aims at identifying a series of most suitable designs. This should be differentiated from single objective optimization or approaches using an optimization weighted function gathering several objectives. In a multi-objective optimization, the aim is to obtain a population of optimized individuals, HCSMR cores in this project.

The Pareto concept is used to determine an optimum population: a population of individuals for which it is not possible to improve any individual on one objective without it deteriorating on at least one other objective. Genetic algorithms are most commonly used to obtain the optimized population. Surrogate models are created to enable large number of solutions to be evaluated as part of the optimization process. At first a research plan is derived to identify the boundaries and behavior of the optimization exercise.

For the HCSMR cores five optimization objectives are considered: the cycle length, the conversion factor, the void coefficient, the maximum fuel rod linear power and the plutonium total mass. Based on the Pareto population obtained, the designers can then select preferred designs depending on the priority set with one objective or another.

The research work objectives set for this work can be summarized as follows:

- Establish the design options of a small under-moderated core;
- Identify the performances of optimized small under-moderated cores;
- Review the added value of multi-objective optimization methods to design under-moderated cores.

This research work is divided into three main areas, reflected in the three parts of the present document. The three parts, their contents and links are highlighted in Figure 0. 1. The research was organized with part one and part two working in parallel, while the last part dedicated to the optimization came at the end, resulting from the knowledge gathered previously. A specific introduction and conclusion are added to each part to support the reader in capturing the main objectives and take-away. The chapters related to each topic identified in Figure 0. 1 are highlighted in red color in the plot.

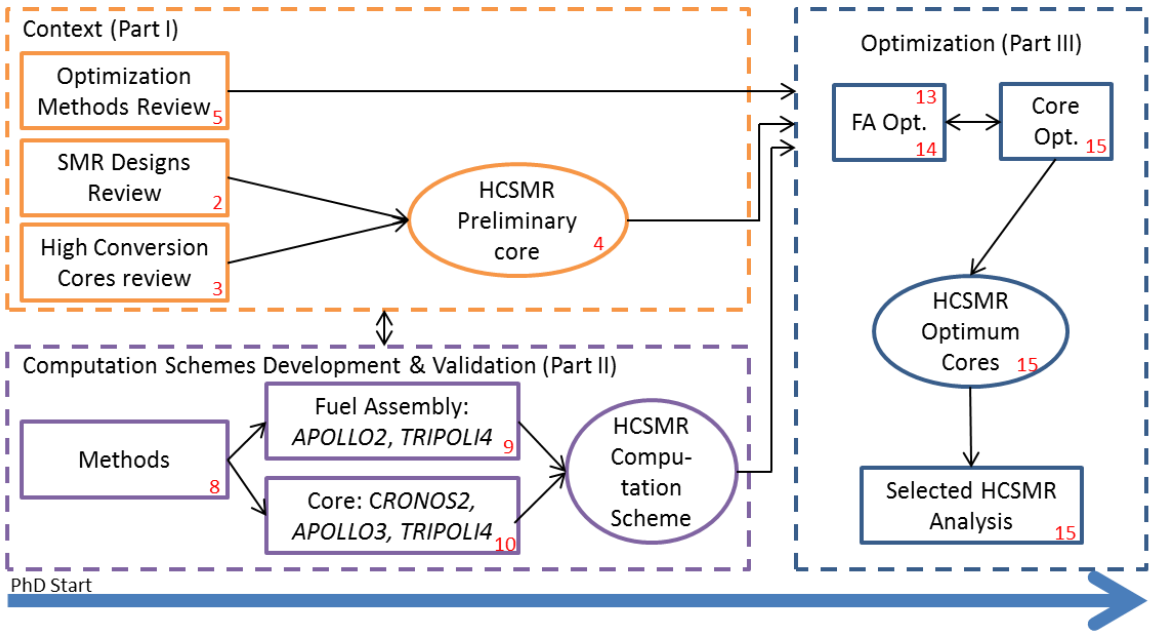

Figure 0. 1: HCSMR Design Research Process Overview

At first an extensive review of existing SMR and high-conversion designs is performed. It enables the creation of a reliable overview of the current status of both subjects. The findings also serve to define the HCSMR objectives and the preliminary design options of the HCSMR core. To benchmark the performances of the HCSMR core, the SMR600 concept is introduced. It is a standard SMR using PWR technology.

In addition, an analysis of reactor physics of under-moderated cores is presented in the first part. This helps emphasize the motivations supporting the design of a small under-moderated

core. Last but not the least, the optimization techniques implemented to design the HCSMR core and the associated theoretical concepts are presented. The URANIE tool, used for the multi-parameters optimization, is also introduced.

The second part is dedicated to the reactor physics models developed to compute the HCSMR core characteristics. Neutron physics codes developed at CEA are used: the deterministic codes APOLLO2 and CRONOS2 as well as the Monte-Carlo TRIPOLI-4® code are the main tools utilized. The deterministic APOLLO3® code under development is also used for benchmarking purposes.

Lattice computations are performed using APOLLO2 while CRONOS2 and APOLLO3® are used for core evaluations. TRIPOLI-4® is employed as a reference computation scheme to benchmark the deterministic results obtained at the fuel assembly and core level. The performances of the HCSMR first core are also presented in the second part.

The last part is dedicated to the actual optimization of the HCSMR core design. The optimization itself is divided into three steps. The first two cover optimizations realized at the fuel assembly level. The definition of an optimum radial zoning in plutonium content is the first exercise's focus. The optimization of fertile fuel rod positions in a MOX fuel assembly is the second optimization exercise at the fuel assembly level.

The last optimization step is dedicated to the entire core optimization. The HCSMR optimization results from an iterative process between those three types of optimization. A population of optimized HCSMR cores is the outcome. Out of the Pareto optimum designs, three cores are selected for a more detailed analysis. The neutron physics characteristics of the selected cores are presented, as well as identifiable steps for further development. A general conclusion terminates the manuscript and summarizes main findings of the research.

Part One

SMR, High Conversion Reactors and Core Optimization Context

TABLE OF CONTENTS

Chapter 1: PART ONE INTRODUCTION

In this first part of the thesis the context of the High Conversion Small Modular Reactor (HCSMR) design is introduced. The HCSMR concept finds its roots both in SMR and high conversion light water reactors (HCLWR) designs. The HCSMR core is carried out using advanced optimization methods based on recent developments in computer science. A review of the current status of the science and technology of those aspects is first performed. The HCSMR main characteristics and design process are defined based on the outcomes presented in the next chapters.

A renewed interest for SMR can be seen worldwide. In Chapter 2 the reasons behind this trend are first investigated. The opportunities and challenges SMR are offering are then discussed. A review of existing SMR designs and SMR currently in development is also introduced. 50 SMR designs are considered and preliminary evaluated. This led to identify nine SMR designs as interesting reference for the HCSMR design. For those nine concepts a detailed review of the main characteristics is performed. Moreover a reference is needed to benchmark the performances of the HCSMR design to be optimized. The SMR600 design is created for that purpose. Its characteristics and performances are introduced and discussed in Chapter 2.

Chapter 3 is dedicated to the review of high conversion cores benefits and main characteristics. To limit the consumption of natural uranium and improve the performances of light water reactors currently being operated, such designs were intensively studied in the last decades. Existing high conversion light water reactor designs and concepts are researched and analyzed. This bibliography work made it possible to identify the interest of the HCSMR design and to define some of its main characteristics. The specificity of high conversion core physics is also introduced in this chapter as well as the key concepts of conversion factor and void coefficient.

To optimize the HCSMR core a first reference is required. The starting HCSMR core is introduced in Chapter 4 with an overview of the first generic design concept, its fuel assembly and core characteristics. The first HCSMR core characteristics are defined using existing knowledge on SMR and high conversion cores. In particular previous studies performed at CEA on large high conversion cores are considered. The general objectives and performances of the optimization exercise are also introduced in Chapter 4.

This work is partly dedicated to the use and development of optimization methods to design the HCSMR core. Nuclear core conception requires conciliating a large number of objectives and boundary conditions. Optimization techniques can provide a support to decision making in complex design exercises, such as core design. Such optimizations have multiple criteria and objectives. Those concepts are introduced in Chapter 5. A review of the existing methods and techniques with regard to the research plan, surrogate models and optimization methods is performed. It is followed by an analysis of the existing approaches, their advantages and limitations which can be found in Chapter 5.

Chapter 6 summarizes the main take away for the HCSMR design optimization.

1. 1 DEFINITIONS

The acronym SMR can refer either to Small and Modular Reactor or Small and Medium Reactor:

- Small and Medium Reactor (SMR)
  The "small" and "medium" adjectives qualify the size of a given design. According to the IAEA, "small reactors" are reactors with an equivalent electric power less than 300 MW and "medium" reactors have an equivalent electric power between 300 and 700 MW [1].

- Small Modular Reactor (SMR)
  Both the design and the construction of SMR can be "modular". Modularity in design refers to multi-modules SMRs: one plant is made of several units. Units can be successively added to the plant at the initial construction time or later. Modularity in construction refers to the shipment of in-factory manufactured modules. This reduces on-site activities, thus the construction time and risks.

The HCSMR design belongs to the Small Modular Reactor definition of SMR.

The SMR designs currently operated or in development worldwide are based on various nuclear technologies. As explained in the next chapters the most mature innovative designs use water as coolant and moderator. They belong to the category of Light Water Reactors (LWR).

- Light Water Reactors (LWR)
  Over 80 % of the current installed commercial nuclear reactors are LWR. In LWR water is used as both coolant and neutron moderator. The neutron spectrum is thermal. LWR are divided between Pressurized Water Reactor (PWR) and Boiling Water Reactor (BWR)

- Pressurized Water Reactor (PWR)
  Among LWR, PWRs have pressurized water as coolant and moderator. Water flows through the primary circuit at very high pressure – usually 155 bars – into steam generators where a secondary circuit is connected. Water from the secondary circuit becomes steam when heated in the steam generator and drives the turbine. Examples include – but are not limited to – EPR, AP1000, VVER and Hualong one reactors.

- Boiling Water Reactor (BWR)
  Among LWR, BWRs have a primary circuit directly connected with the turbine. Water – usually at 70 bars – is heated in the nuclear core into steam which drives the turbine. BWR-6, ABB-3, ABWR are examples of BWR designs.

Within LWR SMR design type almost only PWR technology has been found in the literature as it can be seen in the next chapters.

Chapter 2: SMALL MODULAR REACTORS

2. 1 RENEWED INTEREST FOR SMRS

The first nuclear reactors ever designed were small ones. Experimental cores and sub-marine propulsion designs pioneered the development of nuclear power. The first nuclear-powered submarine, the USS Nautilus (1954), had a power of about 10 MW. In 1958 the Shippingport reactor started operation in the USA with an electrical power output of 60 MWe. The nuclear industry gathered a large experience in designing and operating small cores.

The commercial development of nuclear power led the engineers to develop bigger units. In the 1960s nuclear power plant (NPP) designs became larger and came to have electrical output close to 1000 MWe. The EPR® plants in construction in 2017 have an electrical output above 1600 MWe. This change was driven by the size-scale effect. Since nuclear power plant projects are capital intensive but have low operating costs the profitability tends to increase with larger designs.

As of today there are more than 100 nuclear reactors with an electrical output lower than 700 MWe in operation in the world. However none of them are qualified innovative SMRs. Around the year 2000 several industrial or academic organizations accelerated their activities on SMR development [2]. Since 2010 the trend has expanded and the development and commercialization of newly designed SMRs become a priority for several actors across the nuclear industry [3].

Hence small reactors are not new but the paradigm associated with their current development is. The drivers to support the development of SMRs are different compared to large reactor development. The vision is to deploy successive small modules at one site to form a NPP or address niche-market with simpler design using the economy of numbers and simplification of design rather than the economy of scale used so far to justify large units. SMRs require less capital and reduces investment risks compared to large reactors.

To reach simplification of design for SMRs, several innovation programs were started. In the literature more than 70 SMRs designs currently in development or in operation can be found [1] [4] [5]. They have different levels of maturity and are based on various reactor technologies. Annex A gives an overview of 50 SMR designs. These designs are selected for their development readiness but also to highlight the variety of technologies in SMRs. No under-moderated small core has been found in the literature.

The most mature innovative designs use water as a coolant and moderator [6]. They belong to the category of Pressurized Water Reactors (PWR). Very often their primary circuit is integrated: the core, steam generator and pressurizer are all encapsulated in one reactor pressure vessel (RPV). The development of integrated designs (iPWR) has evolved rapidly in the past years and is directly linked to the renewed interest for small reactors introduced before.

Other SMR technologies exist, including some supported by the Generation IV International Forum (GIF) [8] [9]: Sodium cooled Fast Reactor (SFR), Molten Salt Reactor (MSR), Lead or Lead-Bismuth cooled Fast Reactor (LFR).

2. 2 SMR OPPORTUNITIES AND CHALLENGES

Innovative SMRs share many principles with large reactors. Their designs and safety approach is built upon the many years of experience operating large reactors and in particular PWR. This section aims at presenting the main opportunities and challenges of innovative SMR. A focus is given to the aspects where SMRs bring significant innovation or new philosophy in comparison to large LWR currently in operation. This makes it possible to understand the value of developing SMR designs and setting directions for some design options of the HCSMR concept.

2. 2. 1 Safety and Security

Several aspects support a high safety level for SMRs. As they are of simpler design than large reactors, SMRs require less components and systems which reduces the possible failure and malfunction of systems. This is particularly true for integrated PWR in which for example large Loss Of Coolant Accident (LOCA) are eliminated by design: the direct integration of core, steam generators and pressurizer in the pressure vessel [10] enable the removal of large piping systems.

The small power of the core limits the decay heat being removed compared to large reactors. It requires therefore less mitigation measures in case of accident. For example, in the event of heat removal failure, the NuScale design foresees a 30 days grace period before all the water in the primary circuit boils. After this time, the decay heat has decreased and air-cooling using natural convection only is enough to prevent temperature rise and fuel melting. Designers are referring to the passive and inherent safety features of SMRs.

With regard to security, some innovative SMRs design will be constructed underground to reinforce their protection against external hazards. Other designs will be barge-mounted or placed under the sea level for operations [11]. In general those new deployment schemes reinforce the level of SMR designs' protection against external hazards. In some specific cases it also leads to new requirements and careful assessment of SMR safety and security, since the proposed concepts are new to the nuclear industry. An example is the underwater Flexblue design.

Furthermore some innovations in SMRs bring new safety topics. As an example the NuScale design is willing to operate multiple modules from the same control room. This raises questions with regard to human factors and accident mitigation aspects. Regarding core and fuel topics, some designs foresee a management of the core reactivity performed without soluble boron in the primary coolant. This would ease some operational processes and might reduce design costs but at the same time it raises safety and operability questions [12].

The accident at the Fukushima Daiichi NPP in 2011 in Japan demonstrated the need for the nuclear industry to respond adequately to unexpected circumstances and beyond design-basis

accidents. This applies to all nuclear reactors including SMR designs. In particular NPP must resist extended loss of on- and off-site power. SMR designers showed the capability of their concepts to address Fukushima Daiichi accidental situations [13]. The innovative design features and passive safety approaches of SMRs enable longer grace periods compared to current large reactors.

2. 2. 2 Operability and Flexibility

Most large NPPs currently in operation have a fuel cycle length between 12 and 18 months. After this period a refueling outage takes place to replace part of the irradiated fuel and perform maintenance operations. In SMR technologies the foreseen fuel cycle lengths are longer: at least 2 years and up to 10 years of continuous operation is claimed by designers. This will impact the maintenance and operating philosophy of SMRs.

The simplification of some systems such as the operation in natural convection for the NuScale modules raises questions with regard to flow stability during start-up and shut-down phases as well as in case of partial-load operation. The SMRs ability to operate in load-follow mode is not granted since the nuclear steam supply system (NSSS) flexibility might be limited compared to large reactor. SMRs not using soluble boron in the primary coolant for reactivity control are particularly affected. All designs, including the HCSMR, should fulfill the load-follow requirements described in the European Utility Requirements (EUR) chapter 2.3 [24].

A solution proposed by the designer is to let the core operate at full power at all times and perform load-follow operations via the secondary systems of the unit. Either by routing the steam produced directly to the condenser or by using it via a co-generation system coupled to the plant, for example, to balance the intermittency or renewable energy sources on the grid [26]. Such hybrid systems could support the flexibility of SMRs and their integration in the energy landscape of tomorrow.

2. 2. 3 Licensing

For SMRs developed as modules, the business model will require a high degree of standardization. This can only be achieved with a licensing framework adapted to such requirement. In particular, the licensing of an n^{th} module in a unit should be based on the 1^{st} module license without further requirement. Moreover, real standardization will only be possible when a SMR licensed once in a country could be deployed in several other areas with limited or none additional licensing requirement. A higher degree of licensing harmonization must be reached compared to the current situation to support SMR development. Otherwise adaptation to every specific requirement will decrease the benefit of standardized manufacturing. Several works were published calling for further development in that direction [21] [22] [23].

Whereas it is recognized that a cross-border licensing regime will be difficult to achieve in the near future, a two-step licensing process like the generic design assessment (GDA) developed in the UK [21] could give a generic license to a design concept, leaving only site specific licensing to the responsibility of the respective country's safety authority.

2. 2. 4 Public Acceptance and Emergency Planning Zone

SMR could benefit from an improved public perception compared to large reactors [20]. The increased safety level SMR designers make for good publicity but also the smaller size and land use would support an improved public attitude toward SMRs. This last argument also justifies the reduced emergency planning zone (EPZ) associated with SMR deployment. A reduced EPZ for SMRs compared to large reactors would increase the deployment opportunities and SMR market size. However this will have to be accepted by the respective safety authorities.

2. 2. 5 Fuel Cycle and Proliferation Resistance

Another important aspect for the development of SMRs is their ability to prevent nuclear material proliferation. Compared to large reactors, SMRs have pros and cons with regards to proliferation resistance. The multiplication of small nuclear cores worldwide could increase nuclear proliferation risks. Adequate measures must hence be considered with SMR deployment. In particular SMRs using heavy water as a moderator should receive specific attention and the IAEA has already issued recommendations on this topic [25].

For SMR designs using water coolant such as iPWR, standard enriched UO_2 fuel is usually foreseen. The fuel enrichment is below 5.0 % ^{235}U in agreement with international recommendations on nuclear safeguards. The rather long cycle length anticipated would limit fuel transport and ease oversight. This would support the intrinsic ability of SMR designs to prevent nuclear material proliferation.

2. 2. 6 Economics and Markets for SMRs

The current philosophy in nuclear energy supports the development of large units. The overnight cost (€/MWe) of a given design gets smaller when the unit size increases. The overnight cost refers to a unit cost without financial or risk hedging costs: considering the plant is built over one night. The scaling function 1. 1 illustrates the influence of the reactor size in the unit overnight cost [14].

$$Cost(P_1) = Cost(P_0) * \left(\frac{P_1}{P_0}\right)^n \quad (1.1)$$

$Cost(P_i)$ is the cost of power plant *i* for the unit size P_i [MWe] and *n* the scaling factor ranging from 0.4 to 0.7. The key parameter of this exponential law is the scaling factor *n*. Detailed scaling factors for plant structures, electrical systems, balance of plant, etc. are given in the literature [15]. In equation 1.1 the cost of unit one with power P_1 is derived based unit zero cost with power or size P_0.

The Figure 1.1 from [14] illustrates the scale effect based on French experience [16]. It shows the limited interest of small designs based on overnight costs. It also shows the benefit of building more than one unit in one plant: the "repetition effect". By sharing some systems in a plant, several nuclear units built in one plant benefit from a reduced specific overnight cost. This aspect is also transferable to the economics of SMRs.

2. 2 SMR Opportunities and Challenges

Moreover SMRs have intrinsic advantages supporting their development. Several studies were performed to assess the economics of SMR [3] [17] [18] [19]. Designers refer to a new paradigm and present the following advantages compared to large reactors:

- Reduction of the number of systems due to simplified designs relying on passive features;
- Standardization of design and in factory module production;
- Module shipment via conventional long distance transport[1];
- Installing several modules in one plant as required;
- Innovative financing schemes, e.g. 2nd module deployment paid by the first module generation revenues;
- Reduced risks associated with SMR development;
- Limited cost of capital;
- Suited for non-power applications, e.g. desalination, process heat supply;
- Easier decommissioning and dismantlement thanks to the modularity of construction and size of the units.

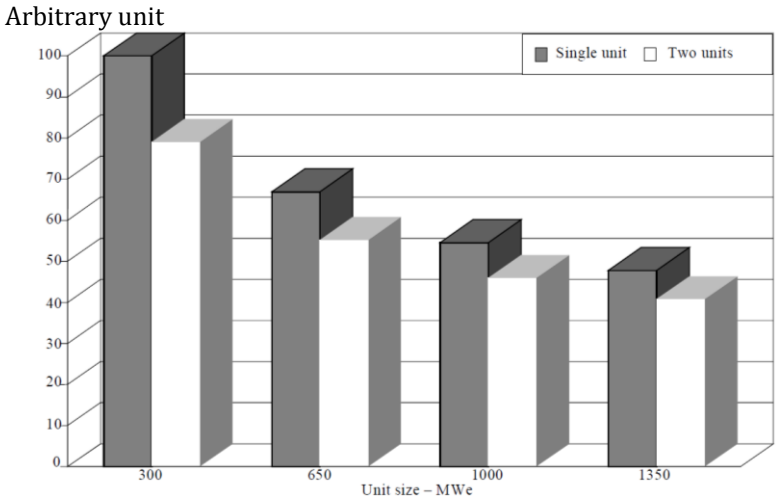

Figure 1.1 : Overnight Cost Ratio for Single or Two Units' Nuclear Plants of Different Power

By taking into account those specific competitive advantages a consensus has emerged [3] [17] [20] to recognize the potential of SMR levelized cost of electricity (LCOE, defined in 1. 2) to be close to large nuclear reactors' LCOE. Those analyses are based on assumptions made by SMR vendors. However the lack of innovative SMR deployment so far prevents the collection of reliable figures on the current economics of SMRs.

$$LCOE = \frac{\sum_t \frac{Investment_t + Fuel_t + O\&M_t + Decommissioning_t}{(1+r)^t}}{\sum_t \frac{Electricity_t}{(1+r)^t}} \qquad (1.\ 2)$$

With $Investment_t$: Investment cost in year *t*.
$Fuel_t$: Fuel cost in year *t*.

[1] This limits the RPV maximum diameter and was considered for the HCSMR design RPV diameter

$O\&M_t$:	Operations and maintenance cost in year *t*.
$Decommissioning_t$:	Decommissioning cost in year *t*.
$Electricity_t$:	Electricity amount generated in year *t*.
r :	Annual discount rate.
t:	year t

The LCOE of large nuclear reactors is mostly influenced by the construction or investment cost. The decommissioning costs are discounted and the fuel and O&M fuel are small compared to investment costs. Therefore the unit overnight costs set the LCOE, provided the unit will generate power as expected. This is why the current delays and investment extra costs in nuclear new builds observed worldwide are quickly and substantially raising nuclear energy LCOE.

For SMRs the ratio between capital costs – investment and decommissioning costs – and the variable costs – O&M and fuel costs – is reduced. Reducing the fuel costs has therefore more impact in a small core to limit the LCOE compared to large core. Moreover the fuel management of small cores is usually designed for long cycle and has a low efficiency (burnup) which offers a real opportunity for improvement [3] [20].

On the other hand it is important to remark the various markets available for SMR deployment [20]. When competing with large nuclear reactors or coal fire units, SMRs will have to become competitive and aim at a low LCOE value to increase their deployment. In niche markets such as isolated power generation the rather high LCOE of SMRs would not disqualify their development.

2. 2. 7 Perspectives for SMR Development

Several countries have expressed interest in SMR technologies. Countries hosting SMR vendors such as Russia, USA, Argentina or South-Korea are at the forefront of SMR development. Three innovative SMR designs are currently in construction: CAREM in Argentina, HTR-PM in China and KLT-40S in Russia [6].

Nuclear new comers countries have also repeatedly expressed their interest to develop SMRs. Their motivations are diverse. The reduced capital costs compared to large reactors is not the only driver. The ability of SMRs to have non-electrical applications, their size adapted to small power grids [3] and their relevance for remote area generation are reasons of interest for new comers.

In the USA the government supports the licensing and development of first of a kind (FOAK) design. NuScale and mPower received financial aid to license their designs, although the mPower project is now on hold. The UK government is willing to offer support to the development of an SMR in its country. Governmental support for FOAK design is certainly a strongly, if not mandatory, enabler of SMR development.

Challenges exist also for SMR development. Factory production of SMR modules is key for SMR competitiveness. This requires a substantial initial investment that only sufficient volumes in

2. 2 SMR Opportunities and Challenges

SMRs development will recover. To move from an economy of scale to the economy of multiple, the standardization of in-factory built modules is important.

This standardization will require a step forward in the harmonization of current licensing regimes. A new approach to module licensing is needed. This comes in addition to the prerequisite for regulators to license SMR innovative passive safety features.

The development of SMR designs is a global trend observed across the nuclear power industry. As with other nuclear technologies, SMRs are also impacted by the recent drop in natural gas prices. Together with the low or non-existing prices for greenhouse gas emissions it does not encourage funding SMR development. A consolidation of the sector is likely to occur. Not all designs will be developed and joint efforts and investments would support SMR future successes.

The following remarks complete the previous statements on SMR development perspectives, by summarizing main opportunities and challenges of PWR SMRs compared to large reactors. The iPWR SMR key specific features and expected advantages are shown in Figure 1.2 based on IAEA work by H. Subki [6].

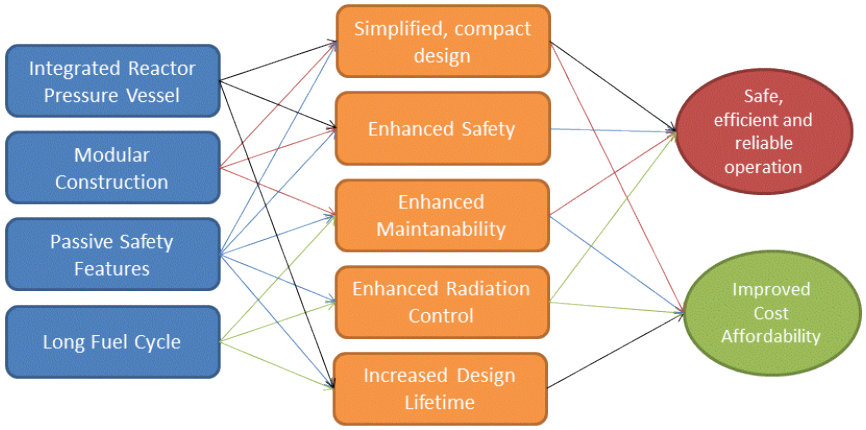

Figure 1.2: iPWR Specific Features and Expected Advantages

2. 2. 7. 1 Opportunities

The items listed below are divided between aspects related to technology and non-technology topics, although interconnections exist between both aspects.

Technology

- Enhanced safety and reliability;
- Design simplicity;
- Long operating cycle;
- Modularization: shorter construction period.

Non-technology

- Lower capital costs: better affordability;
- Adequacy with smaller electricity grids;

- Opportunity to match demand growth by module incremental increase;
- Site flexibility including mobile deployment;
- Suitable for non-power applications, e.g. district heating, desalination.

2. 2. 7. 2 Challenges

Technology

- Maintenance;
- Human factor engineering, e.g. multiple units control room;
- Innovative features licensing;
- Design and operation.

Non-technology

- Economic competitiveness;
- FOAK financing;
- Harmonized licensing approach;
- Infrastructure requirement;
- Availabilities to nuclear new-comers.

The next section presents the main specificities and particular features of selected innovative SMRs compared to large reactors.

2. 3 SELECTED SMR DESIGNS OVERVIEW

Hereafter the main characteristics of nine selected innovative SMRs are presented. A focus on core and primary circuit characteristics is given. The nine designs are foreseen for immediate or near-term deployment with the exception of the Flexblue design planned for mid-term deployment. The designs are selected based on their maturity, degree of innovation, level of information available and possible links with the HCSMR concept. Information on their core, fuel and safety concepts is given in the next paragraphs. A comprehensive overview can be found in Annex B. Some options of the HCSMR design are derived based on a screening of those designs. Several references [3] [4] [6] [9] [12] are used for this overview.

2. 3. 1 CAREM (Argentina)

The CAREM-25 reactor is a prototype currently in construction in Argentina. It aims at validating the concept and technologies developed for the future CAREM commercial design (150-300 MWe). The CAREM-25 prototype has been developed since the 90's. Its construction started in February 2014. It has a thermal power of 100 MW and an electrical power of 27 MWe. The core is made of 61 hexagonal fuel assemblies. Fuel enrichment is 3.10 % ^{235}U. A cycle length of 11 months with half of the fuel assemblies replaced at each refueling is foreseen. Soluble boron is not used for reactivity control. Burnable poisons (Gadolinium) and movable absorbing elements control the core's reactivity. The CAREM-25 is an integral PWR self-pressurized. Twelve identical helical vertical steam generators are located within the pressure vessel. Its

safety systems rely on passive features. Natural circulation is used for the primary coolant in operation as well as in case of anticipated transient or design basis accidents. A passive condenser approach is implemented for the residual heat removal system (RHRS).

2. 3. 2 ACP100 (China)

The engineering entities of the China National Nuclear Corporation (CNNC) are focusing since 2010 on the development of an integral PWR type SMR, the ACP100. Apart from the pressurizer the NSSS is located within the pressure vessel. Two units per plant are foreseen for the deployment of the ACP100. FA are standard 17x17 with a reduced active height of 215 cm. Fuel enrichment is 4.20 % ^{235}U. The core is made of 57 FA. The cycle length foreseen is two years. Reactivity control is performed via soluble boron and 25 CRDM. As an integral PWR the ACP100 benefits from a reduced number of piping compared to a large PWR and therefore no possibility of a large LOCA scenario. The small size of the core enables passive decay heat removal. The reactor and spent fuel pool are located underground to prevent exterior aggression. The ACP100 is foreseen for base load operation. A site in Changjiang, in the Hainan province in southern China is selected to build the demonstration plant. APC100 design passed the IAEA safety review in 2016. First concrete is scheduled for the end of 2017.

2. 3. 3 Flexblue (France)

With Flexblue, its designer DCNS introduced a new and unique type of SMR: a subsea SMR. One Flexblue module has an electrical power of 160 MWe and a thermal capacity of 530 MW. The deployment of several modules at one site is possible. Each module is moored on a stable sea ground at a depth up to 100 m near a coast. A cable transports the electrical power generated by the Flexblue module to the land. The module can be remotely controlled from a control room onshore and can be accessed via an underwater vehicle for maintenance purposes. The Flexblue modules are manufactured and refueled at a shipyard and then transported by ship to the desired location for submerged operation. The Flexblue design is a two-loop PWR type. The core is made of 77 standard 17x17 fuel assemblies with a reduced active height of 215 cm. A cycle length of 38 months is foreseen with all fuel assemblies being replaced at each refueling. Flexblue safety concept is based on inherent safety features. Its operating environment provides an unlimited heat sink. Moreover it is modifying the safety demonstration requirements: seismic analysis or airplane crashes are not comparable to land-based reactors.

2. 3. 4 SMART (Republic of Korea)

The System-integrated Modular Advanced ReacTor (SMART) conceptual design started in 1999. SMART received a standard design approval license in 2012. The SMART design is an integral PWR combining inherent passive and active safety features. It has an electric output of 100 MWe for a thermal power of 330 MW and foresees water desalination in addition to electricity production. The fuel is standard 17x17 with a reduced active height of 200 cm. The core has 57 fuel assemblies enabling a cycle length of 36 months with half of the core replaced at each refueling outage. The reactivity is controlled via soluble boron in the primary coolant, 25 CRDM as well as burnable absorber. Horizontally mounted pumps into the reactor pressure vessel

ensure the circulation of the coolant. Heat removal was first designed to be performed by a combination of active and passive systems. Since 2012 a redesign of the safety features was started. It aims at relying on inherent passive systems only and for example eliminates the need of emergency diesel generators.

2. 3. 5 ABV (Russian Federation)

The ABV design is an integral PWR developed by OKBM Afrikantov. It has a thermal output of 38 MW and a thermal one of 8.5 MWe. The ABV design also enables co-generation with steam or heat supply in addition to electricity. Its deployment is foreseen as barge-mounted unit or land-based plant. The ABV core has 121 hexagonal fuel assemblies with an active axial height of 90 cm. Its batch fuel management enables a cycle length of over 120 months with fuel enrichment at 18.7 % ^{235}U. Fuel enrichment higher than 5 % ^{235}U would challenge the possibility to export such design outside of the Russian Federation. Reactivity control is performed via CRDM, soluble boron and the use of Gadolinium as burnable absorber in the fuel design. As an integral PWR the core and steam generators are located within the pressure vessel. However the pressurizer and CRDM are located outside the pressure vessel. The safety concept is based on both active and passive systems. Emergency core cooling is provided over an unlimited time during design-basis and beyond design-basis accidents.

2. 3. 6 RITM-200 (Russian Federation)

OKBM Afrikantov is the designer of the RITM-200 reactor. It has a thermal power of 175 MW and an electrical one of 50 MWe. The RITM-200 is designed to provide power to ice-breaker ships but its deployment is also foreseen for barge-mounted plants or offshore drilling platforms. The RITM-200 is an integral PWR. The core is made of 199 hexagonal fuel assemblies with an active height of 165 cm. The fuel enrichment is below 20.0 % ^{235}U. This enables a cycle length of 84 months using a batch fuel cycle management. The fuel enrichment close to 20% would challenge the possibility of exporting such a design outside of the Russian Federation, according to international standards (§2. 2. 4). The core and steam generators are located within the pressure vessel. The pressurizer and CRDM are located on the top of the pressure vessel. Reactivity control is performed via control rods but no soluble boron is used. The safety concept uses a combination of both active and passive systems. Passive heat-exchangers, either with atmospheric air or water, are forming the emergency core cooling system.

2. 3. 7 mPower (USA)

Babcock & Wilcox mPower Inc. (B&W) introduced the mPower design in 2009. This iPWR is primarily intended for electricity production and has a nominal output of 180 MWe per module. Twin-unit plant development is foreseen with a combined power of 360 MWe. The pressure vessel incorporates the core, once-through steam generators and the pressurizer. In-vessel Control Rod Drive Mechanisms (CRDM) is a specificity of the mPower design. The core is made of 69 standard 17 x 17 Fuel Assemblies (FA) with a reduced height (240 cm) compared to large PWR (390 cm). Its UO_2 fuel is enriched at 4.95 % ^{235}U. A batch fuel management is foreseen: all FAs are replaced during the refueling outage for a cycle length of 48 months. Horizontally

mounted canned motor pumps located within the pressure vessel ensure the primary coolant circulation. Passive and inherent safety features are designed, including natural circulation only for heat removal in case of design basis accidents. Diesel generators are not required for the safety demonstration. Basic design of the mPower has been completed and some interested utilities were identified. However the project development was scaled down by B&W in 2014 for restructuring reasons.

2. 3. 8 NuScale (USA)

Research and development of the NuScale design started in 2003 with thermo-hydraulic studies on natural circulation. NuScale Power was formed in 2007. The NuScale SMR design is based on small modules of 45 MWe each. Up to 12 modules, two times six, will form a plant. Each module is an integrated PWR. NuScale modules rely on natural circulation not only in case of design basis accident but also during operation. Natural convection drives the water within the pressure vessel instead of pumps. The modules are independent and can be added to the plant in a successive manner as needed. Each module has an individual turbine. The modules are located underground inside a reactor pool. The core of each module is made of 37 FA. The fuel is standard UO_2 17x17 with a reduced height of 1.8 meters. The Nuscale module will be refueled every two years requiring a batch fuel cycle. The safety concept is based on inherent safety features to enable passive long term heat removal during operation or in case of a severe accident. Heat removal occurs through steam generators and heat exchangers submerged in a water pool. The design enables 30 days of water cooling without operator action. After this period air cooling is sufficient to remove the remaining heat. The small size of each core limits the decay heat to be extracted. Early 2017 NuScale submitted an application to the Nuclear Regulatory Commission (NRC) to certify its design. The design certification is foreseen for 2020 with a first commercial operation in 2023.

2. 3. 9 Westinghouse SMR (USA)

The Westinghouse SMR was first introduced in 2011. It is an integral PWR designed using the developments and experience of the AP1000®. The Westinghouse SMR thermal power is 800 MW for an electrical output of 225 MWe. The deployment is foreseen as a stand-alone unit plant, although multiple units can be built at the same site. The Westinghouse SMR core is made of 89 standard 17x17 fuel assemblies with a reduced active height of 240 cm. A cycle length of up to 24 months is foreseen with 36 fuel assemblies replaced by new ones at each refueling outage. As an integral PWR the Westinghouse PWR pressure vessel contains all primary systems such as the core, steam generator and pressurizer. Only the eight external, horizontally mounted primary coolant pumps are located outside of the pressure vessel. The 37 CRDM are located within the pressure vessel. The safety concept relies on passive systems and inherent safety design. The heat removal system is passive and provides a grace period of up to 7 days.

2. 3. 10 Future Trends

The nine designs reviewed in previous paragraphs are foreseen for immediate or near-term deployment with the exception of the Flexblue design planned for mid-term deployment. Nonetheless each design has its own level of maturity and deployment perspectives. Those aspects are evolving rapidly and the anticipated future trends presented hereafter are based on the status Q4 2017.

The CAREM demonstration plant is in construction while the ACP100 is expected to start at the end of 2017. Their completion is anticipated over the coming years. As the first innovative SMRs to be constructed in the 21st century their success will be important for the entire SMR community, both from a scientific and an industrial perspective.

In the USA the NuScale project is leading the path towards innovative SMR deployment. Early 2017 the acceptance by the NRC to review NusCale design certification application marked a major milestone. A site for the first plant has been selected at Idaho National Laboratory, which is encouraging in regards to the implementation of the project. On the other hand the Westinghouse SMR development efforts have been reduced and the mPower project is likely to be abandoned. The lack of a confirmed market for SMRs challenges investors' appetite for SMR technologies.

The SMART deployment plans have been reoriented since 2015 to focus on foreign deployment. The agreement concluded between SMART designers and the Saudi Arabia's King Abdullah City for Nuclear and Renewable Energy (KA-CARE) aims at assessing the potential to develop two SMART units in that country. Studies and constructions plans are planned up until 2018.

In France the Flexblue design is a unique concept. Foreseen for mid-term deployment, the project is on hold as the designer DCNS and its partners, EDF, CEA, TechnicAtom are assessing the opportunity to prioritize the development of a land-based SMR design. As such, the preliminary design of terrestrial concept between 150 and 170 MW is ongoing.

The ABV and RITM-200 designs are planned for deployment according to the designer OKBM Afrikantov but no detailed information is available about an expected location or construction schedule.

The nine designs' specific features introduced in the section §2. 3 show PWR SMR main characteristics. This bibliography review enables the setting of directions for the HCSMR core. In particular information from mPower and Westinghouse SMR regarding the core power, the core active height, the core maximum radius and the cycle length supported the definition of the HCSMR core preliminary features.

Since those industrial designs contain proprietary information it is not possible to obtain all detailed design characteristics. Core design details and fuel utilization information is only partially available. Hence an own design for benchmark purposes is introduced: the SMR600.

2. 3. 11 SMR600

The SMR600 design is developed as part of this PhD thesis for benchmark purposes on neutron-physics performances. The objective is to set a reference to compare iPWR and HCSMR design performances on natural uranium consumption and conversion factor. The SMR600 characteristics are mostly based on the mPower and Westinghouse SMR designs (cf Annex B) and aims at representing a generic iPWR core type.

The fuel is standard 17x17 with enriched UO_2 at 4.95 % ^{235}U and reduced height of 220 cm. The core is made of 69 fuel assemblies and is rated at 600 MW thermal. Two fuel management approaches are considered. First a batch fuel management core: all full assemblies are only used for one irradiation cycle. Secondly a "1/2" fuel management approach is studied. With this approach after each cycle 33 fuel assemblies are reloaded into the core for a second irradiation cycle. The SMR600 detailed core characteristics and loading patterns are introduced in Annex C.

The SMR600 design was modeled using the CASMO5 [27] and SIMULATE5 [28] codes using standard neutron-physics methods and recommended simulation options by the code supplier Studsvik. The computation scheme overview is similar to the one introduced in Part Two for HCSMR cores. First multi-parameters cross sections are generated with CASMO5. The fuel assembly is computed as an infinite medium. The cross sections generated are then used for core simulation performed with SIMULATE5. Core simulations are repeated for eight successive cycles using the identical fuel management and reload scheme to obtain an equilibrium cycle.

The relevant outcomes for benchmark with the HCSMR core are summarized in Table 1.1. With a batch fuel management the SMR600 core reaches a cycle length of over 900 equivalent full power days (EFPD). A "1/2" fuel management enables the attainment of over 600 EFPD. The detailed core characteristics and performances are shown in Annex C.

The cycle lengths observed are in line with the performances of mPower, Westinghouse SMR and Flexblue designs (see Annex B). With a batch fuel management it is possible to achieve cycle lengths of over two years. The associated conversion factor of 0.63 is relatively high. The conversion factor is the ratio between the fissile material mass at the end of irradiation and the fissile material mass at the beginning of irradiation. The concept and mathematical definition are introduced in the next chapter §3. 4. The rather high conversion factor observed is mainly due to the low fuel burnup. The core average burnup at EOC of the SMR600 "batch core" reaches 29 MWd/kgHM only (see Annex C).

Parameter	SMR600 Batch	SMR600 1/2 Fuel Management
Cycle length (EFPD)	924	633
Conversion Factor[1]	0.63	0.48
Core Average Burnup EOC (MWd/kgHM)	29	30

Table 1.1: SMR600 Core Selected Performances

[1]cf §Part One3. 4. 1 for definition.

The SMR600 "1/2 fuel management core" makes is possible to achieve a fuel cycle of almost two years with a conversion factor of 0.48. The fuel discharge burnup is above 41 MWd/kgHM and characterizes an increased fuel utilization compared to the SMR600 "batch core" as expected.

The loading patterns, fuel designs and core characteristics are based on the mPower and Westinghouse SMR and on own trade-off using engineering judgement. The gadolinium enrichment and poisoned fuel rods position are kept similar for all fuel assemblies.

SMR600 is anticipated to operate soluble-boron free. Operating a nuclear core without soluble boron in the primary coolant brings benefits [32]. It enables the removal of the associated system costs and corrosion maintenance needs. It reduces the liquid radioactive waste and doses for on-site staff. It also prevents the scenario of a boron dilution transient and associated safety analysis and measures.

Moreover, reactivity coefficients are impacted by the boron concentration. In particular for core aiming at long cycle length, the excess reactivity at BOC to be compensated is high. If soluble boron is used, its high concentration can lead to a positive moderator coefficient. This aspect is further detailed in §2. 4. The use of boron is also controversial from an environmental perspective, in particular in Europe where the European Chemicals Agency (ECHA) acted in 2010 to include boric acid on a Candidate List of "substances of very high concern", thus targeting borates for eventual classification under the European Union REACH legislation (Registration, Evaluation, Authorization and Restriction of Chemicals). This could lead to additional licensing requirements for soluble boron use in NPP across Europe [33].

As shown in [34] and [35] an iPWR core design without soluble boron requires a detailed optimization of the peak power and linear heat generation. It is not realized for the SMR600 core design. However, the results obtained are relevant as order of magnitude for cycle length and conversion factor. With soluble boron in core the local maximum linear heat generation remains below 475 W/cm[1] for both core designs over the entire cycle length.

The conversion ratio of a standard iPWR SMR ranges hence between 0.45 and 0.65 and is in line with conversion ratio observed for large PWRs. Nevertheless, the fuel utilization is not as optimal as in large PWRs due to the fuel management strategies implemented and low discharge burnup. This aspect is further detailed in the next chapter.

2. 4 PWR SMR CORE AND FUEL

This section focuses on core and fuel specificities of PWR SMRs compared to large reactors. The nine PWR SMRs introduced in §2. 3 are considered. Although several similarities exist between large PWRs and SMRs based on PWR technology, it is relevant to look at the SMR specificities with regards to core and fuel design to support the HCSMR core optimization.

[1] 475 W/cm is an arbitrary value defined based on current German – Konvoi – PWR licensed limits.

2. 4. 1 Fuel Assemblies

Fuel assemblies in PWR SMR are similar to large PWRs fuel. Compared to large core, the number of FA in SMRs is reduced. It varies from one-fifth to half of the fuel assemblies loaded in a large PWR. The ABV and RITM-200 designs are exceptions with around 200 fuel assemblies in core. This makes it possible to reach a very long cycle length (7 to 10 years, details in Annex B).

Standard 17 x 17 fuel assemblies with reduced height are foreseen for six of the nine SMR designs considered. The remaining three designs, the CAREM-25 and Russian SMR designs ABV and RITM-200 use hexagonal fuel. Both fuel types are made of standard UO_2 fuel rods with Zircaloy based fuel rod cladding. The choice of standard fuel enables the reduction of licensing cost and speeds-up the technology readiness and future deployment of those designs.

Reduced height refers to the fuel active zone length. It ranges between 90 cm and 240 cm for the nine SMR designs reviewed. In comparison, the fuel active length in large PWRs ranges between 370 cm and 430 cm. The reduced core power of SMRs motivates the reduction of the active length. It also results from further considerations, for example the thermal-hydraulic boundary conditions contributing significantly to set the core axial size. The need to obtain natural circulation of the core coolant in some designs is a key driver.

The average linear power in PWR SMRs is reduced compared to large PWRs. Table 1.2 and Table 1.3 give an overview of SMR design average linear power compared to typical large reactor designs.

		PWR	BWR	SMR600	SFR
Core power	MW	1400	1200	600	1500
Average linear power	W/cm	180	200	149	255

Table 1.2: Overview of NPP Average Power

		CAREM	ACP100	Flexblue	SMART	ABV
Core power	MW	100	310	530	330	38
Average linear power	W/cm	108	96	121	110	47

		RITM-200	mPower	NuScale	W-SMR
Core power	MW	175	530	160	800
Average linear power	W/cm	Not available	121	90	142

Table 1.3: Overview of Selected SMR Average Power[1]

The reduced size of the core impacts the neutron leakage rate: neutron leakage increases in small core compared to large reactors. This has a negative influence on small cores' performances since, compared to large cores, a larger proportion of neutrons are escaping the core and hence are not used to fission the fuel. This influences the fuel management strategy.

[1] Derived from open-source information [3] [4] [6] [9] [12].

2. 4. 2 Fuel management

In-Core Fuel Management (ICFM) defines the fuel management strategy. It is mainly influenced by:

- the cycle length;
- the fuel type;
- the core loading pattern design;
- the operating flexibility;
- the reactivity management strategy;
- and the neutron dose to the core's surrounding structure.

ICFM is an iterative process that aims at reaching an optimum between the above mentioned aspects, the safety requirements and the economics of the selected ICFM. It results from a trade-off between those criteria.

An introduction to the ICFM definition process can be found in the literature [30] [36]. Large reactor standard ICFMs are based on 12 to 18 month cycles with 1/5 to 1/3 of the core fuel assemblies replaced at each refueling outage, using a fuel enriched ranging from 3.5 to 4.95 % ^{235}U. This ICFM is obtained after several cycles operated with the same ICFM strategy and referred to as an equilibrium cycle. The fresh fuel assemblies should bring enough reactivity for not only the first cycle they are irradiated but for their entire lifetime. This leads to the fuel enrichment definition.

Compared to large reactors, SMR ICFM specificities are mainly driven by three aspects: the reduced size of the core, the willingness to operate long fuel cycle – longer than 24 months – and for some designs to operate without soluble boron in core.

As a consequence, fuel assemblies in SMR are often replaced and have high ^{235}U enrichment compared to large cores. Among the nine SMR designs considered most of them have a one-through fuel management with all fuel assemblies replaced at each refueling outage as summarized in Annex B. This enables, together with high ^{235}U enrichment the loading of substantial excess reactivity in each cycle.

This reactivity excess must be compensated. It is done with soluble boron introduced into the primary coolant and/or with the use of burnable absorbers. Those absorbers – gadolinium, boron, IFBA – are consumed along the cycle by capturing neutrons. Their introduction is particularly important in SMRs using one-through ICFM, since the fresh fuel loaded leads to a distinctive chopped cosine power distribution. In large core the partially burned fuel assemblies compensate this aspect as they have a flatter axial power distribution. Moreover in SMRs operating without soluble boron the use of burnable absorbers is a must. Their introduction is linked to the fuel design and results from an iterative process with the control rods location and level of insertion strategy. Among the designs reviewed all have burnable absorbers as part of their ICFM strategy.

SMR once-through ICFM strategies lead to a lower discharge fuel burnup compared to large reactors. The absence of fuel shuffling reduces the chance of reaching high burnup. Fuel

assemblies are usually expected to be finally discharged after a burnup close to 40 MWd/kgHM. This is lower than the 60-65 MWd/kgHM burnup achieved in large PWRs and influences the fuel costs of SMR design.

2. 4. 3 Safety Criteria

2. 4. 3. 1 Reactivity Feedback

The combined reactivity feedback of an increasing core power should remain negative at all times [38]. In practice it means the reactivity temperature coefficient, referring to the change in reactivity measured in pcm per degree, should be negative. In PWRs the two major reactivity coefficients contributing to the combined temperature coefficient are the moderator and fuel temperature coefficients.

The moderator temperature rises with increasing power and fuel temperature leading to a decreased moderator density and neutrons moderation. This process stabilizes the core power and is known as a negative moderator temperature. The presence of soluble boron in the coolant is contributing, however to increasing the moderator temperature coefficient. The decreased density with rising temperature also leads to limiting the boron density in the coolant and its role in capturing neutrons.

The fuel temperature feedback acts immediately with the power increases. With increasing fuel temperature the absorption of neutrons, also known as Doppler broadening, rises as well. This limits the reactivity increase and depends on the fuel characteristics. A standard PWR fuel with low enriched ^{235}U isotopes has a negative fuel temperature coefficient. With highly enriched uranium fuel or plutonium the fuel temperature coefficient is less negative.

PWR SMR reactivity feedbacks are hence similar to large PWRs. The main difference is a consequence of the high reactivity excess at BOC to enable long cycle length. If compensated with soluble boron only, it is likely to obtain a positive moderator coefficient. It is therefore recommended to limit the initial excess reactivity by introducing burnable absorbers and ideally even remove the use of soluble boron in PWR SMRs.

2. 4. 3. 2 Shutdown margin

The capability to shut down the reactor at any time and ensure sub-criticality must be ensured during normal operation, in case of anticipated operational occurrences including stuck rods events, and in case of abnormal situations such as CRDM ejection or rapid removal.

For PWR SMRs operated with soluble boron, the boron concentration in the primary coolant can be increased to decrease the core's reactivity in addition to the use of control rods. The designs operated without soluble boron can only use control rods for this purpose, often leading to an increase in the proportion of CRDM to the number of fuel assemblies in core in SMRs. For example the mPower design has CRDM above all fuel assemblies.

For designs operating without soluble boron, control rods must also ensure sub-criticality in cold and hot zero power situations. Last but not least, control rod systems must enable reactivity control during power maneuvers in case of load-follow operations or to compensate Xenon effects.

2. 4. 3. 3 Fuel Burnup

PWR fuel is designed and licensed to reach a certain burnup. The fuel must remain below the licensed maximum burnup during operation. Typical fuel assembly average burnup licensed in large PWRs are close to 60 MWD/kgHM. Those limits are unlikely to be reached in SMR designs as explained before. However the smaller cores and flux shapes in SMRs, in particular operated without soluble boron, tend to create higher peaking factor. Since burnup limits also apply to fuel rod and peak pellet burnup, designers must ensure those limits will not be reached, which sometimes requires the development of appropriate simulation tools for this purpose.

2. 4. 4 Operability

Nuclear core designers aim at maximizing the total core power output while minimizing power peaking factors to respect the maximum linear power density defining most operating limits. Beyond the reduced core power in SMRs compared to large reactors, the average linear heat rate is also reduced compared to large reactors as shown in Table 1.3. This designer's choice enables more margins for higher peaking factor, often required due to the ICFM strategy adopted. Indeed the absence of soluble boron and the ambition to operate long fuel cycles could lead to substantial local increase in the power density due to needed control rods insertion.

This is particularly relevant when considering load follow operation with small cores. The feasibility and associated strategies require specific core design developments. On the other hand the small size of SMR core limits Xenon instabilities observed in large core and limit the need for associated mitigation strategies.

The capacity to vary the power and operate in load-follow mode is also constrained by the thermal-hydraulic requirements. In particular for design based on natural circulation for the primary coolant, an issue of coolant stability exists for power transient situations.

The aspects mentioned above describe the specificities of small cores with regards to core and fuel. Those specificities will be considered for the HCSMR core design. Before explaining how in Chapter 4 the next chapter, Chapter 3, introduces the particularities of high conversion cores, their benefits and challenges.

Chapter 3: HIGH CONVERSION CORES

3. 1 MOTIVATION

For more than 50 years LWR have been successfully operated worldwide. Although LWRs benefit from a large positive experience, their conversion factor could be improved: barely only 1 % of the natural uranium required for their fuel is efficiently used and their associated conversion factor – ratio of fuel fissile material quantity at end of irradiation compared to beginning of irradiation – ranges between 0.4 to 0.6 [39] [40].

Nuclear reactors with a fast neutron spectrum, also called fast reactors, such as the ASTRID demonstrator designed at CEA, would enable a conversion factor close to 1.0 [41]. Fast reactors could even have a conversion factor greater than 1.0 and breed fissile material. Such designs produce more fissile isotopes than they consume [42]. Fast reactors are one of the best candidates to close the nuclear fuel cycle and increase nuclear energy sustainability [43]. However due to their complexity and relatively high costs, fast reactors are not developed yet at an industrial scale [42] [44].

It is achievable to increase LWRs conversion factor, which would make them more sustainable and give them the benefit of improved economics. Several concepts of high conversion light water reactors (HCLWR) were studied [40]. Most of them are using a reduced moderation ratio ($\mathrm{MR} = \frac{\mathrm{moderator}_{\mathrm{volume}}}{\mathrm{fuel}_{\mathrm{volume}}}$) – ratio of moderator to fuel volume – which enables the increase of their conversion factor above 0.8. High conversion reactors could ensure a transition towards future nuclear fuel cycles [44], in particular closing the gap between the current fleet of LWRs and future fast reactors' development [45]. This would limit the degradation of plutonium isotopes [46] and provide a dynamic storage of fissile materials [47] compared to current plutonium use in LWRs.

The renewed interest in SMRs offers an additional motivation to develop high conversion cores. Compared to large LWRs, SMRs often have less effective fuel utilization. As explained in §2. 2 the fuel utilization in SMRs can be further optimized [3]. The long fuel cycle, its associated fuel management, the high neutron leakage rate and the low core power density are the main drivers supporting the non-optimal fuel utilization in SMRs. To generate a given energy, an iPWR would require much more fresh fuel than a large PWR. Hence SMRs have a higher natural uranium consumption compared to large PWRs. Moreover iPWR conversion factors are close to 0.6. Increasing the conversion factor of SMRs would enable to reduce their fuel costs and limit natural uranium consumption.

3. 1. 1 LWR natural uranium consumption

It is important to mention some order of magnitude related to uranium consumption in LWRs. The reasoning hereafter contains some simplifications and approximations but enables obtaining a relevant idea of uranium consumption in various LWR designs.

Natural uranium contains 0.72 % ^{235}U, 99.28 % ^{238}U and traces of ^{234}U. To generate 1 GWe over one year in a PWR with an efficiency of 34 % the core must generate 25.8 TWh or $9.27\ 10^{16}$ Joules. The fission of one heavy isotope such as ^{235}U generates around 200 MeV or $3.20\ 10^{-11}$ Joules. To generate 25.8 TWh $\frac{9.27\ 10^{16}}{3.20\ 10^{-11}} = 2.90\ 10^{27}$ nucleus must be fissioned to generate the required energy. Considering fission comes from ^{235}U atoms only with an atomic mass of 235 u, 1132 kg of ^{235}U must be fissioned over the year. If all ^{235}U isotopes contained in natural uranium would be fissioned $\frac{1132}{0.0072} = 157.2$ tons[1] of natural uranium would be required to generate the 25.8 TWh.

It is however not possible to directly fission all the ^{235}U contained in natural uranium. First, a PWR loaded with natural uranium would not become critical, largely due to the neutron capture by water. With their thermal neutron spectrum, PWRs require the fission of isotopes which have large cross-sections[2] in thermal energies, such as ^{235}U. Natural uranium is hence enriched in ^{235}U isotopes and the enrichment tails also contains ^{235}U, currently at about 0.25% ^{235}U. In current PWRs the natural uranium is usually enriched between 3 % and 4.95 % ^{235}U depending on the fuel management options. The ^{235}U isotopes contained in enrichment tails are "wasted"[3].

Secondly the irradiation in PWRs does not enable the fission of all ^{235}U isotopes loaded. At the end of irradiation the fuel still contains between 0.5 % and 1.0 % ^{235}U isotopes[4]. Moreover a non-negligible share of ^{235}U becomes ^{236}U by sterile neutron capture, reducing the ^{235}U fission potential. Overall less than half of the ^{235}U isotopes originally contained in natural uranium are used to fission and generate energy in standard PWRs.

Luckily two main additional physical effects improve natural uranium utilization, defined as the ratio of heavy metal mass burned by fission to the total uranium mass used for making the fuel. First, not only ^{235}U isotopes contribute to fission and power generation: ^{238}U isotopes can be split via fast neutron fission. This accounts for about 7% of overall fission in a PWR. On the other hand, ^{239}Pu is formed during irradiation via neutron capture on ^{238}U. ^{239}Pu has a rather high fission cross section in thermal energies and contributes to 30 % to 40 % of the total fissions observed in PWRs.

Eventually ^{238}U and ^{239}Pu fissions enable the recovery of 80% to 90% of ^{235}U isotopes fission potential [48]. With only 0.72 % ^{235}U in natural uranium, the averaged natural uranium utilization is close to 1 %. BWRs have a slightly improved utilization of natural uranium, thanks to their harder neutron spectrum.

However, iPWR SMRs have a rather low natural uranium (Unat) utilization due to their specific fuel management strategies. To illustrate this reasoning the Unat consumption for large PWRs

[1] Metric tons: 1000 kg.
[2] Cross-sections quantify here the isotopes fission capability with neutrons.
[3] Also referred as *depleted uranium*, enrichment tails can be reused via fuel reprocessing or to manufacture byproducts.
[4] With fuel reprocessing those isotopes can be recovered and further utilize in nuclear fuel.

and for iPWR SMRs designs are derived hereafter. The specific Unat consumption is normalized per energy quantity generated. Unat refers to natural uranium, i.e. uranium ore from mines.

3. 1. 1. 1 Standard PWR Unat Consumption

To illustrate a standard PWR natural uranium consumption, a 1400 MWe PWR pre-Konvoi reactor type is considered. Such design has the general characteristics introduced in Table 1.4 [36] [49]. The fuel management is a yearly (340 EFPD) cycle requiring the replacement of 1/4th of the core every year, hence 48 FA.

The associated natural uranium need is 204 tons Unat per annum. Considering a 100% load factor[1] over the cycle length, the Unat consumption per TWh can be derived: 18 tUnat/TWhe or 6 tUnat/TWhth. Some other PWR types are slightly less efficient than pre-konvoi design with up to 22 tUnat/TWhe required [36]. Considering close to 1% of the irradiated fuel is made of plutonium isotopes [37], a 1400 MWe PWR generates with an early fuel management about 22 kg plutonium.

Parameter	Unit	1400 MWe PWR
Thermal Power	MW	3900
Electrical Power	MW	1400
Pressure	bar	158
Number of Fuel Assemblies		193
^{235}U fuel enrichment	%	3.95
Fuel type		16 x 16
Fuel active height	cm	390
FA heavy metal mass	kg	540

Table 1.4: 1400 MWe PWR Pre-Konvoi Main Characteristics

With the yearly fuel management and the associated equilibrium cycle, the fuel assembly discharge average burnup reaches 55 MWd/kgHM. This shows a rather good fuel utilization.

3. 1. 1. 2 PWR SMR Unat Consumption

The SMR600 design performances introduced in §2. 3. 11 are considered to derive the Unat consumption of an iPWR design. Two fuel management strategies are proposed: a batch fuel management and a "1/2" fuel management. The corresponding cycle lengths are 924 EFPD and 633 EPFD requiring respectively 69 and 33 fresh fuel assemblies to be loaded for each cycle. The UO_2 enrichment is 4.95 %. Accordingly the Unat consumption is 192 tons per cycle for a batch fuel management and 92 tones with the "1/2" fuel management. Normalized to the power

[1] The load factor is the ratio for a given period between the actual generated energy and the theoretical maximum generated energy. A 100% load factor over a cycle is not realistic. Due to operational requirements the load factors observed are in general between 95% and 99%. The 100% assumption is however here valid for the purpose of this study as long as it is kept similar for other benchmark cases.

generated the SMR600 requires 43 tUnat/TWhe with a batch fuel management and 30 tUnat/TWhe when half of the core is reloaded at each cycle.

An increased Unat consumption is observed for iPWRs compared to large PWRs. Mainly the fuel management type explains the differences observed. Moreover the discharge burnup in iPWR cores remains low compared to large PWRs. Beyond fuel management, the size of the core influences uranium consumption: with a smaller core the neutron economy is decreased compared to a large core due to neutron leakage.

The Unat consumption derived here quantifies the tons of uranium actually required to generate a designated energy quantity. It differs from Unat utilization. To assess Unat utilization the composition of the fuel after irradiation must also be considered.

3. 1. 2 Natural uranium utilization and conversion factor

With a conversation factor equal to one, natural uranium can be utilized close to 100%. A conversion factor above one leads to regeneration: more fissile material is generated than consumed in a given irradiation period. PWRs with conversion factors between 0.4 and 0.6 lead to a uranium utilization rate close to 1 % as introduced in previously.

This enables to introduce Figure 1.3 showing the influence of conversion factor on natural uranium utilization rate, proportional to the term $\frac{0.95}{1-C}$ with C the ratio of fissile isotopes generation rate to the fissile absorption rate.

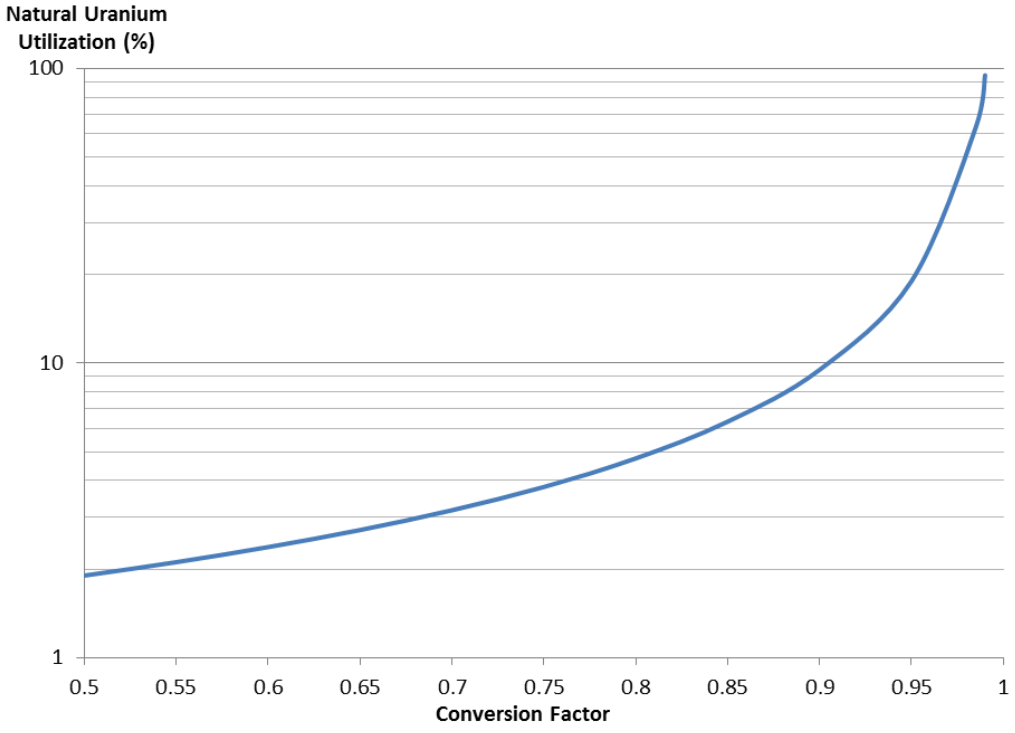

Figure 1.3: Natural Uranium Utilization Rate vs. Conversion Factor

Figure 1.3 assumes the series $1 + c + c^2 + \cdots + c^n$ corresponding to $\frac{1}{1+c}$ quantifying the uranium utilization. In reality all uranium isotopes cannot be burnt. Due to the reprocessing process efficiency, utilizing 100% of natural uranium is only feasible on theory. The decay of ^{241}Pu isotopes out of pile is the main contributor to the limited efficiency. A penalty 5 % is applied (expert judgement) giving $0.95 * (1 + c + c^2 + \cdots + c^n) = \frac{0.95}{1+c}$.

For reactors with a conversation factor greater than one, design options must be implemented to prevent nuclear material proliferation. Such options can include the addition of specific isotopes in the fuel to prevent the generation of plutonium material with a high fissile grade easily recoverable. A detailed analysis of the HCSMR features to prevent material non-proliferation is not performed in this work. Hence an upper limit of one for the conversation ratio is set. With conversion factors between 0.8 and 1.0, natural uranium utilization increases from about 5 to almost 100 %. Improving the conversion factor is hence the relevant parameter to increase fuel utilization and reduce natural uranium consumption.

3. 2 URANIUM RESOURCES & NUCLEAR FUEL CYCLE

Natural uranium resources are limited. The current outlook is encouraging in regards to the availability of uranium to address demand in the coming decades [50]. Hence uranium prices are currently low and uranium and fuel costs of a NPP are not of specific concern. However this might evolve over the years since the long term availability of uranium will depend on the nuclear fleet growth. Tensions on uranium resources could emerge leading to a reinforced interest in developing more efficient nuclear systems with regard to uranium consumption. Moreover increasing the fuel utilization would improve the sustainability of nuclear power and its fuel cycle. Reducing natural uranium consumption is hence a motivation to develop high conversion LWRs.

Two main types of nuclear fuel cycles are currently operated worldwide [51]. In a once-through fuel cycle the fuel is directly disposed after irradiation in a reactor. This is the most common approach. It is implemented in the USA or in Sweden for example.

The closed fuel cycle is a second approach. It aims at recycling the fuel already irradiated to benefit from the remaining energy available in nuclear fuel after irradiation. Following commercial irradiation a spent fuel assembly contains 94 % uranium, 5 % fission products and 1 % plutonium [52]. Both uranium and plutonium isotopes have the potential to be reused for further energy production. A closed fuel cycle using fuel reprocessing is operated in France and Japan. It was also used in Germany until 2005. Both approaches are introduced in Figure 1.4.

The closed fuel cycle enables the recovery of plutonium isotopes via reprocessing. Mixed with depleted uranium – a byproduct of uranium enrichment – plutonium forms the Mixed-Oxide fuel (MOX). Using MOX fuel increases the natural uranium utilization and hence decreases uranium needs for a given energy generated.

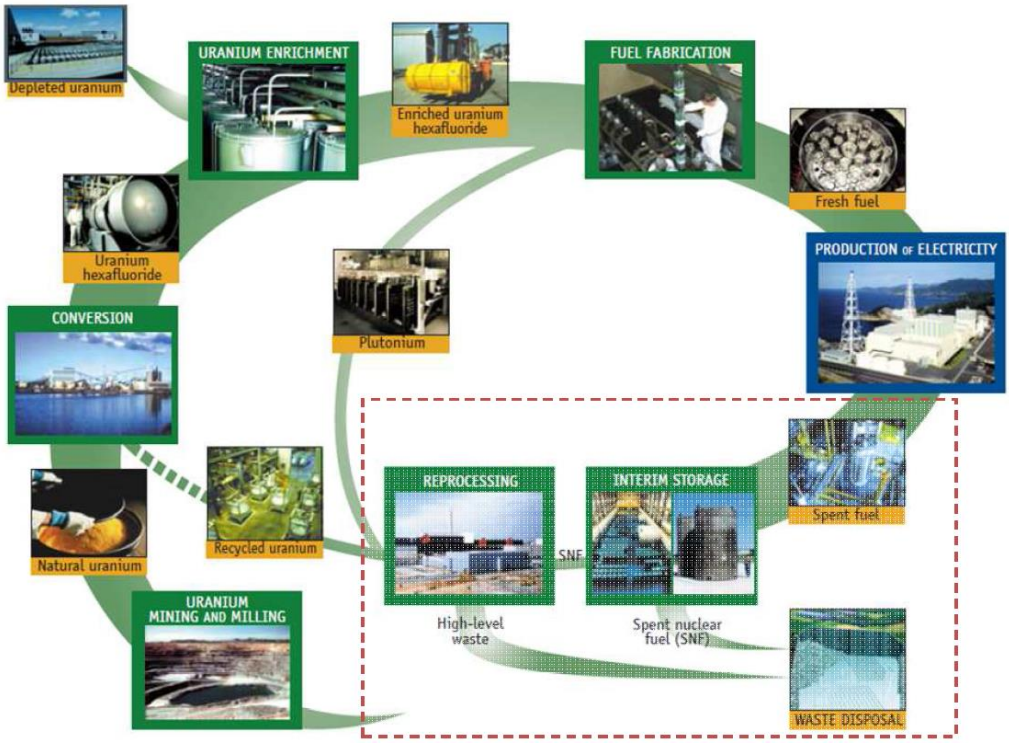

Figure 1.4: Schematic View of the Fuel Cycle with Reprocessing and Recycling from [51]

Some countries such as Japan, Germany or France are using MOX fuel in their conventional LWRs. This permits the further irradiation of the plutonium recovered by fuel reprocessing and hence improves the sustainability of nuclear power. However irradiating MOX fuel in LWRs is not optimum for fuel economy. The thermal neutron spectrum observed in standard LWRs degrades the plutonium vector fissile quality: at the end of irradiation the MOX plutonium contains in proportion substantially less ^{239}Pu and ^{241}Pu isotopes than at the beginning of irradiation. Moreover MOX fuel irradiated in thermal neutron spectrum generates large minor actinides quantities. It further decreases the MOX fuel reactivity and increases challenges for final fuel disposal. Such MOX fuel is currently not reprocessed further as the energy to recover is relatively low if used in LWR[1].

On the contrary a high conversion core using a reduced moderation ratio and hardened spectrum supports a better conservation of the MOX fuel fissile capability. This opens a path towards MOX fuel multiple recycling. When MOX fuel is loaded in an under moderated core the neutron spectrum is hardened further compared to an enriched uranium core. This improves the conversion factor further. To benefit from high conversion cores, fuel reprocessing is hence required [53] and used for this study.

It must be remarked that high conversion cores also require MOX fuel with a rather high content of plutonium. With only low enriched uranium fuel or MOX with less than 10% plutonium

[1] It contains however enough energy reserve via fertile isotopes enabling a further irradiation in fast reactors.

content criticality of the core is difficult to reach in an under-moderated core due to the epithermal neutron spectrum. This is further detailed in §3. 4.

The plutonium required to produce MOX fuel can also come from stockpile from previous reprocessing or military graded plutonium [54]. Irradiating such plutonium isotopes in under-moderated LWRs would preserve the material's energy potential. Moreover this would prevent the natural degradation of the plutonium fissile quality owing to the radioactive decay.

Switching to thorium fuel is also an option to limit natural uranium use. Combined with plutonium or enriched uranium material, irradiating ^{232}Th isotopes in under-moderated lattice is well suited. Several works on associated core design and fuel cycle options assessment were already performed as mentioned in the next section.

3. 3 PREVIOUS WORK

Research and development on high-conversion cores started in the 70's [40]. At first under-moderated lattices were studied. Large R&D programs aimed at developing and validating reactor physics computational tools were set-up [55].

In France experiments to study the neutron-physics behavior of under-moderated lattices were conducted on various research reactors EOLE (ERASME experiment), MELUSINE (ICARE experiment), MINERVE (MORGANE experiment) [56] [57]. The results obtained supported the development and qualification of APOLLO2 neutron-physic code. At the industrial scale the CEA, together with EDF and FRAMATONE, studied various under-moderated core designs between 1984 and 1991 [58] [59].

Professor Edlund [61] [62] worked in the USA, together with BABCOK, to design a 1000 MWe commercial under-moderated PWR in the 70's and 80's [63]. Preliminary studies and research work took place, including studies conducted on the Shippingport reactor [63]. In the same period, studies on under-moderated cores were carried out in Germany [64] [65] [66], and Israel [67].

The designs studied in the 20th century did not lead to commercial developments. In the year 2000's a renewed interest for under-moderated cores is observed. Japan [68] [69] [70], the USA [71] [72] and Israel [73] are working on advanced concepts of HCLWR.

In France [74] [75] [48] large HCPWRs' design were evaluated. The performances reached would enable to operate one year cycle for a 4250 MWt core with a conversion factor above 0.9 and a void coefficient close to 0 pcm.

Recent works emphasize the advantage of developing under-moderated core with a uranium-thorium fuel cycle and not only a uranium-plutonium fuel cycle [39] [77] [78]. Moreover the studies on the IRIS OPEN core rated at 1650 MWth [78] in the USA must be mentioned. It is an upgraded under-moderated version of the IRIS SMR.

Most of the under-moderated cores designed over the last 50 years have in common a high degree of heterogeneity. Neutron absorbers materials are often introduced within the core to

limit the void coefficient. Both axial and radial layers of fertile material are used. As a consequence an accurate simulation of such core design is challenging. Moreover the production of the designed fuel assemblies will have a higher complexity and associated costs. Last but not least the operation and control of heterogeneous core design would require specific considerations. The reviewed under-moderated designs have conversion factors above 0.8.

3. 4 REACTOR PHYSICS OF UNDER-MODERATED CORE

3. 4. 1 Principle

In an under-moderated core, high conversion rates are mainly obtained by a reduction of the moderation ratio (MR).

$$MR = \frac{Moderator\ Volume}{Fuel\ Volume} = \frac{V_{Cell} - V_{Rod}}{V_{Fuel}} \quad (1.3) \text{ with } V_{Rod} = V_{Fuel} + V_{Clad} + V_{Gap} \ (1.4)$$

With reduced moderation ratio, the neutron spectrum is hardened. This enables a better conversion of ^{238}U in ^{239}Pu as well as less production of minor actinides during irradiation. The appearance of ^{239}Pu isotopes compared to their disappearance is increased. Plutonium comes from neutron absorption on ^{238}U via the following path:

$$^{238}U \xrightarrow{(n,\gamma)} {}^{239}U \xrightarrow[T_{1/2} = 23.5\ min]{\beta^-} {}^{239}Np \xrightarrow[T_{1/2} = 2.3\ d]{\beta^-} {}^{239}Pu$$

^{239}Pu is fissile and decays with a period of 24 000 years. ^{239}Pu can also capture neutrons and becomes ^{238}Pu, ^{240}Pu, ^{241}Pu or ^{242}Pu via γ decay or neutrons emissions (n, 2n reactions) as:

$$^{238}Pu \xleftarrow{(n,\ 2n)} {}^{239}Pu \xrightarrow{(n,\gamma)} {}^{240}Pu \xrightarrow{(n,\gamma)} {}^{241}Pu \xrightarrow{(n,\gamma)} {}^{242}Pu$$

The paths presented above are simplified ones showing the direct links of the different isotopes' creation. To find a full chart of the plutonium isotopes' paths one can look at [79] and [80].

A reduced moderation ratio (MR) can be obtained by reducing the pitch between fuel rods (FR). This hardens the neutron-spectrum and hence improves the conversion factor. Using MOX fuel in under-moderated fuel assembly (FA) increases further the LWR conversion factor. This could however lead to a positive void coefficient in case of loss of coolant. To prevent this, small cores – which have a rather high neutron leakage – present advantages compared to large cores.

Loading MOX fuel containing high plutonium mass is also required for under –moderated cores to reach criticality. With MOX fuel containing less than 10% plutonium[1] the reactivity drops as the MR is decreased, as introduced in Figure 1.5. The reactivity values shown in Figure 1.5 are based on APOLLO2[2] computation of fuel assembly in infinite medium. Similar behavior is observed with low enriched uranium fuel. Hence MOX fuel containing at least 10% plutonium is considered for under-moderated cores as in the HCSMR design.

[1] With plutonium vector containing 56 % fissile isotopes as is introduced in Table 1.9.
[2] The APOLLO2 tool is introduced in §8. 2.

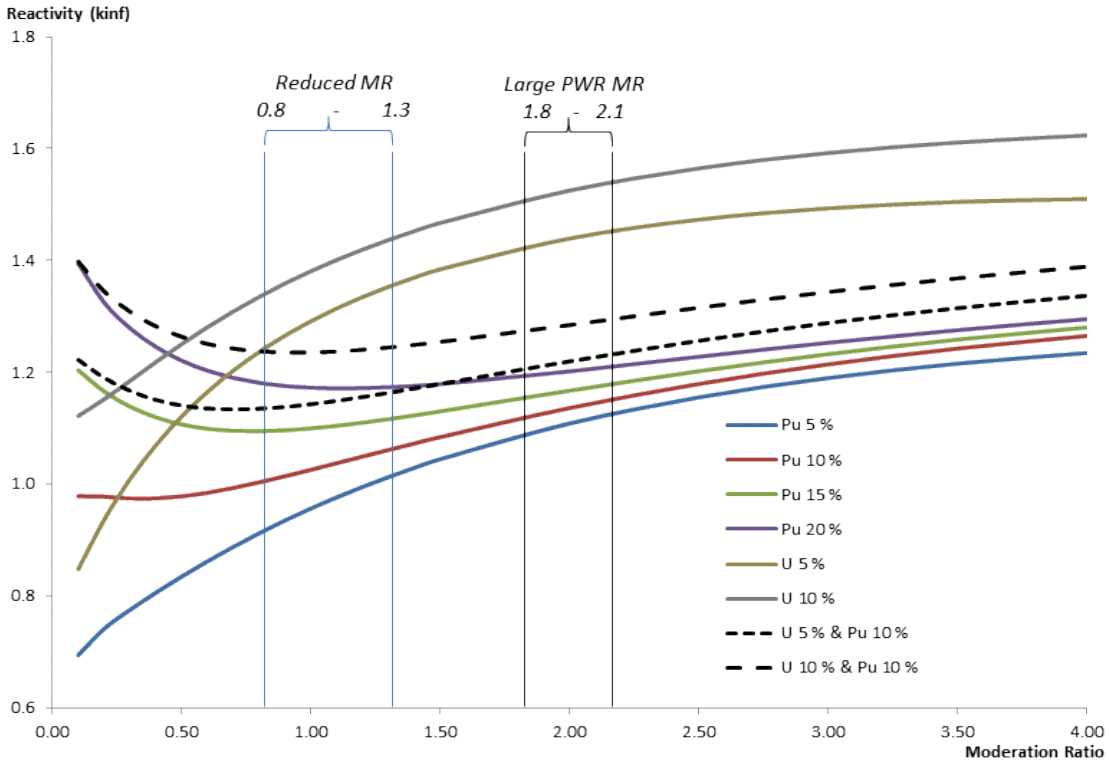

Figure 1.5: Reactivity vs. Moderation Ratio

The conversion rate (CR) is the ratio between fissile isotopes' appearance and disappearance, for a given burnup:

$$CR = \frac{\sum_{Fertile\ nucleus} C_k}{\sum_{Fissile\ nucleus} A_k} = \frac{Fertile\ Capture}{Fissile\ Consumption} \quad (1.5)$$

With A and C respectively the absorption and capture reaction rates for the various isotopes. The conversion rate is an instantaneous information since it depends on the neutron flux. It is illustrated by the absorption rate definition: $A \approx C + F$ with F as the fission rate.

To obtain integral information the conversion factor (CF) is often used. It is expressed via isotopes masses:

$$CF = \int^t CR = \frac{fissile\ mass_{final}}{fissile\ mass_{initial}} \quad (1.6)$$

with t as the irradiation period. The fissile isotopes considered are ^{235}U, ^{239}Pu, ^{241}Pu.

The conversion factor CF is mostly influenced by three parameters:

- The core moderation ratio
- The irradiation period or burnup
- The fuel type; plutonium share and isotopic vector for MOX fuel.

The fuel geometry is often used to vary the core moderation ratio. By modifying the fuel rod pitch, the moderation ratio is influenced. In addition, material densities can be adapted to

modify the moderation ratio. For example a change in the core thermal-hydraulic operating point (moderator pressure, temperature) would influence the moderation ratio.

3. 4. 2 Neutron spectrum

Two aspects are hardening the neutron spectrum in a high-conversion core compared to a standard LWR neutron spectrum. First, the moderation ratio (MR) is reduced. Instead of being around 2.0 in LWRs, e.g. in the EPR design [81], the moderation ratio varies between 0.8 and 1.2 [83]. Consequently, the possibilities for neutrons to be slow-down are reduced and fewer neutrons are reaching the thermal energies in under-moderated cores, compared to standard LWRs. The proportion of neutrons being captured by the large thermal resonances is increased.

The second aspect influencing the neutron spectrum is the type of fuel used. The plutonium isotopes of the MOX fuel have large resonances in the thermal energies. The Table 1.5 shows the main absorption resonances in thermal energies. This increases the neutron capture in the thermal energies. As a result the neutron spectrum is switched towards high energies as plotted in Figure 1.6 obtained with APOLLO2 computations.

Isotope	E (eV)	σ_a (barns)
^{239}Pu	0.3	5450
^{240}Pu	1.1	119650
^{241}Pu	0.3	2410
^{242}Pu	2.7	32192

Table 1.5: Plutonium Isotopes Main Resonances

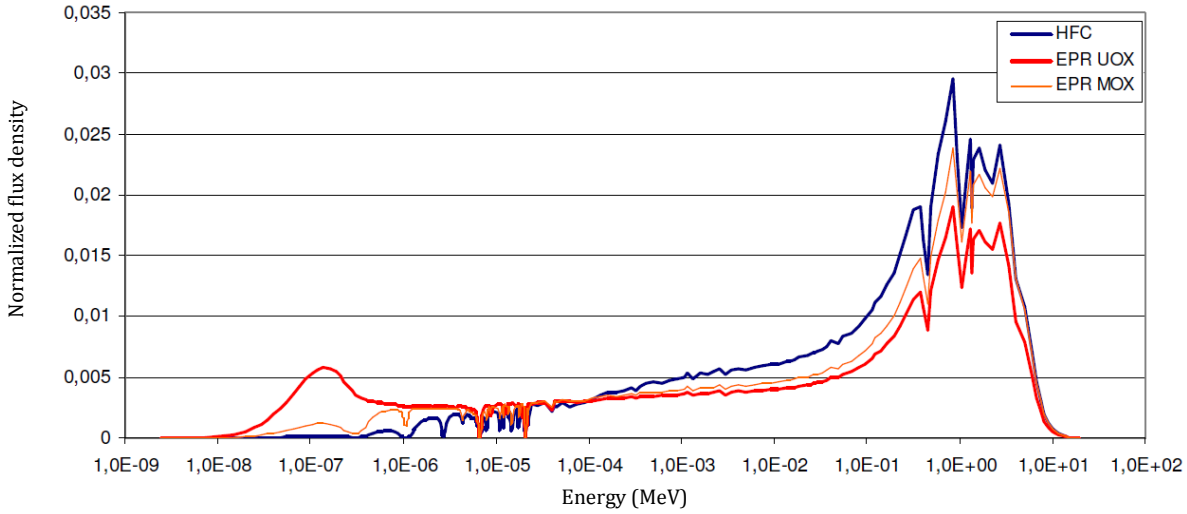

Figure 1.6: Neutron Spectrum of an EPR UOX Core, an EPR MOX Core and a High-Conversion Core

For a given moderation ratio the MOX and plutonium isotopes also limit the reactivity compared to enriched uranium fuel. It is hence required to select MOX fuel with a high content of plutonium as introduced in Figure 1.5. In return, this leads to the void coefficient issue as explained in §3. 4. 4.

3. 4. 3 Reaction rate

In under-moderated design the ratio of neutron capture over fission is modified compared to standard PWRs in particular $\frac{\sum_c {}^{238}U}{\sum_a {}^{239}Pu}$. As the neutron flux is hardened the neutron fission cross section of ^{239}Pu decreases substantially above 4 eV. In parallel ^{238}U capture is increased. Hence the production of ^{239}Pu by neutron capture on ^{238}U is increased. Table 1.6 introduces the reaction rates for ^{238}U by energy groups. More than half of the reactions occur in the epithermal energy domain.

Group	1	2	3	4	5	6	7	8
E sup (MeV)	19.6	4.94 10^{-01}	1.95 10^{-01}	1.91 10^{-03}	4.00 10^{-06}	1.25 10^{-06}	6.25 10^{-07}	1.38 10^{-07}
^{238}U	7.3	5.0	4.9	51.9	6.7	7.4	11.1	5.8

Table 1.6: Energy Group Weighted ^{238}U Absorption Rate Compared to Total Absorption (%)

3. 4. 4 Void coefficient

The void coefficient characterizes the reactivity variation in case the moderator is voided. It is a limiting parameter for the design of high-conversion cores. The void coefficient must be negative[1]. It is defined as the reactivity variation between nominal and voided situation:

$$void = 10^5 . \ln(\frac{keff_{voided}}{keff_{nominal}}) \quad (1.7)$$

Two main opposing effects are observed in voided situations. First the neutron spectrum is hardened. Since no moderator is present the neutron spectrum switches to high energies. Depending on the type of fuel this effect has different consequences. With UO_2 fuel enriched up to 5 % ^{235}U the reactivity will decrease. However with MOX fuel and a rather high (larger than 10 %) enrichment in plutonium isotopes, the reactivity tends to increase. In particular the ratio of capture over fission reaction rates for ^{240}Pu decreases substantially at high energies. This, as well as fast fissions, contributes to increase the reactivity for a MOX fuel with high plutonium content in voided situations. The void coefficient is directly linked to the relative changes between the thermal and fast fission rates. If the loss of coolant leads to an increase of the fast fission rate larger than the thermal fission rate reduction, the core reactivity tends to increase.

The second effect decreases the reactivity. In voided case no more water is reflecting the neutron. A substantial increase of M^2, the migration area, is observed. The rate of neutron escape outside of the core is increasing. This is independent of the fuel type. Moreover the intrinsic characteristic of the core and its tendency to let neutron leaking or not plays a role in the void coefficient. In that sense SMR cores have an advantage since their small size increases the neutron leakage rate, compared to a larger core. In normal operation this would tend to decrease the neutron-physic performances. But in a voided situation this would help to keep a negative void coefficient. The dependency of the neutron flux to the system geometry and size is further introduced in §7. 1.

[1] The relevance of using a strictly negative void coefficient is controversial within the nuclear engineering community, especially based on fast reactor studies, since that aspect is not always the limiting transient.

3. 4. 5 Other considerations

3. 4. 5. 1 Neutron physics coefficients

Negative Doppler and moderator coefficients are needed to ensure intrinsic safety of LWRs[1]. A temperature increase in the core system should lead to a decrease of the reactivity and not the opposite. Standard PWRs are designed to keep the neutron physics coefficients negative during the irradiation cycle [29]. With the coolant soluble boron concentration decreasing along the cycle, the moderator coefficient also decreases.

In an under-moderated core the absence of soluble boron leads to a rather constant moderator coefficient during the entire cycle length. The Doppler coefficient is also similar between the beginning of cycle (BOC) and end of cycle (EOC) since the fuel isotopic content does not vary much during the irradiation cycle.

3. 4. 5. 2 Absorbers and reactivity management

The hardened neutron spectrum in an under-moderated core loaded with MOX fuel reduces the efficiency of neutron poisons usually used in standard LWRs. The efficiency of Ag-In-Cd control rod or soluble boron in the coolant is reduced by a factor of 10 between a standard LWR and an under-moderated core. The use of enriched B_4C control rods or alternative materials, e.g. Hafnium, is needed to control the reactivity. An increase of the control rod numbers per control rod cluster or fuel assembly could also be required.

The small reactivity swing between BOC and EOC in under-moderated cores (below 5 000 pcm for about a two year cycle) reduces the reactivity compensation needs along cycle depletion compared to standard LWRs. The equivalent reactivity swing in a standard LWR is close to 15 000 pcm [30] [31]. Soluble boron is therefore not required to control the core reactivity with under-moderated core. The reactivity management can be designed using control rods only.

The reactor kinetic of an under moderated core is closer to a fast reactor loaded with MOX fuel than a standard PWR. The delayed neutron share (β_{eff}) ranges about 400 pcm whereas β_{eff} is close to 600 pcm in a standard PWR and 350 pcm in a sodium-cooled fast reactor.

The epithermal spectrum also influences the role of Xenon in the core. Xenon is less efficient in under-moderated core compared to standard LWRs due to the change of neutron spectrum. This reduces the need to compensate the Xenon feedback or the challenge of Xenon oscillation. This would ease operability, in particular during transient regime.

With the previous sections the specificities of high conversion cores are introduced. Based on those aspects and the lessons learned on SMR designs reviewed in Chapter 2, the HCSMR design concept and basic characteristics are introduced in the next chapter.

[1] With under-moderated cores negative Doppler and moderator coefficients might also lead to challenges in case of loss of primary pumps, as in fast reactors. A comprehensive transient analysis is needed to assess this aspect.

Chapter 4: HCSMR DESIGN

4. 1 DESIGN PROCESS

This chapter aims at defining the starting point and objectives of the HCSMR core optimization. An image of a first HCSMR core or preliminary design is introduced hereafter. The optimization generic objectives and constraints are also highlighted below. The process to optimize the HCSMR core is illustrated in Figure 1.7.

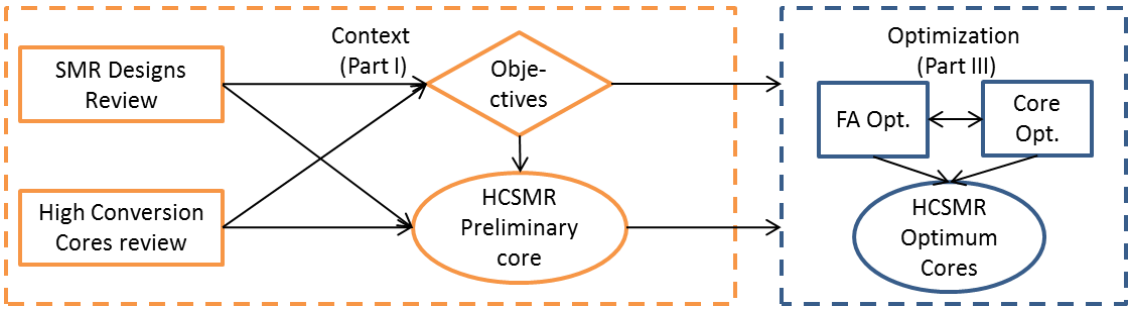

Figure 1.7: HCSMR Design Process Overview: Preliminary Core

The first HCSMR core is established based on engineering judgment and using the literature review outcomes on SMRs and high conversion LWR core design and concepts (Chapter 2 and Chapter 335). A similar process is undertaken to define the generic objectives and constraints of the HCSMR core design and optimization.

4. 2 GENERAL CHARACTERISTICS

The HCSMR has a thermal power of 600 MW and belongs to the category of iPWR. The power of 600 MW is arbitrarily selected[1] inspired by the mPower (530 MW) and Flexblue (530 MW) designs. This choice is also supported by the existing SMR market analysis and economics studies [20].

The HCSMR concept has its steam generators and pressurizer located in one vessel together with the core. This is inspired by integrated SMR designs. A complete design of such a system is outside of this work's scope. An operating point is nonetheless required to perform the core design and optimization and is introduced hereafter.

The fuel considered for the HCSMR core must be based on proven technologies, i.e. fuel rods based on zircaloy cladding and oxide pellet fuel. This boundary condition is set as external requirement for this PhD work. Innovation on fuel materials or fuel technology is out of this study's scope.

[1] The core power itself could be an optimization parameter. This would fit in a broader optimization, including system design and economics, which is out of this work's scope.

The HCSMR general characteristics are introduced in Table 1.7.

Parameters	Unit	Value
Full name		High Conversion Small Modular Reactor (HCSMR)
Reactor type		iPWR with reduced moderation
Coolant & moderator		Light water
Coolant circulation type		Forced
Thermal Power	MW	600
Electrical Power	MW	200

Table 1.7: HCSMR General Characteristics

Furthermore the reactivity management should be realized without soluble boron.

Due to the large number of design parameters of a nuclear core, not all design aspects are systematically optimized in this work. The HCSMR characteristics introduced in this section are generic and are not subjected to optimization, unless otherwise specified. The detailed boundary conditions of the optimizations and its parameters are introduced in Part Three.

4. 2. 1 Fuel Assembly

The HCSMR FA has a hexagonal lattice. It has 13 rows of fuel rods including 30 control rod positions. The number of rows is driven by the maximum feasible assembly pitch according to manufacturing and performance requirements. This design is obtained from previous design and optimization results [39] [59]. HCSMR FA main characteristics are summarized in Table 1.8 and a 2D overview is given in Figure 1.8. A triangular or hexagonal lattice is selected to maximize thermal-hydraulic performances as introduced in §4. 2. 3.

Parameter	Unit	Value
Fuel rod (FR) pitch	cm	1.15
Number of FR		438
Number of Control rods (CR)		30
Instrumentation rod (IR)		1
Fuel pellet diameter	cm	0.82
Cladding thickness	mm	0.65
CR guide tube inner diameter	cm	0.97
CR guide tube outer diameter	cm	1.05
Inter FA water gap	mm	1.0

Table 1.8: HCSMR FA Main Characteristics

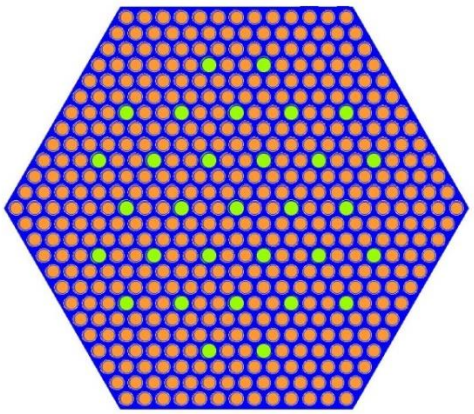

Figure 1.8: HCSMR MOX Fuel Assembly 2D Overview

The cell moderation ratio is 0.83 while it reaches 0.98 at the fuel assembly scale. An optimization of the fuel rod pitch (1.15 cm) and hence the moderation ratio is not performed. It is decided to start from previous CEA work outcomes [39].

A boundary condition to this project is the use of standard oxide fuel in fuel rods with Zircaloy cladding material and spacer grids. Spacing nets, as considered in some fast reactors' design to even further reduce the pitch between fuel rods, are not considered for the HCMSR design.

MOX fuel is considered in this study. The plutonium fraction in the MOX varies between 0 and 25 % with a plutonium fissile content of 56 %. Its isotopic composition is described in Table 1.9 and remains fixed at all optimization steps. The remaining content of the matrix is filled with depleted uranium at 0.2 % ^{235}U. The chosen plutonium vector, also referred to as Pu2035, is selected to be representative of an average MOX fuel in France in 2035.

Isotope	Concentration (%)
^{238}Pu	3,03
^{239}Pu	48,73
^{240}Pu	30,36
^{241}Pu	7,34
^{242}Pu	9,80
^{241}Am	0,74

Table 1.9: MOX Pu Vector

In addition to MOX, enriched uranium fuel is considered for specific applications. The enriched uranium is mixed with plutonium isotopes resulting in a MOX fuel with a matrix enriched in ^{235}U isotopes.

Fertile fuel rods are also considered. They are made of depleted uranium only. The fuel is standard oxide with a density of 10.08 $g.cm^{-3}$. Fuel cladding is standard Zircaloy. Control guide tubes are made of the same alloy and control rods are in B_4C.

A fuel assembly made of fertile fuel rods only (FER FA) is also examined in this study. For such a FA design the guide tube holes are removed and only a central guide tube for instrumentation purposes is kept. Due to the lower neutron flux observed in fertile material, it is indeed not

relevant to place control rods in FER FA. An overview of the FER FA is given in Figure 1.9 as well as its geometrical characteristics Table 1.10. Axially all FA are homogenous: no fertile layers are considered.

Parameter	Unit	Value
Fuel rod (FR) pitch	cm	1.15
Number of FR		468
Number of Control rods (CR)		0
Instrumentation rod (IR)		1
FR diameter	cm	0.82
Cladding thickness	mm	0.65
IR guide tube inner diameter	cm	0.97
IR guide tube outer diameter	cm	1.05
Inter FA water gap	mm	1.0

Table 1.10: HCSMR FER FA Main Characteristics

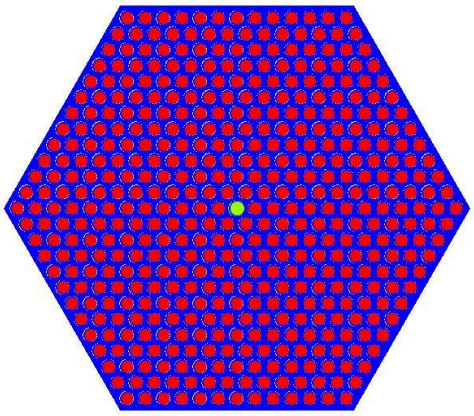

Figure 1.9: HCSMR FER Fuel Assembly 2D Overview

Further combinations of fuel compositions are considered for the optimization of the HCSMR FA. Those characteristics are detailed in Part Two and Part Three. However blankets of fertile fuel materials introduced either radially or axially are excluded of this study's scope.

Radially, an external row of fertile fuel assemblies would increase the production of fissile material and could ease flattening the neutron flux. This is nonetheless not considered for the HCSMR design. The HCSMR aims at increasing conversion factors via fuel utilization and not only by producing fissile materials. A similar reasoning applies for bottom and top blankets of fertile materials which could be considered but are excluded from this work's scope.

4. 2. 2 Core

The HCSMR core has 61 fuel assemblies. The HCSMR core main characteristics are summarized in Table 1.11. They are the starting design options to be further optimized (Part Three). A 2D overview of one HCSMR core is presented in Figure 1.10. In this example the core is made of two types of fuel assemblies: MOX and fertile FA. This is one design option among many possibilities to be evaluated as part of the optimization process.

Parameter	Unit	Value
Power	MW	600
Number of fuel assembly		61
Moderation ratio		1,02
Core width	cm	204
Average heat linear power	W/cm	100

Table 1.11: HCSMR Core Main Characteristics

The average heat linear power is set rather low compared to large commercial PWRs as introduced in Table 1.2 and Table 1.3 in Chapter 2. The intention is to give large margin on peaking factors and enable a reactivity management with control rods only as well as power transient or load-follow operation.

Three types of fuel management are considered with the replacement of 1/2, 1/3 or 1/4 of the FA inventory at each reload outage.

The optimization of the loading pattern impacts substantially the core performances. Automatic loading pattern optimization is itself a research topic [36] [84] and is not the focus of this work. A set of loading patterns designed based on engineering judgment are used for the core performance evaluations.

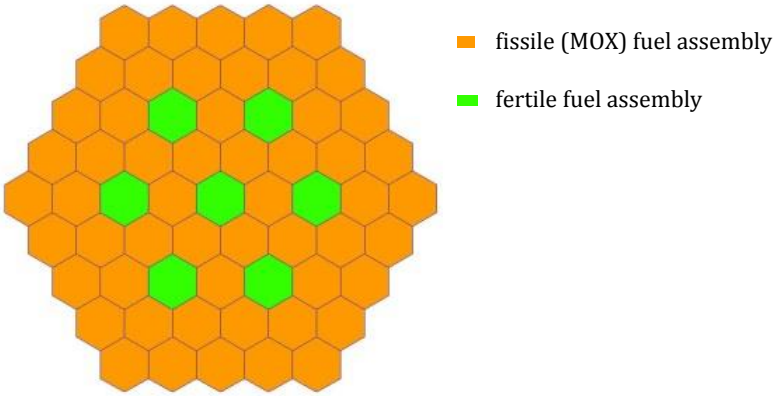

Figure 1.10: HCSMR Core Example 2D Overview

4. 2. 3 Thermal-Hydraulic

4. 2. 3. 1 Operating point

The HCSMR operating point is derived based on mPower design together with basic thermal-hydraulic consideration [85] [86]. The mPower design is chosen for its equivalent core power and design approach. An optimization of the operating point requires simulating the entire HCSMR system. This is outside of this work's scope. The selected operating point and thermo-hydraulic boundary condition are illustrated in Table 1.12.

Parameters	Unit	Value
Pressure	bar	140
Inlet temperature	°C	280
Outlet temperature	°C	310
Flow	$t.s^{-1}$	3.8
Bypass	%	5

Table 1.12: HCSMR Operating Point

4. 2. 3. 2 Square vs. hexagonal lattice

The HCSMR hexagonal or triangular lattice choice is based on thermal-hydraulic consideration. For a given moderation rate, a hexagonal lattice increases substantially the space between fuel rods compared to a square lattice. This increases performances on pressure drop and heat exchange.

Based on §3. 4 and simple geometry, the following can be derived:

Considering equation 1. 3 from §3. 4. 1 the moderation ratio MR is computed as: $\frac{V_{Cell}-V_{Rod}}{V_{Fuel}}$

For a given fuel rod type only V_{Cell} influences the moderation ratio between a square and a hexagonal lattice.

Assuming $V_{cell}^{hexa} = V_{cell}^{square}$ hence $\frac{\sqrt{3}}{2}p^2 = a^2$ (1. 8) with p the pitch of the hexagonal lattice and a the square length, $p = G_{hexa} + 2\,R_{Rod}$ (1. 9) and $a = G_{square} + 2\,R_{Rod}$ (1. 10) with G_{hexa} and G_{square} the gap between the cell border and the fuel rod, respectively for the hexagonal and the square lattice.

Hence $G_{hexa} = 1.075\,G_{square} + 0.149\,R_{Rod}$ (1. 11).

With the fuel rod characteristics from the HCSMR FA given in Table 1.8 the gap with a hexagonal lattice G_{hexa} comes out about 50 % larger than the gap with a square lattice G_{square} .

4. 2. 4 Reflector

The reflector is the structure surrounding the core. Radial, bottom and top reflectors must be defined for the HCSMR core. The reflectors' detailed characteristics are not imposed and can be optimized.

For the HCSMR core the reflector has a particular role. On one hand it should prevent neutron leaking out of the core in normal operation. But on the other hand, in voided situations a reflector enhancing neutron leakage is actually an asset. A good trade-off must be reached.

At first a heavy reflector based on the EPR design is used. For computations its geometry is simplified but the iron content considered is representative of the EPR heavy reflector. The iron content is then varied to assess the impact on the HCSMR core performances.

Compared to a large PWR the HCSMR has a higher neutron leakage rate due to its smaller core size. Considering basic nuclear reactor diffusion theory ([87] and §7. 1) for a cylinder of radius *R* and height *H*, criticality is obtained when geometrical and material buckling are equals, with then μ_0 the fundamental Eigen value given as

$$\mu_0 = \frac{j^2}{R^2} + \frac{\pi^2}{H^2} \quad (1.12)$$

with j = 2,40 (J_0 Bessel Function). This shows the dependency with the reactor geometry and core size.

An optimization of the axial reflector is not considered in this work. Decreasing the enrichment of the fuel top and bottom tends to decrease axial neutron leakage and could provide more fissile material, hence improving the conversion ratio. It is not considered for non-proliferation purposes as it is close to fertile material blankets introduction.

4. 3 DESIGN OBJECTIVES

The HCSMR design aims at combining the benefits of small cores and under-moderated technologies to achieve the following main objectives:

- Conversion factor: higher than 0.8;

Existing under-moderated cores have a conversion factor close to 0.8 (Chapter 3). The HCSMR aims at reaching higher value while remaining below 1.0 to respect non-proliferation recommendations [25]. Conversion factors above 1.0 are nonetheless very difficult to achieve with water as moderator even with under-moderated designs.

- Cycle length: higher than two years;

The cycle length observed for innovative SMRs in development ranges mostly between two and four years (Chapter 2). An increased cycle length and reduced outage number, compared to current large PWRs, would support the economics of small cores [3]. Two years is set as the lower boundary while the optimization will seek at increasing the HCSMR cycle length. An availability factor of 0.95 should be considered in line with modern nuclear designs.

Beyond those two objectives on HCSMR performances the following constraints are carefully considered for the core optimization:

- Void coefficient: less than - 500 pcm;

The safety of a nuclear system comes first. The HCSMR void coefficient must remain negative at all times. Following a conservative approach an arbitrary margin of 500 pcm is applied. This margin covers methodology bias as well as nuclear data uncertainties as introduced in Part Two.

- Maximum linear heat generation rate: less than 400 W/cm;

The fuel cladding is one of the first safety barriers. Its integrity must be ensured at all times. As a consequence, a limitation on linear heat generation rate must be introduced. This parameter should be defined together with sub-channel thermal-hydraulic analysis. Since such evaluation was out of this work's scope we have considered an arbitrary limit of 400 W/cm. This value considers a margin already in line with a conservative approach.

For both the void coefficient and maximum linear heat generation rate, an investigation at the core optimization step will be carried out to analyze the consequences of applying even more conservative limits. Some further constraints and boundary conditions must also be considered:

- Plutonium mass in core.

To ease a potential deployment of an HCSMR core the total mass of plutonium in core should be minimized. The mass of plutonium required influences deeply the initial fuel loading since a large quantity of plutonium is needed at one time. But also impacts the quantity of plutonium to be reloaded at each refueling outage.

4. 4 PRELIMINARY DESIGN

To define a starting point for the HCSMR optimization a preliminary design is established. It is based on the general characteristics introduced in §4. 2. In addition specific choices are applied on fuel material, active height, reflector and fuel management. The preliminary design is also used to develop and validate the neutron physics computation schemes. The performances of this preliminary HCSMR core are introduced in §10. 3.

4. 4. 1 Fuel Assembly

One FA type only is considered for the preliminary HCSMR design. It contains MOX fuel with plutonium at 19%. All 438 fuel rods are made of this fuel type. The active height reaches 220 cm.

Further characteristics are in line with the introduction in §4. 2. 1 and detailed information provided in Table 1.8.

4. 4. 2 Core

The preliminary core contains 61 MOX FA. A heavy reflector is considered radially. The fuel management is made with a 1/3. The associated loading pattern is introduced in Figure 1.11 with the reloading scheme presented in Figure 1.12. Fresh fuel assemblies are noted "M0" and have a "|" reloading mark. Fuel assemblies in their second irradiation cycle are noted "M1" and so on. FA positions in previous cycles are noted in the reloading scheme, e.g. "from position G15".

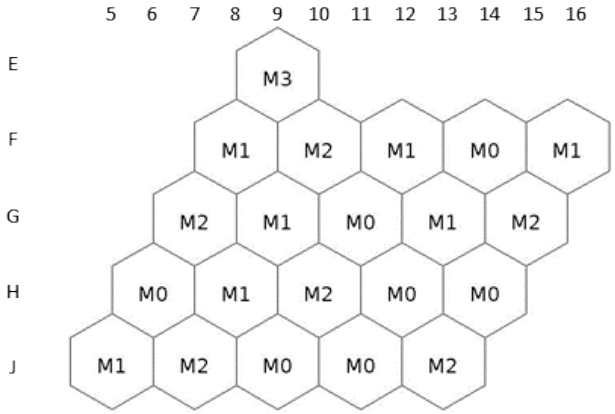

Figure 1.11: Loading Pattern "1/3" FM for Preliminary HCSMR Core

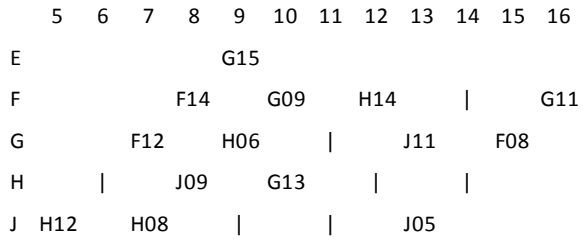

Figure 1.12: Reloading Scheme "1/3" FM for Preliminary HCSMR Core

Chapter 5: OPTIMIZATION METHODS

"*Optimization* theory encompasses the quantitative study of optima and methods for finding them" [88]. *Optimization* supports the decision-making process by providing a set of optimal choices. For a simple optimization exercise it is possible to find a unique optimum solution: the best decision. Real life optimizations are however more complex and have often several objectives and parameters.

Multi-objective optimizations are regularly approached via a general optimization function: a weight is attributed to each objective and a general optimization function gathers all weighted objectives. With this method the multi-objective optimization is transformed into a mono-objective optimization exercise. A unique *best* solution could be identified. This approach is not implemented in this work.

The multi-objective optimization approach used to design the HCSMR core seeks to obtain a group of optimal solutions: a population of optimal HCSMR cores. Neither a weighted approach nor the search for a unique solution is aimed at. The group of optimal solutions should be Pareto optimal. One solution is defined as an individual while the group is referred to as population. The Pareto concept and multi-objectives optimization principles are introduced in §5. 4. 1.

To solve multi-objective and multi-parameter optimization exercises, various methods can be used. The literature classified the methods available in three main categories: calculus-based, enumerative and random methods [89]. Those approaches must be compared regarding two main criteria: their robustness and their rapidity of execution. Hence optimization is a trade-off between robustness and efficiency.

With an enumerative approach all combinations of parameters are assessed. This is robust as long as the parameters' boundary conditions are unchanged. But it is also costly since a large number of combinations exists. Usual engineering exercises have several billions of unique parameters set. A stochastic approach of selecting the combination and performing the assessments can be used to reduce the number of trials as well as the robustness.

To design a new system, the difficulty often lies in the assessment of the optimization function. This is particularly true for nuclear core design as the simulation of one case is costly: it requires substantial computing time. In this case the development of a simplified explicit model can be used: the accuracy of the simulation is reduced to save computing cost.

Another approach is to replace the explicit simulation by a mathematical function, called a surrogate model, which mimics the behavior of the explicit simulation. Polynomial regression and neural network are known examples of surrogate models. Such functions have to be built first. Usually this is done via a learning process based on a set of explicit evaluations. The accuracy of the surrogate model is key to the optimization robustness and largely depends on the learning population size and type.

Research plans are designed in this objective: to define the optimization boundary conditions and research space. To support this process, the use of sensitivity study is appreciable. This

enables an assessment of the type of optimization exercises considered and a qualitative understanding of the dependency between optimization criteria.

This chapter reviews the role and some theory of the different steps introduced: research plan design and sensitivity studies, surrogate model creation and the optimization process itself. The importance of the optimization process, and not only the final outcomes, must be highlighted for engineers since this is a source of valuable information.

5. 1 RESEARCH PLAN

A multi-objective optimization exercise is defined by:

- A set of parameters or criteria with a specific variation range;
- A list of objectives and associated target values.

The objectives are parameters of the optimization functions. Understanding the type of dependency between the optimization parameters and objectives enables a customization of the optimization methods and an increase in study efficiency. This is performed via the design of a research plan also called design of experiment (DoE). An optimization study should start with a research plan phase that aims at assessing the type of problem studied.

First, the parameter ranges are reviewed. At this step, also called scoping study, the objectives and parameters and their dependency are investigated. Parallel coordinates plots provide a useful graphical representation of complex optimization spaces. An introduction to parallel coordinates plots can be found in Annex D.

Sensitivity methods can be used to perform scoping study and review systematically the role and type of the parameters. The literature offers various methods to perform such study. The methods “One At a Time” (OAT), Morris and Sobol indices are used in this work and are introduced hereafter.

Based on the knowledge gained via the sensitivity studies, the research plan is then constructed. Explicit evaluations of the optimization functions are performed. Those evaluations are often “expensive”, they require lots of computation time. Therefore the selection of the parameters and the associated size and meshing of the research plan must be carefully chosen.

The latin hypercube sampling (LHS) method [90] can be used to select the individuals to be evaluated within the research plan. Each parameter range is divided into n domains. An identical probability for each n domain is set. n is the number of individuals to be generated. Each parameter is sampled and n^d sub-domains are generated with d the number of parameters.

The sampling can be performed following a statistical function such as normal or uniform distribution. One individual out of the parametric space is then selected for evaluation and its result is added to the research plan outcomes. The column and line corresponding to this individual are then removed from the parametric space. This approach is illustrated in Figure 1.13 from [91] below. One uniform distribution and one normal distribution are used. The red column and line identifies the forbidden space due to the selection of the top left individual.

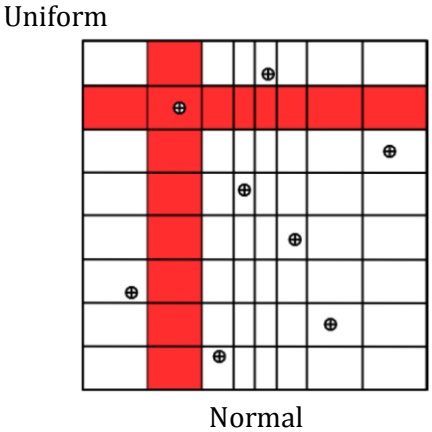

Figure 1.13: LHS Method Illustration.

5. 2 SENSITIVITY ANALYSIS

Sensitivity analysis aims at analyzing the type of optimization exercises considered, characterizing the role and relationship of optimization parameters with regards to the optimization exercise. Three sensitivity analysis methods are reviewed here: the One At a Time method, the Morris indices and the Sobol indices methods. The influence of parameters' range must be carefully considered when implementing such methods. A narrow varying range could undervalue the importance of a very influential parameter and vice versa, depending on other parameters' ranges.

5. 2. 1 One At a Time

The "One At a Time" (OAT) or "One Factor At a Time" (OFAT) method [92] aims at varying one parameter while all others are kept constant. For each parameter a finite number of levels are (nb_{lvl}) are defined. Usually nb_{lvl} is set to two or three. The Figure 1.14 illustrates an OAT method for a function $f(x_1, x_2)$ with two parameters and for nb_{lvl} set to two. From the projection of $f(x_1, x_2)$, the reference in black in the figure, the variation $f(x_1 + \Delta x_1, x_2)$ and then $f(x_1, x_2 + \Delta x_2)$ are evaluated and shown in blue in Figure 1.14. This method makes it possible to characterize the dependency of x_i on y.

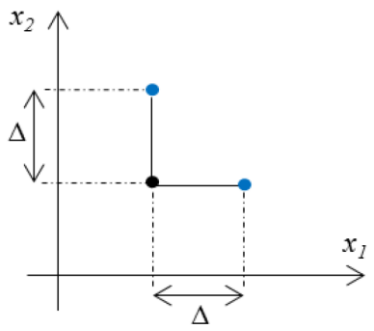

Figure 1.14: OAT Example for a Function with Two Parameters

A function with *d* parameters will have a number of evaluations N_{eval} as:

$$N_{eval} = (nb_{lvl} - 1)\, d\, + 1 \qquad (1.\,13)$$

Finite difference methods can give a simple estimation of each perturbation on *y*:

$$\frac{\partial y}{\partial x_i} \approx \frac{f(x_0,\dots,x_i+\Delta x_i,\dots,x_d) - f(x_0,\dots,x_i,\dots,x_d)}{\Delta x_i} \qquad (1.\,14)$$

5. 2. 2 Morris

The sensitivity analysis approach developed by Morris [93] [94] is a generalization of the OAT method. Parameters (P_i) can be classified in three types:

- P_1 have no influence on the *f* function;
- P_2 have no interaction and/or linear effects on *f;*
- P_3 have interaction and/or non-linear effects on *f.*

In the Morris' method at first *r* points are selected within the entry parameters space. An OAT analysis is performed for each *i* point (with *i* ranges from *0* to *r*) and gives the local variation of the entry x_j on *f*. The average of absolute variations on *f* (noted μ_j) shows the importance of x_i on *f*. The associated necessary number of evaluation N_{eval} is defined as

$$N_{eval} = (d + 1)\, r \qquad (1.\,15)$$

with *d* the number of parameters.

The perturbation effect of output *j* on draw *i* is noted $E_j^{(i)}$ as:

$$E_j^{(i)} = \frac{f(x_1,\dots,x_j+\Delta_j,\dots,x_d) - f(x_1,\dots,x_i,\dots,x_d)}{\Delta x_j} \qquad (1.\,16)$$

Equation 1. 15 leads to:

$$\mu_j = \frac{1}{r}\sum_{i=1}^{r} E_j^{(i)} \qquad (1.\,17) \qquad \text{and} \qquad \mu_j{}^* = \frac{1}{r}\sum_{i=1}^{r} \left|E_j^{(i)}\right| \qquad (1.\,18)$$

The higher $\mu_j{}^*$ is, the bigger is the impact of *f*. The standard deviation σ_j weights the linearity of the model studied with regards to x_j.

$$\sigma_j = \sqrt{\frac{1}{r}\sum_{i=1}^{r}(\mu_j - E_j^{(i)})^2} \qquad (1.\,19)$$

With independent entry parameters and a linear f function, the consequence of a perturbation is independent of x_j value and hence σ_j is null. If σ_j is high the system is non-linear and dependencies exist between the various entry parameters.

The results of an analysis performed with the Morris' method can be plotted as in Figure 1.15 from [95] where σ_j is function of $\mu_j{}^*$ for the function $f(x_1, x_2, \dots, x_8)$.

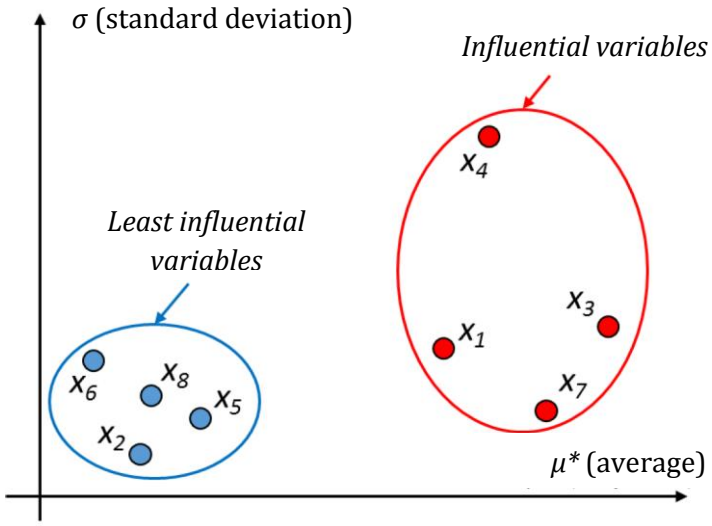

Figure 1.15: Example of Morris' Sensitivity Method Results on a Function *f* with Eight Entry Parameters

5. 2. 3 Sobol

Sobol's indices assume parameters are independent. Sobol [96] extended the Morris' method by introducing standard deviation splitting approach in sensitivity analysis. It starts with the assumption that a function *f* can be split in series of basic functions as:

$$Y = f_0 + \sum_{i=1}^{d} f_i(X_i) + \sum_{i<j}^{d} f_{ij}(X_i, X_j) + \cdots + f_{1,2,\ldots,d}(X_1, X_2, \ldots, X_d) \quad (1.20)$$

Using Hoeffding approach [97], Sobol suggests splitting the variance of *y* as:

$$Var[y] = \sum_{i=1}^{d} V_i(y) + \sum_{i<j}^{d} V_{ij}(y) + \sum_{i<j<k}^{d} V_{ijk}(y) + \cdots + V_{1,2,\ldots d}(y) \quad (1.21)$$

Sobol indices are then defined as:

$$S_i = \frac{V_i(y)}{Var(y)} \; ; S_{ij} = \frac{V_{ij}(y)}{Var(y)} ; \ldots (1.22)$$

With $V_i(y) = Var[\mathbb{E}(y|x_i)]$ and $V_{ij}(y) = Var\left[\mathbb{E}\left(y\middle|x_i x_j\right)\right] - V_i(y) - V_j(y)$

With the global indices encompassing all effects of one parameter on the function as [98]:

$$S_{Ti} = S_i + \sum_{i \neq j} S_{ij} + \sum_{i \neq j,k \neq i,j<k} S_{ijk} + \cdots \quad (1.23)$$

Their interpretation can be summarized as:

- Indices values are between zero and one. The sum of all indices is equal to one.
- If the first order indices S_i is large, the x_i parameter has substantial influence on *y*. The opposite is not necessarily true.
- If the global order indices S_{Ti} is small, the x_i parameter has a limited impact on *y*.
- The second order indices, S_{ij}, show the influence of the interaction between parameters x_i and x_j on *y*.

5. 3 SURROGATE MODELS

Optimization exercises require a large number of calls to the function to be optimized. Although computing performances have substantially increased over the past years, detailed numerical simulations often require long computing times. Such explicit evaluations are referred to as "costly". In practice the deterministic evaluations considered in this work, as part of the optimization process, can last up to several hours.

Surrogate models can be defined as an approached mathematical function to replace a costly explicit evaluation. Different mathematical methods exist to generate surrogate models such as neural network and kriging. Surrogate models are developed by calibration against the results of explicit evaluations. Therefore the approach selected to prepare the surrogate model will influence the results and is key to ensure the accuracy of the models prepared. Surrogate models are usually developed for a specific space and their accuracy is not given outside of the creation and validation space.

Surrogate model quality is not lower compared to explicit evaluations within the validation space. Moreover surrogate models enable the detection of outliers in explicit evaluation results. An evaluation using surrogate models is also often more reliable than with explicit evaluations and hence prevent such outliers.

5. 3. 1 Accuracy

An efficient method used to characterize the accuracy of the surrogate model formed is to quantify the associated R^2 and Q^2. R^2, the training coefficient and Q^2, the predictive coefficient are defined as:

$$R^2 = 1 - \frac{RMSE^2_{training}}{Var(y)} \quad Q^2 = 1 - \frac{RMSE^2_{testing}}{Var(y)}$$

A coefficient of one shows a perfect predictive capability. The lower the coefficient is, the worse the capabilities of the generated surrogate model are.

The Root Mean Square Error (RMSE) between the surrogate model result and the explicit evaluation result is defined as:

$$RMSE = \sqrt{\frac{\sum_{i=1}^{n}(\hat{y}_i - y_i)^2}{n}}$$

with: n: number of evaluation
y: explicit evaluation result
$\hat{y}$: surrogate model evaluation result

The training data base is usually separated from the testing data base. Practically explicit evaluations are divided into two data bases. The testing can also be performed using the training database but a separated approach enhances the confidence of the result obtained.

5. 3. 2 Neural network

Artificial neural networks are one method to generate surrogate models. The concept is based on brain biological neurons observation and was developed in the 80's [99]. Although the name "neural network" is still in use nowadays, the mathematical approach is not directly correlated to biological neuron clusters and their axon connections [100]. With the large scale development of artificial intelligence, machine learning and deep learning approaches, neural networks' use grew substantially over the past years.

A neuron is a non-linear parametric algebraic function taking bounded values. Usually sigmoid functions are used. An open neural network generates an algebraic function of its entry parameters by a crossing functions associated to each neuron. It is illustrated in Figure 1.16 from [95]. Neural network belongs mathematically to regression methods.

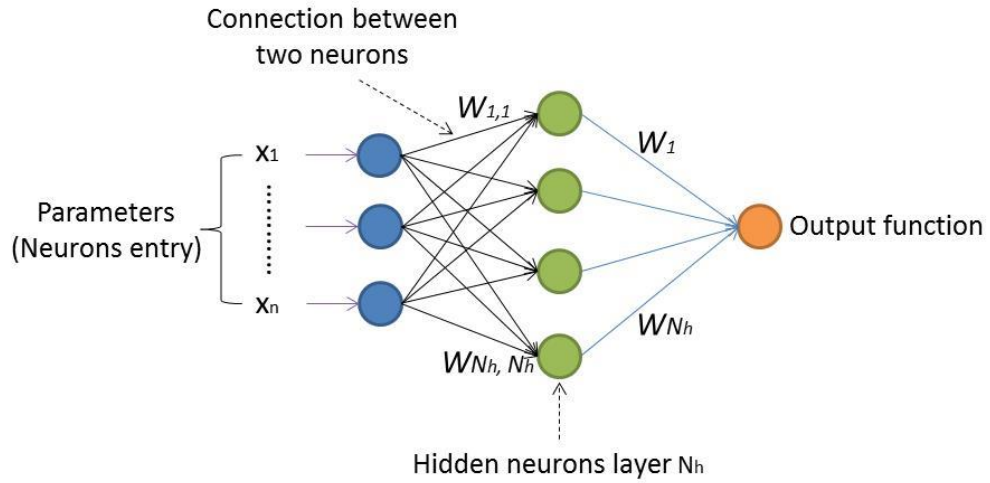

Figure 1.16: Open Neural Network with one Hidden Neurons Layer

The output function is then formalized as

$$f = \sum_{i=1}^{N_h} W_i \, sig(\sum_{j=1}^{N_h} W_{i,j} x_j + W_{0,j}) + W_0 \qquad (1.24)$$

with $W_{0,j}$ and W_0 as constant.

Open neural networks with a layer of hidden neurons are well suited to simulate any non-dynamic physical function. Such model can approach with an arbitrary precision any function [101].

As shown in Figure 1.16 a neuron output function is the sum of the *n* entry parameters to which a specific weight $W_{i,j}$ is associated. The neural network output function *f* is the sum of all neurons output to which a specific weight W_i is associated.

The generation of the neural network is an optimization exercise aiming at defining the most accurate W_i weights. It requires the optimization of non-linear problem. Since the derivative of sigmoid functions can be calculated, the f gradient can be derived. This supports the optimization process [102], in particular the use of metaheuristic methods.

In this work the optimization process and generation of neural networks is performed via the URANIE tool [91]. URANIE is a platform for uncertainties propagation and optimization developed at CEA. It gathers CEA's methods and algorithms on uncertainty, sensitivity and optimization in one global framework. URANIE uses the data analysis framework ROOT [103].

With URANIE an empirical approach is used to select the most appropriate neural network. The number of hidden neurons is varied between *n* and *2n*. The neural network with the lowest Q^2 is eventually selected.

A high number of hidden neurons does not automatically give the best accuracy. An over-learning risk exists. The neural network formed could present non-physical behavior for individuals which were not part of the training space. This advocates using an independent testing data base. The risk of over learning is illustrated in Figure 1.17.

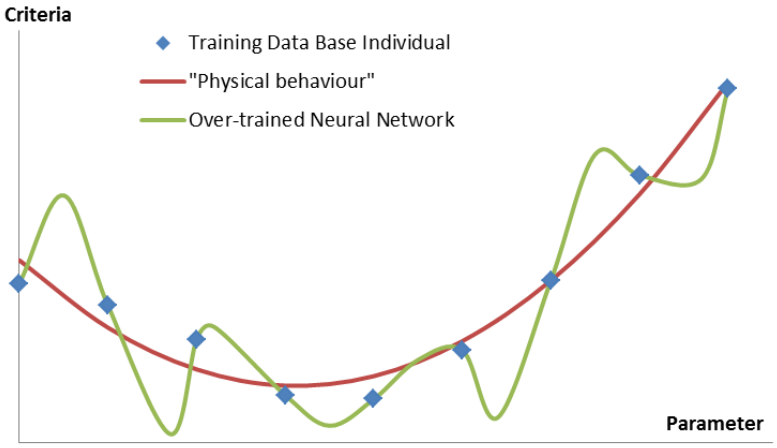

Figure 1.17: Neural Network with Over-Training Example

5. 3. 3 Kriging

The Kriging method was introduced by D. G. Krige in 1951 [104] and formalized in 1970 by G. Matheron [105]. A kriging prediction is a weighted linear combination of values generated out of a training data base. The specific advantage of the kriging method lies in the generation of a linear unbiased prediction for which a bias estimator is available. It is a robust and exact method. The Kriging method belongs mathematically to interpolation methods.

Considering the Gaussian process of *y*, $\hat{y}$, as the sum of a deterministic model *m* and a Gaussian process *z* with a zero-mean distribution

$$\widehat{y(x)} = m(x) + z(x) \qquad (1.25)$$

with *y* a physical quantity of interest and *x* the vector of dimension *d* in which all entry parameters are contained. *n* simulations of *y* are considered.

Kriging aims at minimizing the quadratic average error of $\mathbb{E}[(\widehat{y(x)} - y(x))]$ while $\mathbb{E}\left[\widehat{(y(x)}\right] = \mathbb{E}[y(x)]$ as a non-bias constraint. Solving this system enables the obtainment of the best linear predicator of y without bias.

The deterministic function m can be any simple function, a constant or linear function is adequate as the Gaussian process z simulates the non-linearity between the input variables. Alternatively m can be improved to limit z role. In this introduction m is defined as a linear or constant function with β defining the linear regression parameters:

$$m(x) = \beta_0 + \sum_{j=1}^{d} \beta_j x_j \quad (1.\ 26)$$

The zero-mean distribution Gaussian process z is chosen stationary with its two first moments as

$$\mathrm{E}[z(x)] = 0$$

$$Cov\left[z(x_i), z(x_j)\right] = \sigma^2 N(x_i, x_j) \quad (1.\ 27)$$

with σ the standard deviation of z and N the parametric covariance function, which captures the correlation between two points as function of their distance. The parametric covariance function simulates the regularity of the simulated function. Various parametric covariance functions exist such as generalized exponential function or Matérn covariance function [106]. The Matérn$^{3/2}$ covariance function is implemented in this work. It takes θ and p as parameters and is defined as

$$N_{\theta,p}(x^i, x^j) = \prod_{s=1}^{d} \frac{2}{\Gamma(p_s)} (\sqrt{p(s)}\theta_s(x_s^i - x_s^j))^{p_s} K_{P_s}(2\,\theta_s\sqrt{P_s}) \quad (1.\ 28)$$

With Γ the Gamma function and K_p the Bessel function modified of order p ($p \geq \frac{1}{2}$). It is usual to note the correlation length $l = \frac{1}{\theta}$. A parameter x with a high correlation length has a limited impact on the simulation. On the contrary a parameter with a low l generates important variations on the simulation.

5. 4 OPTIMIZATION

5. 4. 1 Multi-objective optimization

An optimization exercise has objectives and criteria. The type and quantity of the objectives and criteria characterize the type of optimization exercise. For each optimization type various methods can be applied. In the past decades simplified approaches were often used, e.g. parametric studies, enumerative or random methods. The rapidly developing computing capabilities enable the implementation of global optimization methods. Such approaches are particularly relevant to address multidisciplinary optimization exercise [95].

To understand multi-objective optimization (MOO) it is useful to look first at mono-objective optimization. A mono-objective or single-criterion optimization is rather straight forward. The criterion to optimize is defined by an objective function. The best value (usually the minimum in optimization theory) is searched for and directly gives the optimum of the function. The objective function can be linear or not and must consider the constraints imposed by the parameter(s). Various resolution techniques exist, such as gradient methods, the stochastics approach or evolutionary algorithms. An example of a single objective constrained optimization can be summarized as:

$$\begin{cases} Min(J) = f(x) \\ \text{with } x \in A \end{cases}$$

with f(x) the objective function giving *J* the mono- objective and *A* the feasible region of the *x* parameter.

Nuclear core design exercises are complex. They have several optimization objectives. For example to design the HCSMR core the cycle length and the conversion factor should be maximized while the void coefficient must remain negative. As explained earlier (cf §3. 4) those objectives are counteractive. It is often the case in MOO exercises. As a consequence an individual that simultaneously improves all objectives almost never exists.

MOO exercises can be addressed with at least two different approaches. First the scalarization method, also called weighted-sum approach, allocates a weight to each optimization objective. One optimization function is defined which combines all weighted objectives. It can be illustrated as follows:

$$\begin{cases} Min(J) = \sum_{m=1}^{M} w_m f_m(x) \\ \text{with } g(x,p) \leq 0 \\ h(x,p) = 0 \\ x_{i,LB} \leq x_i \leq x_{i,UB}(x,p) \; and \; (i = 1, \dots, n) \end{cases}$$

with the objective function vector *J,* a function of the design vector *x* and fixed parameter *p*; *g* and *h* are inequality and equality constraints.

This method gives preference upfront on some characteristics of the best individual. It can lead to reach Pareto optimum but has several difficulties with complex exercises such as non-convex problems. Several improvements of this approach are proposed in the literature [107].

A second approach to handle MOO are Pareto methods. They aim to obtain a population of individuals for which it is not possible to improve any individual on one objective without it deteriorating on at least one other objective. Such population is called *Pareto* optimal population. A notion of superiority or domination between the population individuals is introduced.

$$x_1 \text{ dominates } x_2 \Leftrightarrow \begin{cases} \forall j \in [1,p] \; f_j(x_1) \leq f_j(x_2) \\ \exists k \in [1,p] \; f_k(x_1) < f_k(x_2) \end{cases}$$

A bi-criterion optimization example can illustrate the domination relationship between the individual. An individual dominates another individual if it is better or equal on one criterion and strictly better on the other criteria. Similarly an individual is dominated by another if at least one criterion exists on which it is strictly better. Only non-dominated criteria individuals are eventually selected and form the *Pareto* front. This example is illustrated in Figure 1.18 where objective *O1* and *O2* should be minimized.

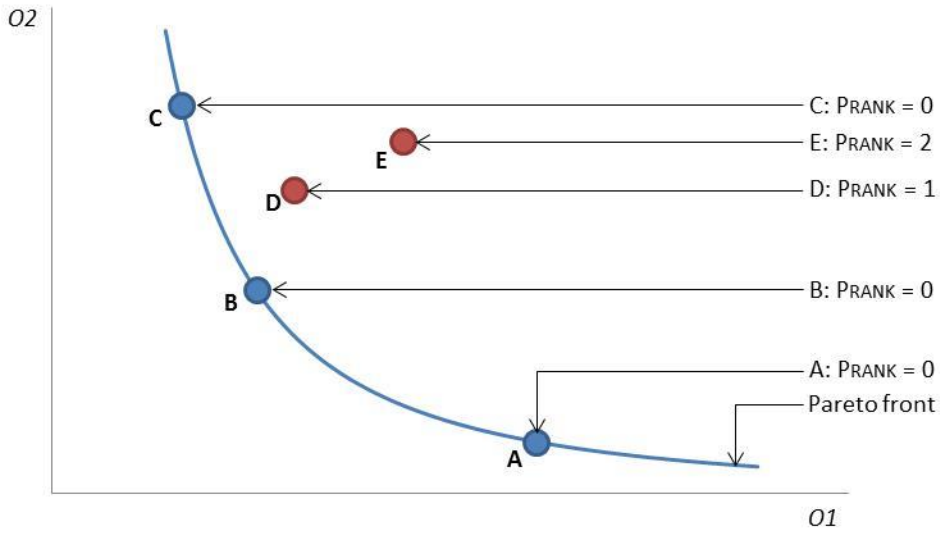

Figure 1.18: Pareto Front Overview

In Figure 1.18 the Pareto front between criteria O1 and O2 is plotted as a curve (blue line). 5 individuals are shown – A to D – with their Pareto rank. The individuals A, B and C are Pareto optimal: their Pareto rank is 0. Those three individuals are non-dominated: it is only possible to improve them on one criterion, e.g. O1, by lowering the other criteria, e.g. O2. Individual D and E, with a respective Pareto rank 1 and 2 are not Pareto optimal. "D" is dominated by "B" and hence has a Pareto rank of 1. "E" is dominated by "D" and "B" and has hence a Pareto rank of 2. The rank is defined as the number of dominance relationships an individual has. In the example shown in Figure 1.18 it is possible to improve the individuals "D" and "E" further to reach the Pareto front. It is however impossible to get individuals on the left domain of the Pareto front curve due to the contradictory objective or criteria of the optimization exercise. This area can be understood as a "forbidden" domain.

With opposing criteria, the Pareto front obtained with two criteria is located on a curve. The Pareto front with three criteria is located on a surface. With *n* criteria, the Pareto front is located in a Pareto hyperspace of *n-1* dimension.

The Pareto rank of each individual is used to optimize a population of individuals. Regardless of the optimization method used, the optimization process starts usually with the evaluation of an initial population covering the optimization domain comprehensively. An iterative process occurs then to evaluate, rank and select a new population to be evaluated, as shown in Figure 1.19. The optimization algorithm seeks to bring all individuals in a non-dominated status, i.e. to have a Pareto rank of 0.

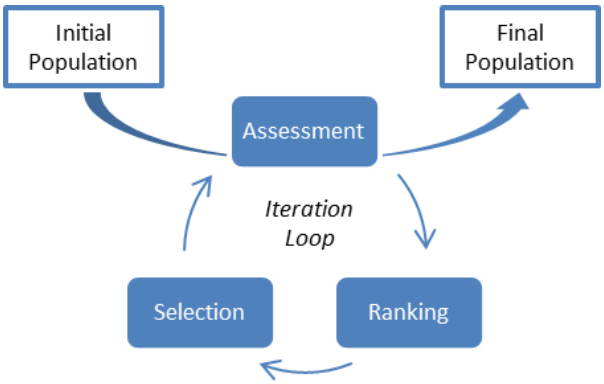

Figure 1.19: Pareto Optimization Process

For nuclear core design this MOO approach generates a population of optimum solutions. It enables a later trade-off based on the criteria of interest and to select the most relevant designs. Preferences are included a posteriori.

The assessment step of the optimization can be performed using explicit evaluations or trained surrogate models (cf §5. 3). A combination of both methods can also be implemented and will be preferred to combine accuracy and efficiency.

Various optimization techniques exist [108]. For this work the optimizations are undertaken using genetic algorithms. Two other approaches, the simplex method and particle swarm are also considered. The specificities of those three methods are briefly introduced below and can further be found in the extensive literature existing on this subject.

5. 4. 2 An Introduction to the Simplex Method

The simplex optimization method was originally developed for mono-criterion optimization in operational research [110]. It was further developed to optimize multi-objective functions. Considering a simplified simplex mechanism aiming at minimizing the function f shown in Figure 1.20 from [95], the process can be described as follow:

- *n+1* points are generated;
- rank generated points according to $f(x_1) < f(x_2) \ldots < f(x_{n+1})$;
- evaluate the barycenter G for *n* first points;
- replace the point x_{n+1} with its symmetrical x'_{n+1} compared to G;
- iterate further from step 2.

At each iteration the least performing point $f(x_{n+1})$ is replaced by its symmetrical.

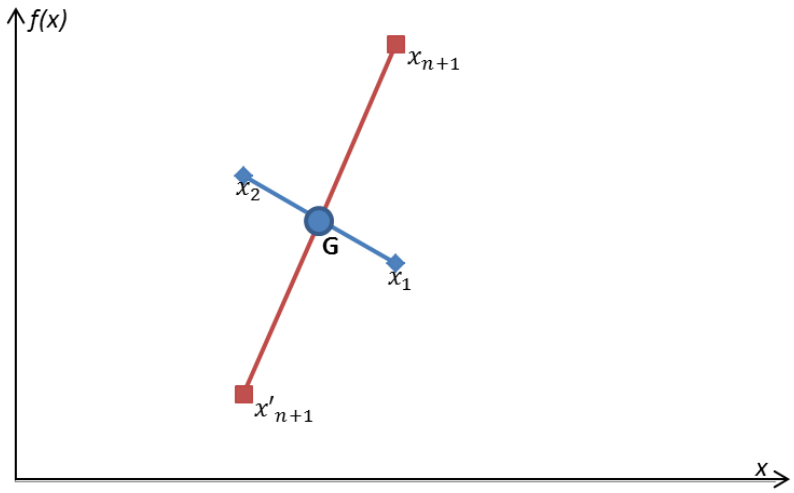

Figure 1.20: Simplex Method Graphical Overview

To solve multi-objective optimization exercises, the simplex method was further developed based on the Pareto rank methodology: individuals are ranked and further optimized according to their dominance relationship. Although the simplex method robustness and efficiency is proven, its limitation to linear objective function prevents its use in optimizing efficiently the HCSMR design.

5. 4. 3 An Introduction to Particle Swarm

The particle swarm optimization method is inspired by natural phenomenon observations [111]. In real life it is common to observe animals moving in groups. A group of birds flying together – a flock –, a school of fish or a swarm of bees are all populations made up of many individuals. Each individual can communicate with its neighbors as well as remembering the best position it had in the swarm. Each individual also knows its velocity and position. To select the next move – or optimization step in optimization theory– each individual has to make a trade-off between:

- Its willingness to come back to its known best position in the swarm;
- Its desire to copy its neighbors to reflect optimal position observed in the neighborhood;
- Its own speed.

A weighted approach of the parameters mentioned above enables the population to become Pareto optimal.

In this work, particle swarm optimization is benchmarked. It may not be prioritized due to the absence of significant benefits compared to the results obtained with genetic algorithms optimization.

5. 4. 4 An Introduction to Genetic Algorithms

Genetic algorithms are evolutionary algorithms developed based on natural selection and genetics observations [88]. They were introduced by John Holland in the 70's and are based on four main principles:

- Optimization is performed within a population of individuals, not on single individuals;
- Best individuals are selected with regards to the objective function, not using derivative or auxiliary knowledge;
- Individuals with heterogeneous characteristics are combined based on genetic observation phenomenon, increasing the possible outcomes and robustness;
- Probabilistic transition rules are used between generations, not deterministic rules.

The optimization starts by generating a population of individuals within the optimization space. Each individual is then ranked according to its performances regarding each objective. The algorithm then selects specific individuals within the population based on natural selection mechanics. A step of cross-breeding and mutation within the selected individuals' parameters can be performed before the new population is evaluated. The evaluation is performed by either an explicit evaluation or by using surrogate models. Those principles are summarized by extending the Pareto optimization concept, as illustrated in Figure 1.21.

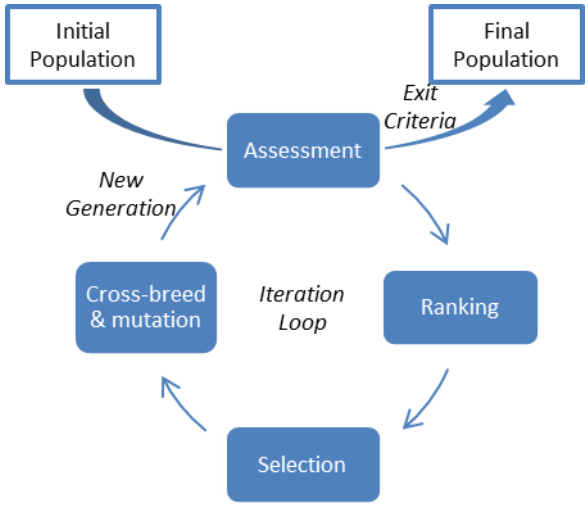

Figure 1.21: Genetic Algorithm Method Overview

Table 1.13 illustrates the corresponding terminology between biological systems genetics and genetic algorithms.

Natural Genetics	Genetic Algorithm
Chromosome	Chromosome, string
Gene	Parameter, feature
Allele	Parameter value
Genotype	Individual's structure
Phenotype	Individual's characteristics

Table 1.13: Comparison of Natural Genetics and Genetic Algorithms Terminology

In natural genetics one or more *chromosomes* form the genetic structure and operation of some organisms. A *chromosome* is also a *chromosome* or *string* in artificial genetic algorithms. The total genetic package in natural systems is called the *genotype* referred to as *structure* in optimization theory. Genetic algorithms used in this work are based on the Vizir package of URANIE. Vizir considers two chromosomes for each structure. Only one of the chromosomes is

active, the dominant one. The *individual* is evaluated on the dominant *chromosome* of the *structure*, also referred as the individual's (visible) *characteristics* or *phenotype* in natural genetics. The second *chromosome* is recessive and will only be used at the cross-breeding and mutation step. A chromosome gathers *parameters* (*gene*) and associated *values* (*allele*). Two types of cross-breeding are considered in Vizir [95]:

- Heterozygous cross-breed

Parameters are randomly selected from both parents to create a child structure as illustrated in Figure 1.22. The selection occurs via two successive steps. First parameters from both dominant and recessive chromosomes are selected for both parents. Then a random selection occurs to determine which parameters go to the dominant or recessive chromosome of the child. Eventually the child inherits of a set of two chromosomes made of parameters from its parents. This process enables the diversification of the individual's characteristics and a thorough overview of the optimization area.

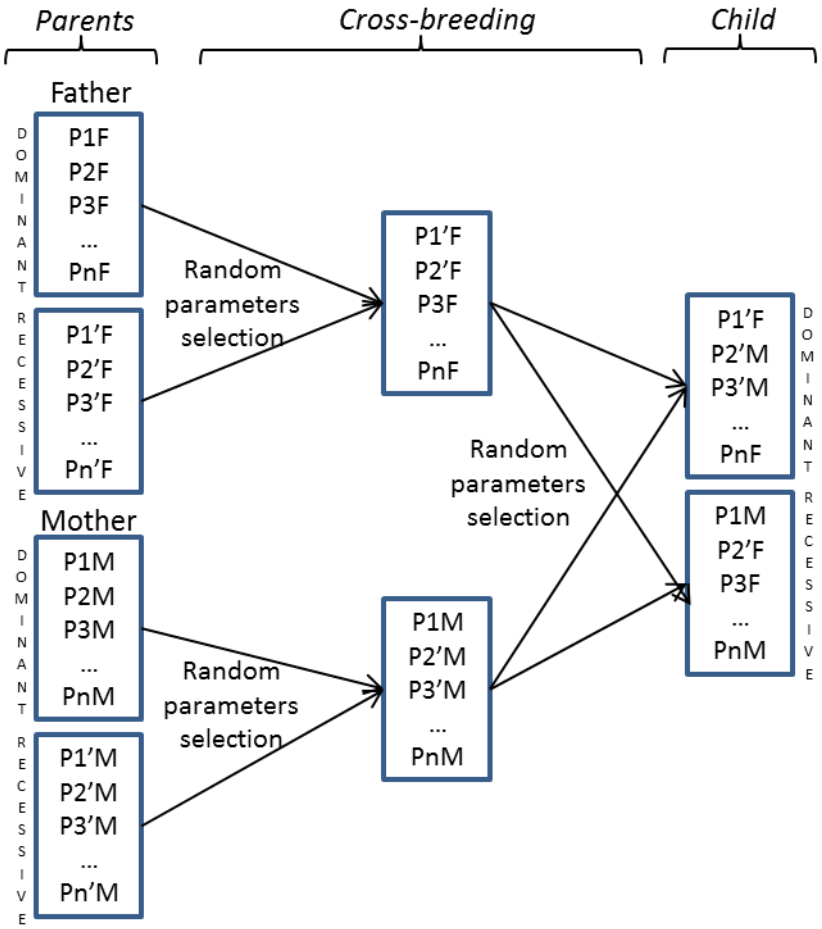

Figure 1.22: Genetic Algorithm Heterozygous Cross-Breeding Process

- Homozygous cross-breed

The homozygous cross-breed also occurs via two successive steps. As for heterozygous cross-breed, a chromosome with parameters randomly selected from father and mother dominant and recessive chromosomes is generated. Then a randomly selected α coefficient is applied to the parameters inherited for both dominant and recessive chromosomes of the child. As a result the child has two identical chromosomes. This is illustrated in Figure 1.23. This process makes it possible to prioritize the best performing individuals of the population.

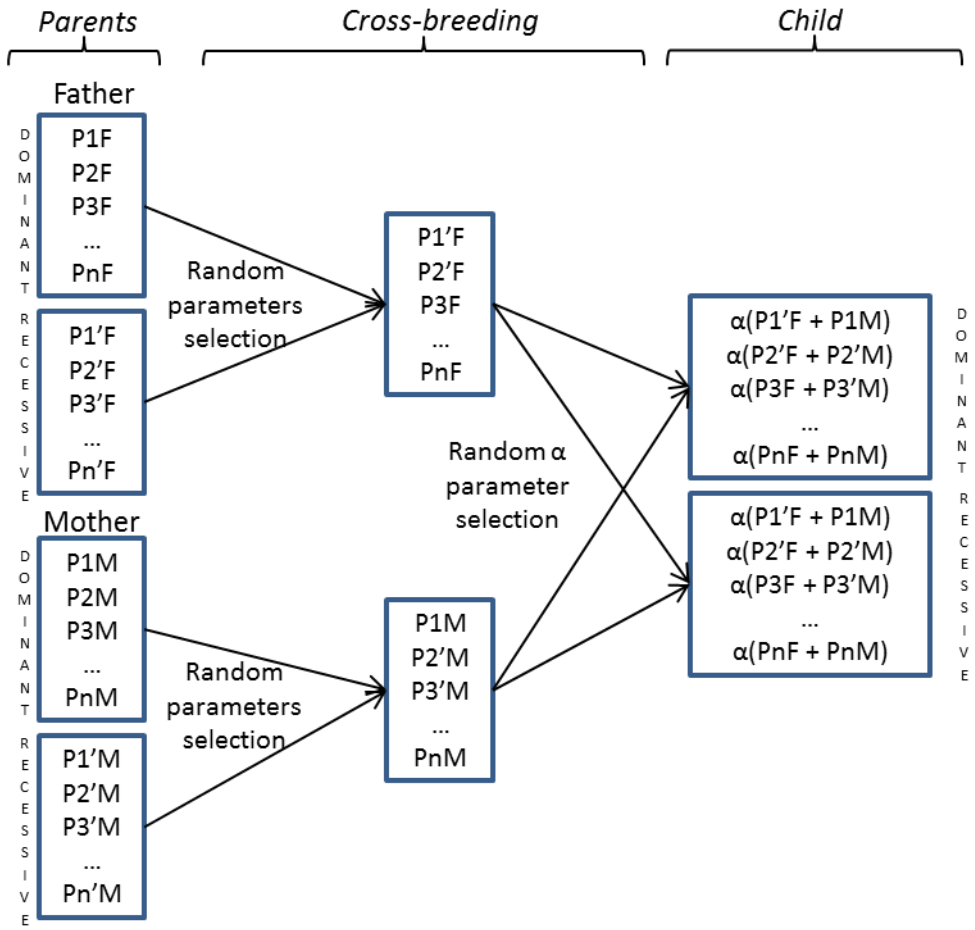

Figure 1.23: Genetic Algorithm Homozygous Cross-Breeding Process

Mutations can also apply to both cross-breeding processes. This can happen for one parameter only or for the entire structure. Mutations are random processes occurring at a relatively low rate. This enables a broad exploration of the optimization domain and makes it possible to avoid finding local optimum only. Overall this ensures genetic algorithms are robust and efficient optimization method as natural systems are, and easily applicable to a wide variety of environments.

Specific adaptations of the genetic algorithm implemented in Vizir are developed to handle the optimization of discrete problems for HCSMR core design. This is introduced in Part Three.

5. 4. 5 Optimization method comparison and accuracy

With multi-objective optimization the comparison of results is complex. A variety of solutions – Pareto optimal individuals – are proposed by each method. Voutchkov [108] introduced criteria to assess optimization method performances:

- Richness: the majority of individuals should be located in the Pareto front;
- Diversity: fronts should be spread with consideration of all objectives;
- Spacing: individuals should be spread along the Pareto front rather than being grouped in clusters;
- Optimality: better optimization methods produce fronts that dominate fronts obtained with another method;
- Globality: as with single objective optimization it is possible to reach local optimum only in multi-objective optimization. This could for example result from using a population too small for the optimization. A better optimization method would ensure the Pareto fronts obtained are global and not local;
- Robustness: due to the meta-heuristic characteristic of multi-objective optimization the exercise must be repeated to confirm the optimization results. Robustness describes the better method when no substantial variation is obtained from an iteration to the next;
- Efficiency and convergence: better optimization method will converge using fewer evaluations.

Quantitative methods [109] bring additional information to assess complex situations. Overall a visual observation remains at first a reliable approach to evaluate the optimization outcomes relevance. Visual observation is also appropriate for simple comparisons.

Chapter 6: PART ONE CONCLUSION

In this first part of the thesis, the motivations to design the HCSMR core are introduced. The HCSMR find its roots at the intersection of SMR and high-conversion light water reactors. A renewed interest for SMR development is observed worldwide. Small core designs bring a new paradigm for nuclear power development. SMRs have passive and intrinsic safety systems, their modularity and simplification, compared to large reactors, advocates for their development. Challenges also exist on the journey toward SMR deployment. The required licensing schemes and business models dedicated to SMRs are not proven yet.

From a reactor physics and fuel management perspective SMRs have low fuel efficiency. The reduced size of the core increases neutron leakage and hence decreases neutron economy. Moreover designers' search for long irradiation cycles fosters fuel management with low shuffling rate, as with batch cores. This reduces the final discharge fuel burnup and fuel efficiency. The HCSMR core aims at tackling those limitations to improve fuel utilization of small cores.

The approach studied in this work focuses on applying high conversion light water reactors' characteristics to small core designs. The high conversion behavior is obtained via a reduction of neutron moderation, mostly attained by tightening the fuel rod pitch. This hardens the neutron spectrum and enables better utilization of the fuel loaded. Such cores are also referred to as under-moderated designs.

HCLWR cores have been studied for many years but so far were not developed industrially as they also have challenges. HCLWR designs' main limitation lies in their behavior in transient situations and in particular in case of loss of coolant as the void coefficient tends to turn positive due to the fuel and core characteristics. To prevent this and ensure a negative void coefficient at all times, various strategies were implemented in previous designs. For the HCSMR the small size of the core itself is an added value to keep a negative void coefficient, since the neutron leakage increase becomes an advantage in voided situations. Similar designs to the HCSMR concept are not found in existing literature.

The review of existing HCLWR designs enables the identification of a starting point to design the HCSMR core. It also permits the analysis of the most promising solutions for application on small cores. The introduction of fertile material is its main illustration. The benefit of loading fertile fuel assemblies for the HCSMR core will be further studied. The introduction of axial layers of fertile material observed in previous designs is not selected however, due to the reduced core height of SMRs. An additional hybrid solution to increase radial heterogeneity in MOX fuel via the introduction of fertile fuel rod will also be considered.

In the first part of this thesis the SMR600 design is also introduced for benchmark purposes. It aims at setting a reference to compare PWR SMR and HCSMR design performances on natural uranium consumption and conversion factor. The SMR600 characteristics are mostly based on the mPower and Westinghouse SMR designs.

The fuel is standard 17x17 with enriched UO_2 and reduced height of 220 cm. The core is made of 69 fuel assemblies and is rated at 600 MW thermal. Two fuel management approaches are considered: a batch fuel management and a "1/2" fuel management approach. The associated cycle lengths reach 924 EFPD and 633 EFPD respectively for conversion factor of 0.63 and 0.48. The corresponding natural uranium needs for the SMR600 amount to 43 tUnat/TWhe with a batch fuel management and 30 tUnat/TWhe when half of the core is reloaded at each cycle. Fuel reprocessing is not considered to derive those values, following the fuel cycle strategies of most advanced iPWR designs.

Using the SMR600 core performances evaluation, a starting point for HCSMR core optimization is defined. The characteristics identified in previous designs, together with the author's personal engineering judgment, made it possible to derive the HCSMR basic characteristics. The core thermal power is rated at 600 MW for an electrical output of 200 MW. 61 fuel assemblies based on a triangular lattice form the core. Each fuel assembly has up to 468 fuel rods with a reduced pitch which enables the reduced moderation behavior. The core height is set at 220 cm and the use of heavy reflectors is considered. Selected characteristics will be further optimized.

Indeed beyond defining a first image of the HCSMR core, this work aims at optimizing the HCSMR core. Under-moderated cores have a high level of complexity. Their optimization is therefore complex and the use of robust optimization methods adds value to design the HCSMR core. For this purpose an analysis of state-of-the-art multi-objective and multi-parameter optimization methods is carried out in this first part. It covers the review of methods to design research plans, perform sensitivity analysis, create surrogate models and perform optimization itself.

The utilization of advanced optimization methods or global methods is not new in engineering but was so far not often considered for reactor core design. This can be explained by the high degree of complexity of reactor core design and in particular the non-linearity and discrete behavior of several aspects in core design. This challenges in particular the optimization method available nowadays and required to strengthen the boundary conditions to use those methods for the HCSMR core design.

To summarize, in this first part of the thesis the motivations and boundary conditions to develop the HCSMR design are introduced. A review of the interest for SMR development, their intrinsic advantages but also the challenges towards their development are discussed. Based on the review of selected existing SMRs, previous HCLWR designs and optimization methods, guidelines for the HCSMR design development are derived.

The next part focuses on neutron-physics. After some theoretical introduction on the science of neutrons in nuclear core, the model and methods used to compute the HCSMR design are reviewed.

Part Two

Neutron-physics Models

TABLE OF CONTENTS

Chapter 7: PART TWO INTRODUCTION

Nuclear core design requires a reliable estimation of neutron production and losses, to determine essential design characteristics and performances. For a given nuclear system the neutron balance is crucial to quantify the reactivity, the power distribution and associated safety margins, to be evaluated with a given accuracy. In this work both deterministic and stochastic or Monte-Carlo methods are used to compute the neutron flux in the HCSMR core as well as the derivative quantities, for example reaction rates and isotopes concentrations.

Deterministic methods aim at solving numerically neutron physics equations. The complexity of the equations governing the neutron population behavior and of the system considered requires using assumptions when deriving the neutron flux. This leads to numerical results containing controlled bias but enables deterministic methods to give fast outcomes.

On the other hand the Monte-Carlo (MC) approach focuses on modeling the nuclear system (almost) exactly and simulates single particle life many times to get large statistics. This approach requires a large number of evaluations. It makes it possible however to get "reference results", since few approximations are used to derive the solution. The results obtained with MC computations are used to benchmark and validate the deterministic models.

For this work aimed at designing the HCSMR core, adequate neutron physics models must be developed. The computation schemes developed must be reliable enough to ensure the adequacy of the optimizations performed. However, highly accurate neutron-physics computation schemes are not mandatory. A trade-off must be reached. Nevertheless, the simulations bias should be known and considered at the optimization step. Thresholds at 500 pcm for nominal reactivity comparison and 3 % for reaction rate comparison are set for maximum difference between stochastic and deterministic results. Those maximum values are not target values but envelope indicators.

This section aims at validating the deterministic computational methods developed to model the HCSMR cores based on comparison with Monte-Carlo methods. An introduction of both deterministic and stochastic computation schemes is given before introducing results for the HCSMR design, first at the fuel assembly level and then at core level as highlighted in Figure 2. 1.

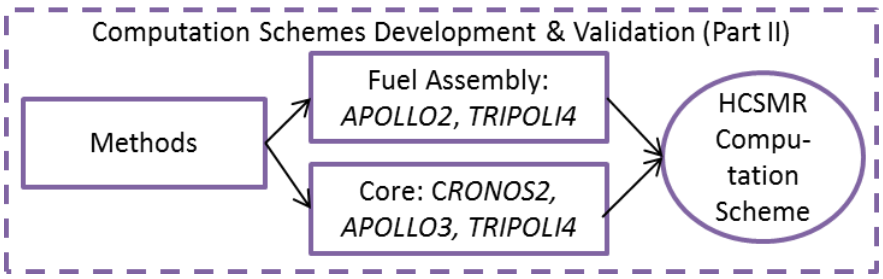

Figure 2. 1: Overview of the HCSMR Computation Schemes Development

An introduction to the fundamentals of neutron-physics focused on the use in this work is presented hereafter.

7. 1 INTRODUCTION TO NEUTRON-PHYSICS

Neutrons are subatomic neutral particles. Their properties and behavior are described by nuclear physics laws [112]. Several authors published comprehensive introductions to neutron-physic fundamentals including [113] [87]. A brief summary is presented hereafter to introduce the main concepts used in this work.

At a given time t and space point $\vec{r}$, the reaction rate τ_i between neutrons traveling at V speed in the direction $\vec{\Omega}$ and an isotope i (assumed motionless) is derived as the product of the neutron density n, the neutron speed V, the isotope density C_i and the microscopic cross section of the i isotope σ_i for a given reaction:

$$\tau_i = nVC_i\sigma_i \quad (2.1)$$

The cross section σ_i quantifies for the isotope i and a given event r (r=fission, scattering or capture) the intrinsic probability of the event r to occur with an incident neutron $n(E)$. The cross section has a surface unit (usually cm^2) and can be seen as a target surface for a neutron reduced to a point size for a given event r. The cross section σ_i depends on the incident neutron energy E and the medium temperature.

Equation (2. 1) can be extended to the total reaction rate between neutrons and the considered medium in which several isotopes are present is given by:

$$\tau = nV \sum_i C_i\sigma_i \quad (2.2)$$

The macroscopic cross section Σ is defined as:

$$\Sigma = \sum_i C_i\sigma_i \quad (2.3)$$

The neutron flux Φ can then be derived from (2. 2) and (2. 3) as:

$$\tau = \Sigma\,\Phi \quad (2.4)$$

The neutron flux unit is $m^{-2}.s^{-1}$. It is a scalar quantity depending on the direction $\vec{\Omega}$.

Three types of interactions between neutron and matter can occur. A neutron can be absorbed by an isotope and disappear. This reaction is usually referred to as *absorption*. A simple collision of a neutron on an isotope can occur. The neutron direction or speed can be modified after the collision. This event is referred to as a *scattering* process. Fission is the third possible interaction type and is usually noted simply as *fission*. The fission process will generate new neutrons immediately after the fission. Those neutrons are referred to as *prompt neutrons*. Fission products results of the fission process. Those products are isotopes which can generate additional neutrons by radioactive decay. The fission products are referred to as *precursors* and the emitted neutrons as *delayed neutrons*.

The neutron balance can be derived with the fundamental equation of neutron-physic, the Boltzmann equation:

$$\underbrace{\frac{1}{V}\frac{\partial\Phi(\vec{r},E,\vec{\Omega},t)}{\partial t}}_{\text{Flux variation}} = \underbrace{-\vec{\Omega}.\vec{\nabla}\,\Phi(\vec{r},E,\vec{\Omega},t)}_{\text{Propagation (leakage)}} \underbrace{-\Sigma_t(\vec{r},E)\,\Phi(\vec{r},E,\vec{\Omega},t)}_{\text{Absorption and scattering disappearance}} +$$

$$\underbrace{\int_0^\infty dE' \frac{1}{4\pi}\int_{4\pi} d\Omega' \Sigma_s(\vec{r}, E' \rightarrow \mathrm{E}, \overrightarrow{\Omega'} \rightarrow \vec{\Omega})\, \Phi\left(\vec{r}, E', \overrightarrow{\Omega'}, t\right)}_{\text{Scattering production}} +$$

$$\underbrace{(1-\beta)\int_0^\infty dE' \chi_p(\vec{r}, E' \rightarrow \mathrm{E}) \upsilon \Sigma_f(E', \vec{r})\, \frac{1}{4\pi}\int_{4\pi} d\Omega' \Phi\left(\vec{r}, E, \vec{\Omega}, t\right)}_{\text{Prompt fission}} +$$

$$\underbrace{\sum_l \chi_l(\vec{r}, \mathrm{E})\, \lambda_l\, \mathrm{C}^l(\vec{r})\, \mathrm{df}}_{\text{Delayed neutrons}} \qquad (2.5)$$

Equation (2. 5) is solved together with the Bateman equation governing the evolution of C^l:

$$\underbrace{\frac{\partial C^l(\vec{r})}{\partial t}}_{\text{Inertia}} = \underbrace{-\lambda_l C^l(\vec{r})}_{\text{Radioactive decay}} + \underbrace{\beta_l \int_0^\infty dE' \upsilon \Sigma_f(\vec{r}) \frac{1}{4\pi}\int_{4\pi} d\Omega' \Phi\left(\vec{r}, E', \overrightarrow{\Omega'}, t\right)}_{\text{Fission products production}} \qquad (2.6)$$

With:

- $\vec{r}$, E, $\overrightarrow{\Omega}$, t are respectively the position, energy (or speed), propagation direction and time variables;
- Σ_t is the total macroscopic cross section gathering fission, absorption and scattering reactions;
- $\Sigma_s(E' \rightarrow \mathrm{E}, \overrightarrow{\Omega'} \rightarrow \vec{\Omega})$ is the differential scattering macroscopic cross section from energy E' and direction Ω' to the energy E and direction Ω ;
- $\upsilon\, \Sigma_f$ is the product of the fission macroscopic cross section and the average number of neutron generated at each fission;
- β_l is the proportion of neutron generated by delayed fission via the decay of a precursor;
- β is the sum of β_l;
- $\chi_p(E' \rightarrow \mathrm{E})$ is the probability for a prompt neutron to be at energy E when generated by fission of a neutron at energy E';
- C^l is the concentration of delayed neutron precursors l;
- λ_l is the decay constant of delayed neutron precursors l;
- $\chi_l(E)$ is the probability of a delayed neutron emitted by a precursor l being of energy E.

The neutron flux in a core $\Phi\left(\vec{r}, E, \vec{\Omega}, t\right)$ can be derived from (2. 5) and (2. 6) $\frac{\partial C^l(\vec{r})}{\partial t} = -\lambda_l C^l(\vec{r}) + \beta_l \int_0^\infty dE' \upsilon \Sigma_f(\vec{r}) \frac{1}{4\pi}\int_{4\pi} d\Omega' \Phi\left(\vec{r}, E', \overrightarrow{\Omega'}, t\right)$:

$$\overrightarrow{\Omega}\, \vec{\nabla}\, \Phi\left(\vec{\mathrm{r}}, \mathrm{E}, \vec{\Omega}, \mathrm{t}\right) + \Sigma_{\mathrm{t}}(\vec{\mathrm{r}}, \mathrm{E}) \Phi\left(\vec{\mathrm{r}}, \mathrm{E}, \vec{\Omega}, \mathrm{t}\right) =$$

$$\int_0^\infty dE' \frac{1}{4\pi}\int_{4\pi} d\Omega' \Sigma_s(\vec{r}, E' \rightarrow \mathrm{E}, \overrightarrow{\Omega'} \rightarrow \vec{\Omega})\, \Phi\left(\vec{r}, E', \overrightarrow{\Omega'}, t\right) +$$

$$\int_0^\infty dE' \chi\left(\vec{r}, E' \rightarrow E\right) \upsilon \Sigma_f(\vec{r})\, \frac{1}{4\pi}\int_{4\pi} d\Omega' \Phi\left(\vec{r}, E', \overrightarrow{\Omega'}, t\right) \qquad (2.7)$$

With $\chi\left(\mathrm{E}' \to \mathrm{E}\right)$ the probability of a prompt or delayed neutron being at energy E when generated by the fission of a neutron at energy E'.

The equation (2. 7) can be considered in a stationary situation. The dependency in time is removed and the k_{eff} is introduced. For preliminary core design purposes stationary computations are enough. Studying rapid transient would require considering the time dependency of the Boltzmann equation. This is not part of this work's scope. The k_{eff} represents the average number of neutrons generated by a fission leading to a new fission event. The stationary neutron flux in a core can then be derived as:

$$\overrightarrow{\Omega}\,\vec{\nabla}\,\Phi(\vec{r},E,\vec{\Omega}) + \Sigma_t(\vec{r},E)\Phi(\vec{r},E,\vec{\Omega}) = \int_0^{\infty} dE' \int_{4\pi} d\Omega' \Sigma_s(\vec{r},E' \to \mathrm{E},\overrightarrow{\Omega'} \to \vec{\Omega})\,\Phi\left(\vec{r},E',\overrightarrow{\Omega'}\right) + \frac{1}{k_{eff}} \int_0^{\infty} dE' \chi\left(\vec{r},E' \to E\right) v\Sigma_f(\vec{r})\,\frac{1}{4\pi} \int_{4\pi} d\Omega' \Phi\left(\vec{r},E',\overrightarrow{\Omega'}\right) \quad (2.8)$$

k_{eff} indicates how stable the reactor system is: $k_{eff} = 1$ is a critical or stationary system. $k_{eff} > 1$ represents an over-critical system – the neutron population increases whereas $k_{eff} < 1$ indicates an under-critical system – the neutron population decreases.

The stationary Boltzmann equation is resolved by discretizing the $\vec{r}, E$ and $\vec{\Omega}$ variables in an iterative manner using neutronic codes. The space variable $\vec{r}$ often gathers several geometric regions where the neutron flux is assumed similar. It is referred to as a geometrical homogenization. The variable E uses energy groups to discretize the neutron energies. It is a necessary simplification of the continuous energies observed in reality. The energy group's choice, both in term of number and characteristics, is critical knowledge in neutronics as it directly impacts the self-shielding approach and the results obtained. The angular variable $\vec{\Omega}$ is handled with two approaches in this work:

- The diffusion approximation is used. The flux is considered isotropic. The scattering cross section Σ_s is assumed isotropic and $\Phi(\vec{r},\mathrm{E}') = \frac{1}{4\pi} \int_{4\pi} \mathrm{d}\Omega' \Phi\left(\vec{r},\mathrm{E}',\overrightarrow{\Omega'}\right)$. Using the Fick's law on the relationship between flux and current, the term $\overrightarrow{\Omega}.\vec{\nabla}\,\Phi(\vec{r},E,\vec{\Omega},t)$ becomes $-\nabla\,\mathrm{D}(\vec{r},E)\,\nabla\Phi(\vec{r},E')$ with D the diffusion coefficient. Considering Σ_t the total macroscopic cross section D can be expressed as $D = \frac{\Sigma_s}{3\Sigma_t}$ [87].
- A transport computation. Several transport methods can be implemented. In this work transport is realized mainly with the methods of characteristics (MOC) and the SN method, solving the transport equation for a finite number of $\vec{\Omega}$.

The computations are usually performed using two steps as described in the next section. Each step can use different methods of resolution of the Boltzmann equation. In general the first level starts with a spatial, angular and energetic discretization at a fuel assembly level using a simplified geometrical environment. At this first level a transport computation in fundamental mode is performed. The cross sections obtained are then used in a second step at the core level with less refined spatial, angular and energetic discretization often using the diffusion approximation to handle the angular variable of the Boltzmann equation.

Chapter 8: COMPUTATION SCHEME OVERVIEW

Figure 2. 2 introduces respectively the deterministic and Monte-Carlo code systems used to simulate the HCSMR core. Further details are given in the following paragraphs.

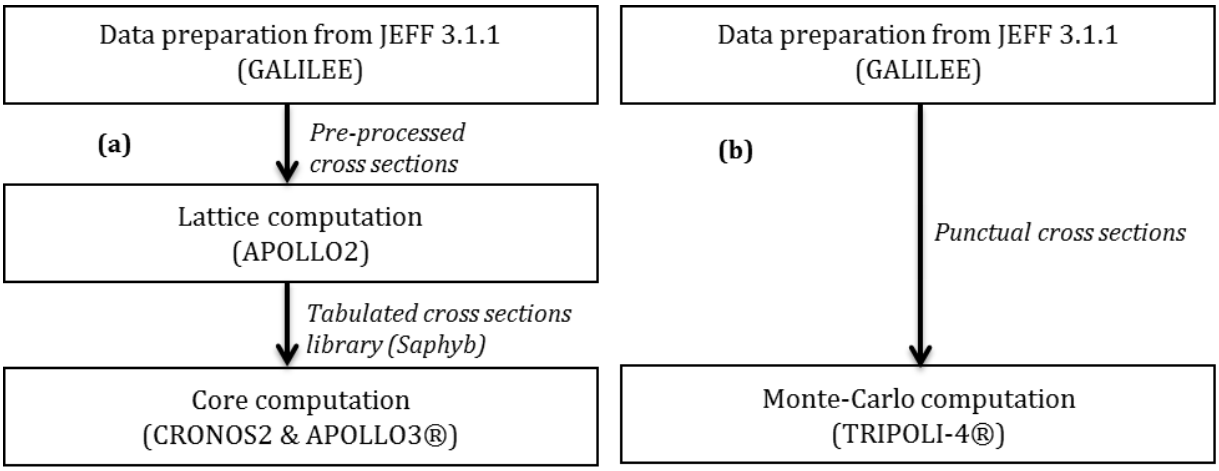

Figure 2. 2: (a) Deterministic and (b) Stochastic Computation Scheme Overview

8. 1 CROSS SECTION LIBRARY

The reference cross-section library is based on JEFF.3.1.1 [114] evaluations. For Monte-Carlo computations the CEA512 pointwise cross section [115] library is used. For deterministic computations the library CEA2005V4 [114] containing multi-energy dependent cross sections and coherent with the CEA512 library is used. Both libraries are prepared using the same approach based on the tool GALILEE [116] developed at CEA. This enables a good adequacy of both libraries, limiting the source of errors and bias due to cross section preparation.

8. 2 TRANSPORT CODE APOLLO2

APOLLO2 is a 2D spectral transport code developed by CEA. Its structure is modular and it has been validated for several applications. The APOLLO2 code is currently used for both research and industrial purposes in various situations [117]. The Boltzmann equation can be solved using the Pij method or the highly accurate method of characteristics (MOC).

The SHEM [118] multi energy group mesh is used for the HCSMR computations. It is optimized for the analysis for LWR reactor. Below 22.5 eV only a Doppler broadening is performed removing the need for an explicit self-shielding calculation.

The cross sections prepared with APOLLO2 at 281 energy groups (SHEM meshing) are collapsed at 2, 8 or 26 groups for the evaluations at the core level using CRONOS2 or APOLLO3®. Tabulated cross section library, called *spahyb*, are prepared containing various fuel assembly conditions characterized by different burnup, fuel temperature and moderator density.

8. 2. 1 Geometry

The HCSMR FA geometry and characteristics are introduced in §4. 2. 1. The FA is hexagonal and contains 13 layers of fuel rods, hence 469 fuel rod or control rod cells. The geometry computed is 1/6 of a FA with the geometry being 1/12 mirror symmetric by design. Each fuel rod is divided into four circumferential regions, giving a total of 176 regions to be depleted. HCSMR fuel assemblies containing fissile material are computed in infinite medium with periodic boundary condition.

For HCSMR FA containing only fertile material a surrounding fissile medium is added, forming a cluster as shown in Figure 2. 3. Periodic boundary conditions are applied to the cluster. A representative MOX medium is used for the fissile medium: a reference HCSMR MOX FA at 30 MWd/kgHM.

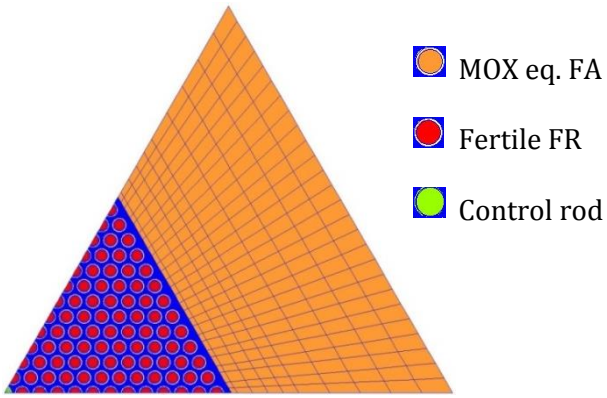

Figure 2. 3: HCSMR Fertile Fuel Assembly Cluster Overview.

8. 2. 2 Self-Shielding

Self-shielded cross sections are computed using the Livolant-Jean-Pierre method. Collision probabilities (Pij) are used to preserve space-dependent multi-group reaction rates. Fuel rods with similar flux magnitudes are grouped and treated together to limit the cost of the self-shielding computation. The resonances of heavy isotopes ^{235}U, ^{238}U, ^{238}Pu, ^{239}Pu, ^{240}Pu, ^{241}Pu, ^{242}Pu, and ^{241}Am as well as Zirconium isotopes for fuel rod cladding are treated with the equivalent mixture method [119] to consider the resonance overlap between these strongly resonant isotopes.

The shelf-shielding computations are performed using assumptions to group similar medium. Instead of considering every medium on its own, 44 groups of mediums are individually self-shielded. Forty-four groups corresponds to 11 types of rods times 4 circumferential regions. The groups are selected to gather fuel rods with similar neutron flux and fission rate conditions. The regions presented in Figure 2. 4 are used for the reference HCSMR fuel assembly. Each color represents one of the 11 self-shielding groups.

The definition of the aggregated geometry was tested to be increased to 12 and 13 groups of fuel rods with similar neutron-physical characteristics, i.e. 48 and 52 self-shielding regions

respectively. This impacted the results at step 0 by less than 2 pcm. Similarly, the number of groups was decreased to 10 and 9. This degraded the results by 10 pcm. No substantial impact of the shelf-shielding regions on the radial power distribution was observed.

Since computing time increases drastically as the number of self-shielded regions increases, it was eventually decided to keep the number of self-shielded regions to 11 for the HCSMR reference fuel assembly. This is a trade-off between computing costs and the results' accuracy.

The HCSMR HET FA uses specific shelf-shielding groups of fuel rods with similar neutron-physical characteristics to reflect the presence of fertile fuel rods. In this case, 13 groups of FRs are used as shown in Figure 2. 4 (right).

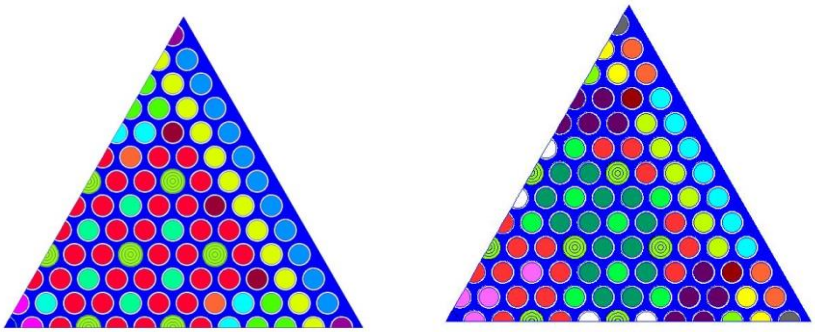

Figure 2. 4: HCSMR Assembly (left) 11 and (right) 13 Self-Shielding Groups.

For both cases since the HCSMR has 13 rows of fuel rods, a 14th row of hexagonal cells has been added to capture the water gap between fuel assemblies for the self-shielding Pij evaluation.

A simplified self-shielding geometry was used for fuel assembly optimization. Only 2 self-shielding groups were considered with one group for the fertile fuel rods and one group for the fissile fuel rods. The relevance of this approach is shown in Chapter 9.

For fertile fuel assembly computations, a specific geometry is used for the self-shielding computations with fuel rods grouped in six radial layers.

8. 2. 3 Flux Computation

Assembly-wide neutron flux is calculated with the highly accurate method of characteristics (MOC) using linear sources enabling fine space discretization of the assembly's heterogeneities [120]. A tracking with a distance between two tracks $\Delta R = 0.1$ cm and azimuthal number of angle $\Delta \varphi = 24$ are used. Cross sections are developed at order 3 of the Legendre polynomial representation. Those parameters are optimized to obtain a good trade-off between result accuracy and computation time.

Infinite medium computations are performed using periodic boundary conditions. The neutron leakage rates are adjusted for APOLLO2 critical computations. The material buckling coefficient B2m defined as the ratio between neutron leakage and the diffusion coefficient is determined by successive iterations. Such computations (B2 critical) are used to compute FA performances for optimization purposes as well as to prepare tabulated cross sections used at the core level. For

validation purposes and comparison with TRIPLOI4® a B2 null is used: leakage is set to zero using optical reflection on volume surface.

Depletion steps are performed at almost every 2.5 MWd/kg. Smaller steps are defined at low burnup to adequately simulate fission products' first production and improve the convergence of the depletion calculation. Resonant isotopes are self-shielded at every depletion step with the flux being recalculated using the method described above. HCSMR FAs are depleted up to 180 MWd/kg. This maximum burnup value is rather high but makes it possible to cover a large burnup domain sometimes required at the core computation step.

8. 2. 4 Saphyb Creation

Saphyb are multi-parameter tabulated libraries. Their purpose is to transmit cross sections and related information prepared with APOLLO2 to core computations performed with CRONOS2 or APOLLO3®. Saphybs are generated with APOLLO2 using a two steps process.

First a nominal depletion of the fuel assembly is carried out. Boltzmann and Bateman equations are solved to derive critical flux at each burnup step as described before. Mediums are stored at each depletion step.

Based on those stored medium, branch computations are then performed in a second step. Branch computations aim at covering the scope of operating conditions to be evaluated at the core level. The fuel temperature, moderator density and material depletion are varied and for each condition a new critical flux is computed. The parameters considered for HCSMR saphybs are:

- Fuel temperature: 280°C, 627°C, 800°C, 1200°C, 1800°C
- Moderator density:
    - Nominal conditions: 780.0 $kg.m^{-3}$ (269.5 °C), 760.4 $kg.m^{-3}$ (281.0 °C), 740.0 $kg.m^{-3}$ (292.0 °C),
    - Voided conditions: 76.04 $kg.m^{-3}$, 7.6 $kg.m^{-3}$, 0.76 $kg.m^{-3}$
- Burnup: 40 steps from 0 to 180 $MWd.kg^{-1}$ with maximum 2.5 $MWd.kg^{-1}$ intervals.

For each fuel assembly characteristics – materials, geometry – a specific saphyb must be created using first the nominal computation and then the branch computation. At both steps the same geometry, self-shielding and flux computation options are used. The computations are performed using 281 energy groups as previously described. An energy condensation to 2, 8 and 26 energy groups is then performed to prepare the cross sections to the required format for core evaluations using the diffusion approximation.

8. 2. 5 Reflector

Simulating accurately the reflector of a nuclear core presents challenges [121]. Historically the treatment is simplified. User-adjusted albedos were the reference to simulate the neutron reflection at the core-reflector interface. This operation was often used to tune the core simulator results to match measurements [122].

For the HCSMR design the reflector is not defined yet and is subjected to optimization of the design. Hence existing reflectors are considered as a preliminary approach. A heavy reflector based on the EPR design is used at first. Its geometry is simplified but the iron content considered is representative of the EPR heavy reflector. The iron content is then varied to assess the impact on the HCSMR core performances.

Three types of reflector must be differentiated: radial, axial bottom and axial top reflectors. Two methods were used to prepare cross-sections to simulate the reflector at the core level. Simulating the reflector aims at generating a set of cross-sections with a low number of energy groups (usually 2, 8 or 26 groups) for core evaluation. The first method is the CEA state-of-the-art approach using APOLLO2 and based on albedo conservation at the interface between the core and the reflector [123].

It consists of designing a 1D slab containing the core and reflector medium and equivalent geometry as shown in Figure 2. 5. The self-shielding computing step is performed on a simplified geometry containing only two fuel assemblies and the reflector. The equivalent mixture method [119] to consider the resonance overlap between these strongly resonant isotopes is used. The reference computation is performed using the S_N method. With an equivalence P0-S2 the sections can then be used for diffusion computations. This first method provides accurate cross sections but is rather costly to set-up.

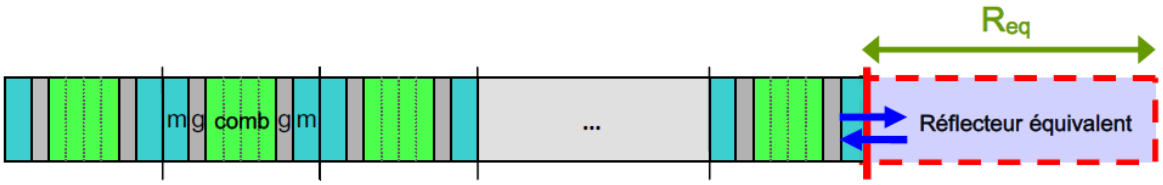

Figure 2. 5: 1D Slab Core-Reflector for Reflector Cross-Section Generation

The second approach "FA cluster approach" is based on the process used to generate HCSMR fertile FA cross sections, as introduced in §8. 2. 1. The reflector medium is located within what is the fertile fuel assembly geometry in Figure 2. 3. This region is surrounded by MOX medium. With a standard flux computation the cross sections for the reflector medium are generated. Although being mathematically not strictly correct, this method is proven to be accurate enough when comparing core evaluations. It makes it possible to quickly vary the reflector medium content and hence generation cross sections for optimization purposes at the core level, as introduced in Part Three.

8. 3 Transport & Diffusion Code CRONOS2

8. 3. 1 General Characteristics

CRONOS2 [124] is a 3D core simulator developed at CEA/SERMA. The neutron flux can be either solved with diffusion or transport methods. For this work CRONOS2 is only used in diffusion with either 2 or 8 energy groups. The fuel assemblies are represented with one or six radial meshes per FA and 16 nodes axially. Radially each hexagon is representing one fuel assembly

and is considered by itself or divided into six triangles. A reflector is modeled both radially and axially. For depletion computation, a depletion chain containing 28 isotopes (20 heavy nuclides and 8 fission products) is used. The other isotopes are grouped in a an equivalent medium with its own macroscopic cross-sections depending on the core parameters, such as burnup, fuel temperature and moderator density.

CRONOS2 uses the branch cross-sections generated with APOLLO2 via the Saphyb. The original cross-sections are condensed at either 2 or 8 energy groups. An equivalence correction to account for diffusion approximation bias on reaction rates and multiplication factor is not performed in the HCSMR computation scheme, as the neutron spectrum considered and the level of accuracy required do not make such correction mandatory.

With the diffusion method a core configuration is assessed in a few seconds. This enables CRONOS2 to run multiple calculations to simulate fuel depletion along an irradiation cycle and to perform equilibrium search computations. This latter type of computation is often repeated in this work to assess the performances of a representative core with a fuel management using multiple fuel assemblies' batches. To obtain an equilibrium core, a fuel management is repeated several times including the reload step at the end of the irradiation cycle, using always the same reload scheme. When the burnups and power distribution have converged an "equilibrium cycle" is reached. It is characterized by converged burnup values of the FA batches at the beginning of cycle (BOC) and end of cycle (EOC). The equilibrium cores obtained are then used to assess the core's characteristics and performances.

8. 3. 2 Thermal-hydraulic

A simplified thermal-hydraulic model is incorporated in CRONOS2. It is based on CRONOS2's modules THERMIC and THERMOC. It uses a 1D (z axis) 2 equations (mass and momentum) model. A 1D cylindrical resolution is also considered for fuel pins to account for thermal effects. The heat transfer coefficient between the cladding and the moderator is based on the Jens-Lottes correlation.

Although simplified this capability enables the consideration of thermal-hydraulic feedback and evaluation of neutron physic coefficients (e.g. moderator, Doppler) as the fuel and moderator temperature, as well as the moderator density, are available.

8. 3. 3 Local Heat Generation Rate

Since the fuel assembly is represented by one or six meshes radially, no pin-wise power distribution is directly available at the core level. In CRONOS2 a pin power reconstruction method does not exist yet. The optimization of the HCSMR design requires knowing the maximum linear heat rate. A simplified method is developed to calculate this quantity. This approached method might not always be conservative but enables analyzing the performance of the HCSMR optimization.

The fuel rod radial peaking factor F_{xy}^{Rod} is defined as:

$$F_{xy}^{Rod} = F_{xy}^{Core} \cdot F_{xy}^{BUgradient} \cdot F_{xy}^{mesh} \cdot F_{xy}^{Ass} \quad (2.9)$$

with:

F_{xy}^{Core} : Relative power of a fuel assembly compared to the core average power per assembly;

$F_{xy}^{BUgradient}$: Within the fuel assembly a burnup and power gradient is observed. For the HCSMR core this effect is considered with a simplified approach: the maximum 1/6th fuel assembly power compared to the fuel assembly average power is the $F_{xy}^{gradient}$ factor;

F_{xy}^{mesh}: The burnup and power gradient in the fuel assembly should on principle also consider the gradient within one computing mesh. This second order factor is neglected and fixed at one.

F_{xy}^{Ass}: Fuel rod maximum relative power compared to the fuel assembly average power computed at the lattice level with APOLLO2.

The F_{xy}^{Ass} itself is indirectly transmitted to the core computations by considering five F_{xy}^{Ass} values per FA tabulated in burnup (at 0, 10, 20, 30 and 60 MWd/kgHM). A linear interpolation is then performed to estimate the current F_{xy}^{Ass}. This approach is designed based on observations on F_{xy}^{Ass}evolution with burnup as shown in Figure 2. 6. For a FA burnup greater than 60 MWd/kgHM, the F_{xy}^{Ass} obtained at 60 MWd/kgHM is considered for the interpolation. This is a conservative approach.

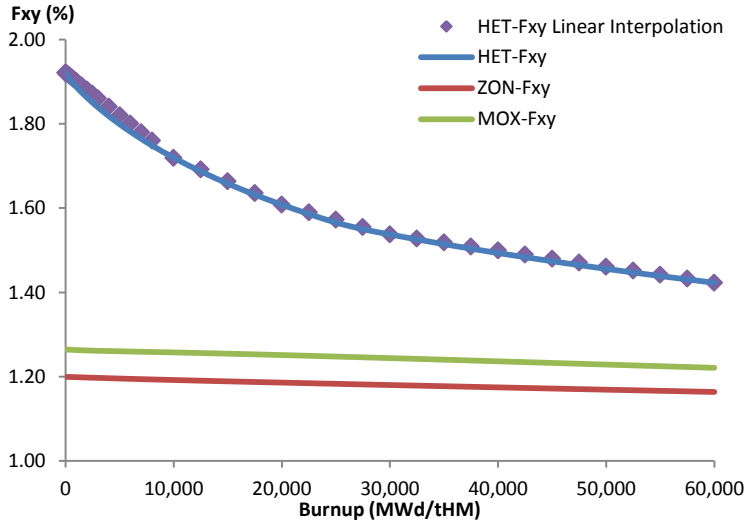

Figure 2. 6: F_{xy}^{Ass} vs. FA Burnup and Linear Interpolation

To reconstruct the maximum linear heat generation, the axial power peaking factor (F_z) is eventually considered. The maximum F_{xy}^{Core} and $F_{xy}^{gradient}$ axially are selected to derive the maximum linear heat generation rate.

8. 4 TRANSPORT & DIFFUSION CODE APOLLO3®

APOLLO3® is a 3D deterministic multi-purpose code developed at CEA [125]. As a neutron-physics lattice and core calculation tool, APOLLO3® is designed to simulate various reactor concepts. In this study APOLLO3® is used at the core level to perform evaluation with both diffusion and transport methods to solve the Boltzmann equation.

The motivation to use APOLLO3® lies in its capability to assess core configuration using transport methods. Only step 0 computations are performed with APOLLO3®. The SN transport method is used to assess heterogeneous HCSMR core configurations. It uses the MINARET solver [126] with the following options:

- Angular order: S8;
- Finite Element Method (FEM) with straight triangles;
- FEM order: 2;
- Max number of outer iterations: 150;
- Diffusion Synthetic Acceleration (DSA) method is implemented.

8. 5MONTE-CARLO CODE TRIPOLI-4®

8. 5. 1 General Characteristics

The 3-D continuous-energy Monte-Carlo code TRIPOLI-4® is developed at CEA. It aims at computing a fuel assembly or core neutron physic characteristics by evaluating different quantities named scores, such as the eigenvalue, the flux and the reaction rates. For comparison purposes in this work, TRIPOLI-4® version 10 is used in critical mode only.

The version 10 of TRIPOLI-4® incorporates the MENDEL code depletion module [115] [127]. This enables the use of TRIPOLI-4® in depletion mode. This option is used to validate the HCSMR fuel assembly computations. In total three types of computation are performed: fuel assembly in static mode, core in static mode and fuel assembly with the depletion mode. Isotherm conditions are considered for HCSMR computations with TRIPOLI-4®.

8. 5. 1. 1 Cross Sections

A punctual cross-section library based on JEFF-3.1.1 evaluations and prepared with GALILEE is used with TRIPOLI-4®. The original cross sections are the same as for deterministic evaluations performed with APOLLO2 to reduce bias for the comparison between stochastics and deterministic evaluations. The punctual cross-sections library is generated via interpolation at a target temperature for heavy isotopes while direct evaluations are used for light isotopes.

8. 5. 1. 2 Geometry

The geometry is created using the ROOT code capabilities [103]. Computations are performed on full HCSMR FA or core and axially the reference height of 220 cm is considered. For core computations the reflector geometry is simulated as in CRONOS2 or APOLLO3®: one additional

row of fuel assembly containing reflector material is added radially. Axially top and bottom reflector volumes are considered filled with reflector material. A detailed geometrical representation of reflector materials is not considered but the medium content and isotopic concentrations are similar between deterministic and stochastics models. Reflective boundary conditions are defined on all boundaries of the geometry. A 2D view of an HCSMR core prepared for TRIPOLI-4® evaluations is introduced in Figure 2. 7.

Volumes are individualized for fuel assembly computations using the depletion mode. Each fuel rod is divided into four circumferential regions. For up to 1752 regions, the coupled Boltzmann and Bateman equations systems are solved at each depletion step and the isotopic composition of all regions is updated.

At the core level, and to evaluate power peak factors, the core is axially divided into 22 meshes of 10 cm each, corresponding to the choices implemented in CRONOS2 and APOLLO3®.

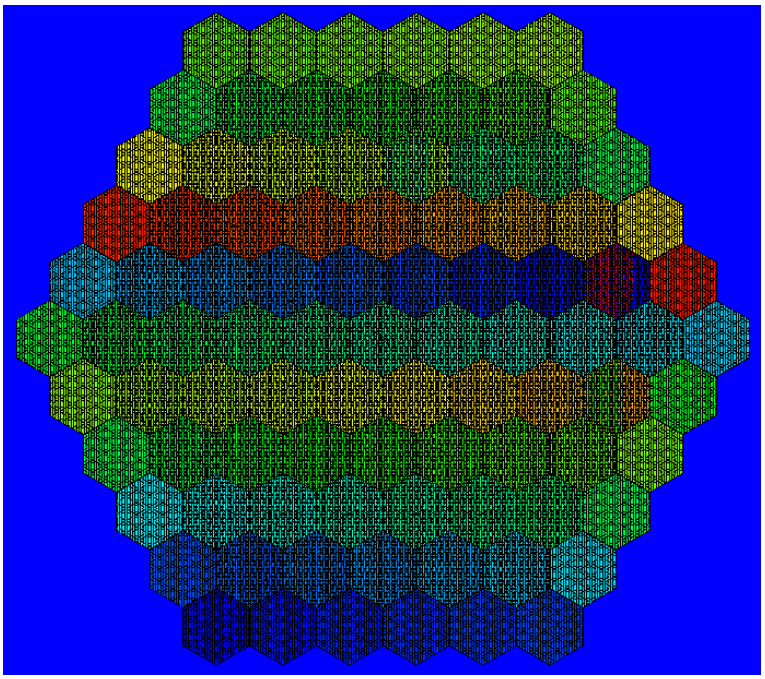

Figure 2. 7: HCSMR Core Geometry Overview for TRIPOLI-4® (a) Radial Views

8. 5. 1. 3 Options and Parameters

A thorough convergence of the results is required to consider the Monte-Carlo approach valid. This is achieved by simulating an important number of neutrons. This can either be performed by increasing the number of neutrons per batch or by increasing the number of batches computed. The 200 first batches – or cycles – computed are often discarded to reduce the bias introduced by the initial fission sources considered. The initial neutron source is isotropic and spatially distributed in all the computed volume, also known as the uniformed source assumption. Energetically it covers a broad spectrum from 10^{-11} MeV to 20 MeV via a Watt spectrum.

For validation purposes investigated here the materials concentration at step 0 and the mediums' temperatures are fixed identically for deterministic and stochastic models.

8. 5. 2 Depletion Mode

TRIPOLI-4® version 10 has a module to compute complex 3D geometry with depletion. An interface enables a coupling between TRIPOLI-4® and the depletion software package MENDEL. The coupling uses the ROOT code capabilities [103] to manage the data and computations steps. The stochastic computation with depletion is performed via a two step process.

First TRIPOLI-4® solves the Boltzmann equation of transport, as in static mode. Scores, such as reaction rates and fluxes normalized to the core power level, are evaluated for each medium to be depleted. This will serve as input to the depletion computation.

In a second step, based on those inputs MENDEL computes the depletion of each isotopic composition based on the requested burnup range. MENDEL solves the Bateman equations, for which the reaction rates from TRIPOLI-4® scores are used. By default the Euler Method (first order Runge-Kutta method) to solve the Bateman depletion equations are implemented. The flux and reaction rates given as input are considered constant during the depletion step. In other words the core is assumed quasi-static at each depletion step.

Second-order depletion methods are also available within TRIPOLI-4®. It enables the reduction of error due to the discretization but requires the increase of computation time, since the transport equations are solved two times at each burnup step. The time convergence with the first order Runge-Kutta method was analyzed.

As for APOLLO2, a depletion chain containing 160 isotopes, including actinides and 126 fission products is used. This supports the consistency of comparisons between stochastic and deterministic calculations. An overview of TRIPOLI-4® depletion mode is given in Figure 2. 8.

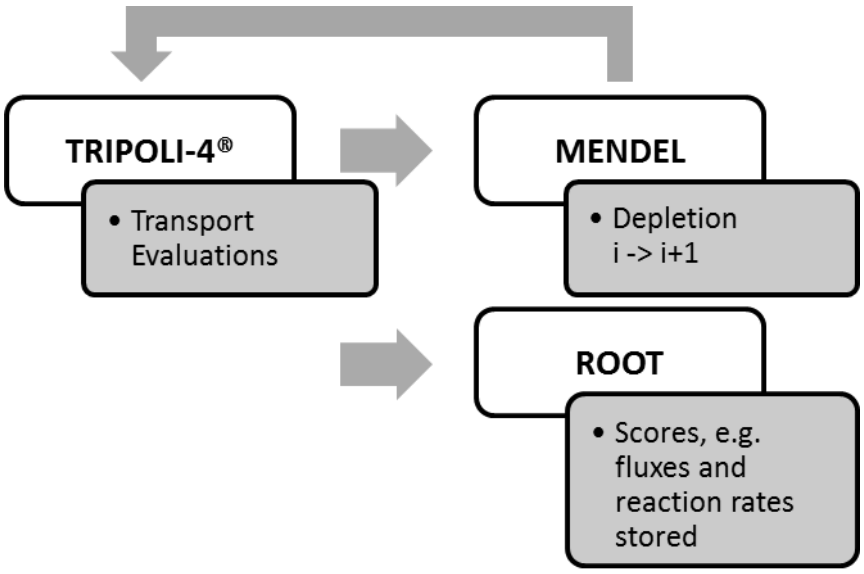

Figure 2. 8: TRIPOLI-4® Depletion Mode Overview

8. 5. 3 Uncertainties with TRIPOLI-4®

Each score evaluated using a transport computation has a statistical uncertainty sigma (σ), the standard deviation measured. The uncertainty mentioned in the results presented in the next sections always corresponds to three σ to ensure a high level of reliability in the results obtained. Assuming a Gaussian distribution, three sigma covers 99.7 % of the results.

The standard deviation can be reduced by increasing the number of neutron history simulated, either by increasing the number of particles within each batch or the number of batches. This increases also the computation time and a trade-off must be reached between uncertainty and computation cost.

The depletion simulation also contains intrinsic uncertainties. Those are due to the discretization of time and space for the Bateman equations to be solved. To limit the bias and cost the depletion steps are first optimized. This is performed with APOLLO2 to reduce the associated costs. The converged depletion steps are then applied to TRIPOLI-4®.

The propagation of uncertainties with depletion steps is a challenge. Two main approaches are available in TRIPOLI-4®. The standard method solves N replication of the transport exercise at each depletion steps. The average results are the input for the depletion evaluation using the Bateman equations. Since the Bateman equations are non-linear the propagation of uncertainties is not trivial. Hence only the static simulation's error on score is available. This method is presented in Figure 2. 9.

The method of independent simulations on the other hand enables the obtention of final concentrations with the associated uncertainty. This latter approach is preferred in this work. It consists of simulating N replica of the TRIPOLI-4® case. These replicas are started with different random seeds. N independent simulations are launched and result in N sets of scores. Combining those results makes it possible to obtain score distributions at each burnup step. With a sufficient number of N simulations, those distributions can be consider Gaussian since the simulations are all independent, and a mean value and standard deviation can be computed for each score of interest. Provided a sufficient number of independent simulations, good estimations standard deviations of scores are hence reached. This process is introduced in Figure 2. 10 and shows the steps to obtain the isotopic concentrations C_i.

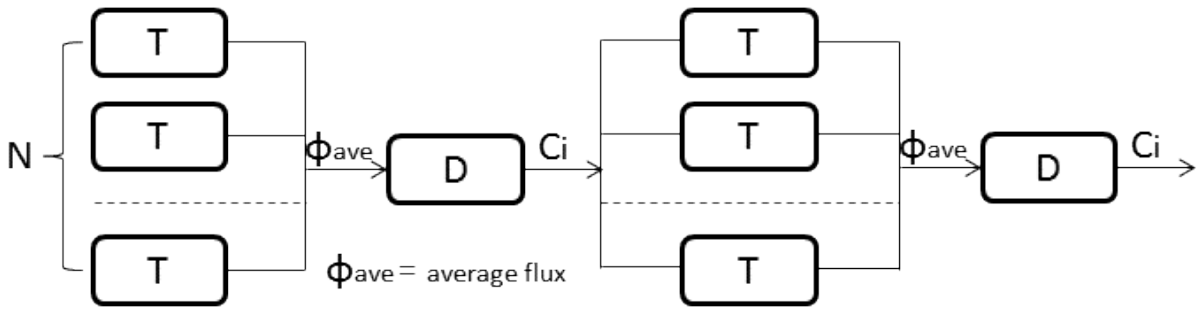

Figure 2. 9: TRIPOLI-4® Depletion using Parallel Transport

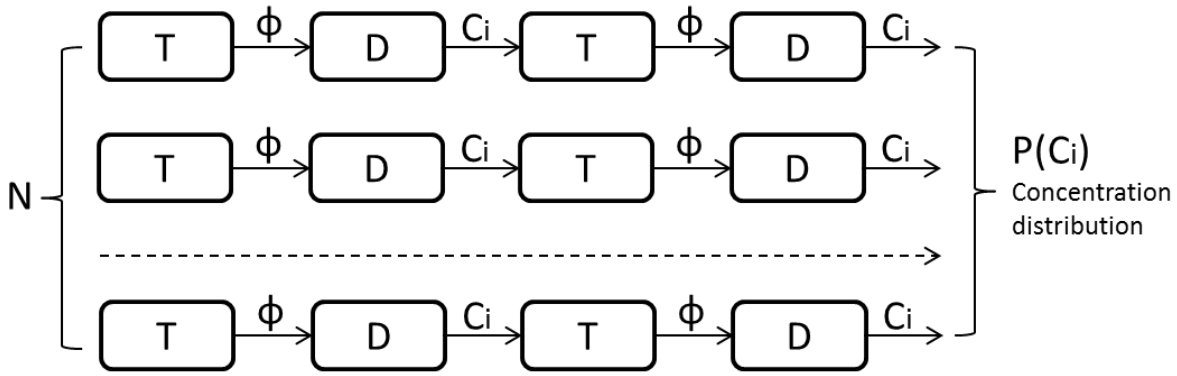

Figure 2. 10: TRIPOLI-4® Depletion using Independent Evaluations

Chapter 9: FUEL ASSEMBLY COMPUTATIONS

9. 1 VALIDATION CASES: FA GEOMETRY AND FEATURES

Three HCSMR fuel assembly designs are considered to validate the lattice computation schemes:

- The MOX fuel assembly contains one type of MOX fuel rods (MOX FA).
- The ZON fuel assembly is made of three types of MOX fuel rods with different plutonium enrichment (ZON FA).
- The HET fuel assembly contains both MOX and fertile fuel rods (HET FA). It is made of 318 MOX fuel rods and 120 fertile fuel rods for the validation exercise addressed here. The optimization of fertile fuel rod positions and quantity is one of the focuses in Part Three.

The three FA geometrical characteristics are identical and introduced in Table 1.8. A 2D view of 1/6th FA for the three FA designs is presented in Figure 2. 11 and the fuel characteristics are introduced in Table 2. 1.

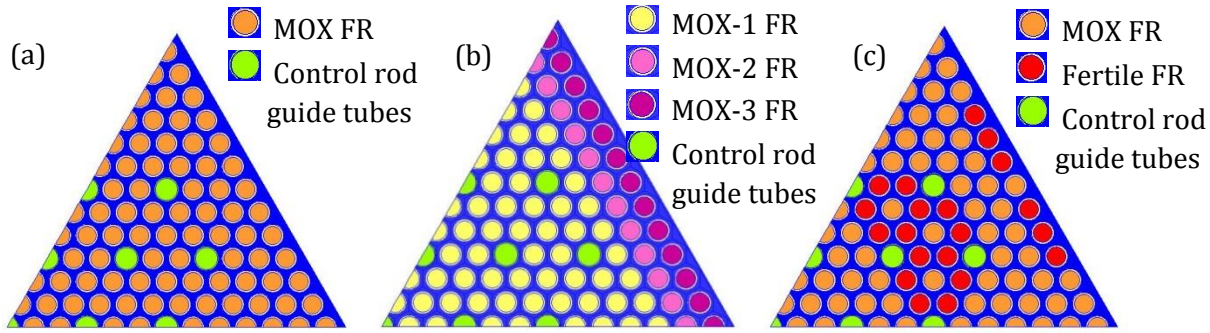

Figure 2. 11: (a) HCSMR MOX FA (b) HCSMR ZON FA (c) HCSMR HET FA 2D View

Each fuel assembly has 30 control rod holes and 1 instrumentation central hole. The average plutonium content is kept constant for the MOX and ZON FA at 19 % Pu equivalent for the validation exercises considered in this chapter. For the HET FA the equivalent Pu content is 18.2 %. The 25.0 % upper plutonium content set as technological limit prevents reaching an equivalent Pu content of 19.0 % as for the MOX and ZON FA.

Parameter	MOX FA	ZON FA	HET FA
MOX FR	438	438	318
Fertile FR	0	0	120
MOX fuel	19 % Pu	-	25 % Pu
Fertile fuel	-	-	0 % Pu
MOX-1 fuel	-	22.7 % Pu	-
MOX-2 fuel	-	12.0 % Pu	-
MOX-3 fuel	-	10.0 % Pu	-

Table 2. 1: HCSMR FA Features

The 3 enrichment zones fuel assembly (ZON FA) was designed to limit the power peak at the outer part of the fuel assembly. The water gap between two fuel assemblies increases the

neutron moderation locally. This can substantially raise the power level in the fuel rods located at the fuel assembly periphery. The 3-zones solution aims at limiting this power increase. The 3-zones definition is described in Figure 2. 11 and Table 2. 2. The choice of the plutonium enrichment triplet in the 3 zones can be optimized and is looked at in part three.

Name	Defined as	%Pu	No. fuel rods
ZON1	rows 2 to 11	22.7	300
ZON2	row 12	12.0	66
ZON3	row 13	10.0	72

Table 2. 2: ZON FA Enrichments Distribution

The neutron physic characteristics were computed for the three FA with deterministic – APOLLO2 – and stochastic – TRIPOLI-4® – methods, as introduced in the previous chapter. The adequacy of the results on reactivity, power distribution and isotopic concentration is looked at in the next section.

The author would like to highlight that some of the results presented in this section were published in ICAPP2016 [128].

9. 2 VALIDATION RESULTS

The FA reactivity is compared using the eigenvalue obtained in nominal and voided situations with deterministic and stochastic models, without neutron leakages.

For the power distribution the heavy isotope fission rates are compared. Only the fission on the following heavy isotopes is considered: ^{234}U, ^{235}U, ^{236}U, ^{238}U, ^{238}Pu, ^{239}Pu, ^{240}Pu, ^{241}Pu, ^{242}Pu, and ^{241}Am. The fission rate is selected as comparison value since it influences directly the fuel rods' power. For some comparisons the fuel rod maximum relative power compared to the fuel assembly average power computed at the lattice level with APOLLO2 (F_{xy}^{Ass}) is also used.

The isotopic concentrations are computed by tracking the mass of specific isotopes in the fuel assembly and comparing them to the total heavy metal mass.

9. 2. 1 Reactivity

For each fuel assembly type the reactivity in nominal conditions at burnup 0 MWd/kgHM (fresh fuel) is presented in Table 2. 3. The nominal conditions are characterized by a fuel temperature of 924 K and a moderator density of 760.4 kg.m^{-3}.

Parameter	APOLLO2	TRIPOLI-4® (3 σ)	Delta (pcm)
MOX FA	1.15703	1.15824 +/- 20 pcm	-90
ZON FA	1.15803	1.15941 +/- 15 pcm	-103
HET FA	1.16065	1.16450 +/- 10 pcm	-285

Table 2. 3: Reactivity Comparison between APOLLO2 and TRIPOLI-4® at 0 MWd/kgHM

9. 2 Validation Results

The reactivity delta is computed using the equation (2. 10):

$$Delta\ (pcm) = 10^5.(\frac{1}{keff_{T4}} - \frac{1}{keff_{AP2}}) \quad (2.\ 10)$$

The results obtained show a good adequacy between the deterministic and stochastic computations. A difference remains suggesting a potential for further improvement. However for the purpose of fuel assembly and core optimization in this work, the results obtained here are judged satisfying enough.

Beyond the comparison with fresh fuel at 0 MWd/kgHM, also referred to as "step 0" computation, it is relevant to observe the behavior with depleted materials. All fuel assemblies are depleted up to 60 MWd/kgHM with APOLLO2 on the one hand and with TRIPOLI-4® on the other hand. The associated methods are introduced in §8. 2 and §8. 5. The reactivity obtained is presented in Table 2. 4.

Parameter	APOLLO2	TRIPOLI-4® (3 σ)	Delta (pcm)
MOX FA	0.98942	0.99226 +/- 17 pcm	-289
ZON FA	0.99087	0.99378 +/- 14 pcm	-296
HET FA	0.98907	0.99226 +/- 15 pcm	-325

Table 2. 4: Reactivity Comparison between APOLLO2 and TRIPOLI-4® at 60 MWd/kgHM

The delta observed between deterministic and stochastic evaluations slightly increases but the values obtained are good enough to confirm the adequacy of the models developed. Those results are in line with the threshold of maximum 500 pcm set for stochastic and deterministic result differences. This is strengthened when looking at the delta evolution over the depletion steps for the MOX FA in Figure 2. 12.

A verification of the result's convergence obtained with TRIPOLI-4® is introduced in Annex E.

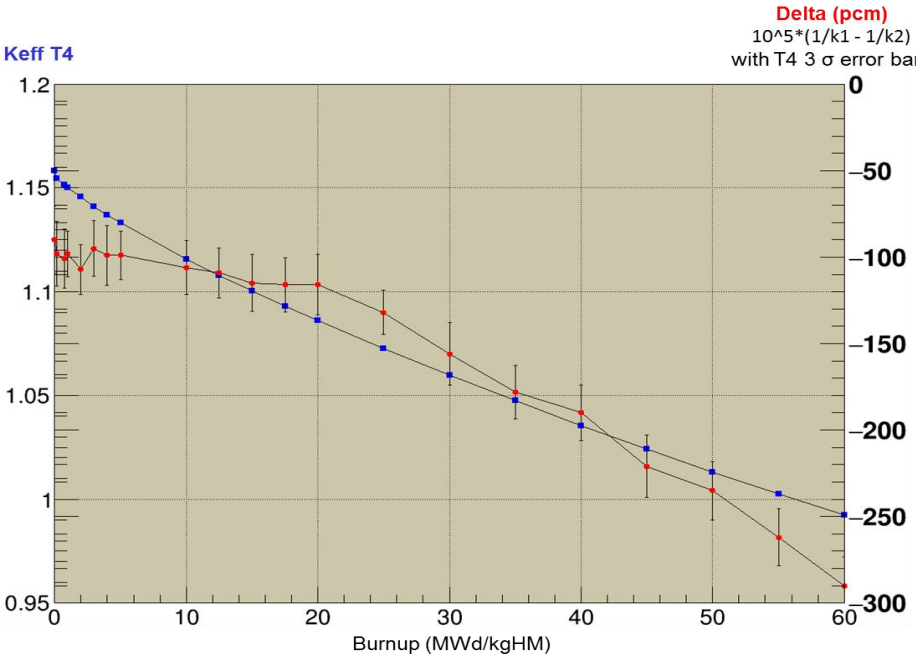

Figure 2. 12: MOX FA Reactivity vs Burnup from TRIPOLI-4® (k1) and APOLLO2 (k2)

A third type of reactivity comparison is undertaken in voided situations for the three fuel assemblies at 0 MWd/kgHM. The moderator density is set to 1 % of the nominal value. The impact of a voided situation on neutron spectrum is illustrated in Figure 2. 13. The reactivity is evaluated with both TRIPOLI-4® and APOLLO2. The results and their comparison are presented in Table 2. 5. Here also the adequacy between stochastic and deterministic methods can be observed, thus confirming the options for APOLLO2 models. Moreover the differences observed are conservative from a safety point of view: the reactivity is over-estimated by APOLLO2 compared to TRIPOLI-4® in voided situations.

The reactivity values obtained from voided situations in Table 2. 5 can be compared with the nominal value from Table 2. 3. This is presented in Table 2. 6. This gives a tendency of the fuel assembly behavior in voided conditions. It remains however an indication only since an evaluation at the core level including real neutron leakage is needed to compute the reactivity swing of a core in voided situations.

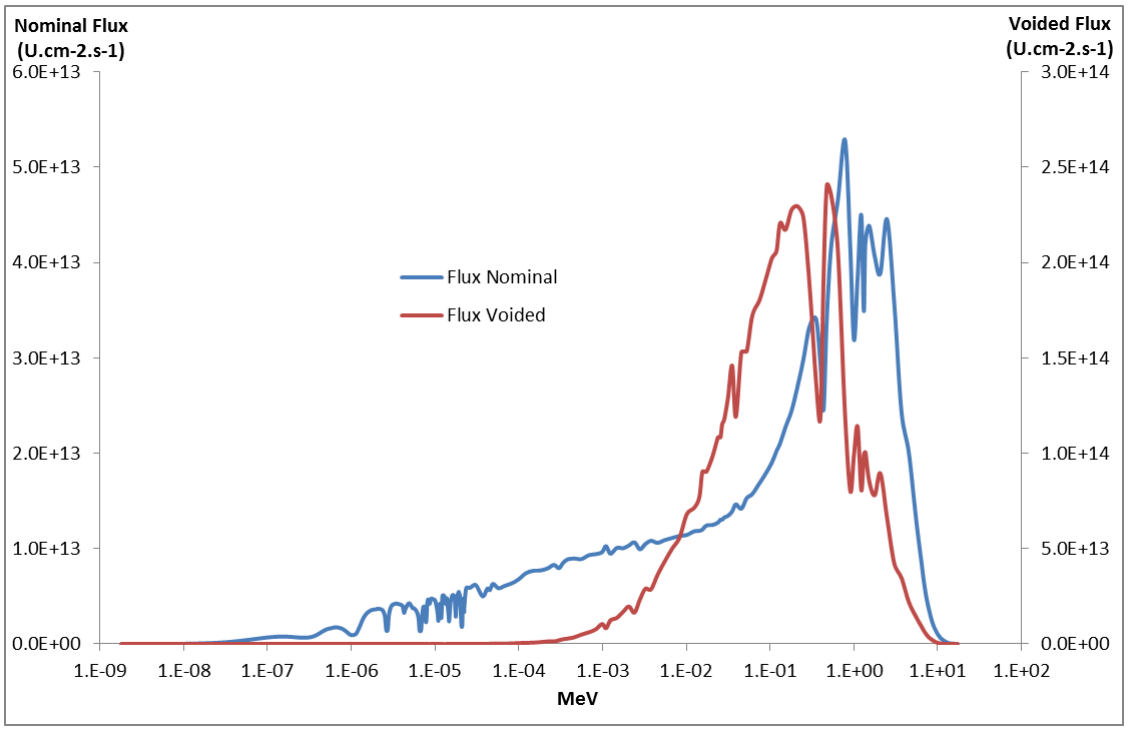

Figure 2. 13: MOX FA Flux in Nominal and Voided Situations Evaluated with APOLLO2

Parameter	APOLLO2	TRIPOLI-4® (3 σ)	Delta (pcm)
MOX FA	1.34651	1.34147 +/- 10 pcm	279
ZON FA	1.34700	1.34208 +/- 11 pcm	272
HET FA	1.31508	1.31141 +/- 12 pcm	212

Table 2. 5: Reactivity Comparison between APOLLO2 and TRIPOLI-4® in Voided Situations at 0 MWd/kgHM

(pcm)	APOLLO2	TRIPOLI-4®	Delta	Delta (%)
MOX FA	15 166	14 686 +/- 22	480	3.3
ZON FA	15 116	14 631 +/- 19	485	3.3
HET FA	12 492	11 881 +/- 16	611	5.1

Table 2. 6: FA Void Coefficient with APOLLO2 and TRIPOLI-4® and Delta

9. 2. 2 Fission Rates

Before comparing the fission rate distribution between TRIPOLI-4® and APOLLO2 models it is first interesting to look at the fission rate distribution within a fuel assembly to identify some of the characteristics of the HCSMR FAs.

The Figure 2. 14 shows the cumulated fission rates for heavy isotopes in the MOX and ZON fuel assembly at step 0. The results in Figure 2. 14 and next ones are shown for 1/6th fuel assembly only.

For the MOX FA an increase of the fission rates in the outer rows of the fuel assembly is observed. The highest values are recorded at corner fuel rods. Physically this is explained by the local increase in moderation due to the water gaps between two fuel assemblies. To tackle this phenomenon the ZON FA is introduced with plutonium enrichment reduced in the outer rows. Figure 2. 14 shows indeed for the ZON FA the outer rows have the lowest fission rates of the FA. This highlights the interest to introduce fuel rods with reduced enrichment on the outer part of an HCSMR fuel assembly. However an increase is observed in the ZON FA at the last row of ZON1 fuel rods (cf Table 2. 2). This emphasizes the need to optimize the plutonium enrichment triplet for the 3 zones to limit the overall power peak.

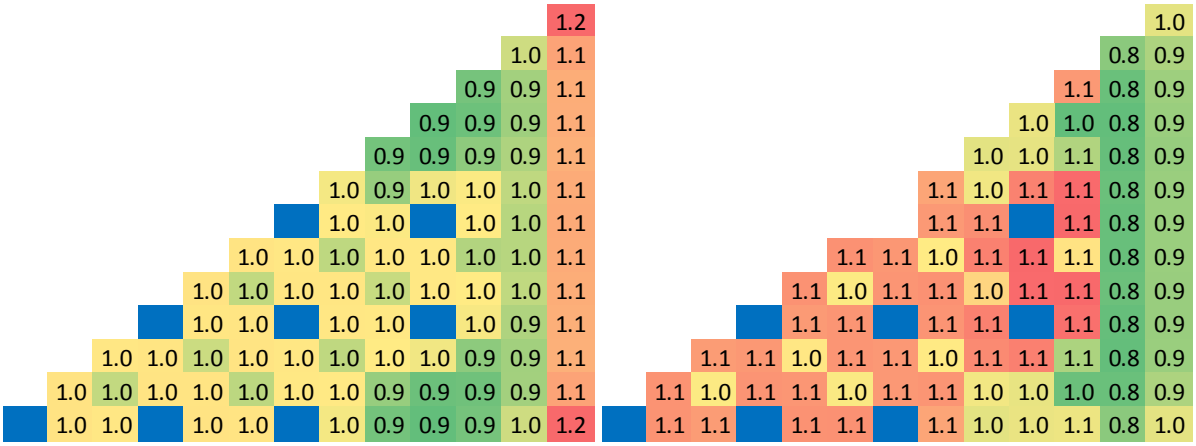

Figure 2. 14: (left) MOX and (right) ZON FA Heavy Isotopes Normalized Cumulated Fission Rates(x10^{12}) at 0 MWd/kgHM

The third type of FA, the HET FA, contains fuel rods with depleted uranium only. HET FA heavy isotope fission rate distribution at step 0 are presented in Figure 2. 15. The position and role of fertile fuel rods is easy to recognize. Since the FA total fission rate is defined by its power, an increase of the fission rates in MOX fuel rods is observed to balance the decrease in fertile fuel rods. This is particularly noticeable in MOX fuel rods next to fertile fuel rods, due to the local

spectrum change. The neutron mean-path is increased next to fertile materials, which thermalizes the neutron spectrum. This then increases the reactivity and fission rates in the neighboring rods. This aspect is particularly true at step 0 and would have to be considered when optimizing the position of fertile fuel rods.

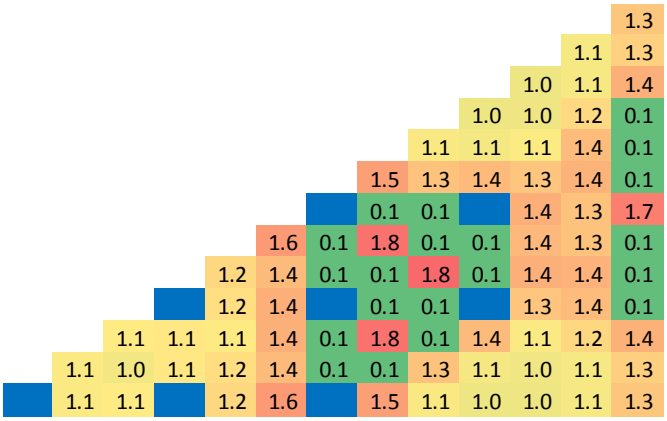

Figure 2. 15: Heavy Isotopes Normalized Cumulated Fission Rates(x10^{12}) HET FA at 0 MWd/kgHM

Figure 2. 16 to Figure 2. 18 are dedicated to the fission rate distributions comparison between TRIPOLI-4® and APOLLO2 models. This step contributes to validating the neutron-physic computation schemes. The next figures show a comparison of the results at 0 MWd/kgHM and at 60 MWd/kgHM for the three fuel assembly types.

The maximum differences rod-to-rod observed are 1.8 % at step 0 and 1.4 % at 60 MWd/kgHM. Considering the TRIPOLI-4® 3 sigma uncertainties, the rod-to-rod delta between APOLLO2 and TRIPOLI-4® change by up to 0.1% only. Those results show the reliability of the deterministic computation schemes developed to compute HCSMR fuel assemblies. The HET FA shows the largest discrepancies between deterministic and stochastic results. This is explained by the high flux changes between fertile and MOX fuel rods.

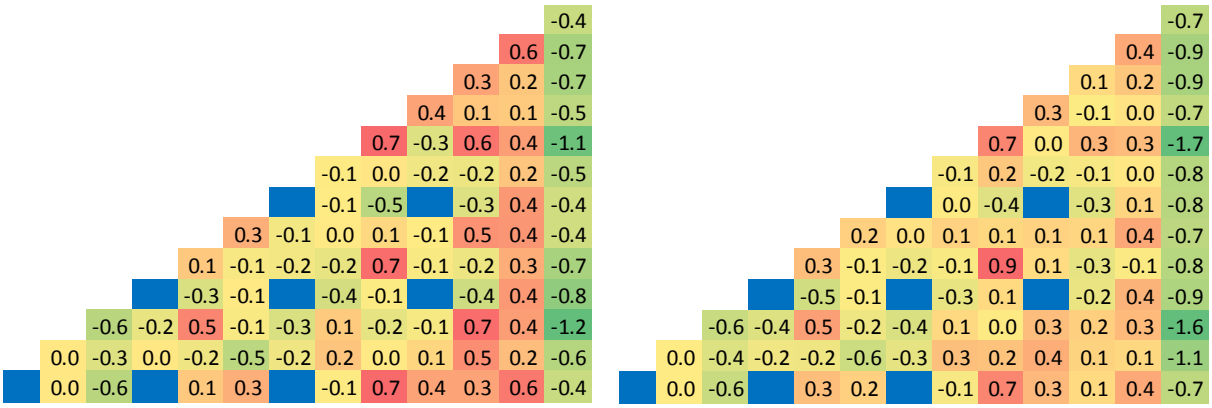

Figure 2. 16: (left) MOX FA (right) ZON FA, 1/6 Heavy Isotopes Fission Rates AP2/T4 Difference (%) at 0 MWd/kgHM.

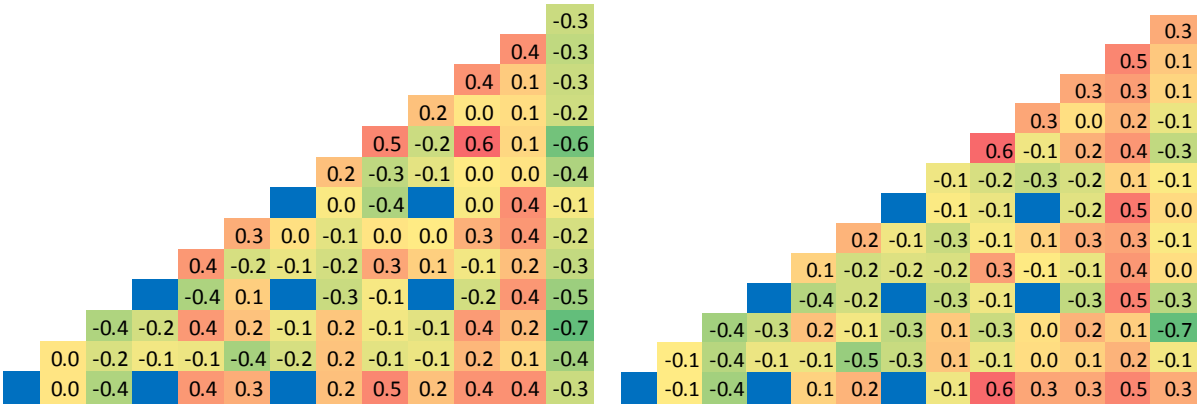

Figure 2. 17: (left) MOX FA (right) ZON FA, 1/6 Heavy Isotopes Fission Rates AP2/T4 Difference (%) at 60 MWd/kgHM.

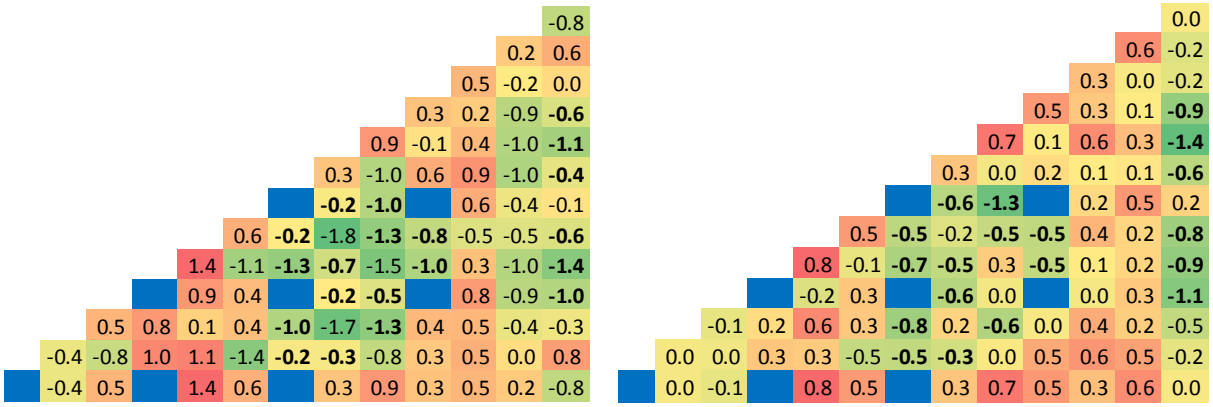

Figure 2. 18: HET FA, 1/6 Heavy Isotopes Fission Rates AP2/T4 Difference (%) at (left) 0 MWd/kgHM and (right) 60 MWd/kgHM

9. 2. 3 Isotopes Depletion

The reduced moderation of HCSMR FA hardens the neutron spectrum. This impacts the production and consumption of heavy isotopes. The Figure 2. 19 shows the evolution of three heavy isotopes ^{238}U, ^{239}Pu and ^{241}Pu for a MOX HCSMR fuel assembly from 0 to 60 MWd/kgHM. Both ^{238}U and ^{239}Pu masses decrease with increasing burnup. ^{238}U isotopes are fissioned or capture a neutron to become ^{239}Pu. ^{239}Pu isotopes are fissioned as well as ^{241}Pu. But since ^{241}Pu concentration is low in fresh fuel – due to the shorter half-life of ^{241}Pu and the fresh plutonium chosen vector Pu2035 – the ^{241}Pu concentration starts by increasing before reaching an asymptotic value until 60 MWd/kgHM.

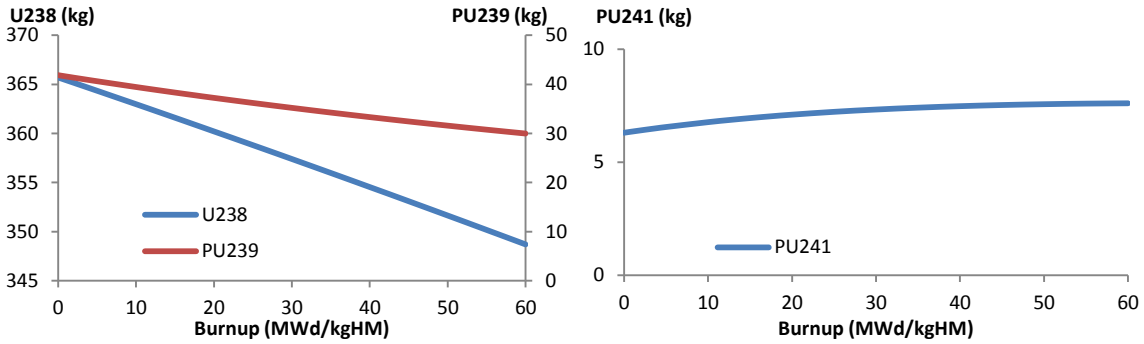

Figure 2. 19: MOX FA (left) ^{238}U, ^{239}Pu, (right) ^{241}Pu Isotopes Mass (kg)

In Figure 2. 20 a comparison of the ^{235}U, ^{238}U, ^{239}Pu and ^{241}Pu masses obtained with APOLLO2 and TRIPOLI-4® computations is presented. The differences are small and no substantial bias is observed. Those results show the adequacy of the deterministic computation schemes developed to evaluate HCSMR fuel assemblies also considering fuel depletion.

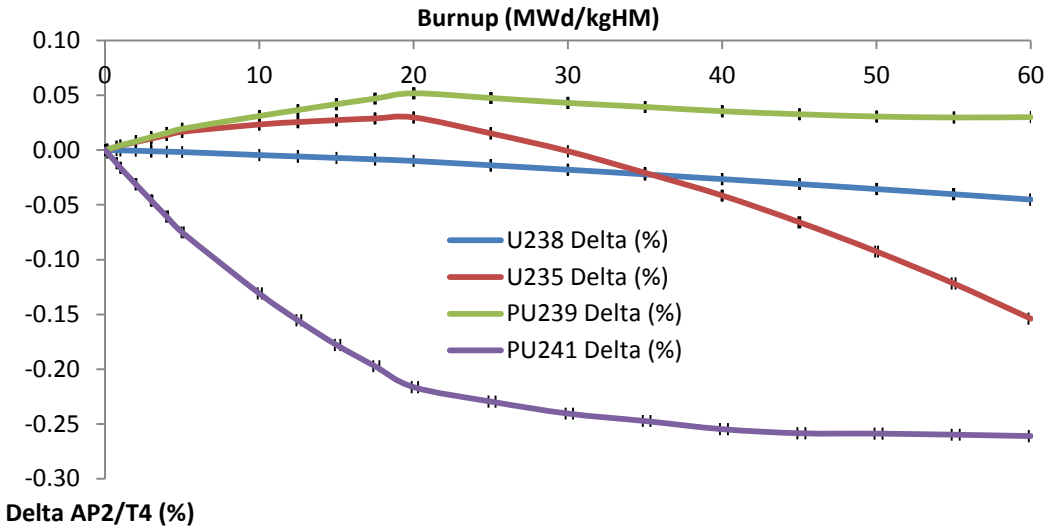

Figure 2. 20: MOX FA Isotopes Mass Difference AP2/T4 (%)

9. 3 Specific Computation Schemes

The HCSMR FA design optimization requires performing computations with broad input parameters. Those parameter ranges are broader than the chosen set of parameters used to validate the computation schemes in previous paragraphs.

The next section extends the validation to further boundary conditions aimed at supporting the robustness of the HCSMR FA computation schemes. Moreover a few specific models and analysis are introduced hereafter.

9. 3. 1 HET FA with Reduced Plutonium Enrichment

The comparison of APOLLO2 and TRIPOLI-4® evaluations is repeated for the HET FA design with reduced plutonium content in the MOX fuel rods: 13.8 % Pu instead of 25.0 % Pu. The plutonium content 13.8 % in MOX fuel rods corresponds to FA average plutonium content of 10.0 % Pu when the fertile fuel rods are also considered. The low plutonium enrichment of 10 % is selected to cover the targeted range of plutonium enrichment later use for FA optimization. The results at 0 MWd/kgHM are presented in Table 2. 7 and Figure 2. 21. The reactivity delta between deterministic and stochastic results is close to 200 pcm. The maximum rod-to-rod heavy isotope fission rate difference is 1.2%. This confirms the computation scheme adequacy is not impacted by the varying plutonium enrichment. This observation and further similar analysis with other boundary conditions ensure the robustness of the HCSMR FA computation schemes.

Parameter	APOLLO2	TRIPOLI-4® (3 σ)	Delta (pcm)
HET-13.8 FA	1.05638	1.05866 +/- 24 pcm	-204

Table 2. 7: HET-13.8 FA Reactivity Comparison between APOLLO2 and TRIPOLI-4® at 0 MWd/kgHM

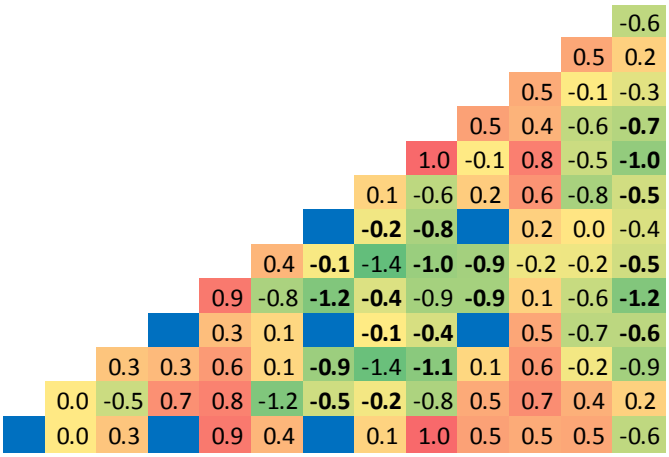

Figure 2. 21: HET-13.8 FA, 1/6 Heavy Isotopes Fission Rates AP2/T4 Difference (%) at 0 MWd/kgHM.

9. 3. 2 Simplified HET FA (HET-S) Model

A simplified APOLLO2 model is proposed to support the HET fuel assembly optimization exercise: the HET-S model. The specificity lies in the simplified self-shielding approach. The fuel rods are grouped in only two self-shielding regions: one region for the fissile fuel rods and the other for the fertile fuel rods. This approach offers two advantages: on the one hand it gives robustness to the model regardless of the fertile fuel rods' position. On the other hand it reduces the self-shielding computation time by a factor of 80 compared to the reference method (4 seconds with the HET-S approach). Since the self-shielding module is required two times for FA optimization– in nominal and voided situations – the saved time is substantial.

The adequacy of this model is validated via comparison with the reference APOLLO2 HCSMR HET FA computation scheme. The results are introduced in Table 2. 8 and Figure 2. 22. The reactivity delta observed between the reference and simplified computation scheme results is below 5 pcm. The differences in heavy isotope fission rates show a rod-to-rod maximum difference of 2.6 %. This remains in line with the objective of maximum 3% set as highest acceptable value. However such delta is not negligible and is clearly a direct consequence of the approximation introduced with the simplified self-shielding approach. Based on this observation an uncertainty factor of 3 % is considered for HET FA maximum peak power at the optimization step as highlighted in Part Three.

Parameter	HET FA	HET-S FA	Delta (pcm)
APOLLO2	1.16065	1.16060	- 4

Table 2. 8: Reactivity Comparison between HET and HET-S FA at 0 MWd/kgHM

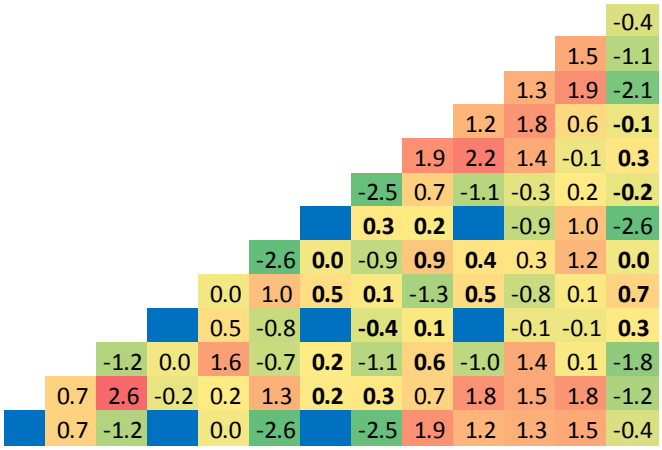

Figure 2. 22: 1/6 Heavy Isotopes Fission Rates HET-S FA/HET FA Difference (%) at 0 MWd/kgHM.

9. 3. 3 Sensitivity to Nuclear Data

The reference nuclear data is the JEFF 3.1.1 library as introduced in §8. 1. The influence of using another nuclear data evaluation is assessed here. It aims at identifying whether the nuclear data source is a substantial factor to consider for the HCSMR core optimization.

The HCSMR MOX and HET FA characteristics are evaluated using the ENDF/B-VII.1 library [129] and compared to the results obtained with the JEFF 3.1.1 library. The evaluations are made with the APOLLO2 reference HCSMR computation scheme. Differences in reactivity are compared in Table 2. 9 and Table 2. 10. Reactivity differences obtained are below 100 pcm.

Parameter	JEFF 3.1.1	ENDF/B-VII.1	Delta (pcm)
MOX FA	1.15703	1.15703	0
HET FA	1.16065	1.16038	- 20

Table 2. 9: Reactivity Comparison between JEFF 3.1.1 and ENDF/B-VII.1 at 0 MWd/kgHM

Parameter	JEFF 3.1.1	ENDF/B-VII.1	Delta (pcm)
MOX FA	0.98942	0.98850	-94
HET FA	0.98907	0.98860	- 48

Table 2. 10: Reactivity Comparison between JEFF 3.1.1 and ENDF/B-VII.1 at 60 MWd/kgHM

When looking at the heavy isotope fission rate differences between an evaluation using the JEFF 3.1.1 library and the ENDF/V-VII.1 library for the MOX FA, introduced in Figure 2. 23, differences lower than 0.1 %, both at 0 MWD/kgHM and 60 MWd/kgHM, are observed. Overall this highlights the limited influence of the nuclear data library on the power distribution and hence radial form factor for the HCSMR fuel assembly. This confirms the robustness of the HCSMR model developed and provide assurance to the optimization step.

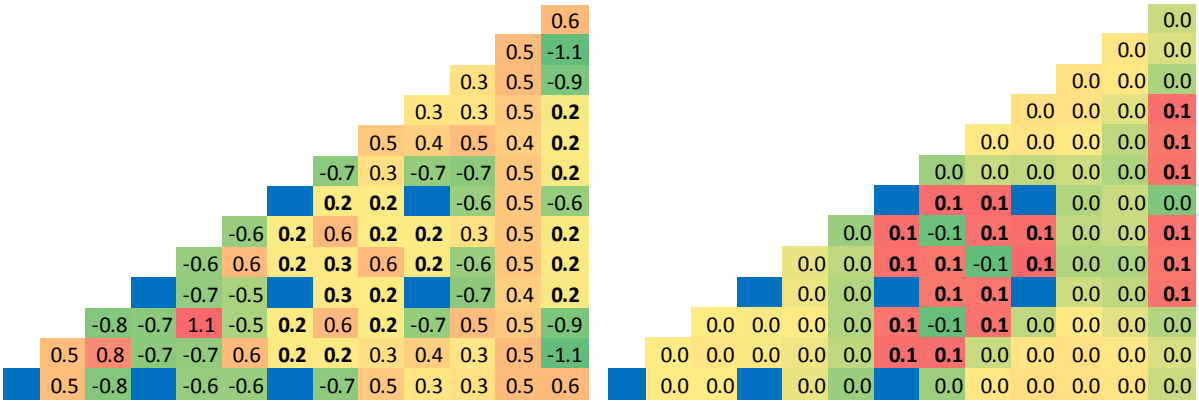

Figure 2. 23: 1/6 HET FA Heavy Isotopes Fission Rates JEFF 3.1.1/ENDF-BVII.1 Difference (%) at (left) 0 and (right) 60 MWd/kgHM.

9. 3. 4 Plutonium Content Influence

Before looking at the HCSMR FA optimization it is instructive to observe some characteristics of reference MOX, ZON and HET FAs. In this paragraph the average plutonium content is varied and the influence on three parameters is observed: the FA reactivity (K_{inf}), the void coefficient (*void*) and the peaking factor (F_{xy}). The peaking factor F_{xy} was introduced earlier as F_{xy}^{Ass}.

The FA averaged plutonium content is varied between 12 and 20 % Pu for the MOX and ZON FA with 1 % steps. For the HET FA 18% is the highest average plutonium content considered. Above this value the actual fuel enrichment would have been higher than the 25% Pu limit. In the ZON FA the enrichment ratio between the three zones is kept identical, while the average enrichment is varied. The computations are performed using the methods introduced previously but with critical reflective boundary conditions (B2 critical).

Results in Figure 2. 24 confirm the relationships between plutonium enrichment, reactivity and void coefficient already expressed. The higher the plutonium content is, the higher the reactivity and void coefficient are. Peaking factors (F_{xy}) have a low dependency on plutonium content. Yet a

global trend is however observed: the higher the plutonium content is the lower the radial peaking factors at the fuel assembly level are. A detailed analysis of design parameters influence on the FA performances is made using sensitivity analysis methods in Part Three.

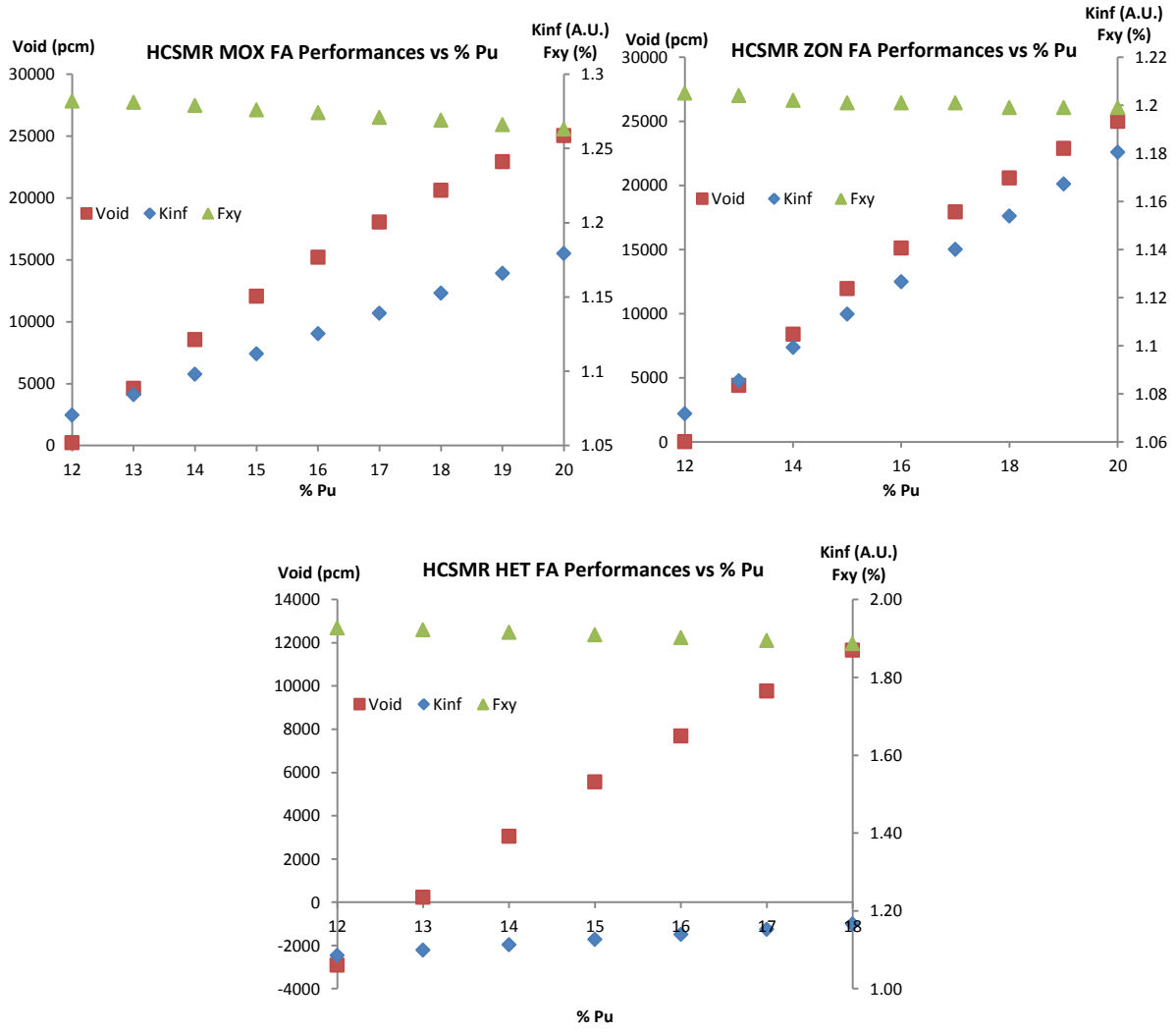

Figure 2. 24: HCSMR FA Performances (top left) MOX FA (top right) ZON FA (bottom) HET FA vs % Pu Average Enrichment.

Chapter 10: CORE COMPUTATIONS

10. 1 VALIDATION CASES: CORE GEOMETRY AND FEATURES

Three core configurations are assessed to validate the computation scheme at the core level:

- MOX core: HCSMR core with only MOX fuel assemblies.
- HET core: HCSMR core with only HET fuel assemblies.
- FER core: HCSMR core with both MOX and FER fuel assemblies.

The HET and FER cores are two designs in which fertile materials, depleted uranium at 0.2 % ^{235}U enrichment, are inserted either at the core level or at the fuel assembly level. The introduction of fertile materials aims at keeping the core void coefficient negative, as introduced in §3. 4. The MOX core is only loaded with MOX FA. It does not contain fertile medium.

The three core configurations MOX, HET and FER are presented in Figure 2. 25. For each core, the external layer contains the radial reflector medium. The loading patterns are similar for the MOX and HET cores whereas a different one is used for the FER core due to the introduction of fertile FA. A rotational symmetry "by third" is used to design the loading patterns. Only one batch of FER fuel assemblies is considered.

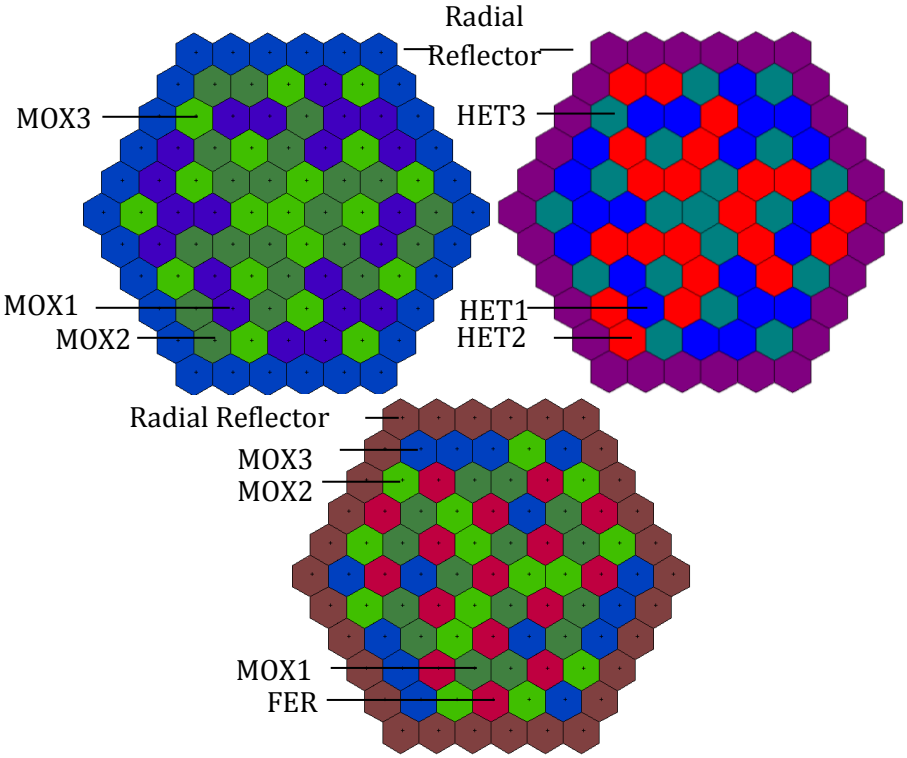

Figure 2. 25: HCSMR (top left) MOX Core (top right) HCSMR HET Core (bottom) HCSMR FER Core

The loading patterns are created to mirror equilibrium cores using a "1/3" fuel management, for which one third of the fuel assemblies (20) is replaced by fresh ones at each reload outage.

The first FA batch (MOX1) average plutonium content is kept constant for the MOX and FER cores at 17 % equivalent. For the FER core the actual MOX1 enrichment is set at 23 %, what is equivalent with regards to the plutonium mass loaded in core to the 17 %, since fertile FA are also loaded in the core. The HET core has a first batch (HET1) average plutonium content of 16 %. Each depleted FA batch (MOX2, MOX3 and HET2, HET3) then has a different plutonium content representing the real FA average batch burnup with regards to reactivity (k_{inf}). The equivalent plutonium contents are selected based on the performances observed on equilibrium HCSMR cores for each core type MOX, HET and FER. In other words, fresh FA have an adjusted plutonium content to represent the reactivity at BOC per batch obtained on an equilibrium cycle. The fuel material depletion is hence indirectly considered.

This approach enables feeding both deterministic and stochastic computations with the same medium compositions. A more realistic approach would have considered depleted materials for MOX2 and MOX3 medium composition requiring approximation in the detailed isotopic compositions. The FA types and enrichments for each core are presented in Table 2. 11. Although the fuel compositions are based on approximations, the physics to be evaluated remains valid. The ZON fuel assembly validated previously is not considered for core validation.

For the FER core, only one type of FER FA batch is considered. It contains fresh depleted uranium. This does not strictly represent the "1/3" loading patterns used later in which also three batches of FER FA are considered. However the FER FA medium evolution remains relatively limited during irradiation, hence supporting the assumption introduced here. At the core level fuel material depletion was not performed. A validation with material depletion at the fuel assembly level was earlier performed as introduced in Chapter 9.

MOX Core	Plutonium average Content (%)	FA Number
MOX1	17.0	21
MOX2	12.8	21
MOX3	9.8	19

HET Core	Plutonium average Content (%)	FA Number
HET1	22.0	21
HET2	15.8	21
HET3	11.5	19

FER Core	Plutonium average Content (%)	FA Number
MOX1	23.0	15
MOX2	16.0	15
MOX3	14.0	15
FER	-	16

Table 2. 11: MOX, HET and FER Cores FA Number and Plutonium Enrichments

The reference reflector (96 % of steel: "heavy reflector") cross sections prepared with CEA state-of-the-art approach are used as introduced in §8. 2. 5. The neutron physic characteristics are computed for the three cores with deterministic – CRONOS2 – and stochastic – TRIPOLI-4® – methods. APOLLO3® is also used as deterministic code to benchmark some results obtained

with CRONOS2. Overall this step aims to validate the deterministic models developed with CRONOS2 to compute HCSMR cores. For this purpose the adequacy of the results on reactivity and power distribution is looked at in the next section. Some aspects of this work were presented at IYNC 2016 [130].

10. 2 VALIDATION RESULTS

Three parameters are compared between deterministic and Monte-Carlo models to assess the accuracy of the deterministic computation schemes:

- The nominal core reactivity or eigenvalue (k_{eff})
- The core reactivity in case of loss of coolant (void coefficient)
- The power distribution as well as radial and axial power peaking factors (F_{xy} and F_z)

Isotherm core conditions are considered. The same fuel temperatures and moderator density are used between deterministic and stochastic models.

10. 2. 1 Reactivity

The eigenvalue computed for the three cores with TRIPOLI-4® and CRONOS2 are respectively presented in Table 2. 12 and Table 2. 13. In Table 2. 13 the differences between CRONOS2 (CR2) and TRIPOLI-4® (T4) are referred to as "Delta". The reactivity discrepancies are computed using the following formula:

$$Delta\ (pcm) = 10^5.\left(\frac{1}{keff_{T4}} - \frac{1}{keff_{CR2}}\right) \quad (2.\ 11)$$

CRONOS2 eigenvalues introduced in Table 2. 13 result from evaluations with either two energy groups (2-gr.) or eight energy groups (8-gr.).

MOX Core	T4 k_{eff}	3σ error (pcm)	HET Core	T4 k_{eff}	3σ error (pcm)	FER Core	T4 k_{eff}	3σ error (pcm)
keff	1.04899	6	keff	1.04876	5	keff	1.02723	6

Table 2. 12: Monte-Carlo Eigenvalue for the MOX, HET and FER Cores

MOX Core	CR2 2-gr.	CR2 8-gr.	HET Core	CR2 2-gr.	CR2 8-gr.
k_{eff}	1.05304	1.05207	k_{eff}	1.05177	1.05057
Delta	366 pcm	279 pcm	Delta	273 pcm	164 pcm

FER Core	CR2 2-gr.	CR2 8-gr.
k_{eff}	1.03401	1.02312
Delta	638 pcm	391 pcm

Table 2. 13: Deterministic k_{eff} for the MOX, HET and FER Cores and Delta with TRIPOLI-4®

The adequacy of the modeling options is observed with regard to the nominal eigenvalue for the MOX and HET cores. The computations with eight energy groups in CRONOS2 give better results

compared to a computation with two energy groups. The epithermal neutron spectrum of the HCSMR cores explains this observation: modeling more accurately the epithermal and fast energy groups improves the results.

The FER core is more heterogeneous compared to the MOX and HET designs due to the fertile FA (FER) made of fertile fuel rods only. The results observed for the FER core using the diffusion theory at two and eight energy groups give confidence but can be refined. An evaluation at 26 groups with a transport flux solver (SN) in the APOLLO3® code was performed. An eigenvalue of 1.02627 leading to a delta of 91 pcm compared to the TRIPOLI-4® results is obtained. Hence the results based on transport are improved compared to the results presented in Table 2. 13 using diffusion theory. Since the FER core is highly heterogeneous and substantial flux gradients are observed, such a core design digresses from the diffusion theory boundary conditions. The results are hence good enough for screening and preliminary computations but a transport evaluation increases confidence in the results.

10. 2. 2 Void Coefficient

The void coefficient characterizes the reactivity change between the nominal and voided core situations: with only 1% of nominal moderator density. As introduced in §3. 4. 4 the void coefficient must remain negative for the HCSMR core design. The relevance of this constraint can be questioned but remains a driving principle in this work. The optimization of the FA design and core design should enable to reach this goal. The values presented in Table 2. 14 show the results obtained with TRIPOLI-4® and CRONOS2 for the reactivity in a voided situation for the MOX and HET cores. In this situation the neutron spectrum is hardened due to the lack of moderator. The two energy group computation scheme focusing on the thermal energy group is not adequate. Therefore CRONOS2 is used with eight energy groups for void coefficient computations.

The voided computations are performed without thermal-hydraulic feedback and similar fuel temperature between TRIPOLI-4® and CRONOS2. The reflector is not voided in those computations.

MOX Core	T4 (3 σ)	CR2 8-gr.	Delta (pcm)	HET Core	T4 (3 σ)	CR2 8 gr.	Delta (pcm)
keff	0.94682 +/- 9 pcm	0.95656	1075	keff	0.89877 +/- 7 pcm	0.90404	649

Table 2. 14: Reactivity in Voided Situations for the MOX and HET Cores with T4 and CR2

The results obtained show a tendency of CRONOS2 to over predict the reactivity in voided situations. This is conservative with regards to void coefficient for safety analysis purposes. The differences observed are larger than 500 pcm. However since the differences observed are conservative and it is here a voided evaluation the results obtained are good enough to accept the deterministic computation schemes for optimization purpose. For a detailed safety analysis a more refined evaluation would be required.

For the FER core the results are shown in Table 2. 15. The eigenvalue over prediction of CRONOS2 compared to TRIPOLI-4® is further increased. In the FER core the heterogeneity are even more important than in MOX and HET cores. This might explain the tendency to obtain a higher difference between deterministic and stochastic results. Indeed, medium heterogeneities can lead to important local flux variation. This could even question the validity of the diffusion approximation for those highly heterogeneous cores.

A transport computation with 26 energy groups (26-gr.) using APOLLO3® is performed to illustrate this assumption. It gives improved results compared to the Monte-Carlo values. Those results are presented in Table 2. 15. This observation reinforces the interest to perform transport computations for FER core evaluations.

FER Core	T4 (3 σ)	CR2 8 gr.	Delta (pcm)	AP3 26-gr.	Delta (pcm)
keff	0.95362 +/- 9 pcm	0.96929	1695	0.95194	185

Table 2. 15: Voided Reactivity for the FER Core with T4, AP3 and CR2

The deltas between stochastic and deterministic computations on absolute void coefficients are presented in Table 2. 16 for the MOX and HET core and in Table 2. 17 for the FER core.

MOX Core	T4 (3 σ)	CR2 8-gr.	Delta (pcm)	HET Core	T4 (3 σ)	CR2 8 gr.	Delta (pcm)
Void (pcm)	-10 247 +/- 11	-9 517	730	keff	-15 434 +/- 9	-15 021	413

Table 2. 16: Void Coefficient Comparison for the MOX and HET Cores with T4 and CR2

FER Core	T4 (3 σ)	CR2 8 gr.	Delta (pcm)	AP3 26-gr.	Delta (pcm)
keff	-7 436 +/- 11	-5 405	2031	-7 211	225

Table 2. 17: Void Coefficient Comparison for the FER Core with T4, AP3 and CR2

The delta observed for the FER core using diffusion computations is rather high. One area of improvement identified is a better preparation of the fertile FA cross sections. A "cluster method" is used with APOLLO2 at the FA level to generate FER FA cross sections: the FER FA is surrounded by a MOX FA equivalent medium. This equivalent medium is a MOX fuel in nominal condition at 30 MWd/kgHM burnup. It nourishes the FER medium as explained in §8. 2. The same equivalent MOX medium is considered both for FER FA in nominal or voided conditions. This introduces a bias in the FER FA cross sections in voided conditions and could be improved by using a voided MOX equivalent medium when performing the cluster computation.

10. 2. 3 Power Distribution

For each core configuration the maximum radial (F_{xy}) and axial (F_z) FA power peaking factors are derived. F_{xy} and F_z must be understood as maximum radial power and maximum axial node power respectively. Additional FA peaking factor or burnup gradient form factors are not

considered here. Axially the active zone is divided for both deterministic and stochastic models in 22 layers of 10 cm.

$$Fxy = \frac{FA_{max}^{power}}{FA_{avg}^{power}} \qquad (2.\ 12) \qquad\qquad Fz = \frac{FA_{axial\ node\ max}^{power}}{FA_{axial\ node\ avg}^{power}} \qquad (2.\ 13)$$

The results obtained with CRONOS2 and TRIPOLI-4® are presented in Table 2. 18 and delta between CRONOS2 evaluated with two energy groups and TRIPOLI-4® are introduced in Table 2. 19. Overall a good agreement is observed between the maximum F_{xy} and F_z for each core configuration between the evaluations with CRONOS2 and TRIPOLI-4®. Moreover the position of the FA or axial node in which the maximum is observed is always identical.

MOX Core	**T4**	**CR2 2-gr.**	**CR2 8-gr.**	**HET Core**	**T4**	**CR2 2-gr.**	**CR2 8-gr.**	**FER Core**	**T4**	**CR2 2-gr.**	**CR2 8-gr.**
F_{xy}	1.568	1.566	1.571	F_{xy}	1.587	1.583	1.588	F_{xy}	2.179	2.129	2.068
F_z	1.433	1.435	1.437	F_z	1.434	1.441	1.444	F_z	1.441	1.453	1.435

Table 2. 18: Maximum Form Factors for the MOX, HET and FER Cores with T4 and CR2

MOX Core	**Delta (%)**	**HET Core**	**Delta (%)**	**FER Core**	**Delta (%)**
F_{xy}	-0.1	F_{xy}	0.2	F_{xy}	-2.3
F_z	0.1	F_z	0.5	F_z	0.8

Table 2. 19: Delta between T4 and CR2 Maximum Form Factors for the MOX, HET and FER Cores

Figure 2. 26 introduces the FA relative power for the MOX and HET cores obtained with CRONOS2. Only one third of the core is shown since the core is one-third symmetric. The results observed for both cores are similar. This is due to the same loading patterns used for both cores, although the FA are different. Moreover the FA are homogenized at the core level.

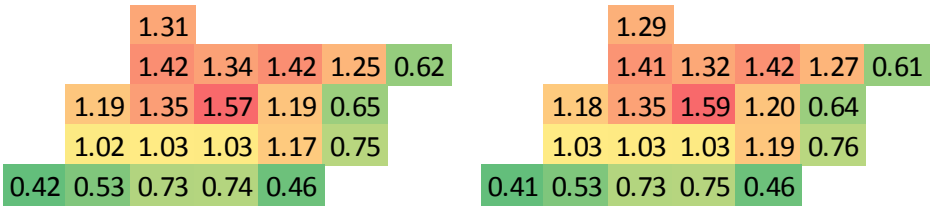

Figure 2. 26: (left) 1/3 MOX Core and (right) 1/3 HET Core FA Relative Power (CRONOS2)

To obtain a sense of the power distribution in 3D an overview of the MOX core is introduced in Figure 2. 28. This overview is prepared with the SALOME [131] platform.

Figure 2. 27 shows the FA power difference between CRONOS2 and TRIPOLI-4® for the MOX and HET cores. A maximum difference of 3% in average FA power is observed at the periphery of the core. The differences observed are in line with the maximum threshold of 3 % delta set to accept the deterministic computation schemes. Since the largest differences are observed at the core's periphery an adaptation of the reflector modeling would improve the results.

For the FER core the FA power distribution and the differences between deterministic and stochastic evaluations are introduced in Figure 2. 29. The FER FA positions are highlighted by bold values. The power generated in FER FA is significantly lower compared to the power

generated in MOX FA. This is a direct consequence of the fissile vs fertile material difference between MOX and FER FA. The low power in FER FA at step 0 increases during the irradiation cycle due to the ^{239}Pu material breeding.

		1.78				
		1.01	1.43	0.47	-0.97	1.08
	0.58	0.30	-0.16	-1.11	2.35	
	-1.72	-1.36	-1.33	-2.58	-1.03	
2.54	1.84	-0.79	-1.63	2.68		

		1.24				
		0.77	1.09	0.33	-0.79	1.29
	0.45	0.19	-0.04	-1.07	2.22	
	-1.17	-1.25	-1.21	-2.15	-0.81	
3.03	2.14	-0.43	-1.17	2.88		

Figure 2. 27: (left) 1/3 MOX Core and (right) 1/3 HET Core FA Power Diff. CR2 (8 gr.)/T4 (%)

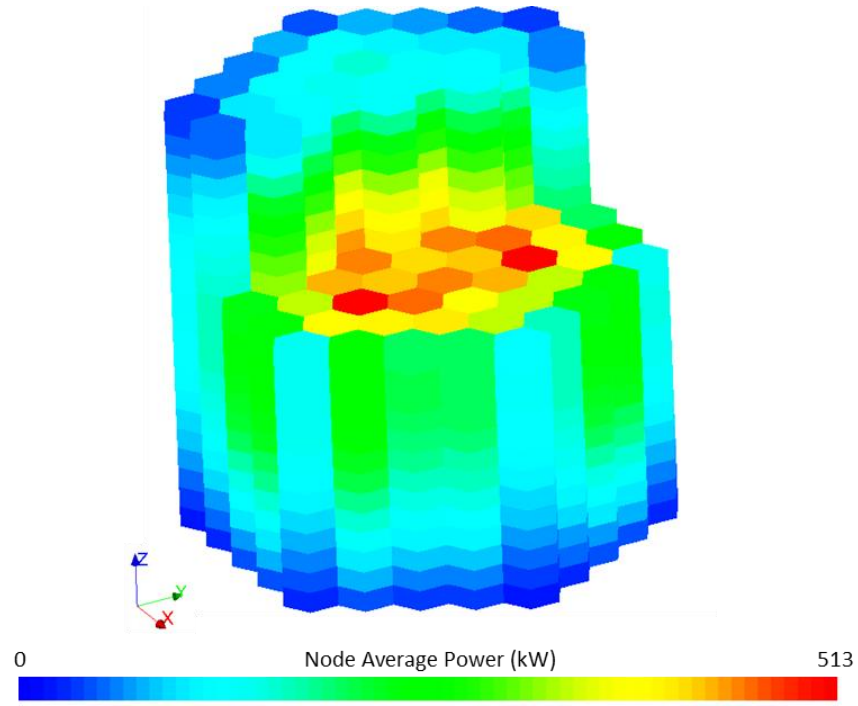

Figure 2. 28: MOX Core Power Distribution 3D Overview Based on APOLLO3 Results

The differences observed in Figure 2. 29 between CRONOS2 and TRIPOLI-4® results show a maximum difference close to 3 %. This is relatively high but in line with the 3 % target. Hence the adequacy of the deterministic model for the HCSMR core optimization is confirmed. A systematic error on fertile fuel assemblies is not observed. On the contrary a radial power difference between deterministic and stochastic model is observed.

		0.38				
		1.76	2.06	**0.37**	1.98	0.89
	1.57	**0.32**	1.53	1.99	1.22	
	0.23	1.40	1.40	**0.23**	0.95	
0.43	0.58	**0.13**	0.59	0.45		

		2.84				
		2.75	1.06	**-1.35**	-1.62	-2.31
	2.81	**1.64**	2.39	-1.74	-2.17	
	-1.97	1.49	2.12	**-2.00**	-1.59	
2.12	2.08	**2.36**	1.67	-1.04		

Figure 2. 29: (left) 1/3 FER Core FA Relative Power and (right) 1/3 FER Core FA Power Differences CR2 (8 gr.)/T4 (%)

The results obtained with APOLLO3 (AP3) using transport computations are introduced in Figure 2. 30. The differences compared to the stochastic model are slightly better compared to the results obtained with CRONOS2 and 8 groups' computation and introduced in Figure 2. 29. A gradient is observed in the differences indicating an improvement could come from a better reflector simulation. This conclusion is in line with the simulation approximation introduced in those exercises.

		-1.66			
		-2.13	-2.05	**-0.95**	-0.37	1.93
	-0.95	**-1.10**	-1.12	-0.38	1.95	
	0.83	-0.92	-0.89	**1.04**	1.99	
2.09	1.27	**1.47**	1.46	1.82		

Figure 2. 30: 1/3 FER Core FA Power Differences AP3 (26 gr.)/T4 (%)

10. 2. 4 Reflector

A detailed reflector design is not considered in this work. Instead a homogenous medium is modeled axially – top and bottom reflectors – and radially an additional FA row is added to the core loading pattern. This outer FA row is filled with reflector medium. The neutron economy and the behavior in voided situations are directly impacted by the top, radial and bottom reflectors' characteristics.

The HCSMR reference reflector contains 96 % of steel referred to as *heavy reflector*. The cross sections for this reference reflector are prepared with the reference method based on a 1D-Slab evaluation as introduced in §8. 2. 5. Additionally reflector cross sections with 10 % and 50 % steel content only are prepared using the "FA cluster" method also introduced in §8. 2. 5. The method is applied to a 96% steel content case for benchmark purposes.

The performances observed for three contents of steel in the radial reflector medium are introduced in Table 2. 20 . The axial reflectors material – top and bottom – are kept as heavy reflector for all computations. Only the radial reflector medium is modified. Those results are obtained with HCMSR MOX core computations using two energy groups.

Radial Reflector Steel content (%)	**CR2 k_{eff} 2-gr.**	**F_{xy}**
10	1.05230	1.546
50	1.05266	1.547
96	1.05314	1.551
96-reference	1.05304	1.566

Table 2. 20: MOX Core with Alternative Radial Reflectors

The result obtained with 96% steel with the two different methods validates the approached methodology using the "FA cluster". Although this method introduces approximations, the results obtained show good accuracy compared to the reference results discussed in previous paragraphs.

With high steel content in the reflector, neutrons bounce back more often, which increases the core reactivity. However this effect is limited due to an opposing effect. The epithermal neutron spectrum of HCSMR cores provides a specific behavior compared to large LWR cores. Since the reflector medium is made of steel and water, the diminution of steel content leads to increase in water content. This additional water volume impacts the outer FA row by increasing the neutron slow-down and hence the reactivity. This effect compensates the decrease of steel neutron reflection capability, which is mostly relevant for fast neutrons.

The influence of the reflector medium on HCSMR core performances will be further evaluated with equilibrium core evaluations in the next section.

10. 3 SELECTED PERFORMANCES: PRELIMINARY DESIGN

10. 3. 1 Design Characteristics

In this section a first set of HCSMR cores' performances is presented. This would define some references of HCSMR cores' characteristics before starting the optimization exercises. The preliminary HCSMR core design introduced in Part One is used as reference for the HCSMR cores evaluated. This preliminary core, introduced in §4. 4, is made of MOX fuel assemblies only, also referred to as "MOX core".

Compared to the results from §10. 2, the performances presented hereafter are based on equilibrium cycle evaluations. As introduced in §8. 3. 1 a given core configuration is evaluated several times until the fuel burnups at the beginning of cycle (BOC) and end of cycle (EOC) converge. The reactivity is not compensated during the cycle depletion computation. The cycle ends is reached when the core's reactivity reaches 10 pcm or less.

Beyond MOX core, the performances of example HET and FER cores are also introduced in this section. Their general characteristics are based on the designs considered for computation scheme validation in §10. 1. The specificities are:

- MOX core: HCSMR core with only MOX fuel assemblies;
  - FA design: MOX FA;
  - Fuel enrichment: 17 % and 19 % plutonium are considered;
- HET core: HCSMR core with HET fuel assemblies;
  - FA design: HET FA with 120 fertile fuel rods per FA introduced in §9. 1;
  - Fuel enrichment: 23.4 % plutonium, 17.0 % equivalent for the entire FA/core;
- FER core: mixed core of FER and MOX fuel assemblies;
  - FA design: MOX and FER FA;
  - Fuel enrichment: 23 % plutonium, 17.0 % equivalent for the core.

The loading patterns and reloading scheme for the three cores are introduced next. The MOX and HET core use the same loading pattern and refueling scheme while the FER core has a specific set of inputs. For the three cores a "1/3" fuel management is considered. Figure 2. 31 and Figure 2. 32 introduces the loading patterns and refueling schemes.

	5	6	7	8	9	10	11	12	13	14	15	16
E					M3							
F				M1		M2		M1		M0		M1
G			M2		M1		M0		M1		M2	
H		M0		M1		M2		M0		M0		
J	M1		M2		M0		M0		M2			

	5	6	7	8	9	10	11	12	13	14	15	16
E					F3							
F				M1		M0		F1		M0		M2
G			M1		F1		M2		M0		M2	
H		F0		M0		M0		F0		M1		
J	M2		M1		F2		M1		M2			

Figure 2. 31: Loading patterns for cores without fertile FA (left) and core with fertile FA (right)

	5	6	7	8	9	10	11	12	13	14	15	16
E					G15							
F				F14		G09		H14		|		G11
G			F12		H06		|		J11		F08	
H		|		J09		G13		|		|		
J	H12		H08		|		|		J05			

	5	6	7	8	9	10	11	12	13	14	15	16
E					F12							
F				F10		|		H12		|		H14
G			H10		H06		J07		|		J11	
H		|		|		|		|		H08	
J	F08		G13		G09		F14		G07				

Figure 2. 32: Reloading Schemes for Cores without Fertile FA (left) and with Fertile FA (right).

10. 3. 2 Results

The results obtained for the MOX cores are introduced in Table 2. 21. With this preliminary design the cycle length is close to two years. The conversion factor reaches about 0.80. Those characteristics are in line with the optimization objectives defined in Part One. The void coefficient is strongly positive highlighting the need of further development of this core. With a maximum linear power below 250 W/cm the power map is relatively flat.

The conversion factor is the ratio between the fissile material mass at the end of irradiation and the fissile material mass at the beginning of irradiation. The conversion factor is further defined in §3. 4. "End of irradiation" can either refer to FA final discharge or the end of the irradiation cycle (EOC). For the conversion factors presented in Table 2. 21 "end of irradiation" is FA final discharge. This approach is always considered in this work unless explicitly specified. When "end of irradiation" refers to EOC, the conversion factors for the cases introduced in Table 2. 21 would be higher than 0.9. The approach selected is hence conservative and in line with the objective of HCSMR design to improve fuel utilization.

Table 2. 22 shows the performances of HET and FER cores. As for the MOX cores, the cycle length and conversion factor are close to the objective set for the HCSMR core. The void coefficient remains positive, although fertile materials are introduced in those cores. Fertile fuel rods or fuel assemblies lead however to a substantial increase of the maximum linear power reaching up to 370 W/cm. The introduction of heterogeneities in those cores explains this behavior.

In Table 2. 21 and Table 2. 22 the void coefficients indicated are evaluated at BOC with one percent nominal moderator content. It is the highest value observed along the entire irradiation cycle for the three core design types. At BOC the plutonium content is maximum leading to the highest reactivity increase in case of loss of coolant. For optimization exercises the void

coefficient is hence always evaluated at BOC with one percent nominal moderator density unless explicitly mentioned.

		MOX Core	MOX Core
Core height	cm	220	220
Pu enrichment	%	**19.0**	**17.0**
Fuel type		MOX	MOX
Fuel management		1/3	1/3
Cycle length	EFPD	853	648
Cycle Burnup	MWd/kgHM	18.529	14.090
FA average discharge burnup	MWd/kgHM	55.297	42.033
Void coefficient	pcm	7559	2849
Conversion factor		0.79	0.84
Plutonium mass BOC	kg	4923	4461
Fxy, max		1.895	1.829
Fq, max		2.458	2.387
Plin, max	W/cm	246	239

Table 2. 21: MOX Cores Selected Performances

		HET Core	FER Core
Core height	cm	220	220
Pu enrichment	%	23.4	23.0 / 0
Fuel type		HET	MOX / FER
Total fertile FR in core		8280	7488
Fuel management		1/3	1/3
Cycle length	EFPD	657	715
Cycle burnup	MWd/kgHM	14.286	15.271
FA average discharge burnup	MWd/kgHM	42.621	53.444/22.972
Void coefficient	pcm	2697	2659
Conversion factor		0.84	0.83
Plutonium mass BOC	kg	4479	4431
Fxy, max		2.803	2.623
Fq, max		3.663	3.436
Plin, max	W/cm	366	344

Table 2. 22: HET and FER Core Selected Performances

For power peaking factors and the maximum linear power, the most penalizing situations are also observed at BOC. The values presented in Table 2. 21 and Table 2. 22 are evaluated at 6 EFPD with Xenon-equilibrium. A core evaluation at 0 EFPD and full power is a non-relevant analysis. A core at beginning of cycle slowly ramps up its power. This approach is in line with standard industrial practices. Therefore the relevant time steps for HCSMR core analyses in optimization exercises are: zero EFPD (BOC), six EFPD and end of cycle (EOC).

10. 3. 3 Reflector

The HCSMR reference reflector is a *heavy reflector* made of 96% steel. In addition, reflectors with 50 % and 10 % steel are considered, as introduced in §10. 2. 4. The HCSMR preliminary core (MOX) assessed with those two reflectors leads to the performances presented in Table 2. 23.

With the reduced steel content in reflector material the cycle length is slightly decreased, as well as the conversion factor and maximum linear power. A similar behavior for the void coefficient is observed. Those differences support the decreased neutron reflecting behavior with reduced steel content in the reflector. However the changes are relatively small. An opposing effect explains this: the increased neutron moderation at the core's periphery due to the additional water content in the reflector.

		Heavy Reflector	50 % Steel Reflector	10 % Steel Reflector
Core height	cm	220	220	220
Pu enrichment	%	19.0	19.0	19.0
Fuel type		MOX	MOX	MOX
Fuel management		1/3	1/3	1/3
Cycle length	EFPD	853	848	845
Cycle Burnup	MWd/kgHM	18.529	18.419	18.367
Void coefficient	pcm	7559	7478	7414
Conversion factor		0.79	0.77	0.77
Plin, max	W/cm	246	233	232

Table 2. 23: Reflector Steel Content Effect on MOX Core Selected Performances

10. 4 REMARKS ON COMPUTATION SCHEMES' VALIDITY

One of the optimization parameters at the core level is the fuel axial length. It ranges between 147 cm and 300 cm. Since the core power remains constant at 600 MW a modification of the core active height influences the power density. The branch computations performed with APOLLO2 consider the reference axial length of 220 cm. With the results shown in Table 2. 24 the adequacy of this assumption is verified.

Cross Sections prepared with		H-220cm	H-220cm	H-147cm	H-220cm	H-300cm
Core height	cm	220	147	147	300	300
Pu enrichment	%	19.0	19.0	19.0	19.0	19.0
Fuel type		MOX	MOX	MOX	MOX	MOX
Fuel management		1/3	1/3	1/3	1/3	1/3
Cycle length	EFPD	853	528	524.9	1150	1144
Cycle Burnup	MWd/kgHM	18.529	17.164	17.070	18.326	18.230
Void Coefficient	pcm	7559	3819	4252	9326	9516
Conversion Factor		0.79	0.81	0.81	0.78	0.78
core HM mass	kg	9005	6028	6028	12282	12283
Plutonium mass	kg	4923	3312	3312	6699	6699
Fxy, max		1.895	1.854	1.856	1.919	1.915
Fq, max		2.458	2.418	2.420	2.456	2.450
Plin, max	W/cm	246	362	362	180	180

Table 2. 24: Axial Length and Power Density Influence on Core Computation Scheme

Branch computations are repeated for a core active height of 147 cm and 300 cm, the minimum and maximum of the active height variation range at the core optimization step. The main

equilibrium cycle outcomes obtained with CRONOS2 are compared with results from the standard computation scheme, with branch computation prepared with an active height of 220 cm but a change in core height at the core level.

Up to 6 EFPD difference on cycle length and 400 pcm on void coefficient are observed. For both cases evaluated the void coefficient obtained with the cross sections prepared with 220 cm core height are smaller compared to the void coefficient obtained with the cross sections prepared with the real active height and hence power density. This is not conservative with regards to safety. Hence a margin of 500 pcm will be applied in core optimization target.

The results obtained for the other parameters of interest: conversion factor, cycle burnup, plutonium mass, maximum linear power are very close between both evaluations and confirm the approach selected.

Chapter 11: PART TWO CONCLUSION

The second part of the thesis focuses on neutron-physics computation schemes developed to calculate the HCSMR core characteristics. After a review of neutron-physics fundamentals for core design purposes, the computation schemes at the fuel assembly and then core level are introduced. The use of benchmark between deterministic and stochastics methods enables the confirmation of the validity of the HCSMR computation schemes developed. The accuracy obtained for the various benchmark cases satisfies the needs for HCSMR core optimization, although it can be further refined.

At the fuel assembly level, APOLLO2 is used to compute the HCSMR FA designs in infinite medium. Three FA designs are evaluated: a MOX FA containing only MOX fuel rods with a unique plutonium content; a ZON FA containing MOX fuel rods with three plutonium contents; and the HET FA containing MOX and fertile fuel rods. The ZON FA design aims at reducing the FA radial power peak due to the local over moderation at the FA outer row. The HET FA is proposed to reduce the reactivity increase in voided situation.

The results obtained with APOLLO2 using deterministic methods are benchmarked against Monte-Carlo results computed with TRIPOLI-4®. The comparisons are performed with fresh fuel and with depleted fuel: at 0 MWd/kgHM and 60 MWd/kgHM. A maximum reactivity delta of 325 pcm is observed for the HET FA at 60 MWd/kgHM. This is in line with the objective of maximum 500 pcm difference set to validate the HCSMR computation schemes.

The heavy isotope fission rates per fuel rod are also compared between APOLLO2 and TRIPOLI-4®. A maximum difference below 2 % regardless of the burnup is obtained for all three FA designs. The largest discrepancies are observed for the HET FA for which local substantial flux changes close to the fertile fuel rods are observed. The accuracy of APOLLO2 to evaluate such design is confirmed however.

Beyond nominal evaluations, voided situations are also computed at the FA level and compared between deterministic and stochastic calculations. The results obtained are assessed with regards to the reactivity evaluated with voided moderator at 0 MWd/kgHM. The maximum difference between APOLLO2 and TRIPOLI-4® remains below 300 pcm and a conservative behavior is observed: APOLLO2 systematically gives reactivity values higher than TRIPOLI-4®. Overall those performances confirm the relevance of the computation schemes developed at the FA level to evaluate and optimize the HCSMR core design.

For the HET FA a simplified deterministic computation scheme, HET-S, is also introduced. This APOLLO2 model aims at reducing the computational cost of FA evaluation, in particular to enable optimization with explicit APOLLO2 computations as introduced in Part Three. This computation scheme is also validated against reference cases. The comparison gives satisfying results. A maximum bias of 2.8 % is identified for heavy isotopes fission rates. Hence a penalty factor of 3 % will be applied for linear power evaluation at the core level for cores loaded with HET FA. This makes it possible to keep a conservative approach. The HET-S reduces the self-shielding computation time by a factor of 80, which decreases substantially the time of a nominal evaluation. This is highlighted in Table 2. 25 with some HCSMR FA computation times.

	MOX, ZON, HET FA				HET-S
Type	Nominal	Evolution 0 – 180 MWd/kgHM	Evolution 0 – 60 MWd/kgHM	Branch (Saphyb)	Nominal
Code	APOLLO2	APOLLO2	TRIPOLI4	APOLLO2	APOLLO2
CPUs	1	1	60	20	1
Time	12’	6 hours	96 hours	2 hours	7’

Table 2. 25: HCSMR FA Computation Time

At the core level CRONOS2 and APOLLO3® are used to compute HCSMR cores. Three core designs are considered to validate the computation schemes developed with CRONOS2 against TRIPOLI-4® results:

- MOX core: HCSMR core with only MOX fuel assemblies.
- HET core: HCSMR core with only HET fuel assemblies.
- FER core: HCSMR core with both MOX and FER fuel assemblies.

The comparison with TRIPOLI-4® are only performed with fresh fuel. Core depletion evaluations are not investigated. MOX fuel rods with three different plutonium contents are considered for each core. To compare similar cores’ images and take core fuel management into account, the three plutonium contents are used to simulate fuel material depletion. This makes it possible to compute cores which are representative of equilibrium core layout at BOC.

For the MOX and HET cores the reactivity differences remain below 400 pcm, both using 2 and 8 energy groups in CRONOS2. For the FER core, up to 600 pcm difference is observed with TRIPOLI-4®. The highly heterogeneous FER core challenges the diffusion approximation. This is confirmed by a transport computation performed with APOLLO3®. The reactivity delta is then below 100 pcm.

This observation highlights the limits of the diffusion approximation for highly heterogeneous HCSMR cores on the one hand. On the other hand it shows good preliminary results can be obtained with CRONOS2 using eight energy groups computations. This will be considered for HCSMR optimization exercises. The comparison of fuel assembly relative power at the core level confirms for the three cores the relevance of the simulation options with differences observed remaining below 3 %.

The accuracy obtained with APOLLO2, CRONOS2 and APOLLO3® matches the requirements needed for this study, aiming at screening various HCSMR core configurations for optimization purposes. The computation times observed for core evaluations are introduced in Table 2. 26.

			MOX, HET, FER CORE		
Type	Nominal Diffusion	Equilibrium Cycle 0 – 180 MWd/kgHM	Nominal Diffusion	Nominal SN	Nominal
Code	CRONOS2	CRONOS2	APOLLO3	APOLLO3	TRIPOLI4
CPUs	1	1	1	8	60
Time	< 1’	10’	<1’	30’	6 hours

Table 2. 26: HCSMR Core Computation Time

Part Three

Optimization

TABLE OF CONTENTS

Chapter 12: PART THREE INTRODUCTION

The evaluation of the HCSMR preliminary core enables the identification of the main challenges associated with the HCSMR core design. Limiting the linear heat generation rate and ensuring a negative void coefficient are the main challenges when increasing cycle length and conversion ratio. Those challenges can be tackled by adequate design choices both at the FA and core level.

Accordingly three optimization exercises are selected to optimize the HCMSR design: two at the fuel assembly level and one at the core level. Figure 3. 1 gives an overview of the links between the three optimization exercises (highlighted in red boxes) and the overall HCSMR optimization process. Figure 3. 1 also summarizes the organization of this part of the thesis and the chapters related to each topic are highlighted in red color in the plot.

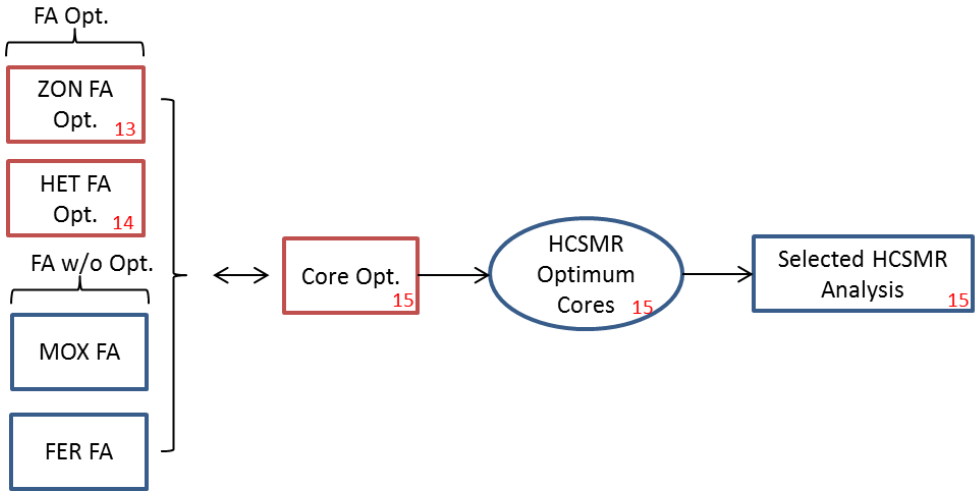

Figure 3. 1: Optimization Process Overview

The optimization process contains iterations between fuel assembly and core optimizations. The nature of neutron-physic computations requiring fuel assembly branch cross sections for core evaluations forced this iterative process. A feedback loop is introduced as shown in Figure 3. 2.

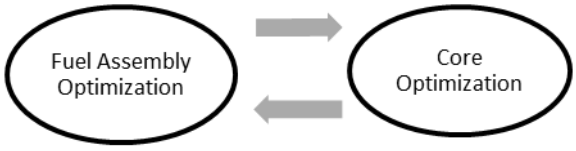

Figure 3. 2: Iterative Optimization Process Overview

As introduced in §5. 4 the optimizations considered in this work are multi-objective and multi-criteria optimization. It aims at obtaining a population of optimum individuals – fuel assembly or core design – but not necessarily at obtaining *the* best design. The population of Pareto optimum individuals can then be used to select one single design for further analysis.

To perform the optimization a screening is first realized to determine the boundary conditions, the domains of the parameters of interest and objectives. This step is also known as establishing a research plan or design of experiment (DoE). Based on the evaluations performed to generate

the DoE, surrogate models using neural networks can be developed to substitute explicit computations. This enables the reduction of the overall computational costs. The associated methods are introduced in Chapter 5.

The actual optimization is then performed using genetic algorithms. Other optimization methods such as particle swarm are also looked at for benchmark purposes. As indicated, the optimization aims at identifying the Pareto front or surface for each optimization exercise. This is obtained when all individuals of the population are Pareto optimal. The definition of a Pareto optimal population and the process to obtain it are shown in Figure 1.19 in Chapter 5. Only optimization methods adapted with specific developments to address the HCSMR core optimization cases are introduced hereafter.

Two concepts are identified at the fuel assembly level to improve the preliminary MOX fuel assembly in line with the HCSMR design objective. First the introduction of three zones of plutonium contents is proposed to reduce the power peak increase observed at the outer fuel rods' row. This is referred to as ZON fuel assembly optimization

The local power increase is a consequence of the enhanced neutron moderation due to the water gap between two fuel assemblies. This phenomenon is explained in §9. 2 and further illustrated in Figure 3. 3. A 13 % increase is observed in the outer row average fission rate compared to the FA average value. The FA maximum F_{xy} reaches 1.27. Those increases are obtained with a MOX FA next to another MOX FA. When a MOX FA is loaded next to a fertile (FER) FA, the outer row average fission rate can increase by up to 40 % compared to the FA average value. This is due to the neutron flux's further thermalization in the adjacent fertile medium.

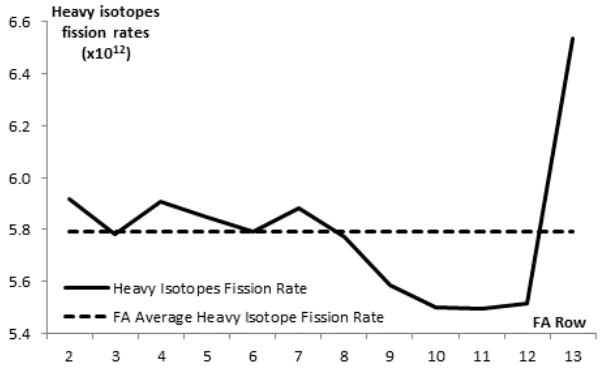

Figure 3. 3: MOX FA Heavy Isotopes Fission Rates per FA Row

In the ZON FA, the MOX fuel rods are grouped in three radial zones and the plutonium concentration is adapted in each of the radial zones. This simple exercise enables better familiarity with the methods and techniques used for research plan creation, surrogate model training and multi-objective optimization. The ZON FA optimization is introduced in Chapter 13.

The second optimization exercise at the fuel assembly level aims at limiting the reactivity increase in case of voided core. Fertile fuel rods are positioned within a MOX fuel assembly for this purpose and form a heterogeneous (HET) fuel assembly. This approach is illustrated in Figure 3. 4 in which an example HET FA containing 120 fertile fuel rods is shown.

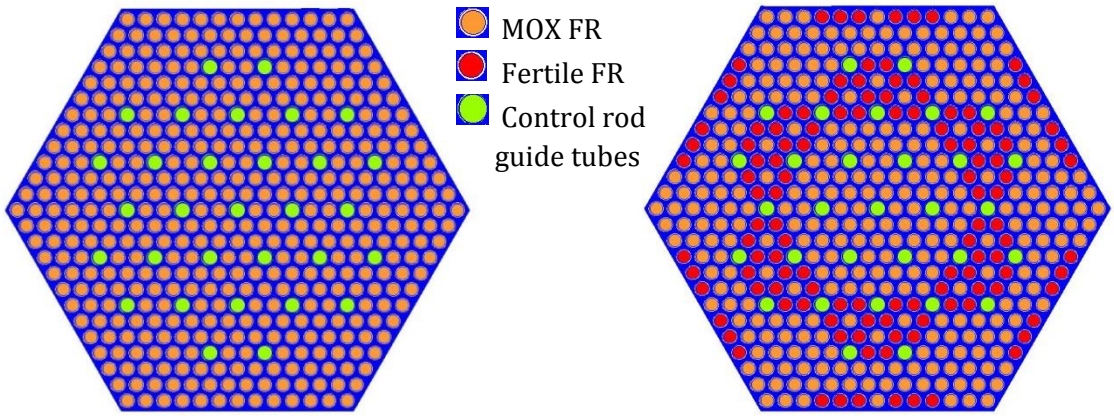

Figure 3. 4: MOX FA and Example HET FA 2D Overview

The consequences in reactivity and power peaks computed with APOLLO2 are introduced in Table 3. 1. The MOX fuel in the MOX FA contains 19 % Pu while the MOX fuel in the HET FA contains 25 % plutonium content for an equivalent plutonium content of 18.2 % at the FA level. Further details are introduced in §9. 2. The reactivity delta between nominal and voided situations computed as void coefficient substantially decreases for the HET FA compared to the MOX FA. It must be remarked that those values are evaluated at the fuel assembly level only. They are not representative of core configurations including neutron leakage. The high increase in the power peak observed for the HET FA motivates the second fuel assembly optimization exercise.

Parameter	Nominal Reactivity (kinf)	Voided Reactivity (kinf)	Void Coefficient (pcm)	F_{xy}
MOX FA	1.15703	1.34651	15166	1.266
HET FA	1.16065	1.31508	12492	1.884

Table 3. 1: MOX and Example HET FA Reactivity and F_{xy} Computed with APOLLO2

The optimization exercise aims at better positioning the fertile fuel rods. It is performed on $1/12^{th}$ of fuel assembly, taking advantage of the FA symmetries. Out of the 44 fuel rods' positions in $1/12^{th}$ FA, up to 12 fertile fuel rods are positioned (up to 144 fertile fuel rods for the entire FA). Identifying where the fertile fuel rods should be located is the aim of the HET FA optimization. This exercise has a discrete behavior and requires specific developments of the genetic algorithm implemented. HET FA optimization is presented in Chapter 14

The optimization exercise at the core level is presented in Chapter 15. The various design options discussed in this work, from the fuel assembly type to the reflector design are considered. The objectives, constraints and parameters in line with the overall HCSMR core design objectives are further detailed in §12. 1.

The surrogate models developed for core design assessment are also introduced in Chapter 15. An optimized population of HCSMR cores is the outcome of the core optimization exercise. Out of the Pareto optimal population a few individuals are then selected for a more detailed analysis.

This makes it possible to highlight some key characteristics of the HCSMR core as well as to identify designs of interest for further developments. To finish, a brief assessment of the results' robustness is performed, by looking at optimization uncertainties and assess the relevance of the results obtained.

12. 1 OPTIMIZATION BOUNDARY CONDITIONS

The HCSMR core generic optimization objectives and boundary conditions are introduced in §4. 3 and can be summarized as follow:

- **Conversion factor** should be maximized and higher than 0.8;
- **Cycle length** should be maximized and higher than 2 years;
- **Void coefficient** should be minimized and less than -500 pcm;
- **Maximum linear heat generation rate** should be minimized and less than 400 W/cm;
- **Plutonium mass** in core should be minimized.

Those generic criteria should apply to the three optimization exercises considered for the HCSMR design. For the two optimizations at the fuel assembly level those criteria must however be adapted. For example the maximum linear heat generation rate is relevant at the core level but not for fuel assembly evaluations since those are based on 2D computations. The F_{xy} at the FA level is the equivalent relevant criteria. Hence the three optimization exercises have their own parameters, objectives and boundary conditions. The main characteristics are summarized in Table 3. 2 and Table 3. 3, for FA and core optimization respectively.

	ZON & HET FA	
	Parameter	**Objective**
Conversion factor	-	-
Cycle length	K_{inf} nominal	*maximize*
Void coefficient	K_{inf} voided	*minimize*
Maximum linear heat generation rate	F_{xy}	*minimize*
Plutonium mass	-	-

Table 3. 2: FA Optimization Objectives

	Core	
	Parameter	**Objective**
Conversion factor	Conversion factor	*maximize*
Cycle length	Cycle length	*maximize*
Void coefficient	Void coefficient	*minimize*
Maximum linear heat generation rate	max. linear heat generation rate	*minimize*
Plutonium mass	Core plutonium mass at BOC	*minimize*

Table 3. 3: Core Optimization Objectives

Each optimization exercise has also its own parameters. A summary of all parameters considered is introduced in Table 3. 4 for FA and core optimization. The ranges of the various parameters are indicated in the next chapters for each optimization case.

ZON FA	HET FA	Core
MOX fuel rods enrichment	Fertile FR position	Fuel type
		Fuel enrichment
		Fuel management
		Loading pattern
		Reflector
		Active height

Table 3. 4: FA Optimization Parameters

Some information on boundary conditions for the optimization exercise must also be taken into account. At the fuel assembly level the pitch between fuel rods and hence the moderation ratio is kept constant in all FA types. This choice, introduced in §4. 2, is based on previous optimization work realized on a similar FA design. The FA geometry and fuel material type (oxide) is also kept constant. At the core level, both the thermal power and number of fuel assemblies are kept constant. Beyond the considered loading patterns and explicit optimization of the loading patterns is not part of this work's scope.

Chapter 13: ZON FUEL ASSEMBLY OPTIMIZATION

The ZON fuel assembly optimization exercise is based on the ZON fuel assembly introduced in Chapter 9. The ZON FA is originally designed to reduce the power peak at the fuel assembly outer layer caused by the local over-moderation. This is due to the proximity of the water gap between FAs. The optimization exercise aims at reducing the FA power peaking factor (F_{xy}) by varying the plutonium content in three types of MOX fuel rods located in three-zones of the FA. Some aspects presented in this chapter are published in PHYSOR 2016 [132].

The geometry of the HCSMR ZON FA is shown in Figure 3. 5. Table 3. 5 describes the types of fuel rods and range of plutonium enrichment considered for each fuel rod type. The fuel assembly average plutonium content is kept constant for each optimization case. To confirm the repeatability of the results obtained, the optimization exercise is performed first with an average plutonium content of 13 % Pu (case ZON.13) and then of 19% Pu (case ZON.19). 25% is the maximum plutonium content in MOX fuel rods due to industrial manufacturing limits.

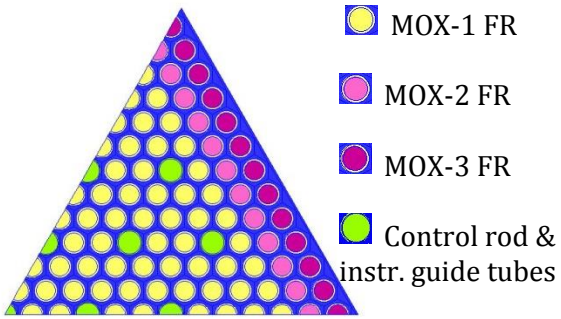

Parameter	ZON FA	No. fuel rods
ZON FA	13 or 19 % Pu	438
MOX-1 fuel	0 - 25 % Pu	300
MOX-2 fuel	0 - 25 % Pu	66
MOX-3 fuel	0 - 25 % Pu	72

Table 3. 5: ZON FA Fuel Rods Type

Figure 3. 5: ZON FA Geometry

The plutonium content in each fuel rod zone $ePu_{ZON(i)}$ is linearly linked to the fuel assembly average content ePu_{FA}:

$$ePu_{FA} = \frac{1}{N_{FA}^{FR}} \sum_{i=1}^{3} ePu_{ZON(i)}\, N_{ZON(i)}^{FR} \qquad (3.\ 1)$$

with N_{FA}^{FR} the total number of FA fuel rods (438) and $N_{ZON(i)}^{FR}$ the number of fuel rods in each zone.

This linear relation between the plutonium content in each zone (MOX-1, MOX-2 and MOX-3) and the fuel assembly average content directly reduces the theoretical boundary given in Table 3. 5 to the values presented in Table 3. 6. Since the weight of MOX-1 fuel rods is higher than MOX-2 or MOX-3, and lower (0 %) and upper (25%) plutonium content limits exist, the available plutonium content range is reduced.

The optimization objectives are the reactivity (k_{inf}), the void coefficient (*void*) and the peaking factor (F_{xy}). The optimization parameters are the enrichment triplet ($ePu_{ZON(1)}$, $ePu_{ZON(2)}$, $ePu_{ZON(3)}$) with $ePu_{ZON(1)}$ linearly derived from $ePu_{ZON(2)}$ and $ePu_{ZON(3)}$.

The fuel rods geometrical repartition in three zones is kept constant in all optimization exercises. Optimizing the geometrical definition of the enrichment zones could be a further development step.

Parameter	ZON.13	ZON.19
ZON FA	13 % Pu	19 % Pu
MOX-1 fuel	8 - 19 % Pu	16 - 25 % Pu
MOX-2 fuel	0 - 25 % Pu	0 - 25 % Pu
MOX-3 fuel	0 - 25 % Pu	0 - 25 % Pu

Table 3. 6: ZON FA Fuel Rods Boundary Enrichments

13. 1 RESEARCH PLAN

13. 1. 1 Overview

Based on the boundary conditions introduced in the previous paragraph, two research plans are designed: one for the ZON.13 optimization exercise and one for the ZON.19 optimization exercise. The research plan for ZON.13 has 2 000 individuals while the one for the ZON.19 optimization exercise has almost ten times more individuals: 18 680. The population sizes were selected differently for both optimization exercises to assess the influence of this parameter. For each research plan, the parameters medium2 and medium3 are sampled using the LHS method (introduced in §5. 1). Medium1 is then linearly derived. Parameter ranges of both populations are presented Table 3. 7. This defines ZON.13 and ZON.19 research plans' boundary conditions. APOLLO2 explicit evaluations are used to evaluate the individuals in each research plan.

Parameter	ZON.13			ZON.19		
	Min	Max	Range (max-min)	Min	Max	Range (max-min)
$\boldsymbol{ePu_{ZON(1)}}$	7.6	18.8	11.2	16.3	24.9	8.6
$\boldsymbol{ePu_{ZON(2)}}$	0.0	25.0	25.0	0.0	25.0	25.0
$\boldsymbol{ePu_{ZON(3)}}$	0.0	25.0	25.0	0.0	25.0	25.0
k_{inf}	1.08360	1.09473	1113 pcm	1.16543	1.17838	1295 pcm
void (pcm)	363	487	124	2188	2290	102
F_{xy}	1.108	2.455	-	1.087	1.950	-

Table 3. 7: ZON FA Surrogate Model Parameter Ranges

The parameters ranges observed for both research plans are similar and show comparable behavior in both cases. The upper limit of 25 % plutonium content for MOX fuel rods tends however to constraint the ZON.19 research plan cases more than the ZON.13 cases. With the ZON.19 case it is not possible to observe cases with 0% Pu content in both $ePu_{ZON(2)}$ and $ePu_{ZON(3)}$ while having a average plutonium content of 19 %. Such a situation is possible though for the ZON.13 case when an average plutonium content of 13 % is the target. The impact of this bias in the boundary conditions is hence limited.

Sensitivity analyses are performed to further characterize the influence of the optimization parameters.

13. 1. 2 Sensitivity Analyses

Sensitivity analyses are first performed to identify which type of optimization exercise ZON.13 and ZON.19 are. The aim is to identify the relationship between the objectives and parameters. The Morris and Sobol indices are used, as introduced in Chapter 5.

13. 1. 2. 1 Morris

Since medium1 enrichment depends linearly on medium2 and medium3 enrichments it is only relevant to study the sensitivity of those last two parameters on the optimization objectives reactivity (K_{inf}), peaking factor (F_{xy}) and void coefficient (*Void*). The Morris method enables the quantification of parameters' influence on the optimization objectives.

The analysis is performed using 100 explicit APOLLO2 computations for each analysis, with medium2 and medium3 being varied within their definition ranges: 0 to 25 % Pu. The outcomes are introduced in Figure 3. 6. Each parameter is plotted as a function of its average variation (μ) on the target parameter and its variance (σ) given in the parameter's unit.

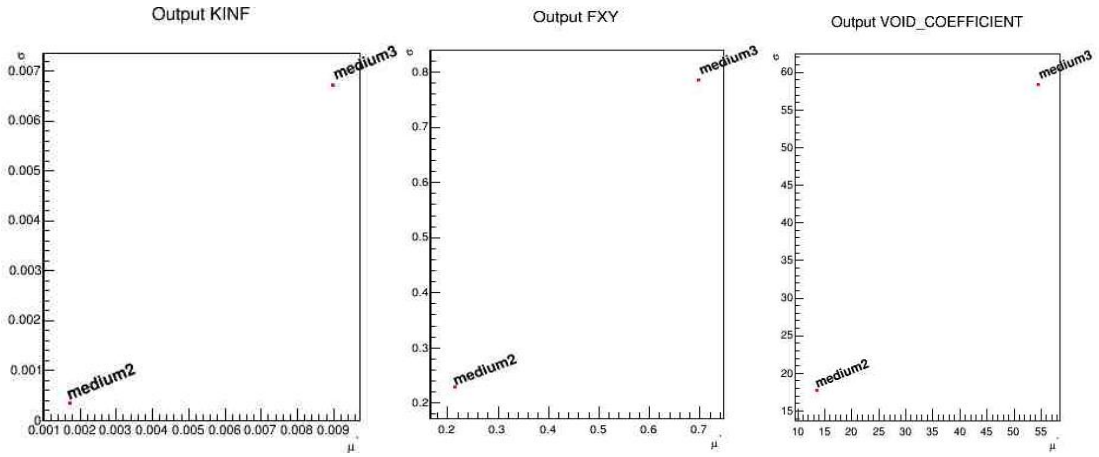

Figure 3. 6: ZON FA Sensitivity Analysis with Morris Method on K_{inf} (left), F_{xy} (center) and *Void* (right)

For the three objective K_{inf}, F_{xy} and *Void*, the parameter medium3 has the largest influence: associated to a variation of medium3 a high average variation (μ) associated to a high variance (σ) is observed.

13. 1. 2. 2 Sobol

The Sobol method is relevant to assess independent parameters. Since medium2 and medium3 considered here are independent, the method can be applied. The Sobol method is a costly analysis, requiring a large number of evaluations of the target function. To save computation time, surrogate models were used instead of explicit APOLLO2 computations. The surrogate models created are introduced in section §13. 2.

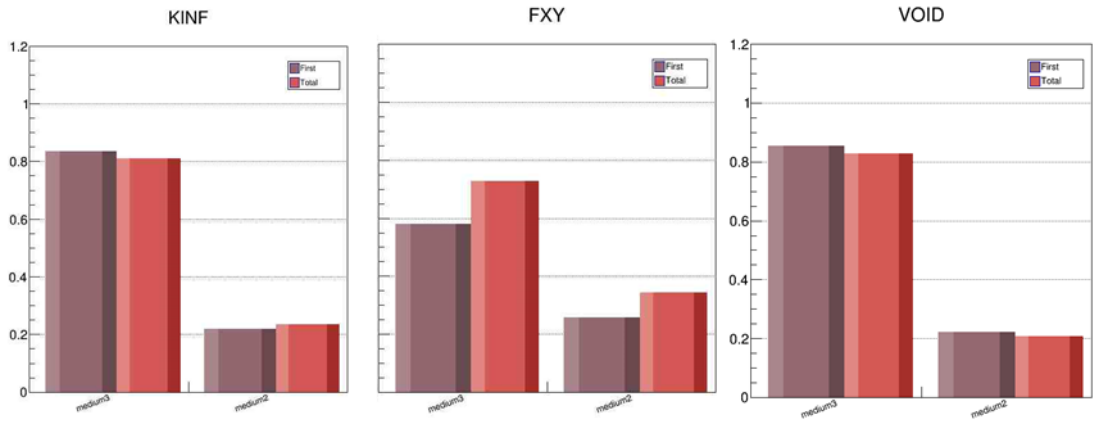

Figure 3. 7: ZON FA Sensitivity Analysis using the Sobol Indices

For the objectives K_{inf}, F_{xy} and *Void*, the Sobol method also shows medium3 has a higher first order and global indices compared to medium2 as illustrated in Figure 3. 7. Medium3 influence on the objective is greater than medium2. The results obtained with the Sobol indices confirm the Morris sensitivity analysis outcomes. It is also in line with expectations from a physical perspective. Since the external layer is in close contact with an increased moderated neutron spectrum its characteristics influences the FA behavior substantially.

13. 2 SURROGATE MODELS

When later using computer-intensive optimization techniques, such as genetic algorithms, a large number of cases must be evaluated. One case or individual is here defined by a given enrichment triplet ($ePu_{ZON(1)}, ePu_{ZON(2)}, ePu_{ZON(3)}$), with $ePu_{ZON(1)}$ linearly derived from $ePu_{ZON(2)}$ and $ePu_{ZON(3)}$. To reduce the computational cost, surrogate models can be used. The benefits and principles of surrogate models are introduced in Chapter 5. Two types of surrogate models are constructed using the URANIE platform: surrogate models based on neural networks and using the kriging theory.

To create surrogate models a training and an independent testing database are used. The database are populations of individuals based on the research plan prepared for ZON.13 and ZON.19 cases and introduced in §13. 1. The respective sizes of the databases are given in Table 3. **8**. In both training and testing populations the parameters' range is similar. The role of the population size is discussed in the next section.

Population	ZON.13	ZON.19
Training	1 000	14 101
Testing	1 000	4 579

Table 3. 8: ZON FA Surrogate Model Training and Testing Populations

Three surrogate functions are created for each optimization exercise: one for each objective: the reactivity (k_{inf}), the void coefficient (*void*) and peaking factor (F_{xy}). The input parameters of each created function are the three enrichments $ePu_{ZON(1)}, ePu_{ZON(2)}, ePu_{ZON(3)}$. The surrogate models' accuracies are then tested against the testing database cases also containing individuals

explicitly evaluated with APOLLO2. The next section introduces the surrogate models' characteristics and accuracies obtained.

13. 2. 1 Neural network

The number of hidden neurons for each surrogate function is illustrated in Table 3. 9 and results from an internal optimum search for each surrogate model. The comparisons between the surrogate function's accuracy and the explicit evaluations are illustrated in Figure 3. 8 to Figure 3. 10 and in Table 3. 9.

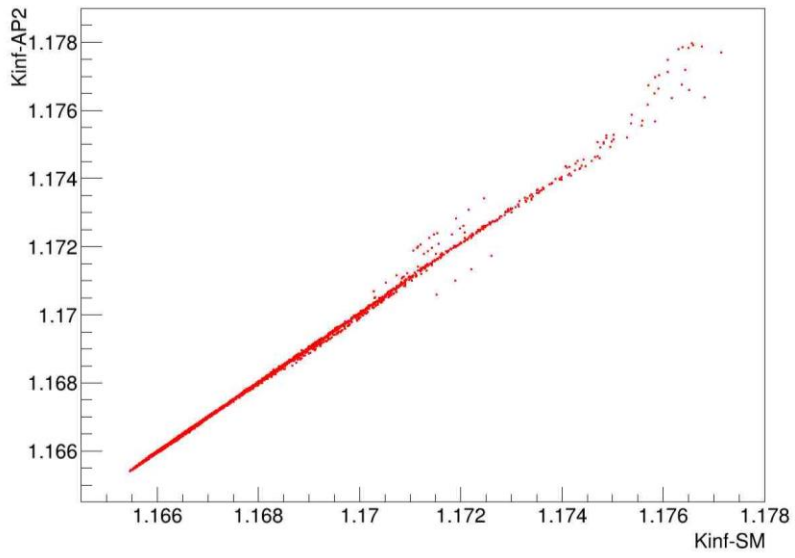

Figure 3. 8: ZON.19 Reactivity (k_{inf}) Neural Network Accuracy Check

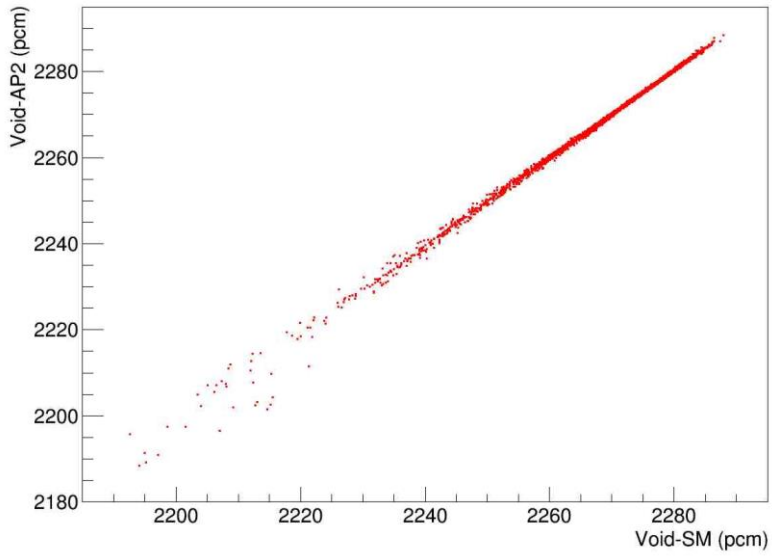

Figure 3. 9: ZON.19 Void Coefficient (*void*) Neural Network Accuracy Check

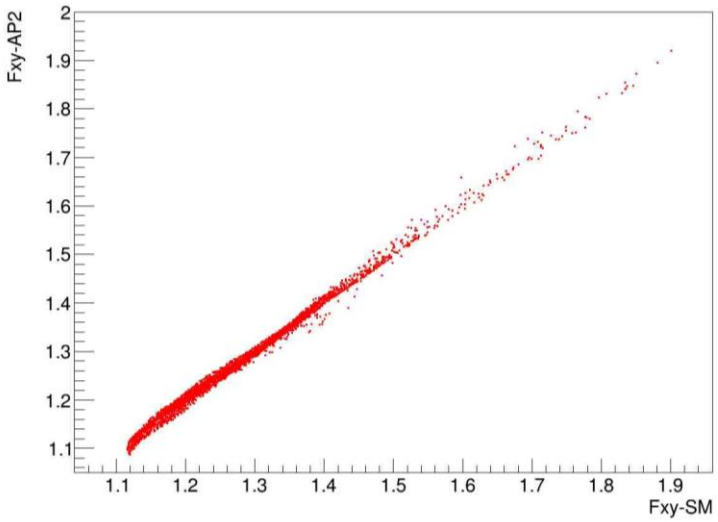

Figure 3. 10: ZON.19 Peaking Factor (F_{xy}) Neural Network Accuracy Check

	ZON.13			**ZON.19**		
	k_{inf}	*void*	F_{xy}	k_{inf}	*void*	F_{xy}
Number of hidden neuron	12	13	12	9	14	8
RMSE	5 pcm	< 1 pcm	< 0.01	6 pcm	< 1 pcm	< 0. 01
95% cases error	6 pcm	1 pcm	0.01	7 pcm	1 pcm	0.02
R^2	0.9998	0.9999	0.9994	0.9621	0.9641	0.9618
Q^2	0.9994	0.9998	0.9992	0.9973	0.9972	0.9948

Table 3. 9: ZON FA Surrogate Performances on Independent Testing Population

The surrogate models constructed using neural network show a high accuracy. Assuming a Gaussian distribution in the neural network prediction, quantiles are derived and the a 95 % confidence interval. The fuel assembly nominal reactivity (k_{inf}) is evaluated using neural networks with a maximum error of 13 pcm for 95% of the individuals considered. The void coefficient (*void*) evaluations have an error smaller than one pcm for 95 % of the individuals while the peaking factor (F_{xy}) error is maximum 0.02 for 95 % of the individuals. The differences observed between explicit APOLLO2 computations and surrogate model evaluations are small and justify using those functions for optimization purposes.

The R^2 training coefficient and Q^2, the predictive coefficient, show good results for all cases. The size of the research plan for training or testing influences the results' quality. This is explained by the increased variety and existence of non-relevant individuals in the research plan. The Kriging method enables an improvement of this aspect.

Further plots illustrate the surrogate function's accuracy in Annex F with the relative error shown for k_{inf} defined as $10^5(\frac{1}{\text{Explicit Kinf}} - \frac{1}{\text{Surrogate Kinf}})$. The results observed for both cases ZON.13 and ZON.19 confirm the accuracy of the surrogate model created.

Furthermore, the size of the learning and testing populations do not show substantial improvements of the surrogate models' accuracy between the ZON.13 and ZON.19 exercises. To confirm this observation an additional comparison is presented in Table 3. 10. The creation of surrogate models using neural network is repeated for k_{inf} using a learning data base of 100 and

500 individuals using the ZON.13 optimization exercise. The results are compared with the 1000 individuals' population outcomes.

k_{inf}	ZON.13		
Learning individuals	100	500	1000
Number of hidden neuron	9	11	10
RMSE	29 pcm	6 pcm	5 pcm
95% cases error	26 pcm	7 pcm	6 pcm

Table 3. 10: Learning Population Size Influence on k_{inf} Neural Network Performances (FA ZON.13)

With only 100 individuals the surrogate models have a rather high inaccuracy. With 500 individuals in the training population the results obtained are similar to the results obtained with a population of 1000 individuals. The accuracy obtained matches this study's requirements. This highlights again the efficiency of neural network to create surrogate models.

Two limitations of the created surrogate models must be mentioned. First the good performances of neural networks created for the ZON FA are obtained for a given domain. When used outside of the creation boundary conditions the surrogate function do not generate reliable results. To illustrate this, the ZON.13 neural networks are tested on a research plan of 1000 individuals with average plutonium of 15 % (ZON.15). The results obtained are presented in Table 3. 11. The large discrepancies between explicit and surrogate results show the importance of limiting the use of surrogate models within their boundary conditions.

	ZON.15 evaluated with SM ZON.13		
	k_{inf}	*void*	F_{xy}
Number of hidden neuron	10	13	9
RMSE	1640 pcm	54 pcm	0.06
95% cases error	1751 pcm	70 pcm	0.07

Table 3. 11: ZON.13 Neural Network Applied to ZON.15 Testing Dataset

The second limitation of the surrogate models is also related to the training boundary conditions: the surrogate function's accuracy is reduced in domain with only few individuals in the research plan. The Figure 3. 8 to Figure 3. 10 highlight the uneven distribution of the individuals and associated challenge: the areas with few individuals have a higher error between explicit and neural network evaluations.

13. 2. 2 Kriging

The creation of surrogate models using the Kriging method is also performed with the URANIE tool. The methodology and parameters are introduced in Chapter 5. Beyond the accuracy of the Kriging interpolation method, it also enables the integration of "Leave One Out" (LOO) approaches.

It is not unusual to have in the research plan individuals resulting from wrongly evaluated cases, for example due to a code failure. The surrogate model learning algorithm would by default include such individuals. The LOO approach provides a barrier against such behavior.

The LOO approach aims at assessing the difference between an individual value from the research plan and from an evaluation with the Kriging model. With an error greater than five sigma the individual is not considered to form the Kriging model. Five sigma corresponds to less than 10^{-4} % chance (considering a Gaussian distribution), which is statistically highly improbable. The error can also come from inadequate parameters selected for the Kriging model creation. This also gives hints at possible further improvement. More details on the LOO approach applied to the Kriging method can be found in [133].

	ZON.13		
	k_{inf}	*void*	F_{xy}
RMSE	8 pcm	< 1 pcm	< 0. 01
Q^2	0.9986	0.9992	0.9999

Table 3. 12: ZON.13 Kriging Surrogate Model

The surrogate models created with the Kriging method show good accuracy. The LOO makes it possible to obtain Q^2 close to one as shown in Table 3. 12.

13. 2. 3 Compared Performances

The surrogate models created with neural networks and Kriging methodology show good results. The performances obtained with neural networks are however slightly better than the ones obtained with the Kriging method. Moreover the time required to create the surrogate function is substantially reduced when using neural networks compared to the Kriging method. A similar tendency is also observed when the surrogate functions are used to evaluate an individual: evaluations using neural network based surrogate models are about ten times quicker than evaluations using surrogate models based on the Kriging method.

Those observations advocate to further use the surrogate functions created with neural networks for the HCSMR ZON FA optimization. The FA optimization and use of surrogate models is the focus of the next section.

13. 3 OPTIMIZATION

The optimization objectives are the reactivity (k_{inf}), the void coefficient (*void*) and the peaking factor (F_{xy}). Whereas *void* and F_{xy} should be minimized, the reactivity *kinf* should be maximized. The optimization parameters are the enrichment triplet ($ePu_{ZON(1)}$, $ePu_{ZON(2)}$, $ePu_{ZON(3)}$) with $ePu_{ZON(1)}$ linearly derived from $ePu_{ZON(2)}$ and $ePu_{ZON(3)}$. Hence only $ePu_{ZON(2)}$ and $ePu_{ZON(3)}$ belong to optimization parameters. The optimization is performed with two methods: with genetic algorithms and then using the particle swarm method. This enables the assessment of both approaches with the ZON optimization exercise.

13. 3. 1 Genetic Algorithms

As introduced in §5. 4 genetic algorithms (GA) are evolutionary algorithms developed based on observations of natural selection and genetics. The Vizir module of the Uranie platform [91] is used to perform the optimization. A population size of 1000 individuals is used, resulting from a

trade-off between computation time and outcomes' relevance. The surrogate models created with neural networks are used to evaluate the individuals' characteristics (*kinf*, *void*, F_{xy}). The optimization is continued until all individuals have reached a null Pareto rank. This means all individuals could not be optimized further on one objective without deteriorating another objective. If the predefined maximum number of evaluations (fixed at one million) is reached before all individuals are of Pareto rank null, the optimization is stopped. The results are shown in the next plots. Figure 3. 11 shows the Pareto front and surface obtained with the optimized population. The parallel coordinates plot in Figure 3. 12 shows the entire optimized population.

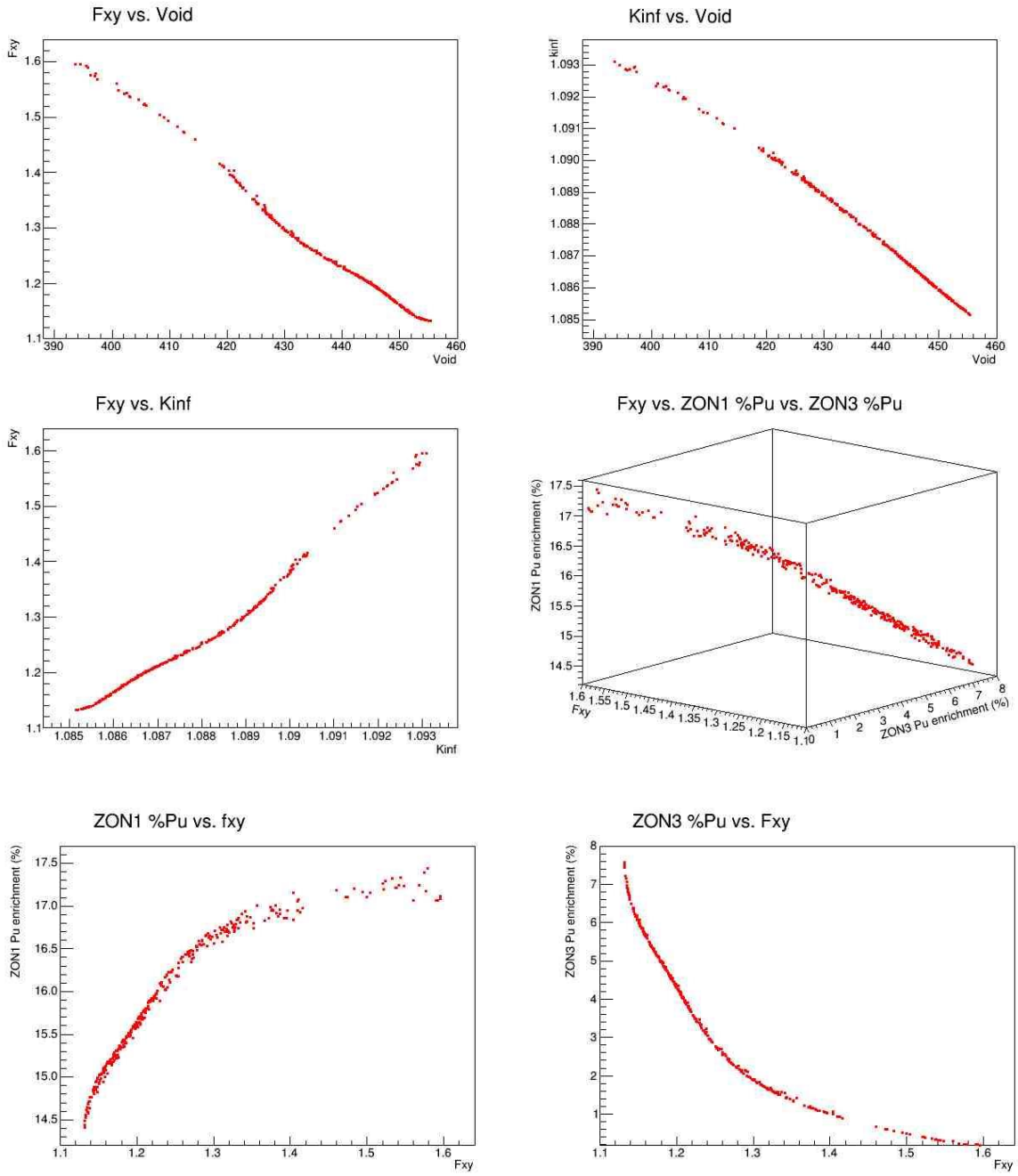

Figure 3. 11: ZON.13 Optimization with Genetic Algorithms Pareto Front

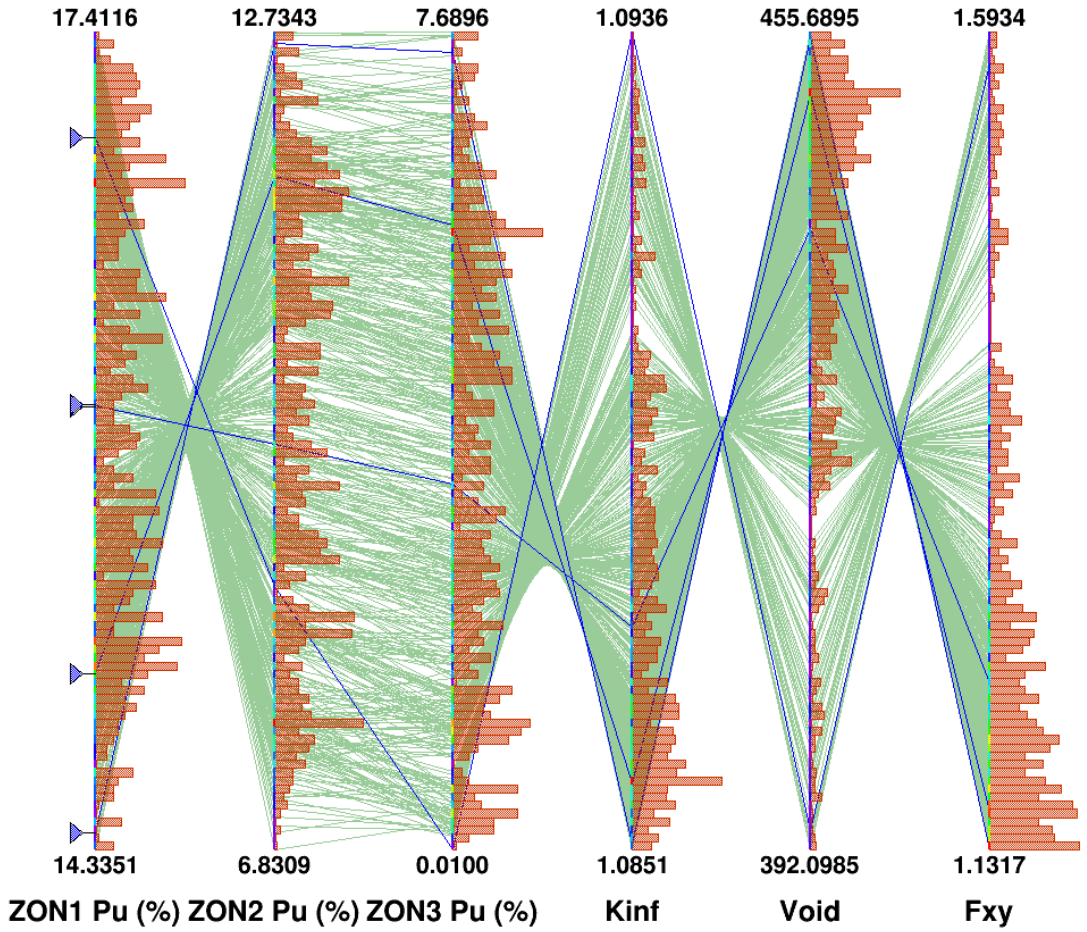

Figure 3. 12: ZON.13 GA Optimization Pareto Population and Selected Individuals (blue)

The optimization outcomes presented in Figure 3. 12 contain interesting physical behavior. First the range of the objectives obtained is comparable to the research plan derived at first. The optimization process has well covered the entire domain of interest. Mostly two types of individuals can be identified in the optimized population. Individuals with a rather low reactivity (k_{inf}) a high void coefficient (*void*) and low peaking factor (F_{xy}). This is observed for individuals with rather high plutonium enrichments in the two external rows of fuel rods, i.e. in ZON2 and ZON3 regions. In Figure 3. 12 this behavior is illustrated by the two blue lines originating at the bottom left of the plot: low ZON1 plutonium content.

A second category of individuals have high reactivity (*kinf)*, low void coefficient (*void*) and high peaking factor (F_{xy}). This is observed when the enrichment in ZON2 and ZON3 is low or extremely low with enrichment in ZON3 below 1%. In Figure 3. 12 this behavior is illustrated by the blue line originating at the top left of the plot: high ZON1 plutonium content. Such fuel assembly design can also be described as an introduction of fertile fuel rods on the outer part of the fuel assembly since the plutonium concentration is very low. A similar approach will be looked at in Chapter 14 where fertile fuel rods are formally introduced. Physically the added value of fertile fuel rods can be understood as the introduction of an escape route for neutrons in case of voided situation. The diversity in the population observed illustrates well the Pareto surface concept as all individuals best in one objective are kept.

13. 3. 2 Particle Swarm

The HCMSR ZON FA optimization exercise is repeated for the ZON.13 case using the particle swarm method. This aims at assessing whether another optimization method, beyond genetic algorithm, should be implemented to optimize the HCSMR design.

The results from particle swarm optimization are plotted in Figure 3. 13. Very similar outcomes are obtained between particle swarm optimization and genetic algorithm optimization. The ranges (minimum, maximum) of the parameters and objectives are close with both methods. This confirms the robustness of the Pareto population obtained. A difference is observed in the distribution of individuals between Pareto's populations. With genetic algorithm the concentration of individuals is related to the optimization objectives, whereas this is not the case for the Pareto population obtained using the particle swarm method. This is highlighted by the orange histograms in both Figure 3. 12 and Figure 3. 13. Overall this shows the particle swarm method does not bring specific added value to the results compared to genetic algorithm.

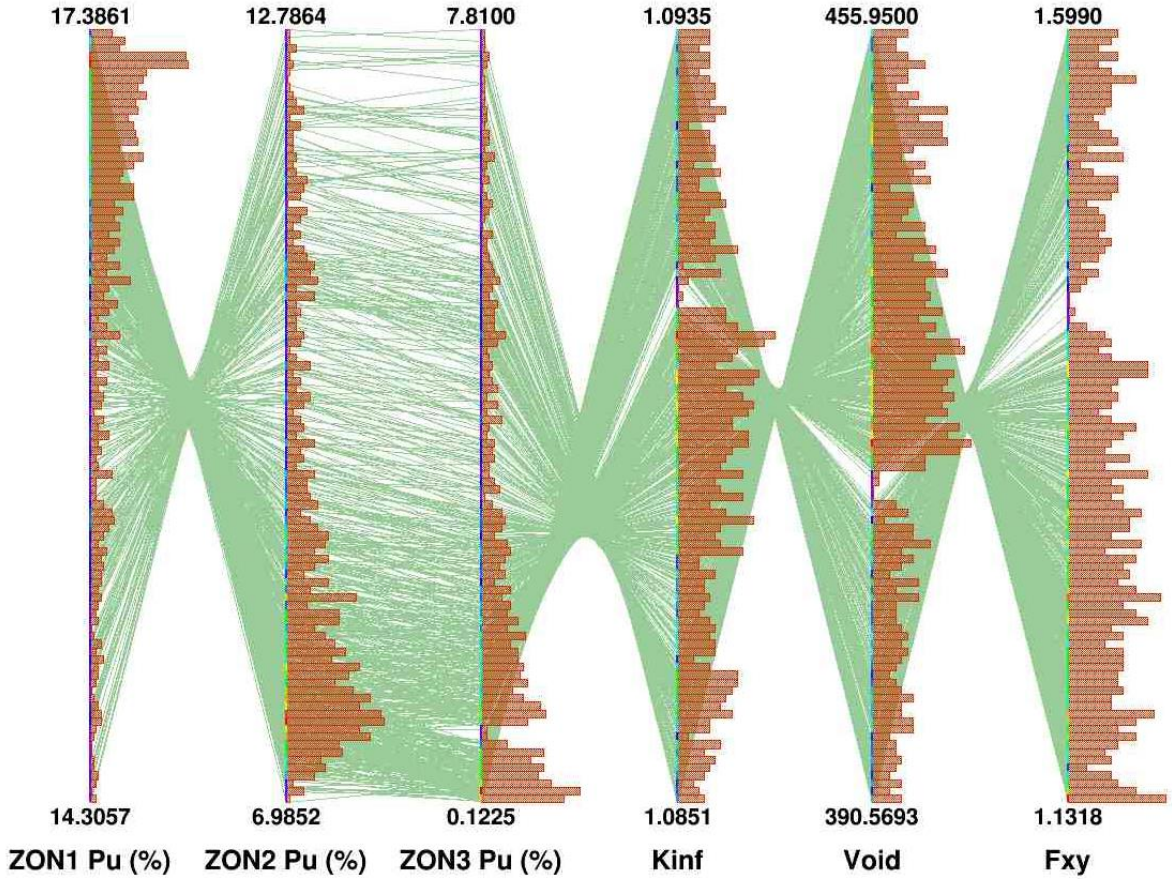

Figure 3. 13: ZON.13 Optimization with Particle Swarm Method

The costs of the optimization are different, however. To optimize a population of 1000 individuals 13 seconds are needed using the particle swarm method whereas 33 seconds are needed for the genetic algorithm optimization. These remain acceptable computing times for both methods.

13. 4 OUTCOMES

The HCSMR ZON FA optimization exercise is performed either using genetic algorithms or particle swarm optimizations. Both methods use surrogate models to evaluate the individuals in the population and obtained a Pareto optimum population. The results from both methods are very similar as explained previously and highlighted in Figure 3. 14 showing the Pareto population obtained with both optimization methods together.

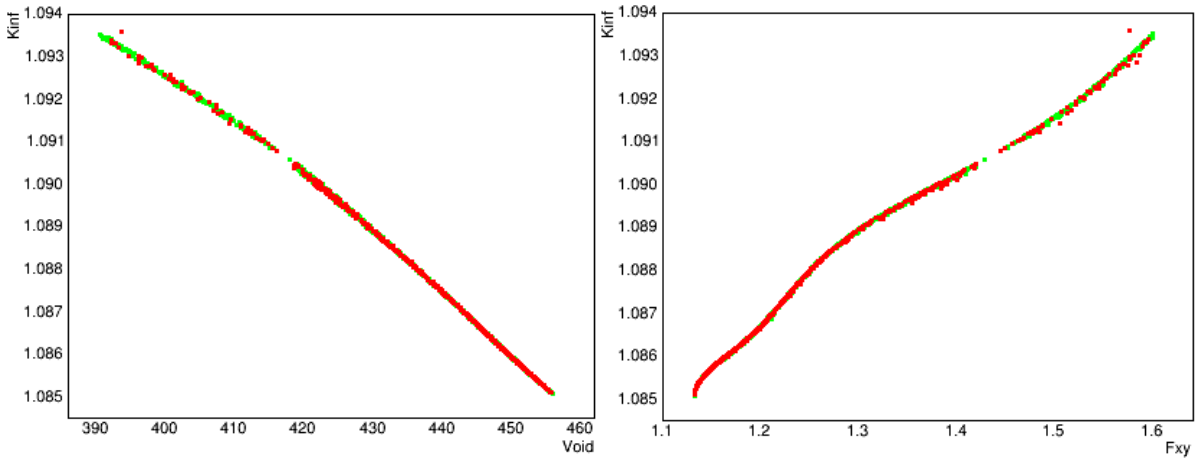

Figure 3. 14: ZON.13 Pareto Fronts with Particle Swarm Population (green) and Genetic Algorithm Population (red)

Base on the results obtained, four individuals are selected as ZON FA design input for the core optimization. Those four individuals are selected to cover the extrema of each optimization objective while all being Pareto optima. The four individuals are marked in blue in Figure 3. 12 and introduced in Table 3. 13.

Case	ZON1 Pu (%)	ZON2 Pu (%)	ZON3 Pu (%)
1	14.4	12.5	7.5
2	17.0	8.7	0.0
3	15.0	11.8	5.6
4	16.0	9.8	3.4

Table 3. 13: ZON.13 Optimization Selected Cases Performances

The performances of the four individuals selected are recalculated with the code APOLLO2. This aims at validating the accuracy of the results obtained. The comparison results are shown in Table 3. 14.

A maximum of 6 pcm difference on reactivity (kinf) is observed. The void coefficient (void) is evaluated within 2 pcm maximum difference and a maximum of 0.02 % difference on peaking factor (Fxy) is observed. Those accuracies are good and remain within the errors associated with the created surrogate models as introduced in Table 3. 9. The reactivity delta is evaluated using equation 3. 2.

$$Delta\ (pcm) = 10^5.(\frac{1}{kinf_{AP2}} - \frac{1}{kinf_{SM}}) \quad (3.2)$$

Case	Kinf SM	Kinf AP2	Delta (pcm)	Fxy SM	Fxy AP2	Delta	Void SM (pcm)	Void AP2 (pcm)	Delta (pcm)
1	1.08495	1.08489	5	1.132	1.123	< 0.01	455	447	2
2	1.09357	1.09351	5	1.592	1.572	0.02	404	405	1
3	1.08561	1.08556	4	1.152	1.162	0.01	451	449	2
4	1.08743	1.08736	6	1.227	1.239	0.01	440	438	2

Table 3. 14: ZON.13 Optimization Selected Performances SM vs. AP2

13. 4. 1 Input to Core Optimization

At the core level, having only one level of the plutonium content (13% used for the ZON.13) limits the optimization possibilities. The HCMSR ZON FA optimization is hence repeated for other plutonium content: 15%, 17%, 19% and 21%. The method used for the ZON.15, ZON.17, ZON.19 and ZON.21 cases is similar to the one implemented with the ZON.13 case. The optimization is performed using genetic algorithms. The detailed outcomes are introduced in Annex G and are used to select the ZON FA designs to be evaluated at the core level. The same principle as for the ZON.13 case is used: four individuals (ZON FA designs) out of the Pareto optimum population are selected to cover broadly the population and its extrema. Table 3. 15 shows the list of selected ZON FA for HCSMR core optimization. For those 20 FA design full branch computations (saphybs) are prepared with APOLLO2.

Case	Pu average content (%)	ZON1 Pu (%)	ZON2 Pu (%)	ZON3 Pu (%)	Kinf	Fxy	Void (pcm)
1	13.0	14.4	12.5	7.5	1.08489	1.123	447
2		17.0	8.7	0.0	1.09351	1.570	405
3		15.0	11.8	5.6	1.08556	1.161	449
4		16.0	9.8	3.4	1.08736	1.239	438
5	15.0	20.2	7.7	0.2	1.12032	1.516	1136
6		16.6	14.6	8.9	1.11168	1.119	1199
7		19.5	10.9	0.1	1.12100	1.665	1133
8		18.2	12.0	4.3	1.11298	1.217	1188
9	17.0	23.7	4.9	0.1	1.14864	1.736	1745
10		18.7	16.1	10.9	1.13867	1.115	1733
11		21.3	16.0	0.1	1.14835	1.806	1801
12		20.5	14.6	4.8	1.14081	1.204	1790
13	19.0	24.9	12.6	0.0	1.17777	1.632	2210
14		24.0	17.0	0.0	1.17811	1.801	2208
15		20.5	18.6	12.9	1.16667	1.103	2275
16		22.0	17.3	8.0	1.16769	1.162	2271
17	21.0	24.9	24.8	1.5	1.19723	1.621	2676
18		22.4	21.8	14.3	1.19138	1.093	2689
19		24.9	21.8	3.8	1.19418	1.341	2660
20		23.0	21.2	12.5	1.19190	1.113	2690

Table 3. 15: ZON Selected Cases Out of GA Optimization

The HCSMR ZON FA optimization exercise enables the introduction of the tools and methodology used to optimize the HCSMR design. First a research plan is created using the LHS sampling method. Surrogate functions are then created based on APOLLO2 explicit evaluations to reduce the computational costs of the optimization. The optimization itself is performed using either genetic algorithm or the particle swarm method. Beyond the lessons learned on optimization processes, the outcomes of this exercise are 20 optimized HCSMR ZON FA designs. Those designs will serve as input to the core optimization. Before looking at core optimization the next chapter is dedicated to another optimization at the fuel assembly level: the introduction and positioning of fertile fuel rods within a fuel assembly, referred as the HCSMR HET FA optimization exercise.

Chapter 14: HET FUEL ASSEMBLY OPTIMIZATION

The HET fuel assembly optimization exercise is based on the HCSMR HET fuel assembly introduced in Chapter 9. The HET FA type is designed to reduce the reactivity increase in case of loss of coolant. Also referred to as a voided situation, a loss of coolant can lead to a reactivity increase characterized by a positive void coefficient. Such behavior can be observed in particular in under-moderated cores. For safety reason the void coefficient must remain negative. Those aspects are further presented in §3. 4. Some outcomes presented in this chapter are published in PHYSOR 2016 [132].

Here the optimization exercise aims at reducing the void coefficient (*void*) by introducing fuel rods containing fertile fuel only. As introduced in §3. 4 fertile materials reduce the reactivity increase in case of loss of coolant due to the absence of Plutonium in it. In parallel the reactivity (k_{inf}) should be maximized while the peaking factor (F_{xy}) should be minimized. A multi-objective optimization exercise is considered for the HET fuel assembly as introduced in Chapter 5.

The optimization challenge lies in the positioning of the fertile fuel rods. Figure 3. 15 introduces a possible positioning of 10 fertile fuel rods out of 44 in $1/12^{th}$ of HCSMR fuel assembly, corresponding to the introduction of 120 fertile fuel rods at full FA scale. Since FA designs are periodically symmetric, this optimization exercise is performed on $1/12^{th}$ of FA only. The fertile fuel rods positions shown in Figure 3. 15 correspond to the HET FA design used for the computation scheme validation (Chapter 9).

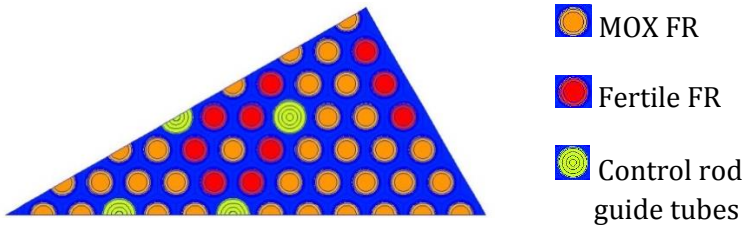

Figure 3. 15: HET FA Design Example

Several strategies can be implemented to position fertile fuel rods within the fuel assembly. They can be positioned in the FA outer row, next to guiding tubes or even randomly. A large number of combinations exist. The optimization exercise has hence a large dimension and a discrete behavior. Considering the introduction of 1 to 43 fertile fuel rods out of the 44 positions in the $1/12^{th}$ fuel assemblies, $1.76\ 10^{13}$ combinations exist to position the fertile fuel rods. This is derived from equation 3. 3.

$$\sum_{i=1}^{43}\binom{44}{i} = \sum_{i=1}^{43}\frac{44!}{i!(44-i)!} \qquad (3.\ 3)$$

Empirical observations show the size of this discrete optimization exercise with over 10^{13} possible combinations is too large to obtain converged optimization outcomes. The total number of combinations is influenced by the number or quantity of fertile fuel rods to be introduced on the one hand; and by the position available to locate fertile fuel rods on the other hand.

To limit the optimization exercise's size first the quantity of fertile fuel rods to be introduced is fixed: only four cases of fertile fuel rods' introduction are considered, with 5, 8, 10 and 12 fertile fuel rods out the 44 fuel rods positions. Those exercises are referred to as HET.05, HET.08; HET.10 and HET.12. Simplifications are also considered to limit the available positions for fertile fuel rods and are introduced later on.

The introduction of fertile fuel rods decreases the fuel assembly's average plutonium content and hence the reactivity. Increasing the plutonium content in the FA MOX fuel rods makes it possible to compensate this effect. This is however constrained by the technological limit in maximum plutonium content of 25 %. Hence the maximum of 12 fertile fuel rods out the 44 positions investigated. This is further illustrated in Table 3. 16.

Avg. Pu (%)	**21.0**	**20.0**	**19.0**	**18.0**	**17.0**	**16.0**	**15.0**	**14.0**	**13.0**	**12.0**	**11.0**
Nb FER FR (for 1/12)	**MOX FR Pu (%)**										
5	24.3	23.2	22.0	20.9	19.7	18.5	17.4	16.2	15.1	13.9	12.7
6	25.1	23.9	22.7	21.5	20.3	19.1	18.0	16.8	15.6	14.4	13.2
7	26.0	24.7	23.5	22.3	21.0	19.8	18.6	17.3	16.1	14.8	13.6
8	26.9	25.6	24.3	23.1	21.8	20.5	19.2	17.9	16.6	15.4	14.1
9	27.9	26.5	25.2	23.9	22.6	21.2	19.9	18.6	17.3	15.9	14.6
10	28.9	27.5	26.2	24.8	23.4	22.0	20.7	19.3	17.9	16.5	15.2
11	30.1	28.6	27.2	25.8	24.3	22.9	21.5	20.0	18.6	17.2	15.7
12	31.3	29.8	28.3	26.8	25.3	23.8	22.3	20.9	19.4	17.9	16.4
13	32.6	31.1	29.5	28.0	26.4	24.9	23.3	21.7	20.2	18.6	17.1
14	34.1	32.4	30.8	29.2	27.6	26.0	24.3	22.7	21.1	19.5	17.8
15	35.7	34.0	32.3	30.6	28.9	27.2	25.5	23.8	22.1	20.4	18.7

Table 3. 16: HET FA Average Plutonium Content and MOX Plutonium Content

A minimum number of fertile fuel rods is required to observe a relevant effect of fertile medium introduction. This is illustrated in Figure 3. 16 and is a motivation to set at five the minimum number of fertile fuel rods to be introduced within the 44 fuel rods positions.

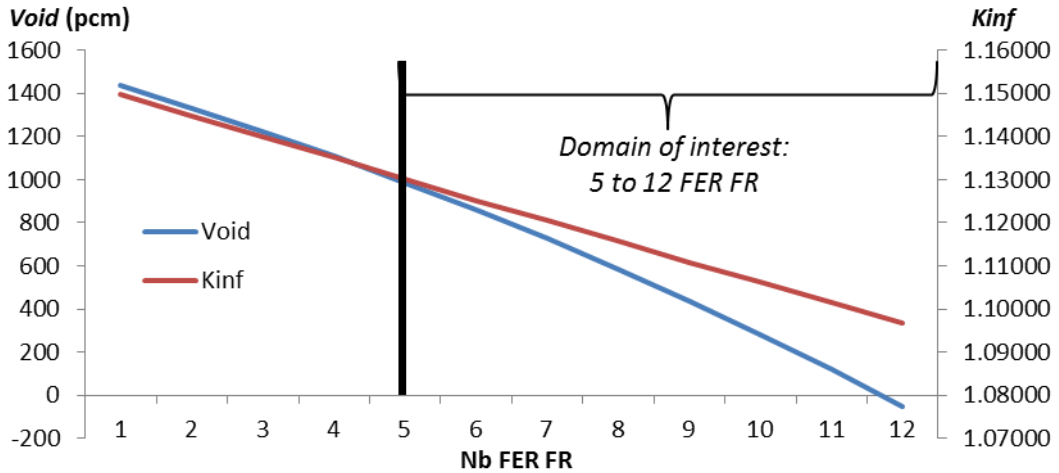

Figure 3. 16: HET FA Kinf and Void vs. Number of Fertile FR

Figure 3. 16 shows the reactivity and void coefficient for HET fuel assemblies with one to twelve fertile fuel rods. The positioning is based on Figure 3. 15 design with ten fertile fuel rods. Below ten fertile fuel rods, the fertile fuel rods are arbitrarily removed from top to bottom and left to right based on the Figure 3. 15 plot. The two additional fertile fuel rods needed to reach twelve fertile fuel rods are added on the outer row from top to bottom.

The four cases HET.05, HET.08, HET.10 and HET.12 are further defined with the research plan introduction in the next paragraph. The discrete behavior of this optimization exercise influences the optimization process. First a sensitivity analysis using the Morris method is only available with continuous parameters. According to literature on the subject [134] Sobol indices could be used with discrete parameters. However, the implementation in URANIE is not completed yet; hence this has not yet been performed for the HCSMR HET optimization and could be addressed in future work.

The absence of rigorous sensitivity analysis does not mean the author is blind in understanding the HET FA optimization guiding principles. The observations from the ZON FA optimization applies to some extent to the HET FA design. For example, fertile fuel rods positioned in the FA outer row, next to the water gap between fuel assemblies, or next to guide tube water holes influence substantially the void coefficient, while limiting the peaking factor increase. On the contrary, single fertile fuel rods in a cluster of MOX fuel rods have a limited impact. The neutron mean free path in under-moderated designs supports this reasoning. Those principles and the further knowledge gained via HET FA optimization research plans help to adjust the optimization process.

The discrete aspect of the HET FA optimization exercises also impacts the creation of surrogate models. Each fuel assembly or individual is defined by 44 Boolean input variables, defining either a fertile or fissile fuel rod. Accurate surrogate model creations are not successful. The limit lies in the size of the initial research plan. To cover the various discrete cases a very large number of explicit evaluations with APOLLO2 are needed, which is costly in computation time. As a consequence the optimization is directly performed using explicit APOLLO2 evaluations. The optimization itself is performed with a specific genetic algorithm developed for this purpose based on the URANIE platform tools.

14. 1 RESEARCH PLAN

14. 1. 1 Overview

Each fuel assembly or individual is defined by 44 Boolean input variables, defining either a fertile or fissile fuel rod. To create the research plans, the positions of the fertile fuel rods are randomly selected among the 44 fuel rods, respecting symmetry rules and the targeted total number of fuel rods in each case (HET.05, HET.08, HET.10 and HET.12). Several plutonium enrichments are considered to assess the impact of this variable on the research plans' outcomes. Overall eight research plans are prepared as introduced in Table 3. 17. The size of the research plans or number of cases evaluated are also introduced in Table 3. 17. The evaluations are based on explicit computations performed with the simplified APOLLO2 computation

schemes HET-S introduced in §9. 3. 2. The ranges of the objectives parameters k_{inf}, *void* and F_{xy} for the eight research plans are presented in Table 3. 18.

Case	RP Name	No. fertile FR (1/12th FA)	No. fertile FR (Full FA)	Pu (%) in MOX	FA Pu eq. (%)	Population size
1	HET.05-1	5	60	19.0	16.4	5000
2	HET.05-2	5	60	22.0	19.0	2000
3	HET.08-1	8	96	19.0	14.8	3000
4	HET.08-2	8	96	15.4	12.0	3000
5	HET.08-3	8	96	21.0	16.4	5000
6	HET.10	10	120	19.0	13.8	5000
7	HET.12-1	12	144	19.0	12.8	5000
8	HET.12-2	12	144	21.0	14.1	5000

Table 3. 17: HET FA Optimization Research Plans

Case	Min Kinf	Max Kinf	Abs Delta (pcm)	Min Void (pcm)	Max Void (pcm)	Abs Delta (pcm)	Min Fxy	Max Fxy	Abs Delta
1	1.12694	1.13098	404	978	1011	33	1.312	2.208	0.896
2	1.15929	1.16281	352	1465	1494	29	1.311	2.217	0.906
3	1.11067	1.11583	516	583	625	42	1.400	2.609	1.209
4	1.07475	1.07972	497	-219	-177	42	1.401	2.624	1.223
5	1.13035	1.13566	531	939	981	42	1.394	2.594	1.200
6	1.12793	1.13352	559	819	867	48	1.487	2.76	1.273
7	1.08982	1.09571	589	-46	4	50	1.607	3.133	1.526
8	1.10720	1.11293	573	337	385	48	1.606	3.121	1.515

Table 3. 18: HET FA Research Plans' Ranges

A graphical representation with a parallel plot provides limited insights due to the high number of input variables. A screening of the best evaluated cases with regards to the three optimization objectives makes it possible to guide the further optimization steps: pattern similarities are observed when looking at the best case for each optimization objective. This was further used to design predefined layouts as introduced in the next section.

14. 1. 2 Patterns

The high number of combinations existing to position fertile fuel rods in the HET FA is a challenge for the optimization. Empirical observations show optimizations are not converging with over two million possible combinations to position fertile fuel rods. Two million combination are reached when positioning six fertile fuel rods or more. To reduce the exercise size and the number of combinations, some fuel rods are forced as either fertile (FER) or fissile (FIS) fuel rods. This reduces the number of available positions (LIB) for the optimization and hence the number of combinations. This is illustrated in Table 3. 19 introducing the number of FER and FIS fuel rods set for the HET.08, HET.10 and HET.12 cases.

With this approach a bias is introduced. Therefore the optimizations are repeated with different predefined cases. The predefined cases, also referred to as patterns, define the position of FIS and FER fuel rods. Those patterns are obtained after analysis of research plans.

Nb FER Total	Nb FER fixed	Nb FIS fixed	Nb FER to be positioned	Nb LIB	Available Combination (million)
5	0	0	5	44	1.1
8	0	0	0	44	177.2
8	2	6	6	36	1.9
10	0	0	0	44	2481.3
10	4	5	6	35	1.6
12	0	0	0	44	21090.7
12	5	10	7	29	1.6

Table 3. 19: HET FA Available Combination and Domain Reduction (1/12th FA)

To obtain such patterns, a statistical analysis is performed. Research plan populations are sorted according to the three objectives k_{inf}, *void* and F_{xy}. For each objective the occurrence of fertile fuel rods for each fuel rod position is statistically computed considering only the best ten percent of individuals according to the objective. Patterns are then obtained by looking at the fuel rod positions with the most often occurring fertile fuel rods. This is illustrated, for example, based on the HET-08.1 research plan, with patterns for best k_{inf}, best *void* and best F_{xy} in Figure 3. 17.

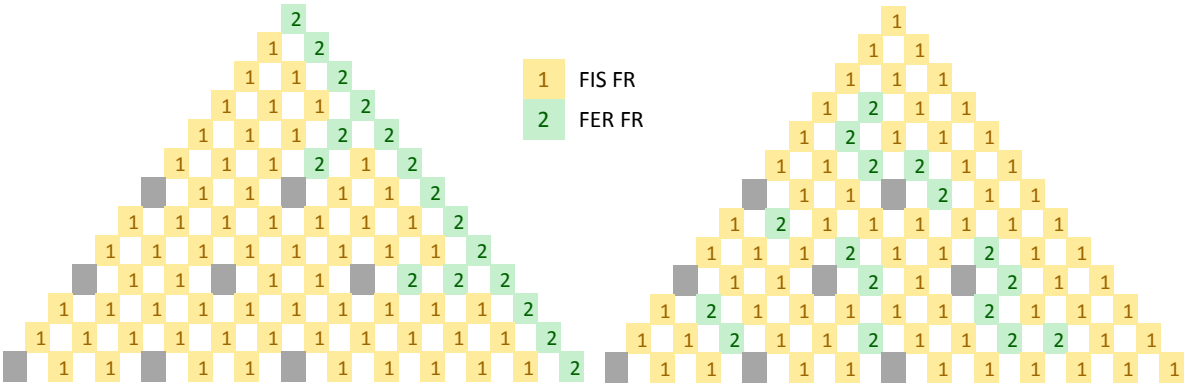

Figure 3. 17: HET FA Patterns Best K_{inf} and *Void* (left) and Best F_{xy} (right)

Figure 3. 17 as well as the next plots in this section show 1/6th of a FA being 1/12th symmetric. All observations show the same patterns for best k_{inf} and best *void*. Hence only two types of patterns are considered for optimization: one for best k_{inf} and best *void* on the one hand and one for best F_{xy} on the other hand.

This exercise is repeated for various plutonium contents using the research plan created (HET.08 for example) or different population sizes in the research plan (HET.05). Observations show this does not influence the result of the best positions' statistical occurrence. This outcome encourages considering only one reference statistical analyze for each of the HET.08, HET.10 and HET.12 cases. For the HET.05 no predefined patterns are used since the dimension of the exercise is small enough.

Based on the patterns obtained the fixed FIS and FER fuel rods are selected. Those predefined cases are varied and repeated to ensure the robustness of the approach implemented. Looking at the HET.08 example further, two FER and six FIS fuel rods should be selected. One possible option is shown in Figure 3. 18.

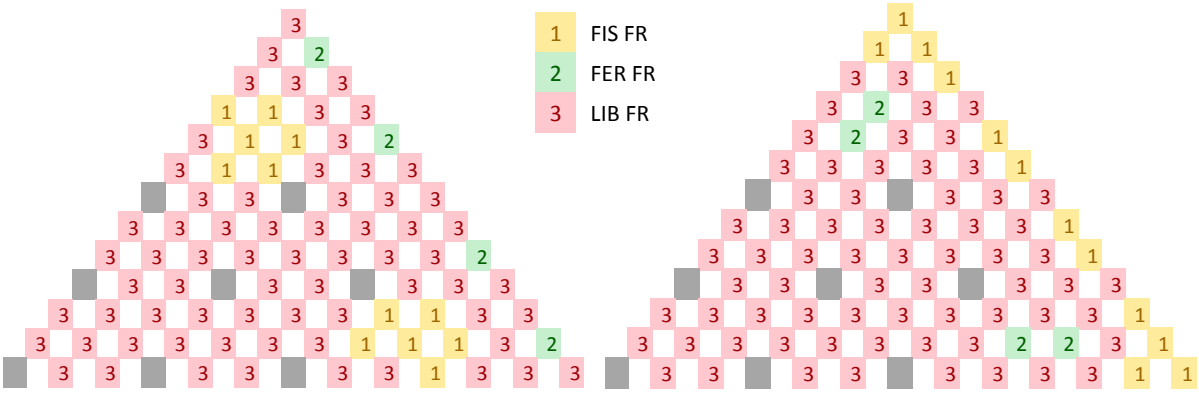

Figure 3. 18: HET FA Predefined Optimization Layout for Best K_{inf} and *Void* (left) and Best F_{xy} (right)

The choice of the fixed FER and FIS positioned are based on engineering judgment. For each optimization case, four predefined patterns are considered to increase the possible optimization outcomes and reduce the risk of a systematic bias being introduced. The four predefined patterns are divided into two for best k_{inf} and *void* and two for best F_{xy}. The other two patterns for HET.08 are introduced in Figure 3. 19 as an example. All predefined patterns are introduced in Annex I.

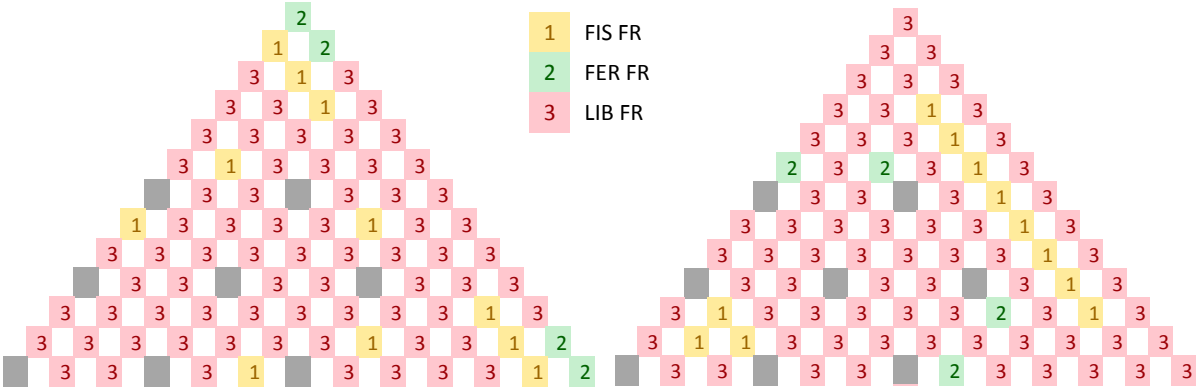

Figure 3. 19: HET FA Predefined Optimization Layout for Best K_{inf} and *Void* (left) and Best F_{xy} (right)

14. 2 Optimization

The HET FA optimization has three objectives: to maximize the reactivity (k_{inf}) while minimizing the void coefficient (*void*) and peaking factor (F_{xy}). There are 44 parameters, being either fertile or fissile fuel rods. To reduce the optimization exercise size and enable convergence, optimizations are limited to cases offering up to two million combinations. The use of predefined

patterns, as introduced in the previous paragraph, enables this. With those patterns some fuel rods are imposed as fissile or fertile fuel rods.

The HET FA optimization is performed with genetic algorithm. The optimization process is introduced in §5. 4. An initial population is evaluated, ranked and then new individuals are defined for the next evaluations. The process is stopped when all individuals are Pareto optimum (Chapter 5) or when the maximum number of evaluations is reached. A specific genetic algorithm is developed to handle the discrete aspect of this optimization process. This algorithm is introduced in the next paragraph.

A starting population of 1000 individuals is evaluated using an explicit simplified APOLLO2 computation scheme. The optimization process is repeated independently for the HET.05, HET.08, HET.10 and HET.12 optimization exercise and with each predefined patterns (except for HET.05). Moreover to assess the influence of the plutonium enrichment in the optimization outcomes the HET.08 case is repeated for two plutonium contents. The list of optimization cases is summarized in Table 3. 20.

Case	Nb FER FR ($1/12^{th}$ FA)	Pu (%)	Item "Best"	Predefined pattern
1	5	22.0	-	-
2	8	21.8	Kinf & Void	A
3	8	21.8	Kinf & Void	B
4	8	21.8	Fxy	C
5	8	21.8	Fxy	D
6	8	15.4	Kinf & Void	A
7	8	15.4	Kinf & Void	B
8	8	15.4	Fxy	C
9	8	15.4	Fxy	D
10	10	23.4	Kinf & Void	E
11	10	23.4	Kinf & Void	F
12	10	23.4	Fxy	G
13	10	23.4	Fxy	H
14	12	23.8	Kinf & Void	I
15	12	23.8	Kinf & Void	J
16	12	23.8	Fxy	K
17	12	23.8	Fxy	L

Table 3. 20: HET FA Optimization Cases

14. 2. 1 A Specific Algorithm

The discrete optimization of fertile fuel rod positions requires a specific development of the genetic algorithm available in the URANIE platform. The main characteristics of the genetic algorithm implemented for the HCMSR HET FA optimization are described hereafter. The process can be divided into six main steps and is described using a pseudo-code with some comments instead of the original C++ to enhance clarity.

1/Boundary conditions' definition

Objective: *define the boundary conditions*

Method:

Problem parameters

- Set total number of fuel rods in FA (44), number X of fertile Fuel Rod (FR) to position
- Set FR type for each position: either "must be Fertile" (FER), "must be Fissile" (FIS), or "can be either FER or FIS" (LIB).
- Set FR weight: FR positioned on symmetry axis are weighted 1/2 while other FR are weighted 1.

Genetic algorithm parameters

- Set the ratio between heterozygous and homogenous cross-breed method (R)
- Set (M) the mutation rate
- Set (Y) the population size.
- Set *maxeval* the maximum number of calls to the evaluation function or code.

2/Initial population generation

Objective: *Based on the boundary conditions generates an initial population of Y individuals.*

Method:

- Each individual (or son) has two chromosomes.
- Each chromosome has 44 parameters (also defined as FR position).
- Each parameter value can be either FER or FIS. The selection occurs as follow:

```
count = 0
For all Parameters (forced position loop)
        If Parameter value is set as FER in boundary conditions
                -> Parameter value is set as FER
                -> count = count + position weight
While count is less than X (filling LIB position for X FER)
        ->randomly choose one free position in the initial free position set
                If Parameter value is still not set
                        -> Parameter value is set as FER
                        -> count = count + position weight
                        If position weight = 1/2
                                -> memo = position
If count = X+1/2
        -> memo parameter value is set to FIS
For all parameters value (filling FIS position)
        If value is not set
                -> Parameter value is set as FIS
```

Remark: the process described above is repeated two times: first for the son's dominant and then for the recessive chromosome. Only the dominant chromosome parameters' values are selected for evaluations.

3/Population evaluation

Objective: *evaluate the performances of son's characteristics*

Method:

- Either using explicit APOLLO2 code or surrogate model.

4/Ranking and selection

Objective: *select individuals for next generation*

Method:

- Determine Pareto rank
- Test if population is converged

5/Cross-breeding

Objective: *increase diversity and robustness*

Method:

- Choice between heterozygous and homogenous cross-breeding method respecting R.

Remark: by default R is set to 50% heterozygous and 50 % homogenous cross-breed in Vizir.

Heterozygous cross-breeding

- Cross-breeding is divided in two steps: first, parameters values are selected for each parent among its two chromosomes to form a "cross-breed chromosome".
- Then both parents "cross-breed chromosome" parameters are considered to select the child dominant and recessive chromosomes. Both steps apply the same method principle as described below.

Step 1:

countD = 0 **D for dominant chromosome*

countR = 0 **R for recessive chromosome*

For all parameters *(fixed positions loop)*

    If parameter value is FER in both chromosomes

        -> Child parameter value is set as FER

        -> countD = countD + position weight

        -> countR = countR + position weight

    If parameter value is FIS in both chromosomes

        -> Child parameter value is set as FIS

For all parameters *(free symmetric position loop)*

    If parameter value is not identical in both chromosomes

        If position weight = 1

            If countD + 1 > X

                -> Child parameter value is set as FIS

                -> countR = countR + position weight

            Else If countR + 1 > X

                -> Child parameter value is set as FER

                -> countD = countD + position weight

            Else If random > 50%

                -> Child parameter value is set as FIS

                -> countR = countR + position weight

            Else

                -> Child parameter value is set as FER

                -> countD = countD + position weight

For all parameters *(free axial position loop)*
    If parameter value is not identical in both chromosomes
        If position weight = 1/2
            If countD + 1/2 > X
                -> Child parameter value is set as FIS
                -> countR = countR + position weight
            Else If countR + 1/2 > X
                -> Child parameter value is set as FER
                -> countD = countD + position weight
            Else If random > 50%
                -> Child parameter value is set as FIS
                -> countR = countR + position weight
            Else
                -> Child parameter value is set as FER
                -> countD = countD + position weight

Outcome: *for each parent a "cross-breed chromosome" is obtained with parameters values depending on the parameter values from dominant and recessive chromosome for each parent respectively.*

Step 2:

- Both parents "cross-breed chromosomes" are considered. Aim is to create two child chromosomes: one dominant and one recessive.

countD = 0 *D for dominant chromosome
countR = 0 *R for recessive chromosome

For all parameters *(fixed positions loop)*
    If parameter value is FER in both chromosomes
        -> Dominant parameter value is set as FER
        -> Recessive parameter value is set as FER
        -> countD = countD + position weight
        -> countR = countR + position weight
    If parameter value is FIS in both chromosomes
        -> Dominant parameter value is set as FIS
        -> Recessive parameter value is set as FIS

For all parameters *(free symmetric position loop)*
    If parameter value is not identical in both chromosomes
        If position weight = 1
            If countD + 1 > X
                -> Dominant parameter value is set as FIS
                -> Recessive parameter value is set as FER
                -> countR = countR + position weight
            Else If countR + 1 > X
                -> Dominant parameter value is set as FER

-> Recessive parameter value is set as FIS
-> countD = countD + position weight
Else If random > 50%
-> Dominant parameter value is set as FIS
-> Recessive parameter value is set as FER
-> countR = countR + position weight
Else
-> Dominant parameter value is set as FER
-> Recessive parameter value is set as FIS
-> countD = countD + position weight

For all parameters *(free axial position loop)*
If parameter value is not identical in both chromosomes
If position weigth = 1/2
If countD + 1/2 > X
-> Dominant parameter value is set as FIS
-> Recessive parameter value is set as FER
-> countR = countR + position weight
Else If countR + 1/2 > X
-> Dominant parameter value is set as FER
-> Recessive parameter value is set as FIS
-> countD = countD + position weight
Else If random > 50%
-> Dominant parameter value is set as FIS
-> Recessive parameter value is set as FER
-> countR = countR + position weight
Else
-> Dominant parameter value is set as FER
-> Recessive parameter value is set as FIS
-> countD = countD + position weight

Outcome: A child pair of chromosomes, one dominant and one recessive with parameter values randomly selected from parents "cross-breed chromosomes".

Remark:

- Cross-breeding is performed randomly on all parents within the population to produce the required number of viable children.
- It can be observed both step 1 and step 2 loops are similar as well as axial and symmetrical positions loops. For the implementation in C++ in URANIE a shared code structure is used.

Homogenous cross-breeding

- Identical to heterozygous cross-breeding but the son gets only one chromosome generated from its parents – using a process similar to heterogeneous cross-breed – which is then repeated two times as dominant and recessive chromosome.

6/Mutations

Objective: *increase diversity and explore broadly the search space*

Method:

- Mutations are considered for all individuals within the population as follow:

If mutation should be made according to M
    For Chromosone in [dominant, recessive]
        fer = randomly choose a free position (LIB in boundary conditions)
    While fer parameter value is FER
        fis = randomly choose a free position
    While fis parameter value is FIS and fis weight = fer weight
        -> fer parameter value is set to FIS
        -> fis parameter value is set to FER

Loop: steps 3 to 6 are repeated until all individuals have reached a Pareto rank of 0 or the maximum number of evaluations *maxeval* is reached.

14. 2. 2 Results

With a maximum of 25 generations all individuals have reached the Pareto surface: it is not possible to further improve one individual on one optimization objective without degrading other objective(s). The results obtained led to the identification of preferred fertile fuel rod positions with regards to the best k_{inf}, *void* and F_{xy}.

A graphical representation of all results obtained is not trivial due to 44 parameters involved. Instead, the three objectives k_{inf}, *void* and F_{xy} boundaries are shown in Table 3. 21 for all Pareto optimum populations. The results obtained indicate large variations of F_{xy} whereas k_{inf} and *void* differences are rather small. The benefit of multi-objective optimization seems hence limited here. Cases with only constraints on parameters k_{inf} and *void* are also investigated but do not provide better outcomes with regards to the Pareto optimum populations.

The HCSMR design optimization requires selecting a few Pareto optima HET FA for core optimization. This is based on the optimization outcomes and arbitrary decision using engineering judgment. To reflect the diversity in an optimized population with regards to the three optimization objectives, two types of patterns are selected for each number of fertile fuel rods introduced. This is introduced in the next section together with visual representation of the selected optimized fuel assemblies.

When comparing the results obtained from Table 3. 21 with the related research plans introduced in Table 3. 18 an improvement of the objectives boundaries is observed, showing the interest of the optimization performed. The outcomes of the HET.08 optimization with two different plutonium contents lead to similar outcomes with regards to fertile fuel rods' positioning. This supports the observation that the number of fertile fuel rods influences more the positioning of fertile fuel rods than the plutonium content considered.

Case	Nb FER FR (1/12th FA)	Pu (%)	Min Kinf	Max Kinf	Min Void	Max Void	Min Fxy	Max Fxy
1	5	22.0	1.16237	1.16400	1456	1483	1.307	1.810
2	8	21.8	1.14323	1.14445	1058	1068	1.623	2.083
3	8	21.8	1.14327	1.14464	1059	1068	1.621	2.037
4	8	21.8	1.14015	1.14187	1081	1093	1.379	1.987
5	8	21.8	1.14067	1.14199	1080	1090	1.400	1.995
6	8	15.4	1.07480	1.07972	-219	-177	1.401	2.624
7	8	15.4	1.07473	1.07966	-213	-180	1.400	2.601
8	8	15.4	1.07538	1.08100	-202	-166	1.328	2.512
9	8	15.4	1.07524	1.07957	-201	-163	1.351	2.568
10	10	23.4	1.14602	1.14732	1024	1033	1.617	1.916
11	10	23.4	1.14609	1.14720	1024	1034	1.618	2.002
12	10	23.4	1.14224	1.14538	1048	1071	1.466	1.956
13	10	23.4	1.14152	1.14499	1045	1064	1.478	2.016
14	12	23.8	1.13761	1.13837	779	785	2.027	2.265
15	12	23.8	1.13784	1.13846	780	785	2.026	2.197
16	12	23.8	1.13200	1.13489	808	824	1.585	2.095
17	12	23.8	1.13263	1.13503	808	829	1.567	2.009

Table 3. 21: HET FA Optimization Cases Outcomes

14. 3 OUTCOMES

Pareto optimum populations obtained from HET FA optimization provide thousands of optimized HET FA design. Only a few can be selected to perform branch computations and participate to the HCSMR core design optimization.

The analysis of Pareto optimum populations shows that two main types of optimized HET FA design exist. Accordingly two patterns are selected among the optimized populations for the four cases of fertile fuel rods' introduction HET.05, HET.08, HET.10 and HET.12. One pattern focuses on FA configurations enabling the best k_{inf} and *void* on the one hand (noted "-a" hereafter) and one pattern focuses on configurations enabling the best F_{xy} on the other hand (noted "-b" hereafter).

The Figure 3. 20 to Figure 3. 24 show the positioning of fertile fuel rods for the selected HET FA. For the HET.10 case two additional patterns are selected to increase diversity at the core level. The plutonium contents are varied for each case up to five times to enlarge the research space for the core optimization. The observations from HET FA optimization justify using a same FA design with various plutonium contents.

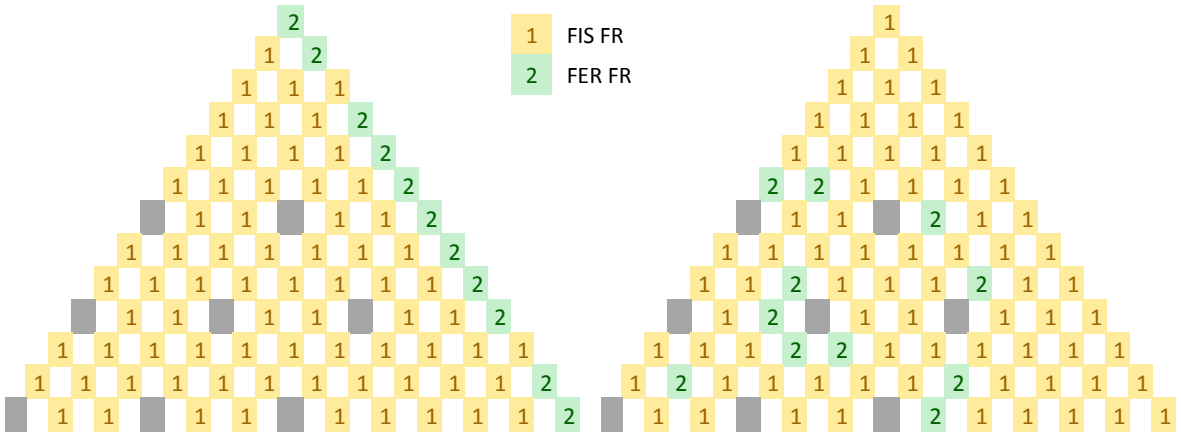

Figure 3. 20: HET.05 Optimized FA for Best K_{inf} and *Void* (left, HET.05-a) and Best F_{xy} (right, HET.05-b)

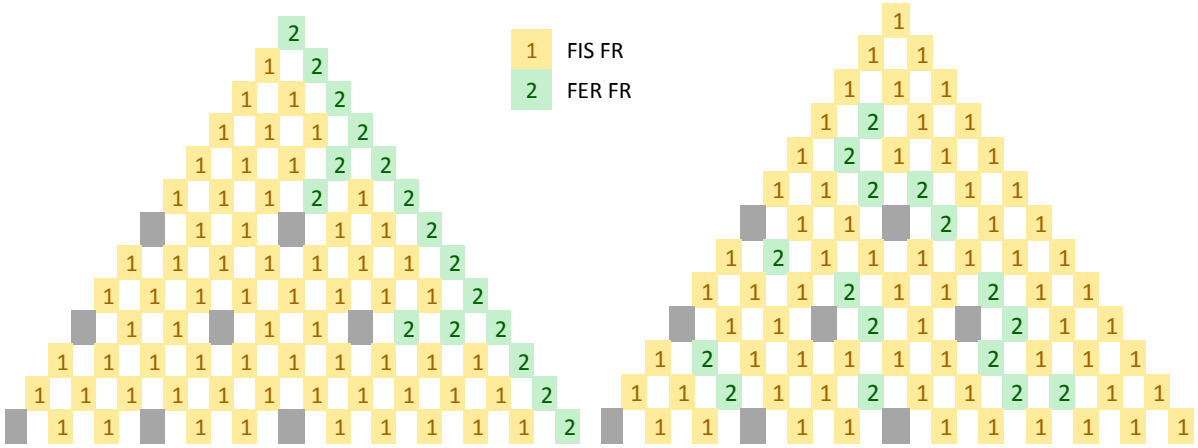

Figure 3. 21: HET.08 Optimized FA for Best K_{inf} and *Void* (left, HET.08-a) and Best F_{xy} (right, HET.08-b)

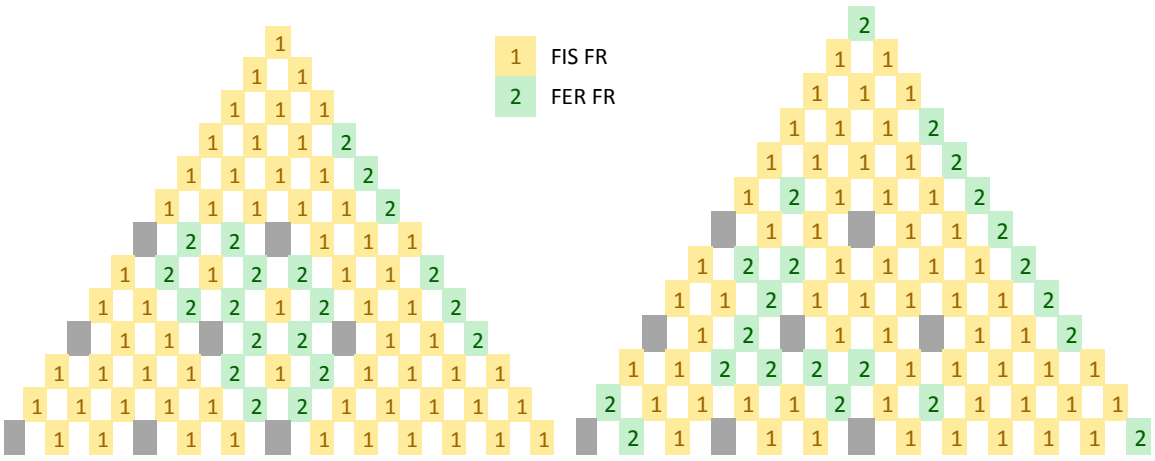

Figure 3. 22: HET.10 Optimized FA for Best K_{inf} and *Void* (left, HET.10-a) and Best F_{xy} (right, HET.10-b)

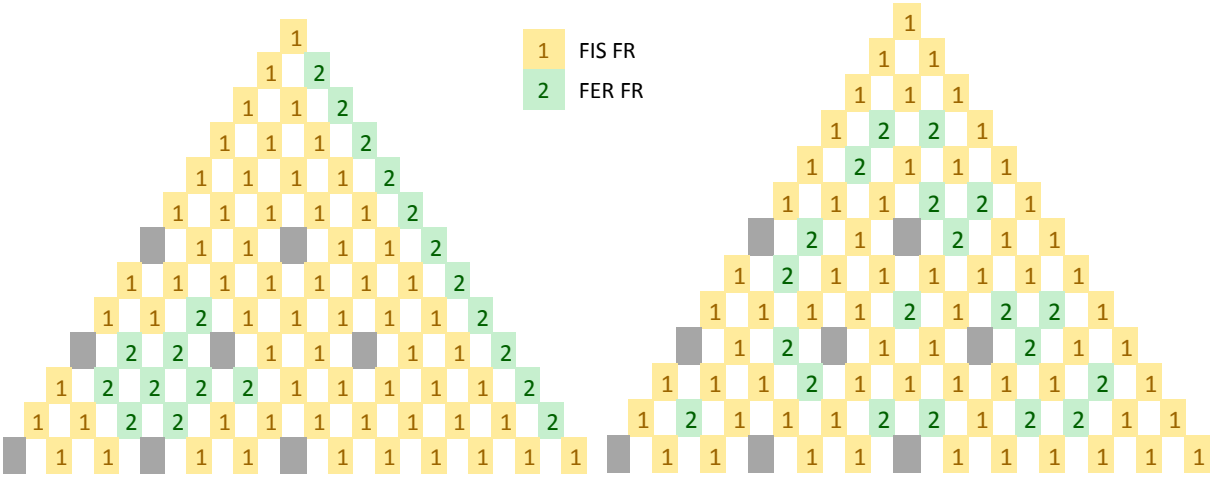

Figure 3. 23: HET.10 Optimized FA for Best K_{inf} and *Void* (left, HET.10-c) and Best F_{xy} (right, HET.10-d)

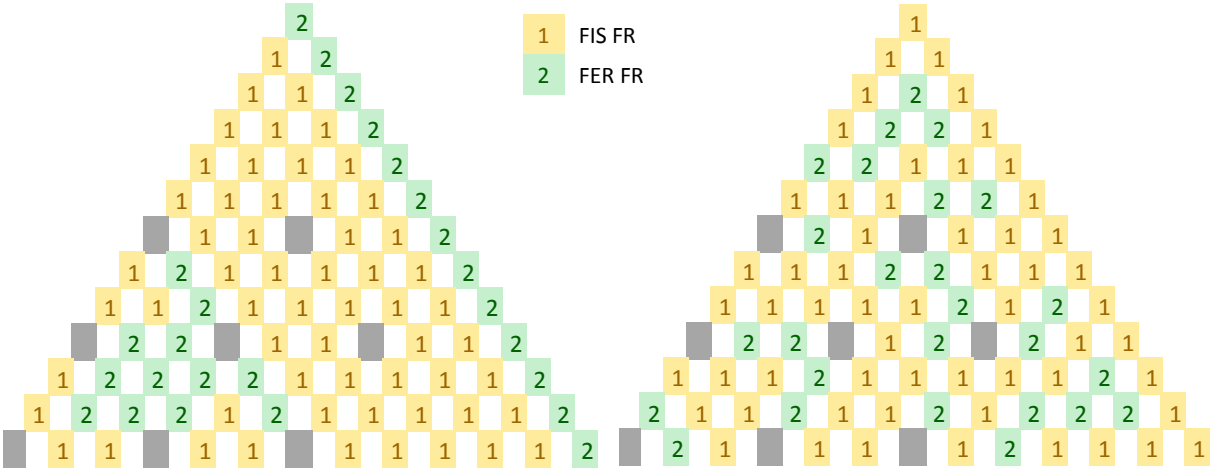

Figure 3. 24: HET.12 Optimized FA for Best K_{inf} and *Void* (left, HET.12-a) and Best F_{xy} (right, HET.12-b)

Table 3. 22 summarizes the 47 HET FA design considered for HCSMR core optimization. The types of HET FA (noted "-a" or "-b") are also reported in the table. Additionally the number of fertile fuel rods on the outer layer of the fuel assembly is introduced to characterize further the differences between the various HET FA designs. This differentiation is needed at the core optimization step to distinguish between the different patterns (e.g. the one noted "-a" or "-b").

Case	Nb FER FR (1/12th FA)	FER Design Name	Nb FER FR Outer Row	Pu average content (%)	Pu content (%)	Kinf	Void (pcm)	Fxy
21	5	HET.05-a	5	11.0	12.7	1.06329	-563	1.822
22	5	HET.05-a	5	13.0	15.1	1.09171	410	1.818
23	5	HET.05-a	5	15.0	17.4	1.11879	1152	1.808
24	5	HET.05-a	5	17.0	19.7	1.14556	1752	1.796
25	5	HET.05-a	5	19.0	22.0	1.17193	2242	1.782
26	5	HET.05-b	0	11.0	12.7	1.06065	-539	1.326
27	5	HET.05-b	0	13.0	15.1	1.08878	439	1.327
28	5	HET.05-b	0	15.0	17.4	1.11570	1183	1.327
29	5	HET.05-b	0	17.0	19.7	1.14238	1784	1.326
30	5	HET.05-b	0	19.0	22.0	1.16876	2275	1.325
31	8	HET.08-a	6	11.0	14.1	1.06851	-576	2.149
32	8	HET.08-a	6	13.0	16.6	1.09558	343	2.142
33	8	HET.08-a	6	15.0	19.2	1.12344	1108	2.128
34	8	HET.08-a	6	17.0	21.8	1.15094	1724	2.110
35	8	HET.08-a	6	19.0	24.3	1.17695	2209	2.091
36	8	HET.08-b	0	11.0	14.1	1.06535	-552	1.389
37	8	HET.08-b	0	13.0	16.6	1.09181	371	1.392
38	8	HET.08-b	0	15.0	19.2	1.11925	1137	1.393
39	8	HET.08-b	0	17.0	21.8	1.14646	1754	1.394
40	8	HET.08-b	0	19.0	24.3	1.17229	2238	1.394
41	10	HET.10-a	3	13.8	19.0	1.10933	649	1.956
42	10	HET.10-a	3	11.0	15.2	1.07175	-595	1.972
43	10	HET.10-a	3	13.0	17.9	1.09850	328	1.962
44	10	HET.10-a	3	15.0	20.7	1.12602	1093	1.948
45	10	HET.10-a	3	17.0	23.4	1.15225	1690	1.933
46	10	HET.10-b	4	11.0	15.2	1.07214	-598	1.970
47	10	HET.10-b	4	13.0	17.9	1.09892	325	1.960
48	10	HET.10-b	4	15.0	20.7	1.12646	1089	1.946
49	10	HET.10-b	4	17.0	23.4	1.15270	1686	1.930
50	10	HET.10-c	6	11.0	15.2	1.07265	-601	2.057
51	10	HET.10-c	6	13.0	17.9	1.09958	322	2.050
52	10	HET.10-c	6	15.0	20.7	1.12723	1087	2.039
53	10	HET.10-c	6	17.0	23.4	1.15355	1685	2.025
54	10	HET.10-c	6	18.1	24.9	1.16800	1969	2.018
55	10	HET.10-d	0	11.0	15.2	1.06767	-560	1.476
56	10	HET.10-d	0	13.0	17.9	1.09421	363	1.476
57	10	HET.10-d	0	15.0	20.7	1.12163	1128	1.476
58	10	HET.10-d	0	17.0	23.4	1.14785	1724	1.476
59	10	HET.10-d	0	18.1	24.9	1.16227	2007	1.476
60	12	HET.12-a	6	11.0	16.4	1.07575	-647	2.320
61	12	HET.12-a	6	13.0	19.4	1.10353	0	2.304
62	12	HET.12-a	6	15.0	22.3	1.13009	-972	2.286
63	12	HET.12-a	6	16.7	24.9	1.15356	1582	2.268
64	12	HET.12-b	0	11.0	16.4	1.07076	-608	1.577
65	12	HET.12-b	0	13.0	19.4	1.09799	342	1.578
66	12	HET.12-b	0	15.0	22.3	1.12423	1077	1.577
67	12	HET.12-b	0	16.7	24.9	1.14754	1617	1.576

Table 3. 22: HET Selected Cases Out of GA Optimization

14. 3. 1 Input to Core Optimization

91 FAs are selected to be used at the core optimization step. They come from four main types of HCSMR fuel assembly as presented in Figure 3. 25:

- ZON FA: 20 three-zones fuel assemblies (Chapter 13) with five average plutonium contents: 13.0, 15.0, 17.0, 19.0 and 21.0 % Pu.
- HET FA: 47 HET fuel assemblies containing 60, 96, 120 or 144 fertile fuel rods with various patterns considered. The average plutonium varies from 11.0 to 19 % Pu.
- MOX FA: 23 MOX FA designs containing only one type of fuel rod: MOX at different plutonium content, 11.0 % to 25.0 %. For 8 FA enriched ^{235}U is also added as shown in Table 3. 23.
- FER FA: 1 FA design containing only fertile fuel rods. The inclusion of FER and MOX FA is motivated by their simplicity and use in other designs [75].

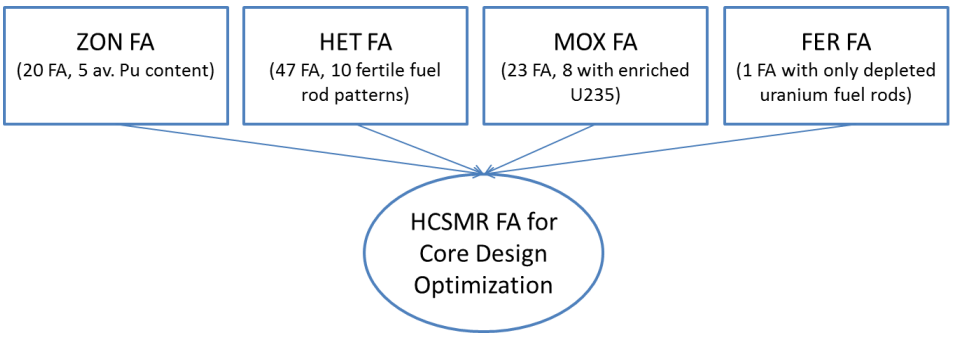

Figure 3. 25: HCSMR FA for Core Design Optimization Origins

Case	Pu Content (%)	235U (%)	Kinf	Void (pcm)	Fxy
68	11.0	0	1.05679	-472	1.283
69	12.0	0	1.07049	23	1.282
70	13.0	0	1.08424	463	1.278
71	14.0	0	1.09800	855	1.278
72	15.0	0	1.11173	1207	1.276
73	16.0	0	1.12542	1522	1.274
74	17.0	0	1.13905	1806	1.271
75	18.0	0	1.15259	2062	1.269
76	19.0	0	1.16602	2293	1.266
77	20.0	0	1.17936	2502	1.263
78	21.0	0	1.19261	2692	1.26
79	22.0	0	1.20573	2864	1.258
80	23.0	0	1.21874	3020	1.255
81	24.0	0	1.23162	3161	1.252
82	25.0	0	1.24438	3290	1.25
83	11.0	5	1.16478	1120	1.259
84	11.0	10	1.25100	1880	1.244
85	13.0	5	1.18358	1640	1.257
86	13.0	10	1.26468	2222	1.241
87	15.0	5	1.20355	2075	1.254
88	15.0	10	1.27986	2514	1.239
89	17.0	5	1.22420	2241	1.25
90	17.0	10	1.29603	2765	1.236

Table 3. 23: MOX selected FA for Core Optimization

Figure 3. 26 introduces, via a parallel plot, the characteristics of the selected FA except the FER FA. In total 91 FA are selected. From left to right the fuel average plutonium content, the fuel plutonium actual content, the number of fertile fuel rods in 1/12th FA, the ^{235}U enrichment are given as parameters. It continues with their performances: the reactivity (k_{inf}), void coefficient (*void*) and peaking factor (F_{xy}) are then introduced.

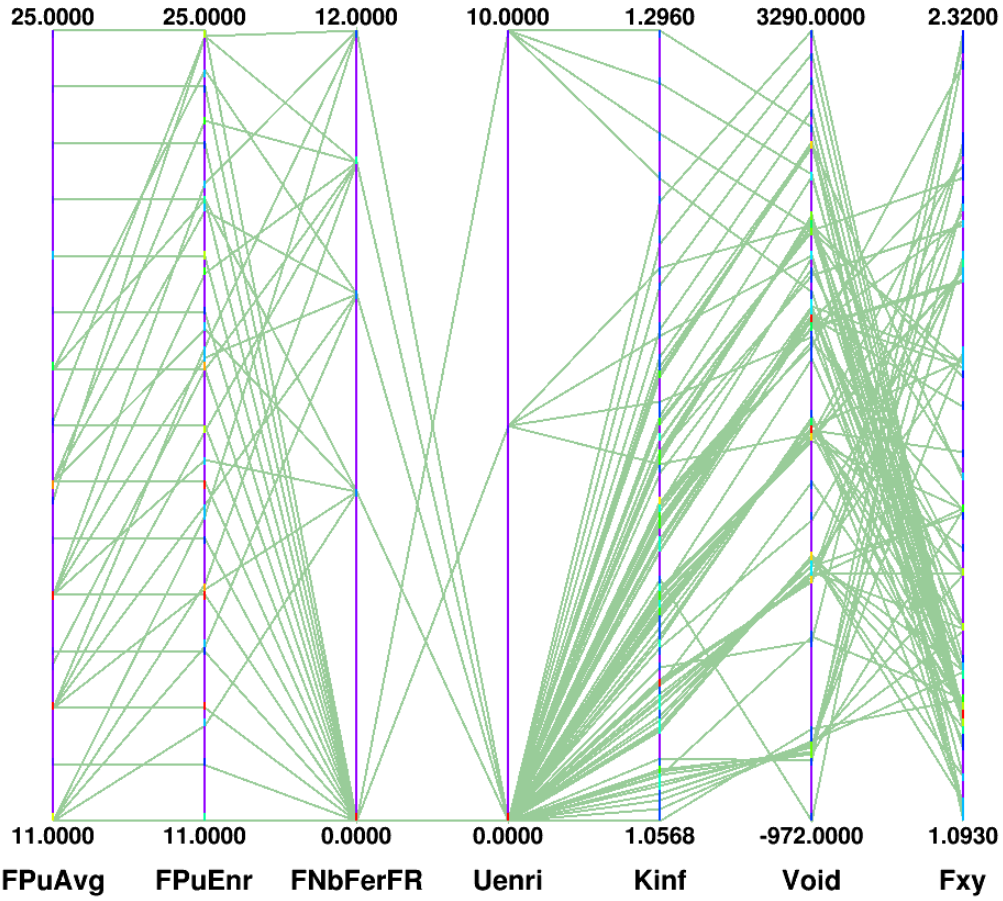

Figure 3. 26: Selected FA for Core Design Optimization Overview

Figure 3. 27 shows for the three performance indicators, kinf, void and Fxy the 90 selected FAs in red (all but the FER FA). In addition the Pareto optimum FAs are shown in black. Those FAs result from an extra Pareto rank evaluation based on all selected FAs. FAs resulting of the ZON and HET optimizations are Pareto optimum within the scope of their own optimization. When combined, and also considering the ad-hoc FA added, some FA can change to no longer be Pareto optimum.

Such a situation is observed and only 48 FA out of the 91 selected FAs composed the Pareto Optimum population. Their characteristics are further introduced in Figure 3. 28. Nevertheless to broaden the research plan at the core level, all 91 selected FAs are considered for core optimization.

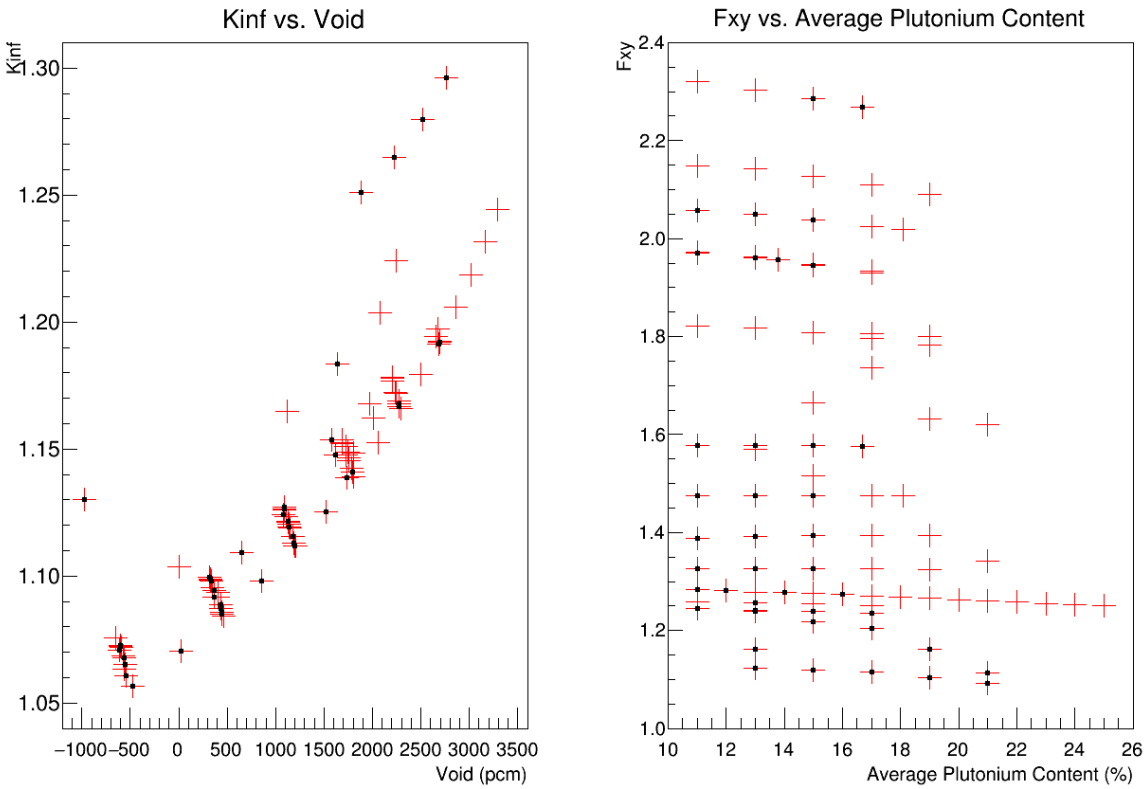

Figure 3. 27: Selected FA for Core Design Optimization Performances Overview

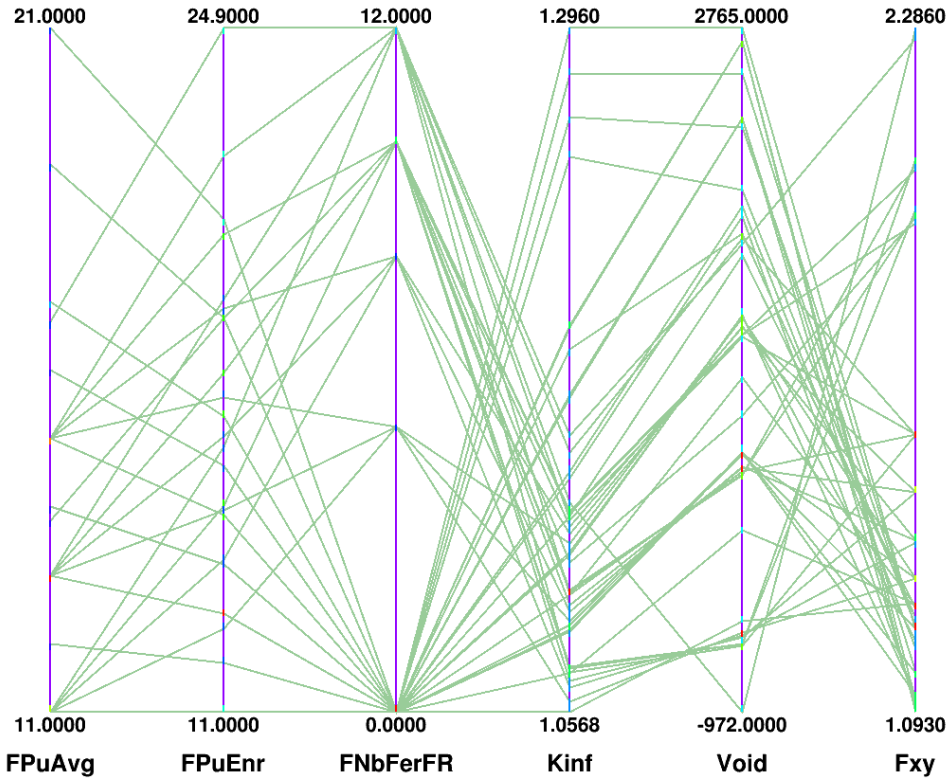

Figure 3. 28: Selected FA for Core Design Optimization Pareto Optimum

Chapter 15: CORE OPTIMIZATION

The HCSMR core design optimization is the third and final optimization exercise investigated in this work. It is also the main optimization step as it contains the outcomes of fuel assembly optimization and several parameters are considered. As in previous optimization exercises, a multi-objective optimization is performed at the core level. The outcomes of the selected optimization realized previously at the FA level are major inputs to the core optimization.

The core optimization has five objectives and ten parameters. The ten parameters are divided between six parameters defining the fuel assembly type and four setting the core's specific characteristic. The objectives are introduced in Chapter 4 and can be summarized as presented in Table 3. 24:

Objective	Target
Void Coefficient	Minimize
Cycle Length	Maximize
Conversion Factor	Maximize
Linear Power	Minimize
Plutonium Mass	Minimize

Parameter	Abbreviation	Range
Active Height	CHeight	147 cm – 300 cm
Fuel management	Cfuelmgmt	1/2; 1/3; 1/4
Fertile Fuel Assembly	CFER	Yes / No
Reflector type	CREF	1; 2; 3
Fuel type	Ftype	MOX ; ZON ; HET
Plutonium average content	FPuEnr	11 % – 25 %
Plutonium content in outer row fuel rods	Fm3enri	0 % – 14.3 %
Fertile fuel rod number (1/12th FA)	FNbCrFer	0 ; 5 ; 8 ; 10 ; 12
Fertile fuel rod number outer FA row (1/12th FA)	FORNbCrFer	0 – 6
^{235}U enrichment	FUenri	0.2%; 5.0%; 10.0%

Table 3. 24: Core Optimization Objectives (left) and Parameters (right)

The ten parameters introduced in Table 3. 24 and their ranges or discrete characteristics are selected based on four main aspects:

- Engineering judgment based on literature reviews (Chapter 3) and the author's ideas;
- The optimization work undertaken at the fuel assembly level;
- The outcomes of the sensitivity studies performed at the core level;
- An iterative process between the outcomes from core and fuel assembly optimization.

On principle all possible combinations between the ten parameters are considered. However, some limitations exist, either by design or inherently:

- Cores containing fertile fuel assemblies (FER) can only be loaded with either MOX or ZON fuel assemblies. Adding HET fuel assemblies to fertile fuel assemblies (FER) does not introduce enough fissile material to obtain critical cores;
- Enriched uranium is only introduced in MOX fuel assembly types;

- The fuel assemblies selected for core evaluations must be available in the fuel assemblies list introduced in §14. 3. 1. Only for those predetermined fuel assemblies are branch computations available.

This latter condition requires the introduction of a specific algorithm as part of the research plan evaluation or at the optimization step: a search is done to identify the closest fuel assembly available according to the selected parameters. This algorithm considers the parameters with different priorities or weights. First the fuel assembly type (MOX, ZON or HET) is looked at. Then a search for the closest average plutonium content is performed. Depending on the fuel assembly type, the selection continues by looking at the number of fertile fuel rods (HET FA), the plutonium content in the fuel assembly outer fuel rods row (ZON FA) or the enriched uranium content (MOX FA). This cascade continues until all characteristics are considered and the closest available FA is identified. The final characteristics of the selected fuel assemblies are communicated back to the optimization or research plan process.

The core fuel management substantially impacts the core performances. For the three fuel managements considered – 1/2, 1/3 and 1/4 – specific loading patterns are developed. Each fuel management requires two loading patterns: one with fertile fuel assembly and one without. Moreover to assess the influence of the loading pattern design itself, two sets of loading patterns for the fuel management 1/3 are considered: 1/3 "1" and 1/3 "2". This led to optimizing eight HCSMR loading patterns. This optimization is performed based on engineering judgment. The loading patterns and refueling schemes are introduced in Annex I and are an input to obtain the HCSMR core research plan. A batch or one-through fuel management is not considered.

Three reflector types are available, referred to as "1", "2" and "3". As introduced in Chapter 4 and §10. 2. 4 the steel content is varied between those three types. The steel concentration is respectively 96 % (heavy reflector), 50% and 10%. The reflector design is ultimately linked to the core's neutron doses and mechanical considerations. The three reflector types assessed here as part of the optimization can be also interpreted as a sensitivity study to assess the impact of reflector design on the HCSMR core neutron physics performances.

An equilibrium core search computation is needed to evaluate each core configuration. It is performed with CRONOS2 as introduced in Chapter 10. To reduce the computational costs of the optimization, surrogate models using neural networks are used. Those functions are created based on a research plan established using CRONOS2 explicit evaluations. To assess the influence of the various parameters on the five objectives a sensitivity study is first performed.

Three parameters take continuous values: the core active height (CHeight), the fuel average plutonium content (FPuEnr) and the fuel outer row plutonium content (Fm3enri). All other parameters have a discrete behavior. The content of enriched uranium is continuous on principle but since only three values are considered (0, 5 and 10 %) it is a discrete parameter.

The outcomes of the optimization are Pareto front and surface giving an indication of Pareto optimum solutions. Out of the Pareto optimum results three designs with opposite characteristics are selected for a deeper analysis of their performances. This chapter finishes by an investigation into the robustness of the results obtained via the multi-objective HCMSR core optimization.

15. 1 RESEARCH PLAN

For the HCSMR core optimization one research plan (RP) is designed based on the boundary conditions introduced in the previous paragraph. The size is arbitrary set to 20 000 individuals and their characteristics are selected using a Latin Hypercube Sampling (LHS) method. The CRONOS2 computation scheme set up to evaluate HCSMR core configuration is designed to handle broad types of core configurations. Nevertheless 10 % of the evaluated cases terminate in error. The reasons are both generic system failure (Input/Output error) and non-converged outcomes due to exotic core configuration or code limitation. The boundaries of the valid outcomes obtained are presented in Table 3. 25.

Objective	Unit	Minimum	Maximum
Void Coefficient	pcm	-22977	20827
Cycle Length	EFPD	31	2478
Conversion Factor	-	0.555	0.999
Linear Power	W/cm	143	673
Plutonium Mass	kg	493	2914

Table 3. 25: Research Plan Objective Initial Range

The range of the results obtained is rather large. It is actually too broad compared to the initial objectives set for the HCSMR core optimization introduced in Chapter 4. Hence the following triggers are applied resulting in the population plotted in Figure 3. 29:

- Cycle length > 300 EFPD
- Void < 500 pcm
- Maximum linear power < 500 W/cm

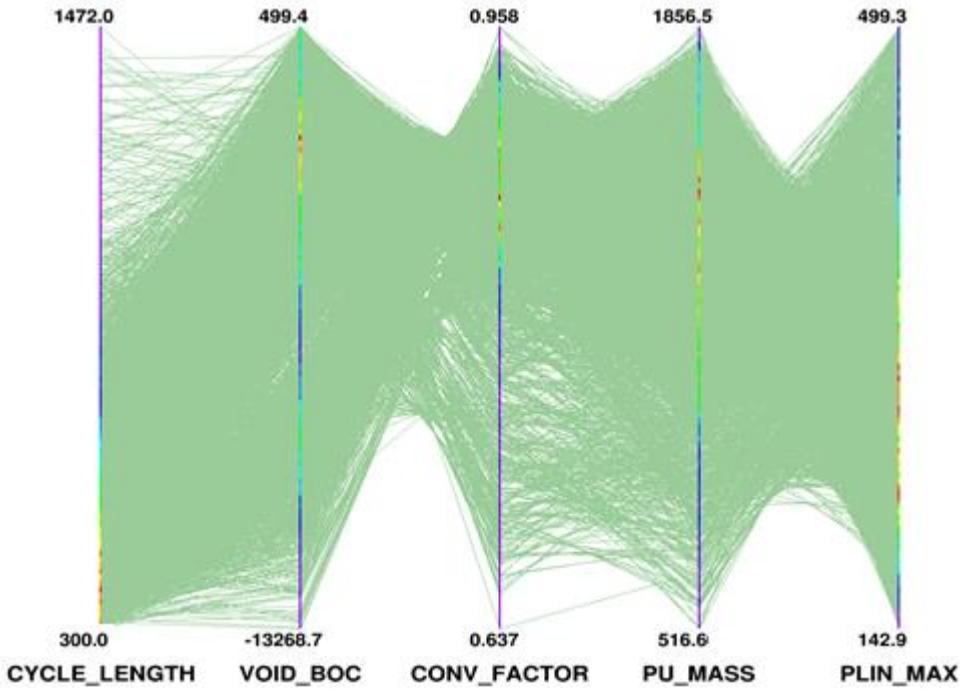

Figure 3. 29: Core Design Selected Research Plan

As a result only 6163 individuals form the research plan population of interest. This population is the basis to creating the core surrogate models and to performing the sensitivity study and core optimization.

Remark: plutonium masses presented in §15. 1, §15. 2, §15. 3. 2, Annex F. 3 and Annex G. 2 correspond to one third of the core plutonium mass. To obtain the core plutonium mass one should multiply those values by a factor three. This apply only to the value presented in those paragraphs.

15. 1. 1 Sensitivity Study

A sensitivity study using the Sobol indices method is performed to identify the parameters influencing most the five optimization's objectives. The outcomes are shown in Figure 3. 30 to Figure 3. 32.

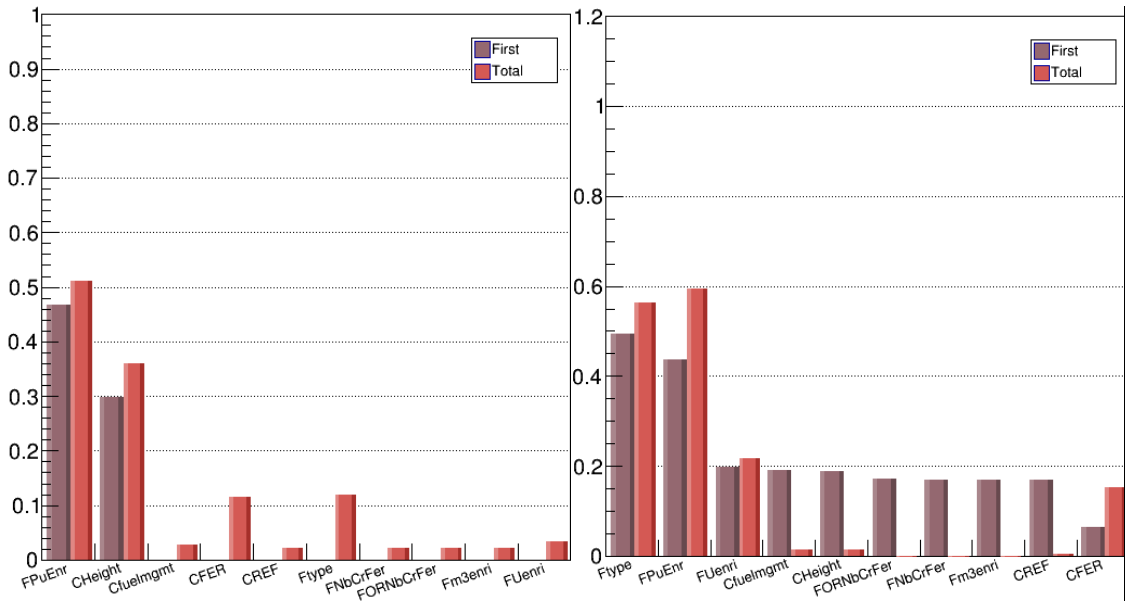

Figure 3. 30: Core Sensitivity Analysis using the Sobol Indices for (left) Plutonium Mass and Conversion Factor (right)

A trend is observed in the parameters that most influence the five objectives. The plutonium content, fuel type and core height are the three parameters with the highest Sobol first and total indices, showing the greatest influence on the five objectives.

The number of fertile fuel rods with HET fuel assemblies, the outer enrichment of the fuel and the reflector type has a second order influence on the five objectives. Those observations highlight the value of including various fuel assembly types for the HCSMR core optimization.

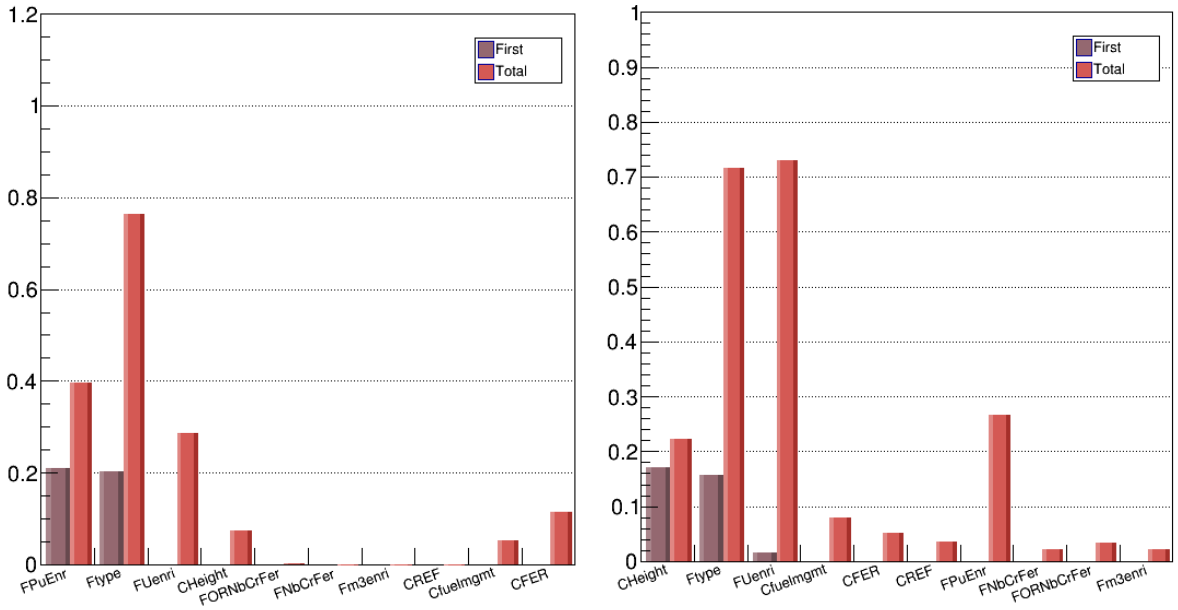

Figure 3. 31: Core Sensitivity Analysis using the Sobol Indices for (left) Cycle Length and Linear Power (right)

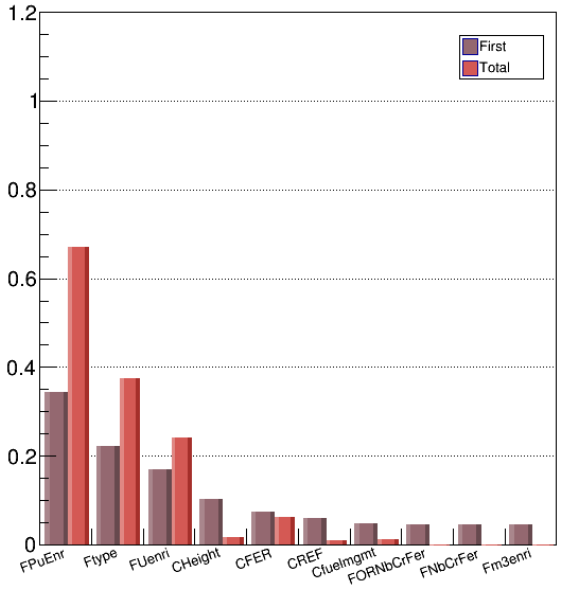

Figure 3. 32: Core Sensitivity Analysis using the Sobol Indices for Void Coefficient

Those results are obtained using surrogate model evaluations. The surrogate model creation and adequacy is introduced in the next paragraph.

15. 2 SURROGATE MODELS

Five surrogate models are created to assess the objectives of the HCSMR core. Based on the research plan obtained with explicit evaluations in the domain of interest (6163 individuals) surrogate models are trained both using the neural network and Kriging methodology. The research plan is split into two databases, one dedicated to initial learning and testing (4000 individuals) and one dedicated to independent testing (2163 individuals). The sizes of the databases are selected arbitrarily based on engineering judgment and previous work performed at the fuel assembly level.

The surrogate models' characteristics are introduced in Table 3. 26. Between 13 and 17 hidden neurons are used. The accuracy obtained is shown in Table 3. 26, Figure 3. 33, Figure 3. 34 and further plots in Annex F.

Neural Network	Cycle Length	Void	Conversion Factor	Plutonium Total Mass	Max Linear Power
Number of hidden neurons	17	16	17	13	17
RMSE	6 EFPD	69 pcm	< 0.01 %	3 kg	5 W/cm
95% cases error	12 EFPD	154 pcm	< 0.01 %	7 kg	11 W/cm
R^2	0.9989	0.9996	0.9995	0.9998	0.9962
Q^2	0.9988	0.9996	0.9995	0.9998	0.9961

Table 3. 26: Neural Network Performances

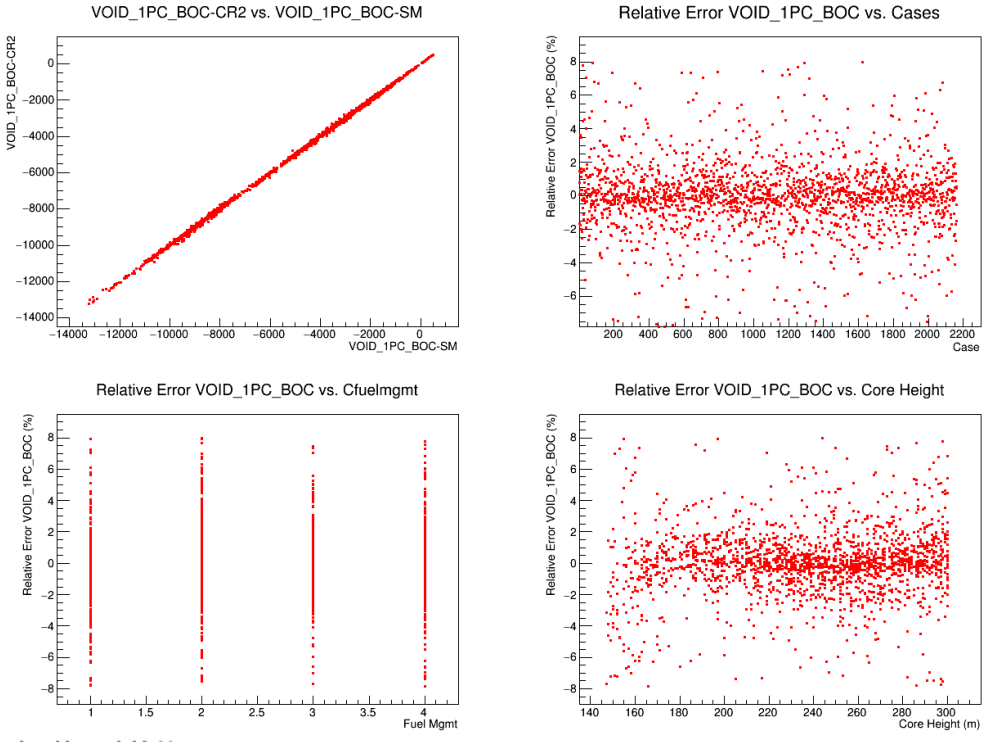

Figure 3. 33: Core Void Coefficient (VOID_1PC_BOC) Surrogate Functions Accuracy Check

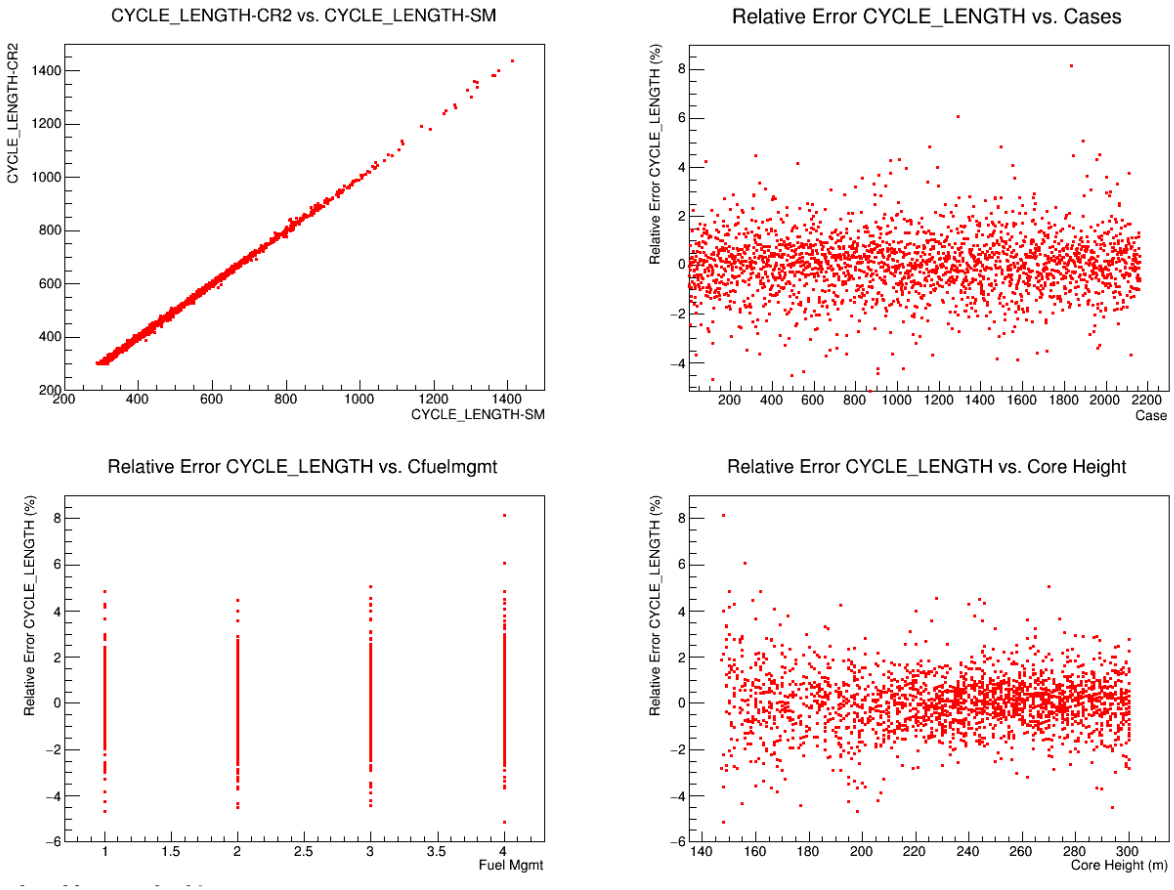

Figure 3. 34: Core Cycle Length (CYCLE_LENGTH) Surrogate Functions Accuracy Check

For the five objectives the accuracy achieved with the surrogate function using neural network is good and justifies using those functions for core optimization. For example, the cycle length is predicted within 12 EFPD for 95 % of the cases. For cycle lengths ranging from 300 EFPD up to over 1400 EFPD, 12 EFPD uncertainties is a very good achievement. Especially knowing uncertainties exist when evaluating the cycle length with CRONOS2 at first. Similar observations can be made for the four other core optimization objectives.

Surrogate models are also created using the Kriging approach. The performances obtained are illustrated in Table 3. 27. Here also the performances are good. Compared to the surrogate model created using neural networks, the performances of the Kriging method are similar or slightly below. This observation associated to the longer time needed to create and evaluate surrogate models based on the Kriging technique motivates the author to prefer using surrogate models based neural networks for the HCSMR core optimization.

Kriging (1000 eval)	**Cycle Length**	**Void**	**Conversion Factor**	**Plutonium Total Mass**	**Max Linear Power**
RMSE	11 EFPD	165 pcm	< 0.01 %	6 Kg	14 W/cm
Q^2	0.9960	0.9974	0.9966	0.9994	0.9665

Table 3. 27: Kriging Performances

15. 3 OPTIMIZATION

15. 3. 1 Characteristics

The HCSMR core optimization has five objectives as introduced in Table 3. 24:

- Void coefficient (minimize);
- Cycle length (maximize);
- Conversion factor (maximize);
- Linear power (minimize);
- Plutonium mass (minimize).

The "minimize" or "maximize" direction defines for each objective the expectations from a designer perspective. However, for some objectives setting a constraint rather than an optimization objective is more effective. For example, according to the HCSMR optimization boundary conditions, the void coefficient must be at least smaller than -500 pcm. It does not necessarily mean a void coefficient of -10 000 pcm is meaningful. A constraint setting the void coefficient below -500 pcm could be enough. For the HCSMR core optimization the most relevant results are obtained with four objectives: cycle length, conversion factor, void coefficient and plutonium mass, and a constraint only for the linear power, kept below 400 W/cm. Moreover constraints are implemented to keep the optimization within the domain of surrogate models validation as introduced in §15. 1.

The optimization parameters are:

- The core active height;
- The fuel management;
- The reflector type;
- The introduction of fuel assemblies with only fertile fuel rods (fertile fuel assemblies);
- The type of fuel assemblies;
- The plutonium average content;
- The plutonium content in fuel assemblies' outer row;
- The number of fertile fuel rods in fuel assemblies;
- The number of fertile fuel rods in fuel assemblies in the outer row;
- The introduction of enriched uranium.

The HCSMR core optimization is performed using genetic algorithms. Genetic algorithms (GA) are evolutionary algorithms developed based on observations of natural selection and genetic observations. GA detailed characteristics are introduced in §5. 4. The Vizir module of the Uranie platform [91] is used to perform the HCSMR core optimization.

Some of the optimization's parameters are continuous whereas some have a discrete behavior. The valid combination of parameters is linked to the research plan boundary conditions considered for this optimization. It is introduced at the beginning of this chapter. The optimizer itself considers only continuous values. An "interpretation step" is performed before and after calling the Vizir module to transform the continuous values into discrete values. This is based on piecewise constant functions.

The optimization population is first set at 10 000 individuals. The maximum number of evaluations is fixed at 100 million. Close to 20 iterations are needed to make all individuals Pareto optimum. This means all individuals could not be further optimized on one objective without deteriorating another objective. All evaluations are performed using the surrogate models created previously to assess the five objectives of the optimization.

The optimization's outcomes are introduced in the next section. The optimization is repeated with initial populations varying in size to confirm the robustness of the optimization's outcomes. In addition, an optimization using the particle swarm method is performed. The results obtained are similar to the one presented hereafter using genetic algorithm. The computing costs are different however. Table 3. 28 summarizes the computational time observed to obtain the optimized populations. It must be remarked that the optimization could be run in parallel mode, using a high number of CPUs to further reduce the computing time. The relative low cost of the optimization has not motivated the implementation of this approach.

	HCSMR Core Optimization				
Algorithm	GA	GA	GA	Particle Swarm	Particle Swarm
Population Size	1000	5000	10000	1000	5000
CPUs	1	1	1	1	1
Time	2'	5h30	42h19	2'	20'
Generation number	20	21	21	37	142

Table 3. 28: Core Optimization Computational Costs

15. 3. 2 Results

Figure 3. 35 and Figure 3. 36 illustrate the optimized populations. All Pareto optimum individuals are shown with regards to the optimization's objectives and parameters. The multi-parameter and multi-objective optimization challenges the readability of the results obtained. A more detailed overview is introduced in Annex G. The range of values obtained for the five objectives are summarized in Table 3. 29.

Objective	Unit	Minimum	Maximum
Void Coefficient	pcm	- 13259	499
Cycle Length	EFPD	300	1471
Conversion Factor	-	0.696	0.958
Linear Power	W/cm	153	469
Plutonium Mass	kg	520	1853

Table 3. 29: Core Optimization Outcomes Objectives Ranges

The Pareto optimum population gathers individuals with various characteristics. Since some parameters, such as the fuel management or fuel assembly type, are discrete and influence strongly the core performances, several smaller populations can actually be identified out of the optimized population.

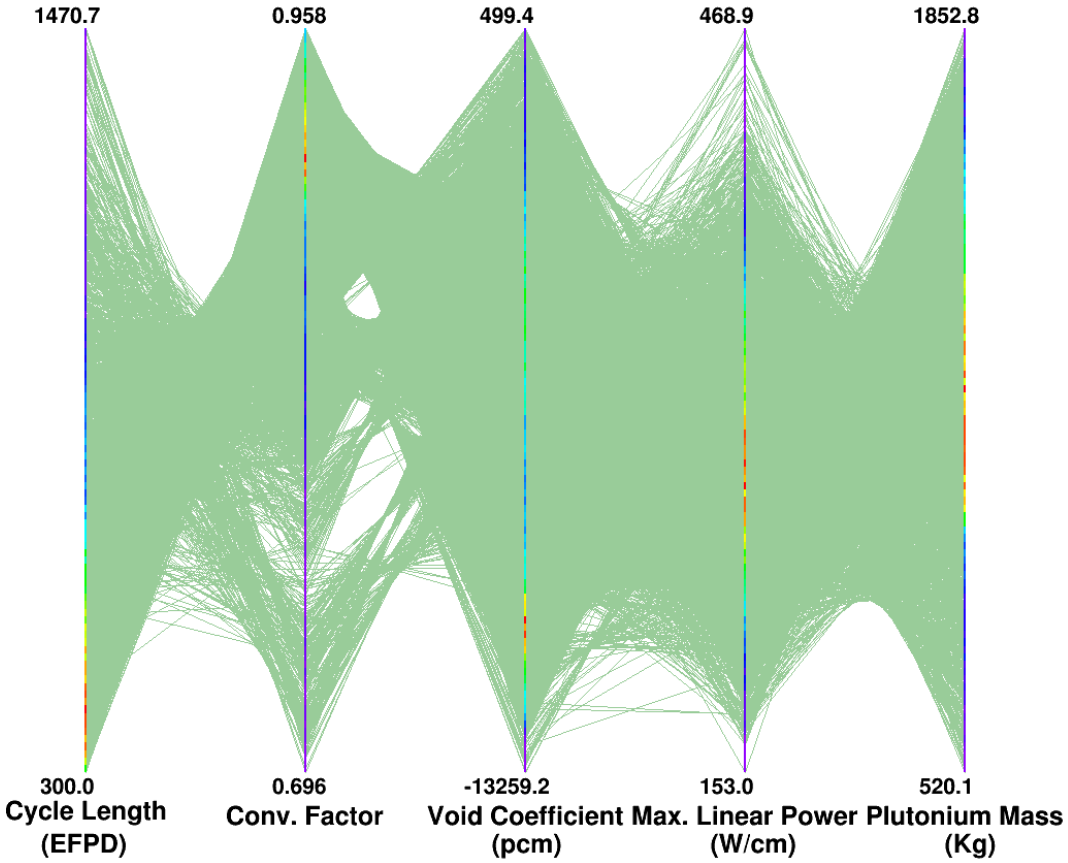

Figure 3. 35: Core Optimization Outcomes on the Five Objectives

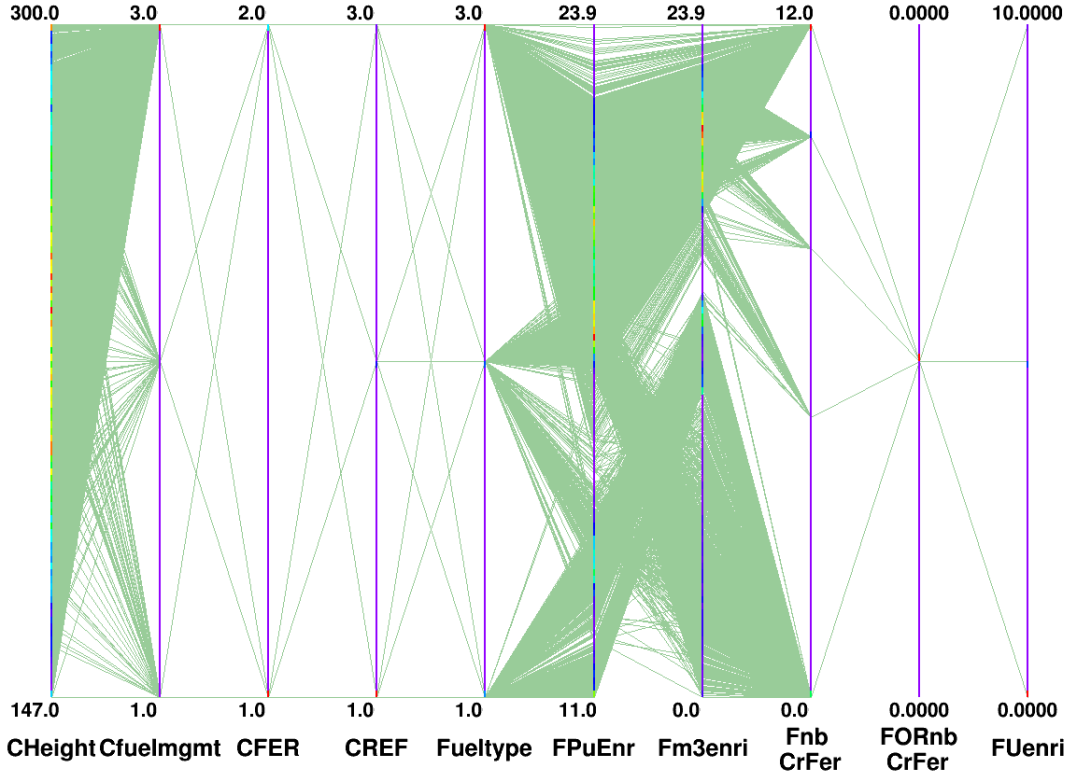

Figure 3. 36: Core Optimization Outcomes on the Ten Parameters

15. 3 Optimization

The optimization is performed with envelope boundary conditions compared to the HCSMR objectives' domain of interest. This aims at giving more freedom to the optimization process and increases the results' diversity. Before analyzing the optimization outcomes, the results are narrowed down to the boundary conditions of the HCSMR core objectives. Triggers are applied on four objectives to discard individuals not complying with the following limits:

- Cycle length > 700 EFPD;
- Conversion factor > 0.8;
- Void coefficient < -500 pcm;
- Linear Power < 400 W/cm.

Out of the 10 000 individuals in the optimized population, 1674 are compatible with the domain of interest identified for the HCSMR design. Figure 3. 37 and Figure 3. 38 show the selected Pareto individuals with regards to cycle length versus plutonium content. Annex G introduces further the characteristics of the optimized population with triggers.

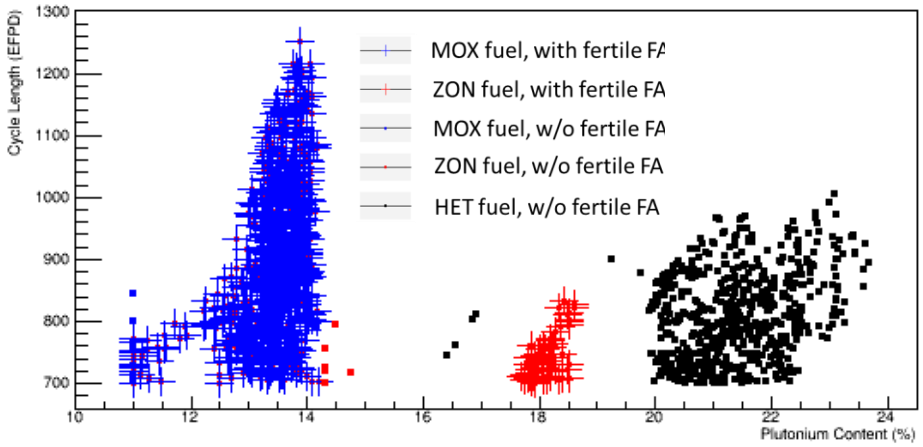

Figure 3. 37: Core Optimization Results Cycle Length vs. Plutonium Content

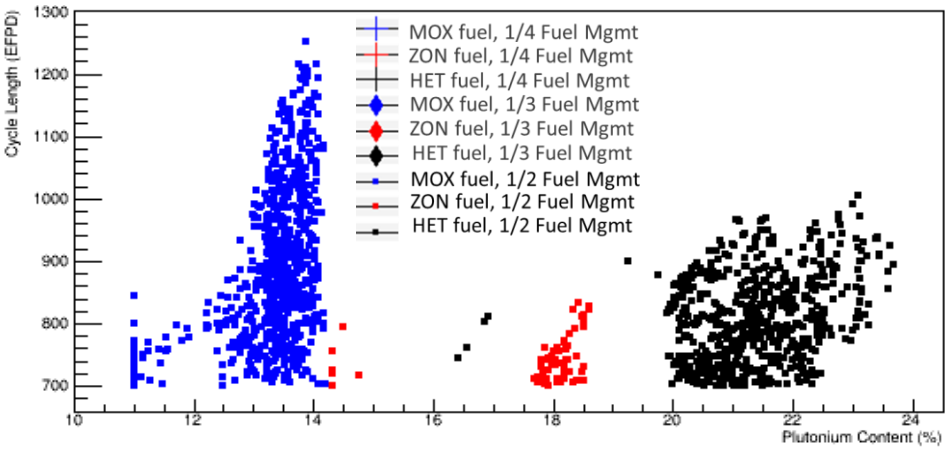

Figure 3. 38: Core Optimization Results Cycle Length vs. Plutonium Content

It must be remarked all optimization exercises are repeated with a different initial population (5 000 individuals for example). The results obtained with the different initial population size are similar, confirming the robustness of the optimization process.

15. 3. 3 Outcomes

The HCSMR core multi-objective optimization results in a population of several optimum HCSMR cores. Rather than understanding the characteristics of each individual core, the analysis performed hereafter focuses on groups of individuals with similar behavior. This enables in particular the identification of which parameter combinations are not part of the optimum core designs.

Table 3. 30 indicates the range of the objectives and parameters for all individuals out of the optimized population to which the triggers introduced in the previous sections are applied. This represents the domain of interest for HCSMR cores.

Criteria	Unit	Minimum	Maximum
Objectives			
Void Coefficient	pcm	- 11180	-502
Cycle Length	EFPD	700	1251
Conversion Factor	-	0.80	0.92
Linear Power	W/cm	170	362
Plutonium Mass	kg	2205	5559
Parameters (continuous)			
Active Height	cm	147	300
Plutonium average content	%	11.0	23.6
Plutonium content in outer row fuel rods	%	0.0	23.6
Parameters (discrete)			
Criteria		**Values**	
Fuel management		1/2	
Fertile Fuel Assembly		Yes / No	
Reflector type		1; 2; 3	
Fuel type		MOX ; ZON ; HET	
Fertile fuel rod number (1/12th FA)		0 ; 5 ; 8 ; 10 ; 12;	
Fertile fuel rod number outer FA row (1/12th FA)		0	
^{235}U enrichment		0%; 5%	

Table 3. 30: Core Optimization with Trigger: Objectives and Parameters Ranges

Some observations can be made based on those results and are summarized in the next sections.

15. 3. 3. 1 General remarks

The optimization results show it is possible to get HCSMR cores matching the HCSMR design minimum requirements defined in Chapter 4. Over 1500 individuals are identified as Pareto optimum and matching those requirements. Their cycle lengths range from two to almost four years. The highest conversion factor reaches 0.92. The maximum linear powers are between

170 W/cm and 362 W/cm. Those levels remain well below 400 W/cm. With regards to the plutonium mass, the values are broadly distributed between 2205 kg and 5559 kg. There is diversity in the optimum cores' characteristics, not only with regards to the objective's values but also on the parameters leading to those performances.

As shown in Figure 3. 37 and Figure 3. 38 the various types of fuel assemblies as well as the choice of loading fertile fuel assemblies or not, influence significantly the HCSMR cores performances. Accordingly, Pareto optimum sub-populations can be identified in both plots. The three fuel types considered (MOX, ZON and HET) lead to Pareto optimum designs. The three reflector types (96%, 50% and 10% steel) are also found in the optimum cores' characteristics. With regards to fuel characteristics, plutonium content ranges from 11 to 23.6 % while ^{235}U at 5 % in MOX fuel also appears in some optimum cores' parameters.

However, 10% ^{235}U is excluded from the optimum population as shown in Table 3. 30. The HET FAs among the cores' Pareto optimum population have 5, 8, 10 or 12 fertile fuel rods out of a $1/12^{th}$ fuel assembly. Only configurations without fertile fuel rods on the fuel assembly outer row are part of the Pareto optimum individuals. With regards to fuel management only the "1/2" reloading strategy is among the optimum population. Those observations are analyzed next.

15. 3. 3. 2 Fertile Materials & Fuel Assembly Types

Among the Pareto optimum cores most individuals contain fertile fuel, either via the introduction of fertile fuel assemblies or by loading "HET" fuel assemblies: FA containing both fertile and fissile fuel rods. Both approaches are found in the Pareto optimum individuals. This shows the relevance of two strategies to limit the void coefficient. In other words, the design heterogeneities can be well managed at different radial levels.

Fertile fuel rods are not found on external row of HET FA. This relates to the findings identified in Chapter 14. The HET FAs without fertile fuel rods on the outer row are designs minimizing the radial peaking factor (F_{xy}). To obtain this behavior the fertile fuel rods are spread within the fuel assembly. On the contrary the HET FAs with fertile fuel rods on the outer row are designs maximizing reactivity and minimizing void coefficient at the fuel assembly level. Among the Pareto optimum cores those latter aspects are tackled with other approaches (fertile fuel assemblies, reflector, etc…) resulting in a preference for HET FA minimizing the radial peaking factor (F_{xy}).

The maximum number of fertile fuel rods positioned in HET FAs (12 fertile fuel rods in $1/12^{th}$ FA or 144 at FA scale) is the most commonly occurring HET FA design among Pareto optimum cores. FA design with 5 or 8 fertile fuel rods (out of $1/12^{th}$ FA) are only found for a small number of optimum individuals. The occurrence of FA design with 10 fertile fuel rods (out of $1/12^{th}$ FA) is half the one observed for the maximum quantity of fertile fuel rods. All configurations present an interest with a clear preference for large numbers of fertile fuel rods in HET FAs.

The Pareto optimum core designs containing no fertile fuel material at all are those with limited plutonium content in fuel (below 15%) and with small core active lengths (below 190 cm). As a result the cycle lengths are limited (below 900 EFPD), the conversion factors are rather low

(maximum 0.82), the void coefficients remains below -500 pcm and the total plutonium mass are among the smallest.

The ZON fuel assemblies are found exclusively for core active heights above 250 cm with plutonium contents in the outer row below 5 %. The FA average plutonium content is between 14 and 18 % and almost all cores loaded with ZON FA also contains fertile fuel assemblies. The conversion factors are above 0.90 with maximum linear powers below 280 W/cm. This highlights the role of radial plutonium content zoning to tackle the maximum peaking factor in case of radially heterogeneous cores due to the introduction of fertile FAs.

15. 3. 3. 3 Core Reflector

The three core reflector types are found among the Pareto optimum core designs. However, there is a clear predominance of the heavy reflector containing 96 % of stainless steel. For 80 % of the Pareto optimum individuals the reflector type "1" (96 % steel, heavy reflector) is found while reflector type "2" (50% steel) and type "3" (10% steel) are respectively found for 15% and 5% of all individuals.

The cores with reflectors containing 50 % or 10% of steel enable low maximum linear power. The associated cycle lengths range from 700 to 1200 EFPD. The performances with regards to void coefficients are below but close to -500 pcm. The reduction of stainless steel content in the reflector enables a decrease in radial power heterogeneities. The following detailed analyses are performed with the heavy reflector design.

15. 3. 3. 4 Fuel Management

As shown in Figure 3. 38 all Pareto optimum individuals are cores with a "1/2" fuel management. A careful review of the optimization objectives justifies this behavior. "Cycle Length", "Conversion Factor", "Void Coefficient" and the "Plutonium Mass" are the four objectives considered for the core optimization with a maximum constraint on the peak "Linear Power". There are no criteria considered with regards to fuel assembly economics.

Since the highest cycle lengths are aimed for and the conservation factors of reloaded fuel assemblies tend to decrease because of the own plutonium consumption, the fuel management with the least fractioning is the best to maximize the cycle length and the conversion factor.

This observation is not entirely satisfactory with regards to the HCSMR objective to limit natural uranium consumption. To quantify this aspect explicitly a further optimization is undertaken with an evaluation of natural uranium needs. A specific method is implemented as introduced in Annex J. This method requires quantifying the equivalent value of plutonium fuel compared to natural uranium (Unat). This topic is rather sensitive and a parametric approach is used. The optimizations are repeated with four equivalent values: 1 kg Pu = 1 kg or 10 or 1000 or 100000 kg Unat.

The four Pareto optimum populations are similar to the Pareto optimum cores obtained without considering the natural uranium requirement. The reason is that no criteria is considered on fuel burnup or fuel assembly costs. With no incentive to increase FA burnup and limit the use of new

FA, the best in term of natural uranium resources utilization is very short cycle length, without fractioning, and an unlimited use of fuel reprocessing. In reality this approach is excluded due to the costs of fresh FA and reprocessing.

The consideration of fuel burnup as criteria for the optimization changes the perspective. A last optimization is performed with an additional objective to maximize the fuel assembly average discharged burnup. The results are shown in Figure 3. 39. Solutions with "1/3" fuel management strategies are among the Pareto optimum cores, together with "1/2" fuel management. "1/4" fuel management strategies are not among the optimum cores. Two reasons explain this observation. On the one hand, cores with "1/4" fuel management strategy tend to have low conversion factors since the fissile material generated during irradiation is consumed along the fuel assembly total irradiation period. On the other hand, the other optimization objective to maximize the cycle length leads to high fuel assembly discharge burnup, above 65 MWd/kgHM, set as maximum acceptable fuel assembly average burnup. Those two aspects prevents finding "1/4" fuel management cores among the Pareto solutions.

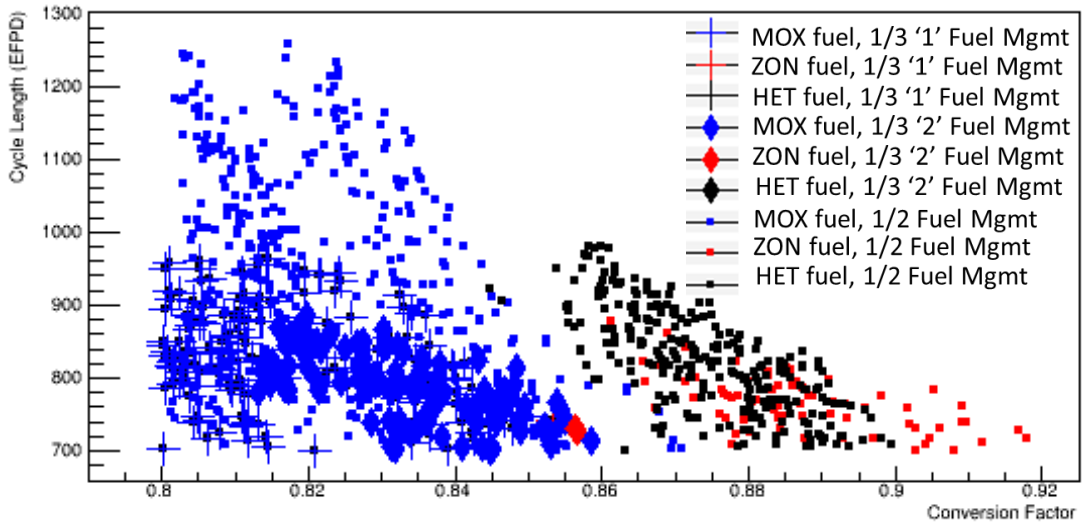

Figure 3. 39: Core Optimization with Burnup: Results Cycle Length vs. Conversion Factor

It can also be observed that the fuel management "1/3" '2' is better represented among Pareto optimum individuals. This shows a better loading pattern design compared to the "1/3" '1' loading pattern with regards to the optimization objectives. The fuel management "1/3" '1' and "1/3" '2' differ by the loading pattern design as introduced in Annex I.

15. 3. 3. 5 Other Observations

MOX FAs with enriched uranium at 5% are among Pareto optimum cores. Enriched uranium enables a rather long cycle length. The introduction of enriched uranium (10%) enables a very high cycle length (>1500 EFPD) but leads to conversion factors below 0.8. Those design options are hence not considered among the targeted Pareto optimum population. Corollary high conversion factors are only achieved without enriched uranium. A continuous optimization of the ^{235}U enrichment could be a further step to refine the outcomes obtained in this work.

Based on the optimized population three specific designs are selected for further analysis of their characteristics. One maximizes the core long cycle length, while the other is best in conversion factor and the third one is a trade-off. The three selected cores are Pareto optimum individuals. They are based on three different fuel assembly types. The choice of those three designs is an educated choice.

15. 4 SELECTED CORE PERFORMANCES

Three designs are selected among the Pareto optimum population to review their detailed characteristics. The selection is performed arbitrarily using engineering judgement and to highlight various possible optimized cores. Their characteristics are presented in Table 3. 31.

Parameter	Unit	A	B	C
Core height	cm	290	300	280
Fuel management	-	1/2	1/2	1/2
Fertile FA	-	YES	YES	NO
Reflector	-	Heavy Reflector	Heavy Reflector	Heavy Reflector
Core pressure	bar	140	140	140
T inlet	°C	280	280	280
Fuel type	-	MOX	ZON	HET
Pu content	%	15.5	18.0	22.3
Pu content in outer row fuel rods	%	15.5	5.0	22.3
Fertile fuel rod number (1/12th FA)	-	0	0	12
Fertile fuel rod number outer FA row (1/12th FA)	-	0	0	0
^{235}U enrichment	%	5.0	0	0

Table 3. 31: Three Selected Cores' Parameters

15. 4. 1 Neutron physics

The main performances of the selected designs are presented in Table 3. 32 and Table 3. 33.

Parameter	Unit	A	B	C
Cycle length	EFPD	1209	706	881
Void Coefficient	pcm	-840	-2369	-2636
Conversion Factor	-	0.81	0.90	0.87
Plin, max	W/cm	201	268	245
Cycle Burnup	MWd/kgHM	19667	11098	15039
Core Burnup BOC	MWd/kgHM	11858	6497	7549
Core Burnup EOC	MWd/kgHM	31525	17595	22588
MOX max. FA Average Burnup	MWd/kgHM	53047	26762	30473
FER max. FA Average Burnup	MWd/kgHM	23627	12049	-
Fxy, max	-	2.03	2.75	2.37
Fq, max	-	2.64	3.65	3.11

Table 3. 32: Three Selected Cores' Performances

Parameter	Unit	A	B	C
Plutonium mass	kg	4383	5298	5103
core HM mass	kg	36393	37875	34839
Unat Consumption[1]	kgUnat/TWhe	7343	5993	4618
Plutonium fissile content BOC	% (mass)	56.3	56.3	56.3
Plutonium fissile content EOC	% (mass)	55.1	54.7	54.2
Production Np	kg/TWhe	1.1	0.4	0.4
Production Am	kg/TWhe	12.1	14.1	14.1
Production Cm	kg/TWhe	2.7	2.6	3.3
Production Pu	kg/TWhe	-48.0	-76.7	-79.8

Table 3. 33: Three Selected Cores' Material Production & Consumption Overview

15. 4. 1. 1 Void Coefficient

Table 3. 34 shows the void coefficients obtained with three moderator densities: at 5%, 1% and 0.1% of the nominal moderator density. All values are negative and below the -500 pcm minimum value set for the HCSMR design.

Parameter	Unit	A	B	C
Void Coefficient 5 % BOC	pcm	-740	- 2467	- 2907
Void Coefficient 1 % BOC	pcm	-840	-2369	-2636
Void Coefficient 0.1% BOC	pcm	-940	-1991	-2566

Table 3. 34: Three Selected Cores' Void Coefficients

15. 4. 1. 2 Reactivity Coefficient

Table 3. 35 introduces three reactivity coefficients evaluated for each selected core: the Doppler coefficient, the moderator coefficient and the power coefficient. All values are negative both at BOC and EOC following a robust safety approach.

Parameter	Unit	A	B	C
Doppler Coefficient BOC	pcm/°K	-3.11	-3.40	-3.34
Doppler Coefficient EOC	pcm/°K	-3.39	-3.55	-3.47
Moderator Coefficient BOC	pcm/°K	-8.60	-9.95	-9.80
Moderator Coefficient EOC	pcm/°K	-11.56	-12.08	-12.04
Power Coefficient BOC	pcm/%Pnom	-9.73	-10.61	-10.46
Power Coefficient EOC	pcm/%Pnom	-9.08	-9.89	-10.29

Table 3. 35: Three Selected Cores' Reactivity Coefficients

15. 4. 1. 3 Reactivity Management

The HCSMR is anticipated to operate without soluble boron in the moderator to control the reactivity. Boron-free PWRs were broadly studied over the past years [32] [135]. For such

[1] With the assumption 1 kg Pu = 10 kg Unat.

designs the reactivity is only controlled using control rod mechanisms and burnable absorbers. Three main aspects must be carefully considered:

- The shutdown margins at all times and in particular at BOC;
- The compensation of the reactivity decrease over the cycle;
- The local power peak and maximum linear power throughout the entire cycle.

The under-moderated aspect of HCSMR cores results in limited excess reactivity at BOC as shown in Table 3. 36.

Parameter	Unit	A	B	C
Reactivity excess hot zero power, BOC	pcm	7720	4739	7186
Reactivity excess full power, BOC	pcm	6461	3456	5860
Reactivity excess full power, 6 EFPD	pcm	6307	3229	5651
Reactivity loss per day	pcm/EFPD	5.3	4.9	6.7

Table 3. 36: Three Selected Cores' Reactivity Excess

The slope of reactivity decrease over the cycle is rather flat compared to large LWRs. As a consequence the excess reactivity to manage at BOC both in hot zero power conditions and at full power is limited. With a maximum of 7720 pcm and considering all fuel assemblies are equipped with a control rod drive mechanisms the maximum anti-reactivity is 127 pcm per control rod cluster.

Due to the epithermal spectrum, the efficiency of standard LWR control rod absorbers is substantially decreased. The use of enriched B_4C control rods or alternative materials, e.g. Hafnium, is needed to control the reactivity. Previous works were performed regarding the reactivity management and efficiency of control rods in high conversion PWRs [136]. Large experience gathered on control rods' behavior and reactivity management can also be found in [137]. B_4C swelling under irradiation is a limitation and mixed Hafnium and B_4C control rods can be a relevant alternative.

A detailed analysis of the most appropriate reactivity management strategy and control rods sequence is not realized in this work and can be part of a follow-up analysis. It must also be remarked that the Xenon poisoning effect is less efficient in the epithermal spectrum and hence less compensation is required also during power transient. This could ease the operation of the HCSMR core without soluble boron even in load-following mode. Moreover the size of the core and its axial length must be carefully considered: a limited axial length reduces Xenon oscillations.

15. 4. 2 Further Considerations

15. 4. 2. 1 Design Lifetime

An expected lifetime of 60 years is anticipated for the HCSMR core. This is a conservative assessment based on current state-of-the-art engineering and material science knowledge. The neutron dose to the pressure vessel is expected to be smaller than for large reactors. The HCSMR neutron fluxes are close to 10^{11} $n.s^{-1}$. However, the impact of the reduced moderation and

epithermal spectrum, leading to a higher dose of fast neutron to the pressure vessel requires a dedicated analysis.

15. 4. 2. 2 Kinetic Aspects

The MOX fuel loaded in HCSMR cores decrease the delayed neutron fraction as well as the prompt neutron generation time. Mostly ^{239}Pu and ^{240}Pu are contributing to this behavior due to their delayed neutron share of 250 pcm. Consequently the core delayed neutron fraction also referred to as β_{eff} is close to 300 pcm whereas it is around 600 pcm in a standard PWR. HCSMR cores behave close to fast reactors with regards to their response to reactivity insertion.

However, since the plutonium isotopes concentration remains almost constant over the cycle the β_{eff} also remains constant during the entire cycle. This is different compared to standard PWRs seeing a decrease β_{eff} at EOC.

15. 4. 3 Uncertainties

15. 4. 3. 1 Cross Sections & Computation Schemes

Several uncertainties are introduced all along the optimization process. At the computation scheme level first the performances of a given core configuration can vary depending on the cross section types – and their own uncertainties – the simplifications considered to simulate the core or even due to the solvers' uncertainties.

The optimization process itself also contains various sources of uncertainties: the surrogate models, although showing high performance, bring their own uncertainties. Moreover the methods to implement genetic algorithms are sources of uncertainties in the choice of objectives.

Margins and penalties are considered at the computation scheme level to ensure conservative results are obtained. The repetition of the successive optimization steps is also reassuring with regards to the level of accuracy obtained for the HCSMR optimum core population. Overall the results obtained are considered robust, in particular compared to the external sources of uncertainties not considered yet: the thermo-hydraulic and system detailed analysis.

15. 4. 3. 2 Thermal-Hydraulic Operating Point

The HCSMR core pressure is set at 140 bars. This is lower than large PWRs for which a core pressure around 155 bars is standard. An optimization of the HCSMR operating point is outside of this work's scope. However, it is relevant to assess the importance of a pressure modification on core performances and in particular with regards to the conversion ratio. Beyond the moderation ratio, the core conversion ratio also depends on the water density.

To assess this effect a comparison of a HCSMR core with an operating point at 140 bars and at 155 bars is performed. The performances are introduced in Table 3. 37. The change in operating points also affects the reactivity coefficients and the core cycle length, which influences the

conversion ratio. Nevertheless the operating point has an observable impact on the conversion ratio. A joint optimization of the operating point could be a follow-up step to this work.

Parameter	Unit	HCSMR 140 bars	HCSMR 155 bars
Core height	cm	220	220
Pu enrichment	%	19.0	19.0
Fuel type	-	MOX	MOX
Fuel management	-	1/3	1/3
Core pressure	bar	140	155
T inlet	°C	280	300
moderator density	$kg.m^{-3}$	0.73	0.69
Moderation ratio	-	1.02	1.02
Cycle length	EFPD	853	635
Cycle Burnup	MWd/kgHM	18529	13799
Void Coefficient	pcm	7559	3292
Conversion Factor	-	0.79	0.839
Plutonium mass	kg	4923	4923
Linear Power, max	W/cm	246	243

Table 3. 37: Cores with two Thermo-hydraulic Operating Points

Chapter 16: PART THREE CONCLUSION

This third part of the thesis presents the HCSMR design optimization process and its outcomes. Three optimization exercises are performed to optimize the HCMSR design: two at the fuel assembly level and one at the core level. The optimization uses iterations between fuel assembly and core optimizations. All exercises are multi-parameter and multi-objective optimizations.

16. 1 ZON FA OPTIMIZATION

The first optimization exercise aims at identifying the optimum plutonium content triplets in three radial zones of a HCSMR ZON fuel assembly (FA). The second exercise purpose is to find optimum positions for the fertile fuel rods introduced in a HET FA. The third and last exercise is performed at the core level. It gathers all parameters considered for the HCSMR design and aims at identifying a population of optimum HCSMR core designs.

For the three optimization exercises the method implemented is similar. First a research plan is established. It focuses on identifying the boundary conditions of the optimization exercises. A sensibility analysis can then be performed to analyze the parameters behavior and relationships. The Morris and Sobol methods are implemented.

Secondly, surrogate models are created. Those are proxy for evaluations performed using explicit neutron physics tools. This step aims at saving time for the optimization process. The surrogate functions are created using neural networks theory implemented via the URANIE platform. Surrogate models based on Kriging methods are evaluated as well.

Surrogate models make it possible to save substantial computing costs to perform the actual optimization step. Moreover surrogate models also offer an added value with regards to its statistical approach: those methods provide an opportunity to identify abnormal behavior and detect erroneous individuals among the research plan. This early detection permits a better understanding of the exercise boundary conditions or to refine the explicit computation scheme.

The optimization itself is performed using genetic algorithms via the URANIE platform and its Vizir module. The results obtained are good and enable the input of optimized ZON fuel assemblies to the core optimization. The ZON FA optimization results in a population of Pareto optimum FA with regards to the reactivity (k_{inf}), the void coefficient (*void*) and the peaking factor (F_{xy}). The optimization parameters are the plutonium contents in three radial zones. Out of the optimized population 20 ZON FA designs are selected with different average plutonium, forming the outcomes of this first optimization exercise. For those designs, FA branch computations are performed. The ZON FA optimization also enables more familiarity with the tools and methodology required to perform a multi-objective optimization.

16. 2 HET FA OPTIMIZATION

The HET FA exercise results in a Pareto optimum population with regards to the reactivity (k_{inf}), the void coefficient (*void*) and the peaking factor (F_{xy}) as well. The optimization parameters are

the positions of the fertile fuel rods. The optimization exercise is repeated for four sub-exercises: with 60 (HET.05), 96 (HET.08), 120 (HET.10) and 144 (HET.12) fertile fuel rods introduced in the HET FA. Due to the large number of possible combinations to position the fertile fuel rods, the optimization exercise size is reduced using templates. Those templates set predefined position for some fissile or fertile fuel rods according to the research plan analysis.

Two main types of fertile fuel rod positioning are observed: on the one hand by positioning most fertile fuel rods on the fuel assembly outer row. This leads to the best reactivity (k_{inf}) and void coefficient (*void*) cases. On the other hand, with fertile fuel rods spread within the fuel assembly, and in particular next to the guide tubes' water holes, the peaking factor (F_{xy}) shows the best performances. Accordingly two types of templates are created for each optimization sub-exercise. The assumptions supporting the introduction of templates are carefully verified by repeating multiple times the analysis.

As a result, the HET FA Pareto optimum populations show two main types of optimized HET FA. Two patterns are selected among the optimized populations for the four sub-exercises HET.05, HET.08, HET.10 and HET.12. For each case, one pattern focuses on FA configuration enabling best reactivity (k_{inf}) and void coefficient (*void*), while one pattern focuses on configurations enabling to obtain the best peaking factors (F_{xy}). In total 47 HET FA are selected for the core optimization.

The specific genetic algorithm developed for the HET FA optimization and its discrete behavior can be further improved. For this work, the cross-breeding process is undertaken without considering the neutron-physic behavior. This could be captured in the optimization exercise: the preferred positioning of fertile fuel rods next to water gap rods could be considered.

In total 90 FAs are selected as input to the core optimization step. Branch computations are performed with APOLLO2 for those FAs. In addition to ZON and HET FA, 23 FA MOX FA are selected. Those fuel assemblies only contained MOX fuel rods, with various plutonium contents and for some FAs the MOX matrix also contains enriched ^{235}U isotopes.

16. 3 CORE OPTIMIZATION

The population of optimum cores obtained confirms the feasibility to design cores satisfying the HCSMR optimization boundary conditions and objectives:

- Conversion factor: higher than 0.8 (maximize);
- Cycle length: higher than two years (maximize);
- Void coefficient: less than - 500 pcm (minimize);
- Max. linear power: less than 400 W/cm (minimize, considered as boundary condition);
- Plutonium mass in core (minimize).

The characteristics of the optimized cores are analyzed using sub-populations. It is first observed that the four types of fuel assemblies considered (MOX, ZON, HET and FER) are among the optimum core designs. This shows a global added value of those approaches to achieve the HCSMR core objectives. A conclusion about whether a type of fuel assembly is better than

another is not made since it depends on the priority given to the different optimization objectives.

MOX FAs with enriched uranium at 5% are among Pareto optimum cores. Enriched uranium enables rather long cycle lengths. The introduction of enriched uranium at 10% leads to very high cycle lengths but significantly degrades conversion factors. A continuous optimization of the ^{235}U enrichment could be a further step to refine the outcomes obtained in this work. Irradiating MOX FA with enriched uranium also permits in an under-moderated small core to limit the required quantity of plutonium. The appropriateness of this approach is therefore confirmed.

The three core reflector types are found among the Pareto optimum core designs. However, there is a clear predominance of the heavy reflector containing 96 % of stainless steel among Pareto optimum individuals.

With regards to fuel management, all Pareto optimum individuals are cores with a "1/2" fuel management. The introduction of another optimization objective "Unat consumption" does not change this conclusion. However, when an additional objective is set on the maximum discharge burnup – to maximize it and limit the need of fresh FA – fuel management with "1/3" strategy are also among the Pareto optimum individuals.

Among the Pareto optimum population three designs are selected for a detailed analysis. Within those three designs the four types of fuel assemblies (MOX, ZON, HET and FER) are represented. Two core configurations contain fertile fuel assemblies. For all designs the reactivity coefficients remain negative at all times. The reactivity coefficients – Doppler, Moderator and Power – remain rather constant over the cycle. Overall those coefficient values are higher than in standard LWR designs. The impact for transient situations, and in particular main steam line break accidents, should be assessed in detail.

Void coefficients remain negative at all time. This satisfies the design requirement set on this objective. Nevertheless, the relevance of this objective should be further analyzed for small under-moderated core with an integrated pressure vessel. A slightly positive void coefficient could enable a further simplification of the core without affecting safety standards since a sudden exit of the entire moderator would be intrinsically impossible in such designs.

The cores selected have rather high active lengths, between 280 cm and 300 cm. This outcome might question the SMR concept, looking to minimize the component size and complexity. However, several advantages exist with such a design. On a neutron-physic perspective this limits the average core power and enhances margins with regards to linear power and even for load-follow operation without soluble boron in the primary coolant. With regards to thermo-hydraulic, a core with a high active length would improve natural circulation. This is particularly relevant for transient situations and could balance the increased pressure drops due to the tightened fuel lattice in under-moderated cores. In a further step those aspects could be optimized together with the core power in an economic assessment.

When comparing the three selected design performances with the HCSMR initial core, or with other under-moderated designs [39] or standard iPWR SMRs (SMR600), improvements are

observed. The cycle length, conversion factors and also natural uranium consumption are improved. Of course, the difference of power output with large under-moderator cores must be noted. But considering a natural resource utilization view, the HCSMR cores bring substantial added value. With regards to the deployment of under-moderated cores, small ones such as the HCSMR also have the advantage of a limited need of initial plutonium mass. Considering a hybrid fleet of NPP combining high conversion and PWR cores [46], high conversion SMRs could well fit the plutonium masses produced and evolve in a symbiotic manner with standard PWRs.

The reactivity management is anticipated without soluble boron. The slope of reactivity decrease over the cycle is rather flat compared to large LWRs. As a consequence the excess reactivity to manage at BOC both in hot zero power conditions and at full power is limited. With a maximum of 6500 pcm and considering all fuel assemblies equipped with a control rod drive mechanism, the maximum anti-reactivity to consider would be 110 pcm per control rod cluster.

The core optimization reveals specific challenges worth a short discussion. The main difficulty identified lies in the joint optimization of the fuel assembly and core design. An iterative process is used to design the HCSMR core. But the transition step from FA to core optimization signifies selecting early on the FA design options. This limits the potential to reach global optimum.

Several options can help tackling those limitations. First, the transformation of fuel assembly cross sections by surrogate model could be one step forward. This would enable a global optimization using surrogate models both at the FA and core levels.

Moreover, the development of computing resources could lead to overall quicker core computations. In this sense, a one-step pin by pin full core evaluation could become possible at a reasonable cost. Such approaches are important when looking at heterogeneous cores since the diffusion approximation has some limitations. Full core 2D or even 3D transport (MOC, SN) would be an important step forward. Developments in those directions are ongoing but are not yet available for optimization exercises due to their still high computing costs.

Conclusion

CONCLUSION

This research work aims at designing and optimizing the high conversion small modular reactor (HCSMR) core design. The HCSMR has a thermal output of 600 MW for 200 MW electrical. It is an integrated PWR with a tightened fuel assembly lattice. The rod-to-rod pitch is 1.15 cm in a hexagonal lattice. As a result the moderation ratio (1.0) is reduced compared to large PWR (2.0) and the HCSMR has an improved ability to convert ^{238}U into ^{239}Pu. The core is loaded with MOX fuel.

The HCSMR core is designed using multi-objective optimization methods. Several optimization parameters are considered: the core active length, the fuel assembly design, the fuel management strategy and the reflector type. Multi-parameter and multi-objective optimization methods are at the heart of this research work. This aims at identifying a population of Pareto optimum core designs. A Pareto optimum population is a population of individuals for which it is not possible to improve any individual on one objective without it deteriorating on at least one other objective.

The HCSMR development is a research project resulting from a cooperation between PreussenElektra GmbH (formerly E.ON Kernkraft GmbH), the Technical University of Munich (TUM) and the French Atomic Energy Commission (Commissariat à l'Energie Atomique et aux énergies alternatives, CEA). It is supported by a cooperation agreement signed in 2010 between E.ON Kernkraft GmbH and the CEA.

The research work is organized in three main parts, reflected in this document's structure. The first part presents a comprehensive review of existing knowledge on SMR, high conversion LWR and optimization techniques. It also serves to define the design objectives and main options of the HCSMR core. The second main work stream is the development of the neutronic model needed to simulate the HCSMR cores performances. The third part is dedicated to the actual optimization of the HCSMR core design.

The HCSMR makes it possible to limit the use of natural uranium and increase its utilization; in particular compared to today's LWRs. Natural uranium low prices currently observed worldwide do not encourage substantial efforts to reduce the uranium consumption of nuclear reactors. However, this situation is likely to evolve in the future and tension on uranium markets could arise. LWRs could become more sustainable with an enhanced ability to convert ^{238}U isotopes into ^{239}Pu.

The HCSMR finds its roots at the intersection of SMR and high-conversion light water reactors. A renewed interest for SMR development can be observed worldwide. Small core designs bring a new paradigm for nuclear power development. SMRs have passive and intrinsic safety systems, their modularity and simplification, compared to large reactors, advocates for their development. Challenges also exist on the journey toward SMR deployment. For example the licensing schemes and business models of SMRs are not proven yet.

More than 70 SMR designs, at various development stages, exist. Among a selection of 50 of the most advanced designs, 24 use PWR technology and 13 have integrated cores concept. An

integrated core concept refers to a reactor pressure vessel containing the core, steam generators and the pressurizer. This approach is also anticipated for the HCSMR core, although a comprehensive system design and analysis is not part of this work's scope.

For nine selected designs a detailed analysis is presented: CAREM-25, ACP100, FlexBlue, SMART, ABV, RITM-200, mPower, NuScale and Westinghouse SMR. One main finding with regards to reactor physics is related to SMR fuel efficiency. From a fuel management perspective SMRs have low fuel efficiency. The reduced size of the core increases neutron leakage and hence decreases neutron economy. Moreover designers' search for long irradiation cycles fosters fuel management with low shuffling rate. Take batch cores as an example. This limits the final discharge fuel burnup and overall fuel efficiency. The HCSMR core aims at tackling those limitations and at improving fuel utilization of small cores. The review of those nine designs also supports the definition of the first HCSMR core characteristics.

Furthermore the SMR600 design is introduced as part of this research work for benchmark purposes. It provides a reference to compare the HCSMR performances on natural uranium consumption and conversion factor with a PWR SMR. The SMR600 characteristics are mostly based on the mPower and Westinghouse SMR designs. The fuel is standard 17x17 with enriched UO_2 and reduced height of 220 cm. The core is made of 69 fuel assemblies and is rated at 600 MW thermal. Two fuel management approaches are considered: a batch fuel management and a "1/2" fuel management approach. The associated cycle lengths reach 924 EFPD and 633 EFPD respectively for conversion factor of 0.63 and 0.48. The corresponding natural uranium needs for the SMR600 amount to 43 tUnat/TWhe with a batch fuel management and 30 tUnat/TWhe when half of the core is reloaded at each cycle. Fuel reprocessing is not considered to derive those values, following the fuel cycle strategies selected for most advanced iPWR designs.

As mentioned, the HCSMR concept partly finds its origins on applying high conversion light water reactors' characteristics to a small core design. The high conversion behavior is obtained via a reduction of neutron moderation, mostly attained by tightening the fuel rod pitch. This hardens the neutron spectrum and enables a better utilization of the fuel loaded. Such cores are also referred to as under-moderated designs.

HCLWR cores have been studied for many years but have not yet been developed industrially as they also have challenges. HCLWR designs' main limitation lies in their behavior in transient situations and in particular in case of loss of coolant as the void coefficient tends to turn positive due to the fuel and core characteristics. To prevent this and ensure a negative void coefficient at all times, various strategies are implemented in the concepts developed until now. For the HCSMR the small size of the core itself is an added value to keep a negative void coefficient, since the neutron leakage rate increase becomes an advantage in voided situations.

The review of existing HCLWR designs also participates to the identification of a starting point to design the HCSMR core. It permits the analysis of the most promising solutions for application on small cores. The introduction of fertile material is its principal illustration. The benefit of loading fertile fuel assemblies for the HCSMR core is analyzed. The introduction of axial layers of fertile material observed in other designs is not selected due to the reduced core height of SMRs. An additional hybrid solution is considered to increase radial heterogeneity in MOX fuel via the

introduction of fertile fuel rods. Similar designs to the HCSMR concept are not found in existing literature.

Under-moderated cores have a high level of complexity. Their optimization is therefore complicated and multi-objective and multi-parameter optimization methods add value to the HCSMR core design. The use of surrogate models based on neural network and multi-objective optimization techniques via genetic algorithm are the preferred methods implemented in this work.

The HCSMR first image contains parameters kept constant for all HCSMR cores, even for the core optimization:

- Core thermal power: 600 MW;
- 61 hexagonal fuel assemblies;
- Fuel rods pitch: 1.15 cm;
- Core moderation ratio: 1.02;

The HCSMR core performances are derived using the neutron-physic codes developed at CEA. At the fuel assembly level, APOLLO2 is used to compute the HCSMR FA designs in infinite medium. Three types of fuel assembly (FA) designs are evaluated: a MOX FA containing only MOX fuel rods with a unique plutonium content; a ZON FA containing MOX fuel rods with three plutonium contents; and the HET FA containing MOX and fertile fuel rods. The ZON FA design aims at reducing the FA radial power peak due to the local over moderation at the FA outer row. The HET FA is proposed to reduce the reactivity increase in voided situation.

The results obtained with APOLLO2 using deterministic methods are benchmarked against Monte-Carlo results computed with TRIPOLI-4®. The comparisons are performed with fresh fuel and with depleted fuel: at 0 MWd/kgHM and 60 MWd/kgHM. A maximum reactivity delta of 325 pcm is observed for the HET FA at 60 MWd/kgHM. This is in line with the objective of maximum 500 pcm difference set to validate the HCSMR computation schemes. Computation schemes with a good accuracy level are needed to successfully carry out the HCSMR core preliminary design. However, very high fidelity computation schemes are not required at this design step.

The heavy isotope fission rates per fuel rod are also compared between TRIPOLI-4® and APOLLO2. A maximum difference below 2 % regardless of the burnup is obtained for all three FA designs. The largest discrepancies are observed with the HET FA for which local substantial flux changes close to the fertile fuel rods are observed. The accuracy of APOLLO2 in evaluating this sort of design is confirmed.

Beyond nominal evaluations, voided situations are also computed at the FA level and compared between deterministic and stochastic calculations. The results obtained are assessed with regards to the reactivity evaluated with a voided moderator at 0 MWd/kgHM. The maximum difference between APOLLO2 and TRIPOLI-4® remains below 300 pcm and conservative behavior is observed: APOLLO2 systematically gives reactivity values higher than TRIPOLI-4®. Overall those performances confirm the relevance of the computation schemes developed at the FA level to evaluate and optimize the HCSMR core design.

At the core level CRONOS2 and APOLLO3® are used to compute HCSMR cores. Three core designs are considered to validate the computation schemes developed with CRONOS2 against TRIPOLI-4® results: the MOX core containing only MOX fuel assemblies, the HET core with only HET fuel assemblies and the FER core loaded with both MOX and FER fuel assemblies.

The comparisons with TRIPOLI-4® are performed with fresh fuel. For the MOX and HET cores the reactivity differences remain below 400 pcm, using both 2 and 8 energy groups in CRONOS2. For the FER core, up to 600 pcm difference is observed with TRIPOLI-4®. The highly heterogeneous FER core challenges the diffusion approximation used for the core calculations.

On the one hand this observation highlights the limits of the diffusion approximation for highly heterogeneous HCSMR cores. On the other hand it shows that good preliminary results can be obtained with CRONOS2. The comparison of fuel assembly relative power at the core level confirms for the three cores the relevance of the simulation options with differences observed remaining below 3 %. Overall the accuracy obtained with APOLLO2, CRONOS2 and APOLLO3® matches the requirements needed for this study, both for the fuel assembly and core computations.

Three optimizations exercises are undertaken to optimize the HCMSR design: two at the fuel assembly level and one at the core level. The HCSMR optimization uses iterations between fuel assembly and core optimizations. All of the exercises are multi-parameter and multi-objective optimizations.

The first optimization exercise aims at identifying the optimum plutonium content triplet in three radial zones of a HCSMR ZON fuel assembly (FA). The second exercise purpose is to find optimum positions for the fertile fuel rods introduced in a HET FA. The third and last exercise is performed at the core level. It gathers all parameters considered for the HCSMR design and aims at identifying a population of optimum HCSMR core designs.

For the three optimization exercises the method implemented is similar. First a research plan is established. It focuses on identifying the boundary conditions of the optimization exercises. A sensibility analysis can then be performed to analyze the behavior and relationships of these parameters. The Morris and Sobol methods are implemented. As a result the research plan space is adapted as required.

Secondly, surrogate models are created. Those are proxy for evaluations performed using explicit neutron physics tools. This step aims at saving computation time for the optimization. The surrogate functions are created using neural network theory implemented via the URANIE platform. Surrogate models based on Kriging methods are evaluated as well. Their performances are good but a clear advantage in comparison to neural networks is not proven. Hence neural network remains the standard approach in this work. The HET FA optimization exercise has a discrete behavior and the creation of a surrogate model is not performed. The explicit code APOLLO2 is directly used to perform the optimization.

Beyond saving substantial computing costs to perform the optimization, surrogate models also offer an added value with regards to their statistical approach: those methods give an opportunity to identify abnormal behavior and detect erroneous individuals among the research

plan. This early detection permits a better understanding of the exercise boundary conditions or to refine the explicit computation scheme.

The optimization itself is performed using genetic algorithms via the URANIE platform and its Vizir module. For the HET FA optimization a specific algorithm is introduced to adapt to the discrete behavior. The results obtained enable the input of optimized ZON and HET fuel assemblies to the core optimization.

The ZON FA optimization results in a population of Pareto optimum FA with regards to the reactivity (k_{inf}), the void coefficient (*void*) and the power peaking factor (F_{xy}). The optimization parameters are the plutonium contents in three radial zones. Out of the optimized population 20 ZON FA designs are selected with different average plutonium content and plutonium content triplet behavior, forming the outcomes of the first optimization exercise. For those selected designs, FA branch computations are performed. The ZON FA optimization also enables the author to become familiar with the tools and methodology required to perform a multi-objective optimization.

The HET FA exercise results in a Pareto optimum population with regards to the reactivity (k_{inf}), the void coefficient (*void*) and the peaking factor (F_{xy}) as well. The optimization parameters are the positions of the fertile fuel rods. The optimization exercise is repeated for four sub-exercises: with 60 (HET.05), 96 (HET.08), 120 (HET.10) and 144 (HET.12) fertile fuel rods introduced in the HET FA (out of a total 438 fuel rods per FA). Due to the large number of possible combinations to position fertile fuel rods, the optimization exercise size is reduced using predefined templates. Those templates set predefined positions for some fissile or fertile fuel rods according to the research plan analysis.

Two main types of fertile fuel rod positioning are observed: either by positioning most fertile fuel rods on the fuel assembly outer row or by spreading the fertile fuel rods within the FA, and in particular next to the guide tubes' water holes. The first approach leads to the best reactivity (k_{inf}) and void coefficient (*void*) performances. The second positioning method leads to the best peaking factor (F_{xy}) performances. Accordingly two types of templates are created for each optimization sub-exercise. The assumptions supporting the introduction of templates are carefully verified by repeating the analysis multiple times.

As a result, the HET FA Pareto optimum populations show two main types of optimized HET FA. Two patterns are selected among the optimized populations for the four sub-exercises HET.05, HET.08, HET.10 and HET.12. For each case, one pattern focuses on FA configuration enabling the best reactivity (k_{inf}) and void coefficient (*void*) while one pattern focuses on configurations enabling the obtainment of the best peaking factors (F_{xy}). In total 47 HET FA are selected for the core optimization.

The specific genetic algorithm developed for the HET FA optimization and its discrete behavior can be further improved. For this work, the cross-breeding process is carried out without considering the neutron-physic behavior. This could be captured in the optimization exercise: the preferred positioning of fertile fuel rods next to water gap rods could be considered.

In total 90 FAs are selected as input to the core optimization step. Branch computations are performed with APOLLO2 for those FAs. In addition to the ZON and HET FA, 23 MOX FA are selected. Those fuel assemblies only contained MOX fuel rods, with various plutonium contents and for some FAs the MOX matrix also contains enriched ^{235}U isotopes.

At the core level the optimization is also performed using surrogate models and genetic algorithms. The objectives and boundary conditions considered are as follows.

- Conversion factor: higher than 0.8 (maximize);
- Cycle length: higher than two years (maximize);
- Void coefficient: less than - 500 pcm (minimize);
- Max. linear power: less than 400 W/cm (minimize, considered as boundary condition);
- Plutonium mass in core (minimize).

The optimization parameters considered are:

- The core active height;
- The fuel management;
- The reflector type;
- The introduction of fuel assemblies with only fertile fuel rods (fertile fuel assemblies);
- The type of fuel assemblies;
- The plutonium average content;
- The plutonium content in fuel assemblies' outer rows;
- The number of fertile fuel rods in fuel assemblies;
- The number of fertile fuel rods in fuel assemblies in the outer row;
- The introduction of enriched uranium.

As a result a population of optimum cores is obtained. Their characteristic confirms the feasibility of designing HCSMR cores satisfying the optimization boundary conditions and objectives. Moreover, key outcomes are identified with regards to the design of a small under-moderated core.

First, the four types of FA considered – MOX, ZON, HET and FER – are found among the Pareto optimum population. This shows the relevance of the approaches considered for HCSMR FA designs. It also confirms the possibility of managing the introduction of fertile material at different levels: within MOX fuel assemblies or by loading FER fuel assemblies.

Furthermore, MOX FAs with enriched uranium at 5% are among Pareto optimum cores. Enriched uranium makes it possible to reach rather long cycle lengths. The introduction of enriched uranium at 10% is not found in the Pareto optimum individuals. The large content of ^{235}U isotopes leads to very high cycle lengths but significantly degrades conversion factors. A continuous optimization of the ^{235}U enrichment could be a further step to refine the outcomes obtained in this work. Irradiating MOX FA with enriched uranium in an under-moderated small core also enables the limitation of the required quantity of plutonium.

Conclusion

The three core reflector types considered – with 10%, 50% and 96% of stainless steel – are found among the Pareto optimum core designs. However, a clear predominance of the heavy reflector containing 96 % of stainless steel is observed among Pareto optimum individuals.

With regards to fuel management, all Pareto optimum individuals are cores with a "1/2" fuel management. The introduction of another optimization objective "Unat consumption" does not change this conclusion. However, when an additional objective is set to maximize the FA discharge burnup – to limit the need of fresh FA – "1/3" fuel management strategies are also among the Pareto optimum individuals.

Based on the Pareto optimum population three designs are selected for a detailed analysis. Within those three designs the three types of fuel assemblies (MOX, ZON and HET) are represented. Two core configurations contain fertile fuel assemblies. For all designs the reactivity coefficients remain negative at all times. The reactivity coefficients – Doppler, Moderator and Power – remain rather constant over the cycle. Those coefficients have values higher than what is observed in standard LWR designs. The impact for transient situations, and in particular for main steam line break accidents, should be assessed in detail.

Void coefficients remain negative at all times. This satisfies the design requirement set on this objective. Nevertheless, the relevance of this objective should be further analyzed for small under-moderated cores using an integrated pressure vessel. A slightly positive void coefficient could further simplify the core design without harming safety since a sudden exit of the entire moderator would be intrinsically impossible in such integrated designs.

The HCSMR reactivity management is anticipated without soluble boron. The slope of reactivity decrease over the cycle is rather flat compared to large LWR. As a consequence the excess reactivity to manage at BOC both in hot zero power conditions and at full power is limited. With a maximum of 6500 pcm and considering all fuel assemblies equipped with a control rod drive mechanism, the maximum anti-reactivity to consider is 110 pcm per control rod cluster.

Overall this research work makes it possible to establish core design options for a small under-moderated core from a reactor-physic perspective. Compared to previous work, the HCSMR design adds value with the HET fuel assembly introduction in particular. The benefits of introducing fertile material radially at the FA level are confirmed. This work also confirms the potential of high conversion for small cores to limit natural uranium consumption and improve uranium utilization. Moreover, loading enriched uranium in MOX fuel to increase fuel cycle length, reduce plutonium mass needs and limit the void coefficient is an approach proven relevant.

The HCSMR performances show the potential of optimized small under-moderated cores. Conversion factors are between 0.80 and 0.92, cycle lengths are close to 1200 EFPD with negative void coefficients, and maximum linear power remains below 400 W/cm. The natural uranium consumption of HCSMR designs depends on their characteristics but is below ten tons per electric TWh generated. Compared to existing PWR operated without fuel reprocessing it is an improvement by at least a factor of two. When comparing the HCSMR performances with innovative PWR SMR designs, the improvement can reach a factor of five. The HCSMR concept is proven from a neutron physics approach with its preliminary core characteristics established.

The added value of multi-objective optimization methods in designing under-moderated cores is confirmed. Some challenges in particular are identified with regards to the iterations needed between core and fuel assemblies' optimization, limiting the search of a global optimum. Recommendations for tackling those aspects are formulated. On a methodology aspect, this works adds value to the discrete optimization undertaken for the HET FA design and the specific algorithm introduced. The methodology implemented can be reused for similar optimization exercises and for handling discrete optimization challenges in general.

This preliminary work towards the design of high conversion under-moderated cores and the HCSMR design opens many paths to further studies. In particular:

- A thermo-hydraulic study using sub-channel methods to verify the margins to critical flux and related thermo-hydraulic properties. This would also enable the confirmation of the fuel assembly grid design, essential to the entire core performance. In addition it would pave the way for a comprehensive multi-physic optimization of the HCSMR core design;
- A neutron-physics study on reactivity management strategy for the HCSMR core. The characteristics identified in this work highlight the advantages of under-moderated cores to operate soluble boron free. A detailed analysis should now suggest concrete approaches in managing the reactivity swing between BOC and EOC as well as to accommodate power manoeuvers and load-following capabilities;
- A system analysis to assess transient situations and the main steam line break accident. in particular the loss of coolant accident is excluded by design since the primary circuit is integrated in one pressure vessel;
- A multi-objective optimization method including adaptive research plans [95]. This would reinforce the accuracy and decrease the cost of the optimization process;
- Repeating such preliminary core designs with a boiling coolant might further improve performance. Compared to a pressurized coolant, an under-moderated BWR core increases the conversion factor by about five points [81]. This would further improve natural resources utilization and nuclear power sustainability.

ACKNOWLEDGMENTS

This PhD research work was a personal project supported by several collaborations. I want to thank the people and their organisations that have enabled this enterprise:

- At the Technical University of Munich (TUM), Prof. Dr. Rafael Macián, Head of the Institute of Nuclear Engineering (NTech), for his supervision and advice;
- At PreussenElektra (PEL), Dr. Wolfgang Faber, Head of the Fuel Operation and Disposal Department, for his tireless efforts to make this project a reality;
- Dr. Michael Fuchs, Senior Vice-President at PEL, for the continuous support of the E.ON/PreussenElektra – CEA collaboration;
- Dr. Erwin Fischer, Chief Nuclear Officer and member of the Board at PEL, for his encouragement and recommendations;
- Mr. Volker Raffel, Head of Energy Economics department at PEL, for his trust and assistance in completing the project;
- At the French Atomic Energy Commission (CEA), Mr. Patrick Dumaz for his support in establishing the project from the beginning;
- Mr. Marc Delpech, Head of Applied Mathematics and Reactor Physics (SERMA) unit at CEA, for his generous and pragmatic support of the project;
- Prof. Dr. Patrick Blanc-Tranchant, Head of CEA Nuclear Energy Division International Affairs, former Head of SERMA unit, for the initial support of the project;
- Dr. Christine Poinot-Salanon, Project Manager at CEA, for her stamina and recommendations to set-up the project.

I want to thank the scientific coordinators who closely supported the project:

- Dr. Marcus Seidl (PEL), reactor physics expert at PEL, for his availability, his recommendations and the time invested in this project;
- Dr. Michel Soldevila, Mr. Siegfried Douce and Dr. Frédéric Damian (CEA), to have pioneered this joint-work, supported the long project hours and shared their knowledge.

Besides the official contributors a large group of colleagues and friends have helped me to complete this adventure. I express my sincere gratitude to them:

- PEL colleagues for their patience and continuous support to this project;
- Mrs. Po Sang Lam at TUM and all the Graduate school staff;
- Ms. Amélie Rouchon, Mr. Karim Ammar, Mr. Cyril Patricot and Mr. Antoine Collin at CEA who shared their own PhD insights and provided me advices on SERMA's tools;
- Dr. Hadid Subki, IAEA SMR Technical Lead, for his advices and recommendations;
- All colleagues at SERMA and in particular at the LPEC group;
- Dr. Fabrice Gaudier, Dr. Gilles Arnaud and the colleagues at the CEA LGLS group.
- Mr. Jean-Baptiste Thomas, for his insight and suggestions;
- Ms. Vivien Ingrams for her patience in reviewing the English language of this document;
- Family and friends for their uninterrupted support. In particular Ms. Hélène Maigne, Mr. Amaël Beauvallet, Mr. Xavier Janin and Mr. Ayoub Nassir for their hospitality in Paris;
- Last but not least Mrs. Marion Janin, who has been my first supporter and confident all along this journey. Thank you!

Bibliography

BIBLIOGRAPHY

[1] V. Kuznetsov. Innovative Small and Medium Sized Reactors: Design Features, Safety Approaches and R&D Trends. IAEA TECDOC-1451, Vienna, 2004.

[2] IAEA. Status of innovative small and medium sized reactor designs 2005. IAEA TECDOC-1485, Vienna, 2006.

[3] OECD/NEA. Current Status, Technical Feasibility and Economics of Small Nuclear Reactors. OECD, Paris, 2011.

[4] IAEA. Status of Small and Medium Sized Reactor Designs. IAEA, Vienna, 2012.

[5] IAEA. Status of Small Reactor Designs Without On-Site Refuelling. IAEA TECDOC-1536, Vienna, 2007.

[6] IAEA. Advances in Small Modular Reactor Technology Developments 2016 Edition, IAEA Booklet, Vienna, 2016.

[7] K. Shirvan *et al*. The design of a compact integral medium size PWR. Nuclear Engineering and Design, 243, 393-403, 2012.

[8] John E. Kelly *et al*. Generation IV International Forum: A decade of progress through international cooperation. Progress in Nuclear Energy, 240-246 (77), 2014.

[9] IAEA. Status of Innovative Fast Reactor Designs and Concepts. IAEA, Vienna, 2013.

[10] B. Middleton, C. Mendez. Integrating Safety, Operations, Security, and Safeguards into the Design of Small Modular Reactors: A Handbook. Sandia National Laboratories, Albuquerque, 2013

[11] K. Shirvan *et al*. Technology Selection for Offshore Underwater Small Modular reactors. Nuclear Engineering and Technology, in press, 2016.

[12] M. D. Carelli, D. T. Ingersoll. Handbook of Small Modular Nuclear Reactors. Woodhead Publishing, ISBN 978-0-857098511, 2015.

[13] IAEA. Design Safety Considerations for Water Cooled Small Modular Reactors Incorporating Lessons Learned from the Fukushima Daiichi Accident. IAEA TECDOC-1785, Vienna, 2016.

[14] OECD/NEA. Reduction of Capital Costs of Nuclear Power Plants. OECD, Paris, 2008.

[15] G. Woite. Capital Investment Cost of NPPs. IAEA Bulletin February, Vienna, 1978.

[16] IAEA. Technical and Economic Evaluation of Potable Water Production Through Desalination of Seawater by Using Nuclear Energy and Other Means. IAEA TECDOC-666, Vienna, 1992.

[17] M. D. Carelli *et al*. Economic features of integral, modular, small-to-medium size reactors, Progress in Nuclear Energy, 52, 403-414, 2010.

[18] J. Vujic. Small modular reactors: Simpler, safer, cheaper? Energy, 45, 288-295, 2012.

[19] G. Locatelli and M. Mancini. Small-Medium sized Nuclear Coal and Gas Powerplant: a Probabilistic Analysis of their Financial Performances and Influence of CO2 Cost, Energy Policy, 38, 2010.

[20] OECD/NEA. Small Modular Reactors: Nuclear Energy Market Potential for Near-term Deployement. OECD, Paris, 2016.

[21] K. Söderholm *et al*. Licensing process characteristics of Small Modular Reactors and spent nuclear fuel repository, Nuclear Engineering and Design, 276, 1-8, 2014.

[22] T. Sainati *et al*. Small Modular Reactors: Licensing constraints and the way forward, Energy, 82, 1092 – 1095, 2015.

[23] WNA (CORDEL). Facilitating International Licensing of Small Modular Reactors, Report 2015/04, London, 2015.

[24] EUR. European Utility Requirements for LWR NPP. Revision D, 2012.

[25] IAEA. Options to Enhance Proliferation Resistance of Innovative Small and Medium Sized Reactors. Nuclear Energy Series No. NP-T-1.11, Vienna, 2014.

[26] D. T. Ingersoll *et al*. Can Nuclear Power and Renewables be Friends? Proceedings of ICAPP 2015, Paper 15555, Nice, 2015.

[27] J. D. Rhodes *et al*. CASMO5 Development and Applications, Proceedings of PHYSOR2006, Vancouver, 2006.

[28] T. Bahadir, S.-Ö. Lindhal. Studsvik's Next Generation Nodal Codes SIMULATE-5, Proceedings of Advances in Nuclear Fuel Management (ANFM) IV, Hilton Head Island, 2009.

[29] R. J. Fetterman. AP1000 Core Design with 50% MOX Loading, Annals of Nuclear Energy, 36, 2009.

[30] M. J. Driscoll *et al*. The Linear Reactivity Model for Nuclear Fuel Management. American Nuclear Society, ISBN 0-89448-035-9, 1990.

[31] M. Schlieck *et al*. Optimized Gadolinia Concepts for Advanced in-core Fuel Management in PWRs, Nuclear Engineering and Design, 205, 191-208, 2000.

[32] J-C Kim *et al*. Nuclear Design Feasibility of the Soluble Boron Free PWR core. Journal of the Korean Nuclear Society, 30, 4, 342, 1998.

[33] ECHA. Recommendation of the European Chemicals Agency of 1 July 2015 for the inclusion of substances in Annex XIV to REACH, ECHA publication, 2015.

[34] E. D. Kitcher and S. S. Chirayath. Neutronics and Thermal Hydraulics Analysis of a Small Modular Reactor, Annals of Nuclear Energy, 97, 232, 2016.

[35] K. E. Ottinger and G. I. Maldonado. SMR Fuel Cycle Optimization Using LWROpt, Journal of Nuclear Engineering and Radiation Science, 2016.

[36] D. Janin *et al*. PWR In-core Fuel Management Optimization of Non-Standard Cycles. Proceedings of Topfuel 2015, Zurich, 2015.

[37] F. N. von Hippel. Plutonium and Reprocessing of Spent Nuclear Fuel. Science, 293, 5539, 2397-2398, 2001.

[38] IAEA. Safety Margins of Operating Reactors: Analysis of Uncertainties and Implications for Decision Making. IAEA TECDOC-1332, Vienna, 2003.

[39] V. Vallet *et al*. Introduction of Thorium-based Fuels in High Conversion PWR, Nuclear Technology, 182, 187-206, 2013.

[40] Y. Ronen. High Converting Water Reactors. CRC Press, 1990.

[41] P. Le Coz et al. Sodium-cooled Fast Reactors: the ASTRID plant project. Proceedings of ICAPP 2011, Paper 11249, Nice, 2011.

[42] P. Boulinier. Les surgénérateurs. Eyrolles, ISBN 2727201095, 1986.

[43] F. Carré, J.M. Delbecq. Overview on the French Nuclear Fuel Cycle Strategy and Transition Scenario Studies. Proceedings of Global2009, Paris, 2009.

[44] M. Kazimi *et al*. The Future of the Nuclear Fuel Cycle, an Interdisciplinary MIT Study. ISBN 978-0-9828008-4-3, 2011.

[45] B. Barré *et al*. Nuclear Reactors Systems, a Technical Historical and Dynamic Approach. ISBN 978-2-7598-0669-0, 2016.

[46] G. Mathonnière *et al*. LWR-SFR synergy for a sustainable nuclear fleet: economic relevance and impact on the competitiveness of SFRs. Proceedings of FR17, Ekaterinburg, Russian Federation, 2017.

[47] OECD/NEA. Plutonium Management in the Medium Term, ISBN 92-64-02151-5, NEA4451, 2003.

[48] D. Greneche, M. Lecomte. Optimisation de l'utilisation des ressources dans les réacteurs à eau légère, RGN, Septembre-Octobre, 2010.

[49] F.C.M. Verhagen *et al*. Recent Developments of the Rosa PWR Code and a Special Loading Pattern Design Application. Proceedings of ANFM 2015, Hilton Head Island, SC, USA, 2015.

[50] OECD/NEA, IAEA. Uranium 2014: Resources, Production and Demand. NEA No. 7209, 2014.

[51] OECD/NEA. The Economics of the Back End of the Nuclear Fuel Cycle, 2013.

[52] L. Patarin *et al*. Le Cycle du Combustible Nucléaire, INSTN-EDP Sciences. ISBN 2-86883-620-8, 2002.

[53] J-B Thomas. Nuclear Power Plants Types and the Management of Plutonium and Minor Actinides in Search of Fuel Cycle Flexibility, C.R. Applied Physics 3, 783, 2002.

[54] D. Haas, D. J. Hamilton. Fuel Cycle Strategies and Plutonium Management in Europe, Progress in Nuclear Energy, 49, 574-582, 2007.

[55] IAEA. Advanced Light and Heavy Water Reactors for Improved Fuel Utilization. IAEA TECDOC-344, Vienna, 1985.

[56] S. Cathalau. Qualification des Propriétés Neutroniques des Réacteurs Sous-Modérés à l'Eau Légère, PhD Thesis CEA / Paris-Sud Orsay University, 1988

[57] J. P. Chauvin. Réacteurs à eau sous-modérés : contribution aux études et à la qualification des outils de calcul neutronique. PhD Thesis CEA / Paris-Sud Orsay University, 1987.

[58] J. P. Millot. Considerations sur les Réacteurs PWR Sous-Modérés. RGN actualités, 4, 405, 1982.

[59] D. Hittner et al. Preliminary Results of the Feasibility on the Convertible Spectral Shift Reactor Concept. Nuclear Technology, 80, 1988.

[60] J. Bergeron *et al*. The French Neutronic Program Addressing The Requirements of Future Pressurized Water Reactors. Nuclear Technology, 80, 1988.

[61] M. C. Edlund. High Conversion Ratio Plutonium Recycle in Pressurized Water Reactors. Annals of Nuclear Energy, 2, 80, 1975.

[62] M. C. Edlund. Physics of Uranium-Plutonium Fuel Cycles in Pressurized Water Reactors. Transactions of the American Nuclear Society, 24, 508, 1976.

[63] R. H. Brogli. Research and Development Efforts for the Light Water High Conversion Reactor. Nuclear Technology, 80, 1988.

[64] H. Märkl *et al*. KWU's High Conversion Reactor Concept, an Economical Evolution of Modern Pressurized Water Reactor toward Improved Uranium Utilization. Nuclear Technology, 80, 1988.

[65] K. Penndorf. Constraints on the Plutonium Recovery Achievable in Homogeneous Pressurized Water Reactors. Nuclear Technology, 80, 2, 1988.

[66] H.-D. Berger. Neutronenphysikalische Untersuchungen zu einem fortgeschrittenen Druckwasserreaktor mit hoher Konversion, PhD Thesis GKSS 85/E/15, Geesthacht, 1985.

[67] Y. Ronon and S. Carmona. Analysis of High Conversion Pressure Tubes Reactor, Nuclear Technology, 73, 210, 1986.

[68] T. Okubo *et al*. Early Introduction Core Design for Advanced LWR Concept of FLWR to Recycle Pu or TRU, Proceedings of Global 2009, Paris, 2009.

[69] T. Iwamura *et al*. Concept of Innovative Water Reactor for Flexible Fuel Cycle (FLWR), Nuclear Engineering and Design, 236, 2006.

[70] Y. Fukaya *et al*. Investigation on Spent Fuel Characteristics of Reduced-Moderation Water Reactor (RMWR), Nuclear Engineering and Design, 238, 2007.

[71] E. A. Hoffman et al. Preliminary Core Design Studies for the Advanced Burner Reactor over a Wide Range of Conversion Ratios, ANL-AFCI-177 Report, 2006.

[72] T. Downar *et al*. Technical Evaluation of the Hitachi Resource-Renewable BWR (RBWR) Design Concept, EPRI Report 1025086, 2012.

[73] R. Rachamin. Conceptual Design of a Pressure Tube Light Water Reactor with Variable Moderator Control, PhD Thesis Ben-Gurion University, 2015.

[74] H. Golfier *et al*. Advanced High Conversion PWR: Preliminary Analysis, Proceedings of ICAPP2007, Nice, 2007.

[75] F. Damian *et al*. Improvement of the Conversion Ratio in PWR, Proceedings of PHYSOR2010, Pittsburgh, 2010.

[76] D. Baldova. Feasibility Study on High-Conversion Th-U233 Fuel Cycle for Current Generation of PWRs, PhD Thesis Prague Technical University University, 2014.

[77] J. G. B. Saccheri *et al*. A Tight Lattice, Epithermal Core Design for the Integral PWR, Proceedings of ICAPP 2004, Pittsburgh, 2004.

[78] E. Greenspan. Advanced Burner Reactor with Breed-and-Burn Thorium Blankets for Improved Economics an Resource Utilization, Proceedings of the 9th International Symposium on Capture gamma-ray spectroscopy and related topics, Budapest, 1996.

[79] R. B. Fireston *et al*. The 8th edition of the Table of Isotopes. NEUP Project 12-3486, 2015.

[80] T. Gray, http://www.periodictable.com/, Wolfram Research Inc., 2016.

[81] F. Damian and R. Lenan. Réacteur à Eau à Haut Facteur de Conversion, RGN, 5, 2010.

[82] P. Barbrault. A Plutonium-Fueled High-Moderated Pressurized Water Reactor for the Next Century, Nuclear Engineering and Design, 122, 1996.

[83] S. Douce *et al*. Improvement of the Conversion Ratio in PWR – Core Performances and Preliminary Study of a Reactivity Initiated Accident, Proceedings of ICAPP 2011, Nice, 2011.

[84] J. M. Do *et al*. Use of Meta Heuristics for Design of Fuel Loading Pattern in light water Reactors comprising some radial and axial Heterogeneities. Proceedings of NIDISC 2011, Anchorage, 2011.

[85] I. E. Idelchik. Handbook of Hydraulic Resistance, Jaico Publishing House, ISBN 978-8179921180, 2005.

[86] N. E. Todreas and M. S. Kazimi. Nuclear Systens, Thermal Hydraulic Fundamentals Volume 1, CRC Press, ISBN 978 1 4398 0887 0, 2012.

[87] J. R. Lamarsh. Introduction to Nuclear Reactor Theory. ISBN 0-894480405, 2002.

[88] D. T. Philipps *et al.* Foundations of Optimizations. ISBN 0 13 330332 2, 1979.

[89] D. A. Goldberg. Genetic Algorithms in Search, Optimization and Machine Learning. ISBN 0-201157675, 1989.

[90] M. D. Mckay. A Comparison of Three Methods for Selecting Values of Input Variables in the Analysis of Output From a Computer Code. Technometrics, 21, 2, 239, 1979.

[91] F. Gaudier. URANIE: the CEA/DEN uncertainty and sensitivity platform, Procedia – Social and Behavioral Sciences, 2, 6, 7660, 2010.

[92] J. P. C. Kleijnen. Sensitivity analysis and related analyses: A review of some statistical techniques. Journal of Statistical Computation and Simulation, vol. 57, pp. 111–142, 1997.

[93] M. D. Morris. Factorial Sampling Plans for Preliminary Computational Experiments, Technometrics, 33, 2, 161, 1991.

[94] A. Saltelli *et al*. Sensitivity analysis, Wiley, ISBN 978-0-470-74382-9, 2008.

[95] K. Ammar. Conception Multi-physique et Multi-objectifs des coeurs de RNR-Na Hétérogènes : Développement d'une Méthode d'Optimisation sous Incertitudes, Université Paris Sud, 2014.

[96] I. M. Sobol'. Global Sensitivity Indices for Nonlinear Mathematical Models and their Monte Carlo Estimates, Mathematics and Computers in Simulation, 55, 271, 2001.

[97] W. Hoeffding. A Class of Statistics with Asymptotically Normal Distribution, The Annals of Mathematical Statistics, 19, 3, 239, 1948.

[98] T. Homma and A. Saltelli. Importance Measures in Global Sensitivity Analysis of Nonlinear models. Reliability Engineering & System Safety, 52, 1, 1, 1996.

[99] W. S. McCulloch, W. Pitts. A Logical Calculus of the Ideas Immanent in Nervous Activity, Bulletin of Mathematical Biophysics, 5, 1943.

[100] G. Dreyfus *et al*. Réseaux de Neurones Méthodologie et Applications, Eyrolles, ISBN 2-212-11019-7, 2002.

[101] K. Hornik *et al*. Multilayer Feedforward Networks are Universal Approximators, Neural networks, 2, 5, 359, 1989.

[102] D. E. Rumelhart *et al.* Learning Representations by Back-propagating Errors, Nature, 323, 6088, 533, 1986.

[103] R. Brun and F. Rademakers. ROOT, an object-oriented data analysis framework. Nucl. Instrum. Methods Section A, 389, 81, 1997.

[104] D. G. Krige. A Statistical Approach to some Mine Valuation and Allied Problems on the Witwatersrand, Master Thesis, 1951.

[105] G. Matheron. La Théorie des Variables Régionalisées et ses applications, les Cahier du Centre de Morphologie Mathématique de Fontaibleau, 5, 1970.

[106] F. Bachoc *et al*. Calibration and improved prediction of computer models by universal Kriging. Nuclear Science and Engineering, 176, 1, 81, 2014.

[107] O. de Weck and I. Y. Kim. Adaptive Weighted Sum Method for Bi-objective Optimization, Proceedings of AIAA Structures Structural Dynamics & Material Conference, Palm Springs, 2004.

[108] Y. Tenne and C.-K. Goh. Computational Intelligence in Optimization Applications and Implementations. Springer, ISBN 978-3-642-12774-8, 2010.

[109] Y. Collette and P. Siarry. Three new metrics to measure the convergence of metaheuristics towards the Pareto frontier and the aesthetic of a set of solutions in bi-objective optimization, Computers & Operations Research, 32, 773, 2005.

[110] J. Nedler and R. Mead. A Simplex Method for Function Minimization. The Computer Journal, 7, 4, 308, 1965.

[111] J. Kennedy and R. Eberhart. Particle Swarm Optimization. Proceedings of IEEE Conference on Neural Networks, Piscataway, 1995.

[112] J. Bussac, P. Reuss. Traité de Neutronique. Herman, ISBN 2-705660119, 1985.

[113] P. Reuss. Neutron Physics. EDP Sciences, ISBN 978-2759800414, 2008.

[114] A. Santamarina et al. The recommended JEFF3.1.1 file and CEA2005V4 library for accurate neutronics calculations. ISBN 978-92-64-99074-6, NEA No. 6807, Paris, 2009.

[115] E. Brun *et al*. TRIPOLI-4®, CEA, EDF and AREVA reference Monte Carlo code, Annals of Nuclear Energy, 82, 151, 2015.

[116] M. Coste-Delclaux. GALILEE: A Nuclear Data Processing System for Transport, Depletion and Shielding Codes, Proceedings of PHYSOR2008, Interlaken, 2008.

[117] R. Sanchez *et al*. APOLLO2 Year 2010, Nuclear Engineering and Technology, 43, 5, 2010.

[118] N. Hfaiedh and A. Santamarina. Determination of the Optimized SHEM mesh for Neutron Transport Calculations, Proceedings of Mathematics and Computation, Supercomputing, Reactor Physics and Nuclear and Biological Applications 2005 conference, Avignon, 2005.

[119] M. Coste-Delclaux and S. Mengelle. New Resonant Mixture Self-Shielding in the code APOLLO2, Proceedings of PHYSOR2004,Chicago, 2004.

[120] S. Santandrea *et al*. A linear surface characteristics scheme for neutron transport in unstructured meshes, Nuclear Science and Engineering, 160, 22, 2008.

[121] J-F. Vidal et al. Analysis of the FLUOLE experiment for the APOLLO2 validation of PWR core reflectors, PHYSOR 2008, Interlaken, 2008.

[122] T. Bahadir. Improved PWR Radial Reflector Modeling with SIMULATE5, Proceedings of Advances in Nuclear Fuel Management (ANFM) V, Hilton Head Island, 2015.

[123] J. Ragusa *et al*. Application of duality principles to reflector homogenization. Nuclear Science and Engineering, 157, 2007.

[124] J.J. Lautard *et al*. CRONOS, A Modular Computational System for Neutronic Core Calculations, IAEA Specialists Meeting, France (1990).

[125] B. Roque *et al*. CRONOS, APOLLO3® Roadmap for a new generation of simulation tools devoted to the neutronic core calculation of the ASTRID prototype, FR13, Paris, 2013.

[126] J.Y. Moller and J.J. Lautard. MINARET a Deterministic Neutron Transport Solver for Nuclear Core Calculations, Proceedings of M&C 2011, Rio de Janeiro, 2011.

[127] A. Tsilanizara *et al*. DARWIN: an Evolution Code System for a Large Range of Applications, ICRS-9, Tsukaba, 1999.

[128] D. Janin *et al*. HCSMR Fuel Assembly Computations with APOLLO2 and TRIPOLI-4® Codes. Proceedings of ICAPP2016, San Francisco, 2016.

[129] M. B. Chadwick *et al*. ENDF/B-VII.1 Nuclear Data for Science and Technology: Cross Sections, Covariances, Fission Product Wields and Decay Data. Nuclear Data Sheets, 112(12):2887-2996, 2011.

[130] D. Janin *et al*. High Conversion Small Modular Reactor (HCMSR): Core Simulations with CRONOS2 and TRIPOLI-4®. Proceedings of IYNC2016, Energy Procedia, Hangzhou, 2016.

[131] C. Chauliac *et al*. NURESIM – A European simulation platform for nuclear reactor safety: Multi-scale and multi-physics calculations, sensitivity and uncertainty analysis. Nuclear Engineering and Design, 241, 3416, 2011.

[132] D. Janin *et al*. HCSMR Fuel Assembly Optimization with APOLLO2 and URANIE Codes. Proceedings of PHYSOR2016, Sun Valley, 2016.

[133] F. Bachoc. Estimation Paramétrique de la Fonction de Covariance dans le Modèle de Krigeage par Processus Gaussiens. Application à la Quantification des Incertitudes en Simulation Numérique. PhD, Paris-Diderot-Paris VII University, 2013.

[134] X-Y Zhang *et al*. Sobol Sensitivity Analysis: A Tool to Guide the Development and Evaluation of Systems Pharmacology Models. CPT Pharmacometrics Syst. Pharmacol, 4, 69-79, 2015.

[135] M-S. Yahya *et al*. Neutronic Feasibility of a Soluble Boron-Free PWR Core Design with the BigT Burnable Absorbers. Proceedings of ICAPP2016, San Francisco, 2016.

[136] E. Saji et al. Control Rod Worth in High Conversion PWR. Journal of Nuclear Science and Technology, 23, 8, 745, 1986.

[137] IAEA. Control Assembly Materials for Water Reactors: Experience, Performance and Perspectives. IAEA TECDOC-1132, Vienna, 1998.

[138] OECD/NEA. Plutonium Fuel – An Assessment, Report by an Expert Group. OECD, 1989.

Annexes

ANNEXES

ANNEX A : OVERVIEW OF SMR DESIGNS IN DEVELOPMENT

Acronym	Full Name	Design Organization	Country of Origin	Reactor Type	Coolant & Moderator	Thermal / Electric Power (MW)	Mode of deployment	Design Status
SMR-160	SMR-160	Holtec International	USA	Integral PWR	Light Water	525 / 160	Land-based	Conceptual
mPower	mPower	Babcock & Wilcox	USA	Integral PWR	Light Water	530 / 180	Land-based, Twin-unit plant	Basic
NuScale	NuScale Power Modular and Scalable Reactor	NuScale Power Inc.	USA	Integral PWR	Light Water	160 / 45	Land-based, 2x6 modules plant	Basic
ACP100	ACP100	NPIC/CNNC	China	Integral PWR	Light Water	310 / 100	Land-based	Detailed
CAREM-25	CAREM-25	CNEA	Argentina	Integral PWR	Light Water	100 / 27	Prototype	Under Construction
SMART	System-integrated Modular Advanced Reactor	KAERI	Republic of Korea	Integral PWR	Light Water	330 / 100	Land-based	Detailed
FlexBlue	FlexBlue	DCNS	France	Loop PWR	Light Water	530 / 160	Under-water	Conceptual
W-SMR	Westinghouse SMR	Westinghouse	USA	Integral PWR	Light Water	800 / 225	Land-based	Conceptual
RITM-200	RITM-200	OKBM Afrikantov	Russia	PWR	Light Water	175 / 50	Twin-unit ice-breaker	Under construction
ABV	ABV	OKBM Afrikantov	Russia	PWR	Light Water	38 / 8.5	Twin-unit barge-mounted or land-based	Detailed
NP-300	NP-300	Areva-TA	France	PWR	Light Water	1000 / 300	Land-based	Conceptual

Acronym	Full Name	Design Organization	Country of Origin	Reactor Type	Coolant & Moderator	Thermal / Electric Power (MW)	Mode of deployment	Design Status
IMR	Integrated Modular Reactor	Mitsubishi Heavy Industries	Japan	Integral PWR	Light Water	1000 / 350	Land-based	Conceptual
DMS	Double MS: Modular Simplified and Medium Small Reactor	Hitachi-GE Nuclear Energy	Japan	BWR	Light Water	840 / 300	Land-based	Basic
IRIS	International Reactor Innovative & Secure	International Consortium	International	Integral PWR	Light Water	1000 / 335	Land-based	Basic
FBNR	Fixed Bed Nuclear Reactor	FURGS	Brazil	PWR	Light Water	218 / 72	Land-based	Conceptual
AHWR300-LEU	Advanced Heavy Water Reactor	BARC	India	Pressure Tube HWR	Light Water & Heavy Water	920 / 304	Land-based	Basic
KLT-40S	KLT-40S	OKBM Afrikantov	Russia	PWR	Light Water	150 / 35	Land-based	Under construction
VBER-300	VBER-300	OKBM Afrikantov	Russia	PWR	Light Water	917 / 325	Land-based or barge-mounted	Detailed
VVER-300	VVER-300	OKB Gidropress	Russia	VVER	Light Water	850 / 300	Land-based	Under construction
VK-300	VK-300	RDIPE	Russia	Integral BWR	Light Water	750 / 250	Land-based	Detailed
UNITHERM	UNITHERM	RDIPE	Russia	Integral PWR	Light Water	30 / 6.6	Land-based or barge-mounted	Conceptual
RUTA-70	RUTA-70	RDIPE and IPPE	Russia	Pool-type	Light Water	70 / N/A	Land-based	Conceptual
SHELF	SHELF	RDIPE	Russia	PWR	Light Water	28 / 6	Under-water	Conceptual
ELENA	ELENA	Kurchatov Institute	Russia	PWR	Light Water	3.3 / 0.07	Land-based	Conceptual

Acronym	Full Name	Design Organization	Country of Origin	Reactor Type	Coolant & Moderator	Thermal / Electric Power (MW)	Mode of deployment	Design Status
HTR-PM	HTR-PM	Tsinghua University	China	Pebble Bed HTR	Helium / Graphite	2 x 250 / 210	Land-based	Under construction
GT-HTR300	Gas Turbine High Temperature Reactor 300 MWe	JAEA	Japan	Prismatic HTR	Helium / Graphite	< 600 / 100-300	Land-based	Basic
GT-MHR	Gas Turbine Modular Helium Reactor	OKBM Afrikantov	Russia	Prismatic HTR	Helium/ Graphite	600 / 285	Land-based	Conceptual
MHR-T	MHR-T	OKBM Afrikantov	Russia	Prismatic HTR	Helium/ Graphite	4x600 / 4x206	Land-based	Conceptual
MHR-100	MHR-100	OKBM Afrikantov	Russia	Prismatic HTR	Helium/ Graphite	215 / 25-87	Land-based	Conceptual
PBMR-400	Pebble Bed Modular Reactor	PBMR SOC Ltd	South Africa	Pebble Bed HTR	Helium/ Graphite	400 / 165	Land-based	Detailed
HTRM-100	Hight Temperature Modular Reactor	STL	South Africa	Pebble Bed HTR	Helium/ Graphite	100 / 35 or 400 / 140	Land-based	Conceptual
SC-HTGR (Antares)	Steam Cycle High Temperature Gas-Cooled Reactor	AREVA	USA	Prismatic HTR	Helium/ Graphite	625 / 272	Land-based	Conceptual
Xe-100	Xe-100	X-energy	USA	Pebble Bed HTR	Helium/ Graphite	100 / 35	Land-based	Conceptual
BREST	BREST	RDIPE	Russia	Liquid metal cooled FR	Lead / -	700 / 300	Land-based	Basic
SVBR-100	SVBR-100	AKME-engineering	Russia	Liquid metal cooled FR	Lead-Bismuth / -	280 / 101	Land-based	Basic
EM^2	EM^2	General Atomics	USA	Gas-cooled FR	Helium / -	500 / 240	Land-based	Conceptual

Acronym	Full Name	Design Organization	Country of Origin	Reactor Type	Coolant & Moderator	Thermal / Electric Power (MW)	Mode of deployment	Design Status
CNP-300	CNP-300	CNNC	China	PWR	Light Water	999 / 325	Land-based	In operation
PHWR-220	PHWR-220	NPCIL	India	Pressure Tube HWR	Heavy Water	755 / 236	Land-based	In operation
CEFR	China Experimental Fast Reactor	CNEIC	China	Liquid metal cooled FR	Sodium / -	65 / 20	Land-based	In operation
PFBR-500	PFBR-500	IGCAR	India	Liquid metal cooled FR	Sodium / -	1250 / 500	Land-based	Under construction
4S	Super-Safe, Small & Simple	Toshiba	Japan	Liquid metal cooled FR	Sodium / -	30 / 10	Land-based	Basic
PRISM	PRISM	GE-Hitachi	USA	Liquid metal cooled FR	Sodium / -	840 / 311	Land-based	Detailed
G4M	Gen4 Module	Gen4 Energy Inc.	USA	Liquid metal cooled FR	Lead-Bismuth / -	70 / 25	Land-based	Conceptual
IMSR	Integral Molten Salt reactor	Terrestrial Energy	Canada	Molten Salt Reactor	Fluoride Salts / Graphite	80 / 33	Land-based	Conceptual
MBIR	Multipurpose fast-neutron research reactor	NIKIET	Russia	Liquid metal cooled FR	Sodium / -	150 / 60	Land-based	Detailed
Modular SSR	Modular SSR	Moltex Energy	UK	Molten Salt Reactor	Fluoride Salts / -	300 / 150	Land-based	Conceptual

Acronym	Full Name	Design Organization	Country of Origin	Reactor Type	Coolant & Moderator	Thermal / Electric Power (MW)	Mode of deployment	Design Status
ThorCon	ThorCon	Martingale Inc.	USA	Molten Salt Reactor	Fluoride Salts / Graphite	500 / 250	Land-based or barge-mounted	Conceptual
CAP150	CAP150	SNERDI	China	Integral PWR	Light Water	450 / 150	Land-based or barge-mounted	Conceptual
ACPR100	ACPR100	CGN	China	Integral PWR	Light Water	450 / 140	Land-based	Conceptual
ACPR50S	ACPR50S	CGN	China	Integral PWR	Light Water	200 / 60	Land-based or barge-mounted	Conceptual

Table A. 1: Overview of SMR Designs in development

ANNEX B : OVERVIEW OF SELECTED iPWR SMR DESIGNS

Acronym	Full Name	Design Organization	Country of Origin	Reactor Type	Coolant & Moderator	Neutron Spectrum	Thermal Power (MW)	Electric Power (MW)
CAREM-25	CAREM-25	CNEA	Argentina	Integral PWR	Light Water	Thermal	100	27
ACP100	ACP100	NPIC/CNNC	China	Integral PWR	Light Water	Thermal	310	100
FlexBlue	FlexBlue	DCNS	France	PWR	Light Water	Thermal	530	160
SMART	System-integrated Modular Advanced Reactor	KAERI	Republic of Korea	Integral PWR	Light Water	Thermal	330	100
ABV	ABV	OKBM Afrikantov	Russia	PWR	Light Water	Thermal	38	8.5
RITM-200	RITM-200	OKBM Afrikantov	Russia	PWR	Light Water	Thermal	175	50
mPower	mPower	Babcock & Wilcox	USA	Integral PWR	Light Water	Thermal	530	180
NuScale	NuScale Power Modular and Scalable Reactor	NuScale Power Inc.	USA	Integral PWR	Light Water	Thermal	160	45
Westinghouse SMR	Westinghouse SMR	Westinghouse	USA	Integral PWR	Light Water	Thermal	800	225

Table B. 1: Selected iPWR SMR designs main characteristics

Acronym	Cycle Management	Cycle length (Full power months)	Fissile Material	Fuel Assembly (FA) type	Active length (cm)	FA Number	CRDM Number	Burnable Absorber	FA Target Burnup (GWd/tHM)
CAREM-25	1/2	11	UO2, 3.10 %	Hexagonal lattice, 108 FRs	140	61	25	Gd	24
ACP100	N/A[1]	24	UO2, 2.3 - 4.20 %	Square lattice 17 x 17	215	57	25	Yes	< 45
FlexBlue	One-through	38	UO2, 4.95 %	Square lattice 17 x 17	215	77	77	Gd	27
SMART	1/2	36	UO2 < 5.0 %	Square lattice 17 x 17	200	57	25	Gd	36
ABV	One-through	> 120	UO2, 18.7 %	Hexagonal lattice, 75 FRs	90	121	N/A	Gd	49
RITM-200	One-through	84	UO2, < 20 %	Hexagonal lattice	165	199	N/A	Gd	51
mPower	One-through	48	UO2, 4.95 %	Square lattice 17 x 17	240	69	69	Gd	37
NuScale	One-through	24	UO2, 4.95 %	Square lattice 17 x 17	183	37	16	Gd	> 30
Westinghouse SMR	1/2.5	24	UO2, 4.95 %	Square lattice 17 x 17	240	89	37	Yes	> 62

Table B. 2: Selected iPWR SMR designs fuel characteristics

[1] Non-available

Acronym	Reactivity Control	Pressure (bar)	T° Inlet (°C)	T° Outlet (°C)	Flow (t.s-1)	Primary Coolant Circulation	RPV Diameter x Height (m)	Lifetime (years)	Mode of deployment
CAREM-25	Control Rods No soluble Boron	123	284	326	0.41	Natural	3.43 x 11.0	60	Prototype
ACP100	Control Rods Soluble Boron	150	282	323	1.30	Forced	3.19 x 10.0	60	Land-based
FlexBlue	Control Rods No soluble Boron	155	288	318	3.16	Forced	3.7 x 3.33	60	Under-water
SMART	Control Rods Soluble Boron	150	296	323	2.09	Forced	6.50 x 18.5	60	Land-based
ABV	Control Rods Soluble Boron	157	248	327	N/A	Forced	> 2.2 x 4.2	40	Twin-unit barge-mounted or land-based
RITM-200	Control Rods No soluble Boron	> 127	280	312	0.90	Forced	2.14 x 4.48	40	Twin-unit ice-breaker
mPower	Control Rods No soluble Boron	141	297	320	4.17	Forced	3.96 x 25.3	60	Land-based, Twin-unit plant
NuScale	Control Rods Soluble Boron	128	248	289	N/A	Natural	2.90 x 17.4	60	Land-based, 2x6 modules plant
Westinghouse SMR	Control Rods Soluble Boron	155	294	324	4.50	Forced	3.5 x 24.7	60	Land-based

Table B. 3: Selected iPWR SMR designs core and primary circuit operating point characteristics

Acronym	Safety Shut-down	Residual heat removal	Emergency Core Cooling System	Containment
CAREM-25	CRDM; passive boron injection	Passive condenser approach RHRS.	Passive pressurized tank for low pressure injection. Rupture disks separating the RPV and accumulators.	Reinforced concrete with stainless steel liner hosting a suppression pool.
ACP100	CRDM	Passive condenser approach RHRS.	2 coolant storage tanks, 2 injection tanks, an in-containment water storage tank and associated injection lines.	Concrete containment with steel plant. Passive heat removal system using two condensers.
FlexBlue	CRDM	2 methods: heat exchanger immersed in water tank or an emergency condenser immersed in seawater.	Passive injection system using direct vessel injection, core make-up tanks, accumulator and safety tanks.	Containment walls in direct contact with ultimate heat sink (UHS).
SMART	CRDM; boron injection active system	Passive removal through heat exchanger submerged in water pool via SG.	4 make-up tanks and 4 injection tanks. Boron safety injection system using high head pump.	Cylindrical, diameter of 44 m. Design pressure of 3.4 bars. Passive cooling via spray.
RITM-200	CRDM	One decay heat removal system (DHRS) per SG connected to 3 heat sinks: the DHRS tank, a water storage tank and an air cooled heat exchanger.	Based on active and passive systems. Hydraulic accumulators connected to SG are actuated passively. Pumps are supplying water to SG. Natural circulation main path.	Passively pressure reduction via use of self-actuated devices at increased pressure in containment.
ABV	CRDM	Combined-type emergency cooldown system (ECDS) using two independent air-cooled heat exchangers channels connected to SG.	ECCS is based on active and passive systems/ It comprises high-head pumps (active) and hydro-accumulators housing a compressed gas (passive).	Passive containment cooling system. Reactor caisson water flooding system available.
mPower	CRDM	Passive removal through auxiliary steam condenser.	Automatic depressurization valves, intermediate pressure injection tanks via accumulators and in-containment refueling water storage tank.	Steel containment vessel passively cooled using an integral water tank.
NuScale	CDRM	Passive removal through heat exchanger submerged in water pool via SG.	Two independent reactor vent valves and two reactor recirculation valves (RRV). Safety injection via RRV.	Submerged metal containment maintained at low pressure during normal operation.
Westinghouse SMR	CRDM; passive boron injection	Passive removal through heat exchanger submerged in water pool via SG.	3 diverse methods: natural circulation and atmosphere steam release; passively cooled condenser; direct vessel injection.	Carbon steel containment vessel submerged in a water pool filled up via two UHS tanks.

Table B. 4: Selected iPWR SMR designs core safety features

ANNEX C : SMR600

C. 1 CHARACTERISTICS

The SMR600 design was developed for benchmark purposes. The objective was to set a reference of an iPWR to compare the performances of the HCSMR design. The SMR600 characteristics are mostly based on the mPower and Westinghouse SMR designs (cf Annex B). The fuel is standard 17x17 with reduced height UO_2 fuel enriched at 4.95 % ^{235}U. The fuel assembly characteristics are presented in Table C. 1. Input data are given in cold conditions (293 K) with highlighted exceptions.

Parameter	Unit	Values
Fuel rod (FR) pitch	cm	1.26
Number of FR	-	265
Number of Control rods (CR)	-	24
Fuel pellet diameter	cm	0.82
Cladding thickness	mm	0.57
CR guide tube inner diameter	cm	0.57
CR guide tube outer diameter	cm	0.62
Cell moderation ratio[18]	-	1.68
Active height	cm	220
Inter FA water gap	mm	0.84

Table C. 1: SMR600 fuel assembly characteristics

The core is made of 69 fuel assemblies. Two types of fuel management are studied and accordingly two loading patterns are used. First a batch fuel management core was designed: all full assemblies are only used for one irradiation cycle (SMR600.A). A second loading patterns using a "1/2" fuel management approach (SMR600.B) was designed and is introduced in Figure C. **1**.

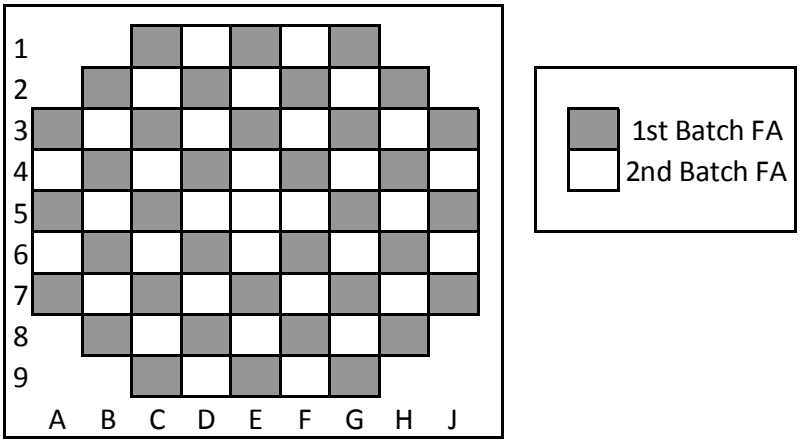

Figure C. 1 : SMR600 "1/2" fuel management core loading pattern

The batch fuel management is using UO_2 fuel enriched at 4.95 % 235U with 24 Gd fuel rods per fuel assembly as shown in Figure C. 2. The "1/2" fuel management fuel has 16 Gd fuel rods per fuel assembly as shown in Figure C. 2. Standard PWR reflectors both axially and radially are considered. The core characteristics are introduced in Table C. 2.

[18] in hot conditions (141 bars, 300°C)

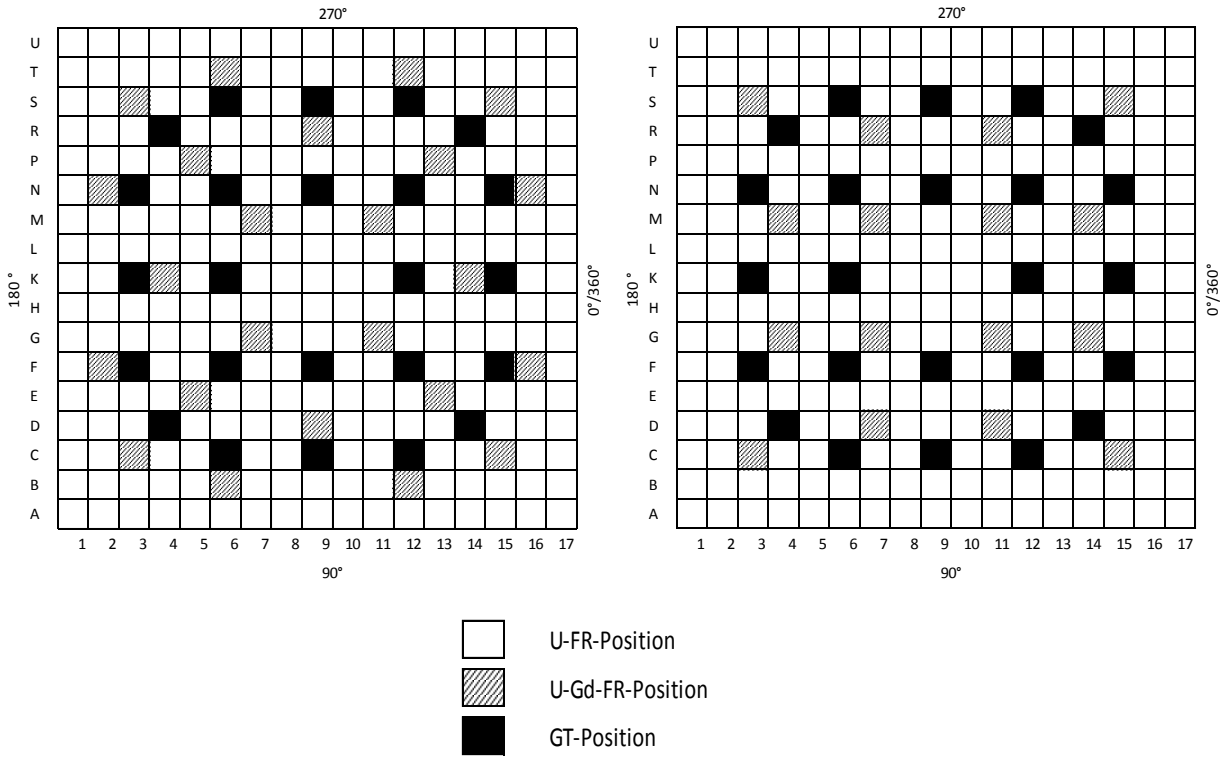

Figure C. 2 : SMR600 (a) 24-Gd FR and (b) 16-Gd FR fuel assembly top view

Parameter	Unit	Value
Power	MW	600
Number of Fuel Assembly	-	69
Core moderation ratio[19]	-	1.99
Active height	cm	220
Core width	cm	194
Average heat linear power	W/cm	149
Primary pressure	bar	141.3
Inlet temperature	°C	291.0
Core flow	t.s-1	4.17
Core flow bypass	%	6

Table C. 2: SMR600 Core Main Characteristics

The SMR600 design was modeled using the CASMO5 [27] and SIMULATE5 [28] codes based on industrial standard neutron-physic methods and recommended simulation options by Studsvik. CASMO5 performed the lattice computation using the nuclear data library ENDF/B-VII.0 with 586 energy groups' spectra to generate energy condensed cross sections. The eigenvalue and flux distribution are computed using 2D-characteristics based transport calculation with 19 energy groups. For Gd fuel rods, ten radial rings are used for depletion. At the core level SIMULATE5 solves the multi-group diffusion equations in 3D with both radial and axial discretization.

[19] in hot conditions (141 bars, 300°C)

C. 2 PERFORMANCES

The main performances of both SMR600 designs are introduced in Table C. 3.

Parameter	Unit	SMR600 Batch	SMR600 1/2 Fuel Management
Cycle Length	EFPD	924	633
Conversion Factor	-	0.63	0.48
Core Average Burnup BOC	MWd/kgHM	0	9
Core Average Burnup EOC	MWd/kgHM	29	30
FA Average Discharge Burnup	MWd/kgHM	29	41
FA Maximum Average Burnup	MWd/kgHM	43	48

Table C. 3: SMR600 Cores Performances

As illustration of the burnup distribution the FA average values are plotted in Figure C. 3.

	J	H	G	F	E	D	C	B	A
1			0.0	22.8	0.0	25.8	0.0		
2		0.0	31.5	0.0	22.8	0.0	33.7	0.0	
3	0.0	33.6	0.0	9.4	0.0	8.0	0.0	31.5	0.0
4	25.8	0.0	8.0	0.0	12.9	0.0	9.4	0.0	22.8
5	0.0	22.8	0.0	12.9	7.8	12.9	0.0	22.8	0.0
6	22.8	0.0	9.4	0.0	12.9	0.0	8.0	0.0	25.8
7	0.0	31.6	0.0	8.0	0.0	9.4	0.0	33.7	0.0
8		0.0	33.7	0.0	22.8	0.0	31.6	0.0	
9			0.0	25.8	0.0	22.8	0.0		

	J	H	G	F	E	D	C	B	A
1			8.0	33.6	12.9	36.2	7.8		
2		9.4	46.1	22.8	44.1	22.7	47.9	9.4	
3	7.8	47.9	25.8	38.5	31.5	37.4	25.8	46.1	8.0
4	36.1	22.7	37.4	33.6	44.8	33.7	38.6	22.8	33.6
5	12.9	44.1	31.5	44.8	40.8	44.9	31.5	44.1	12.9
6	33.6	22.8	38.5	33.6	44.9	33.7	37.5	22.8	36.2
7	8.0	46.1	25.8	37.4	31.5	38.6	25.8	47.9	7.8
8		9.4	47.9	22.8	44.1	22.8	46.1	9.4	
9			7.8	36.2	12.9	33.6	8.0		

Figure C. 3 : SMR600 1/2 fuel management FA average burnup at BOC (left) and EOC (right).

ANNEX D : PARALLEL COORDINATES PLOT INTRODUCTION

Parallel coordinates plots enable to show a large number of data and some of their characteristics in one graphical view. It is particularly useful to illustrate research plans and optimization exercises with a large number of parameters and objectives.

As an example in Figure D. 1 and Figure D. 2 the hourly power prices (Epex SPOT prices) from 2015 in France and Germany are plotted. The population has 8760 individuals in total. Each individual is characterized by its time parameter: month (1 to 12), day (1 to7), hour (0 to 23) and criteria: price for France or Germany (in €/MWh). Every green line represents one individual. The parallel coordinates plots show the range of the parameters and objectives with minimum and maximum values. Orange bars give a visual representation of the population distribution.

In Figure D. 2 a trigger highlights in blue the individuals with negative power prices in Germany. Looking at the days parameter for those blue individuals a concentration on day 7 (Sunday) is observed. This shows negative power prices mostly occur on Sunday in Germany. This is expected due to the reduced power demand on Sundays. A correlation with low power prices in France is also observed although prices are above 0 €/MWh.

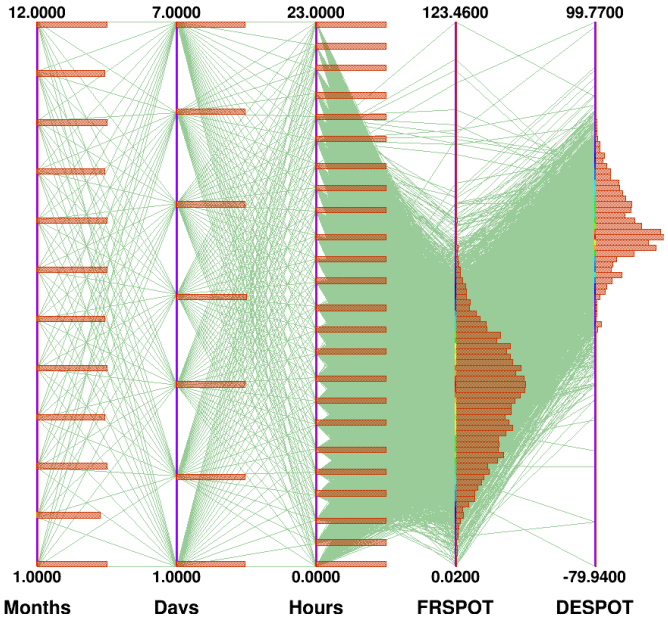

Figure D. 1: 2015 hourly Power Epex Prices in France and Germany

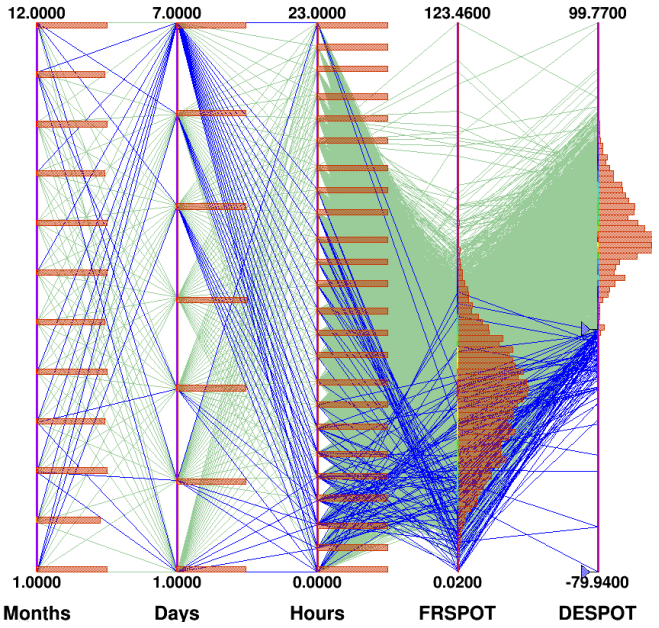

Figure D. 2: 2015 Germany hourly negative Power Epex Prices (blue)

ANNEX E : HCSMR FUEL ASSEMBLY TRIPOLI-4® COMPUTATION

The Figure E. 1 give an overview of the ^{239}Pu fission rate computed with TRIPOLI-4® for the HCSMR MOX fuel assembly introduced in §0. By comparing the symmetrically identical fuel rod, an assessment of the Monte-Carlo evaluation convergence was performed and is presented in Figure E. 2. The symmetrical differences on the ^{239}Pu fission rate are all below 0.2 % showing the good convergence obtained for the TRIPOLI-4® evaluation.

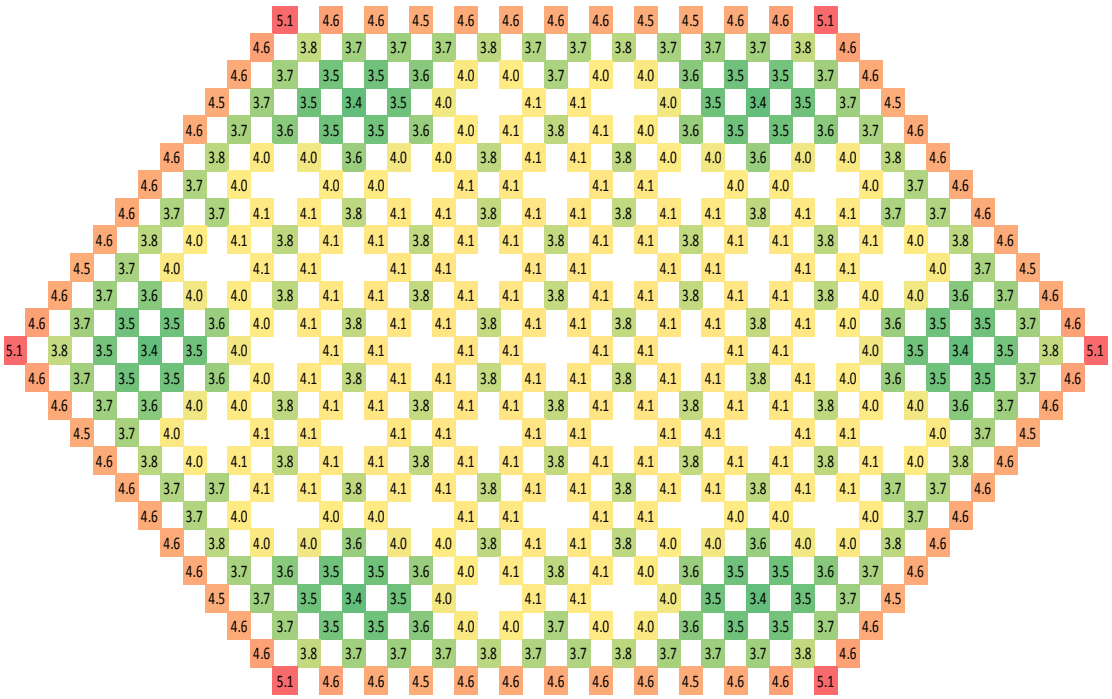

Figure E. 1: ^{239}PU fission rates(x10^{12}) MOX FA at 0 MWd/kgHM

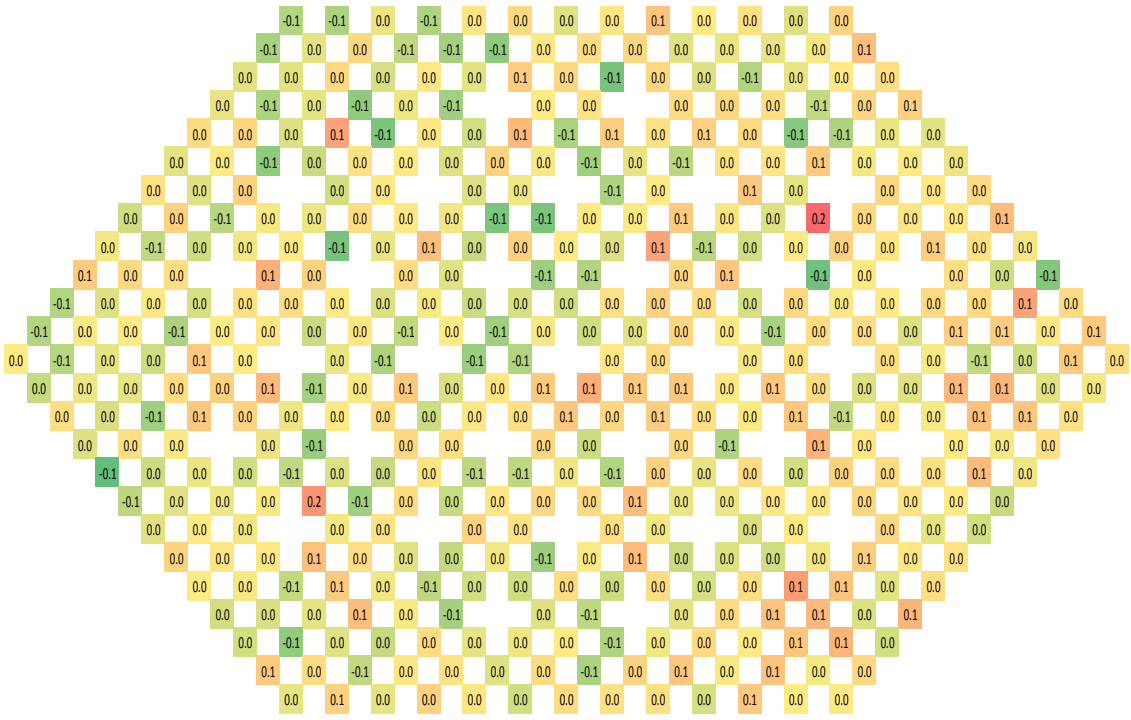

Figure E. 2: ^{239}PU fission rates symmetrical comparison to rod average (%) MOX FA at 0 MWd/kgHM

ANNEX F : SURROGATE MODEL ACCURACY

This section illustrates via plot the accuracy of surrogate models created to optimize HCSMR fuel assembly and core.

F. 1. ZON-19 FUEL ASSEMBLY

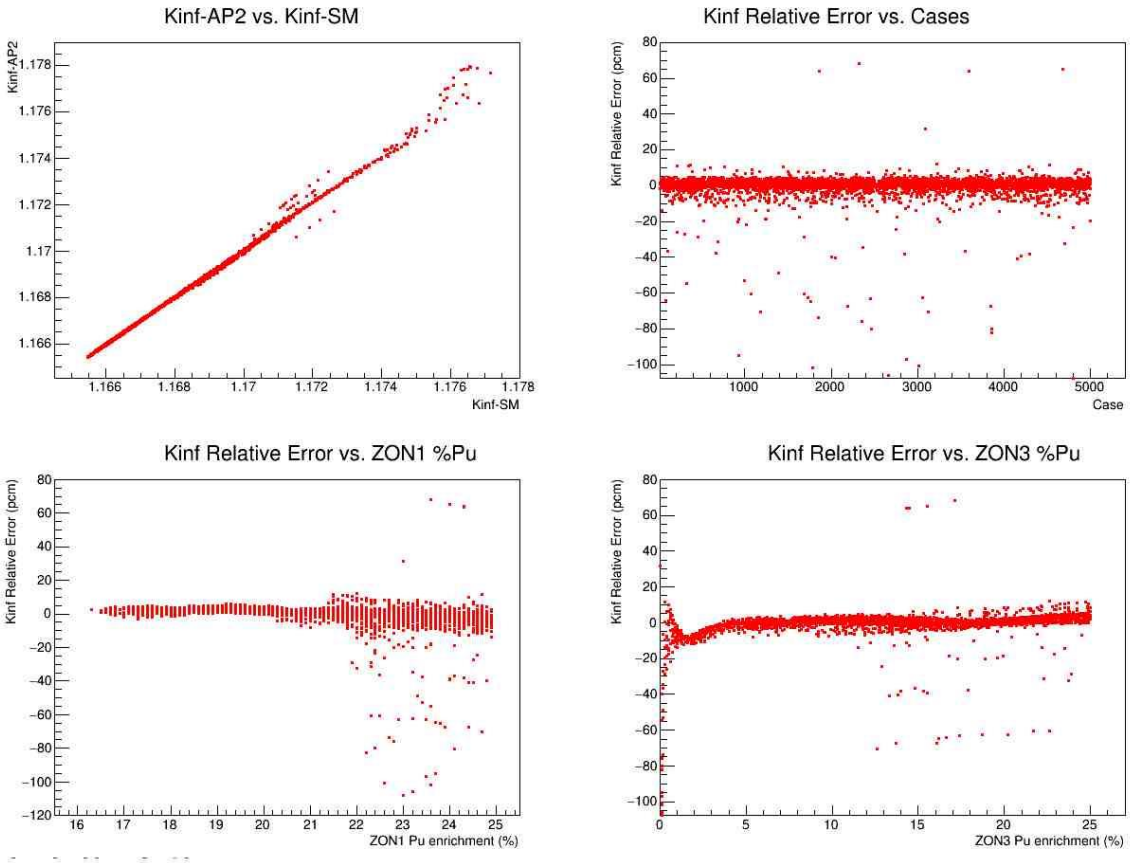

Figure F. 1 : HCSMR ZON.19 reactivity (Kinf) surrogate functions accuracy check

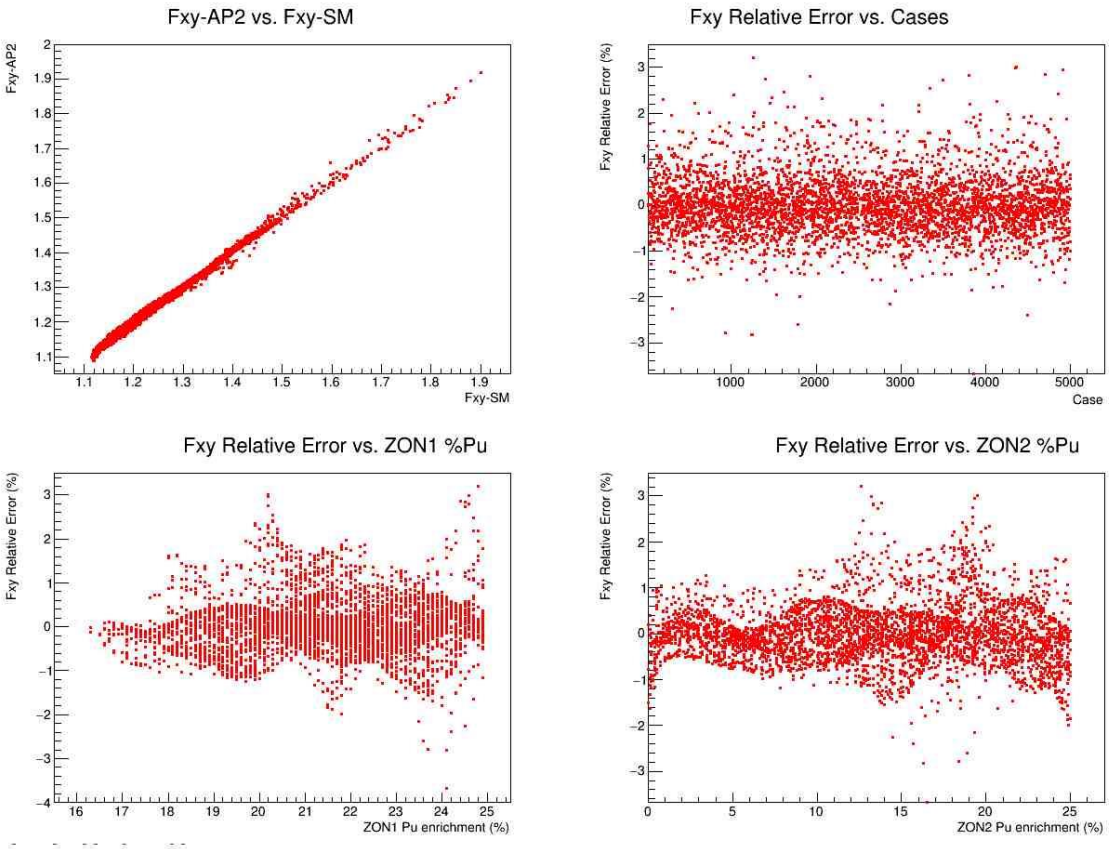

Figure F. 2 : HCSMR ZON.19 peaking factor (Fxy) surrogate functions accuracy check

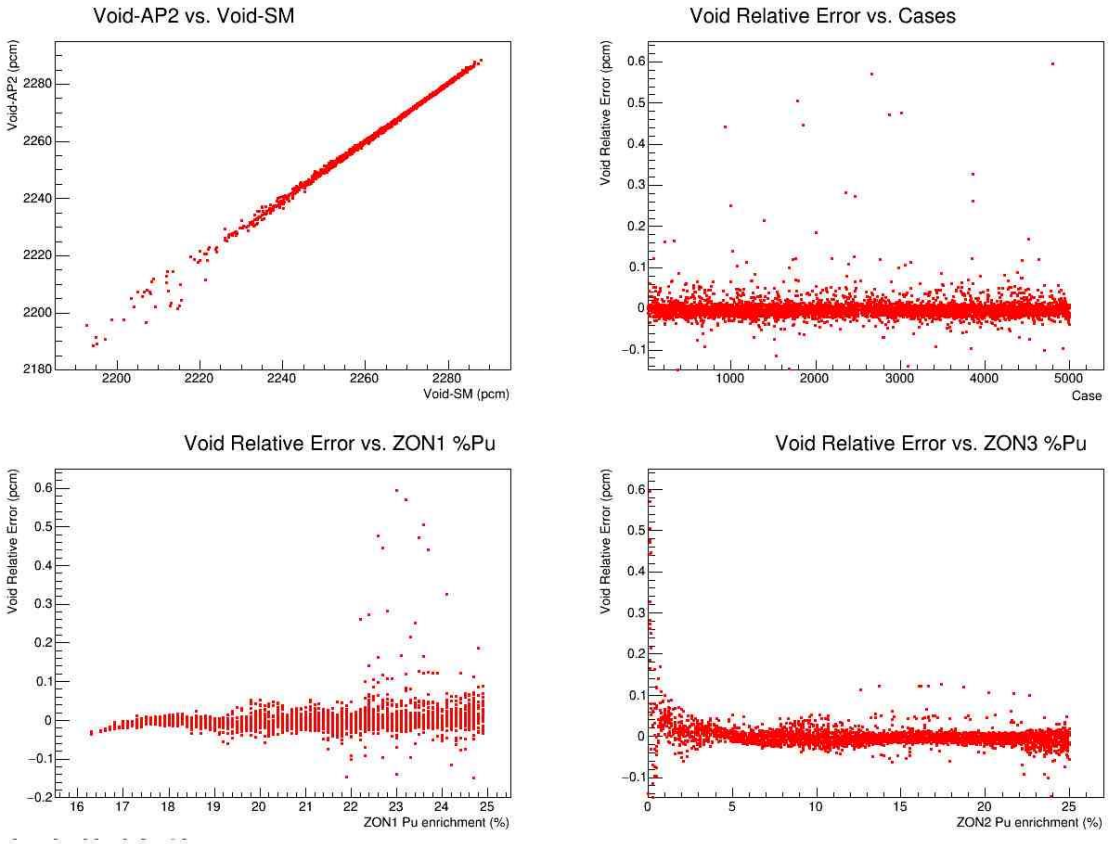

Figure F. 3 : HCSMR ZON.19 void coefficient (Void) surrogate functions accuracy check

F. 2. ZON-13 FUEL ASSEMBLY

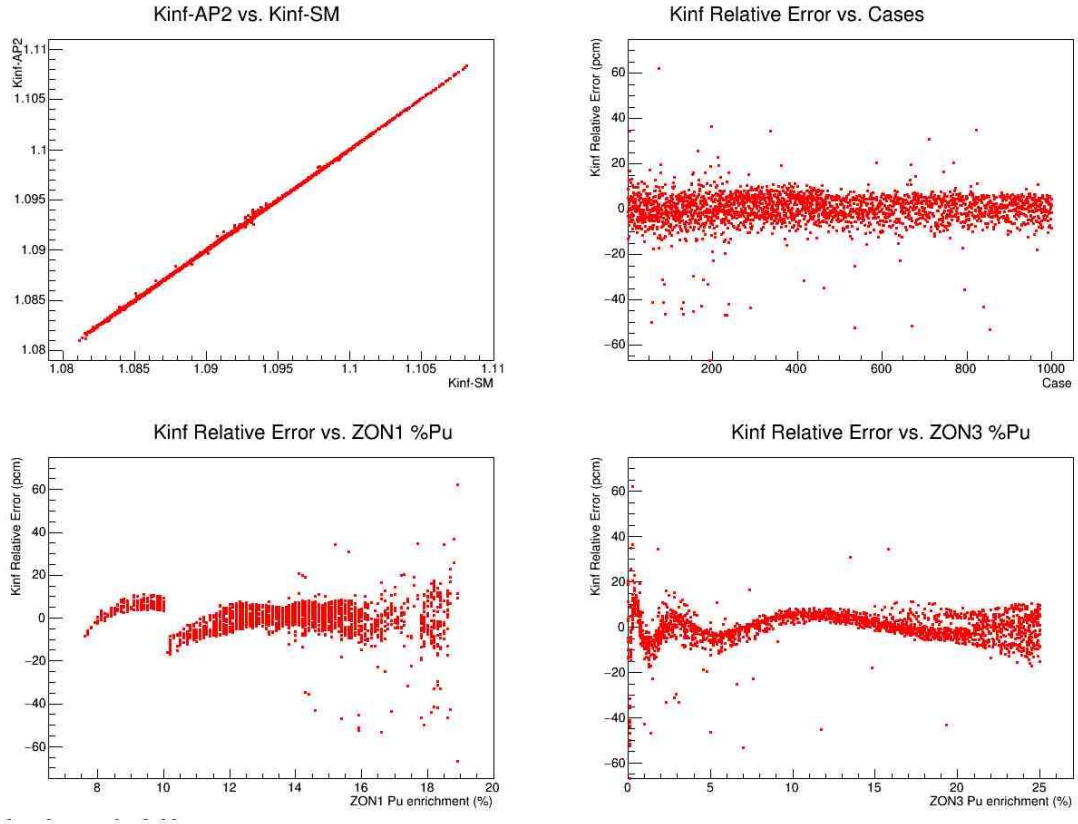

Figure F. 4 : HCSMR ZON.13 reactivity (Kinf) surrogate functions accuracy check

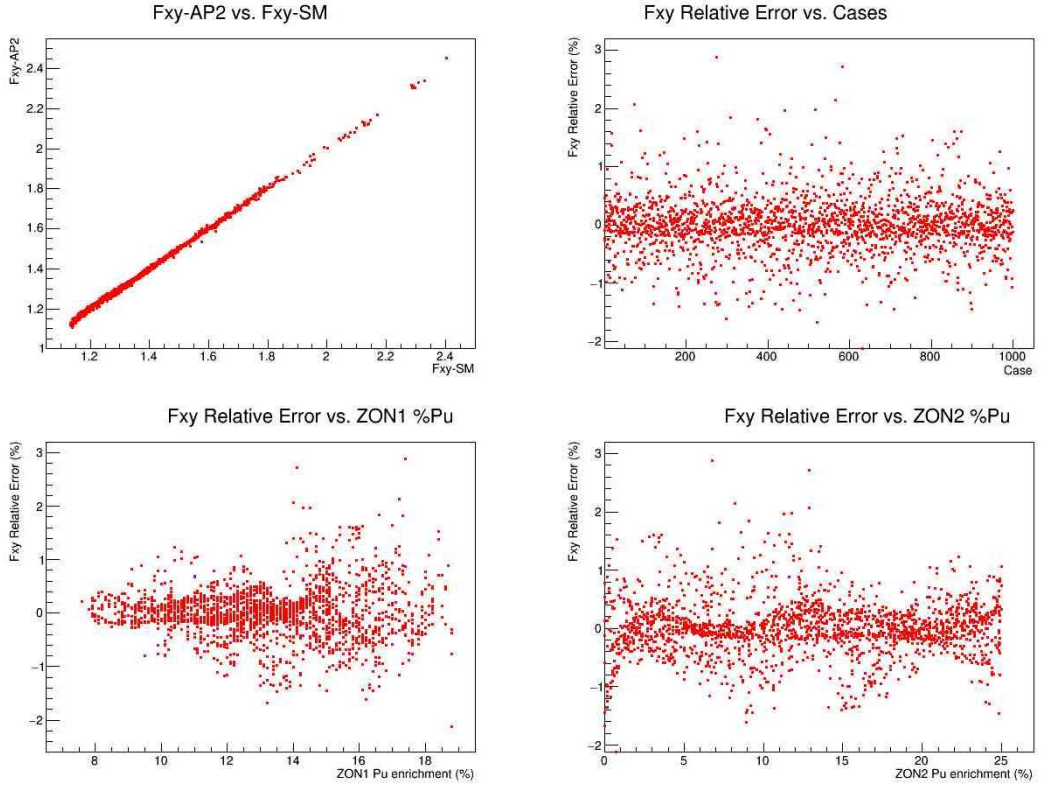

Figure F. 5 : HCSMR ZON.13 peaking factor (Fxy) surrogate functions accuracy check

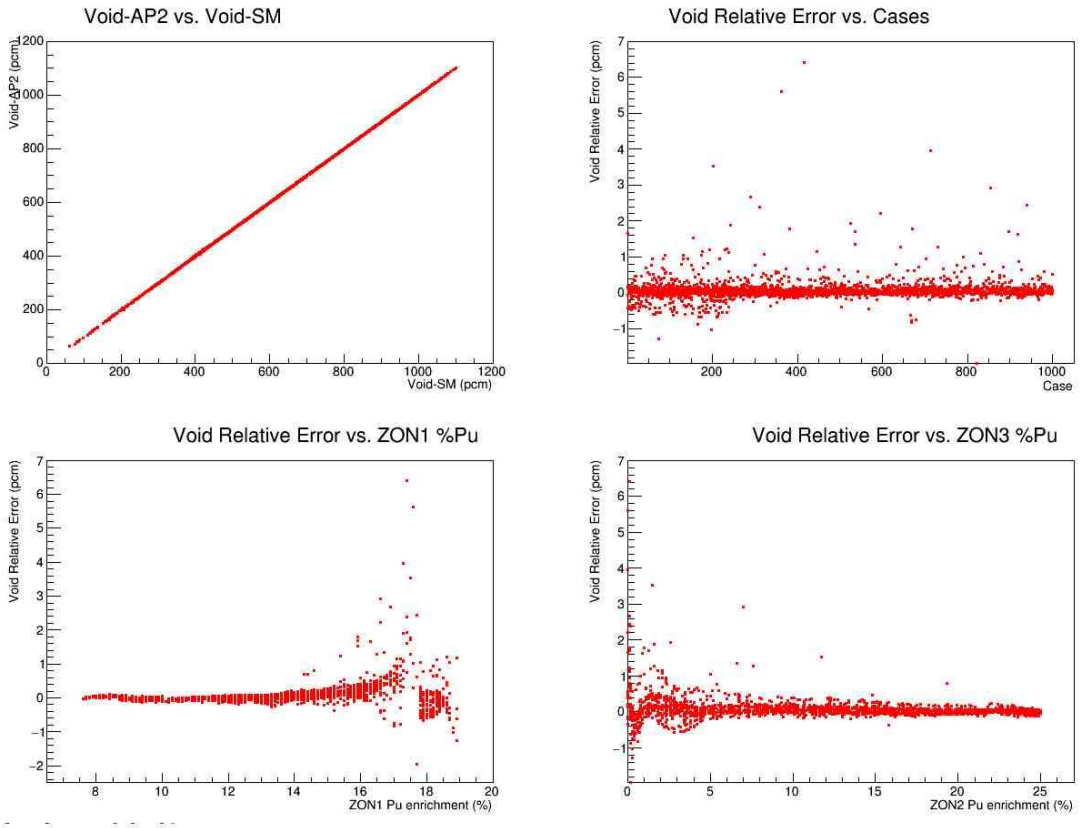

Figure F. 6 : HCSMR ZON.13 void coefficient (Void) surrogate functions accuracy check

F. 3. HCSMR CORE

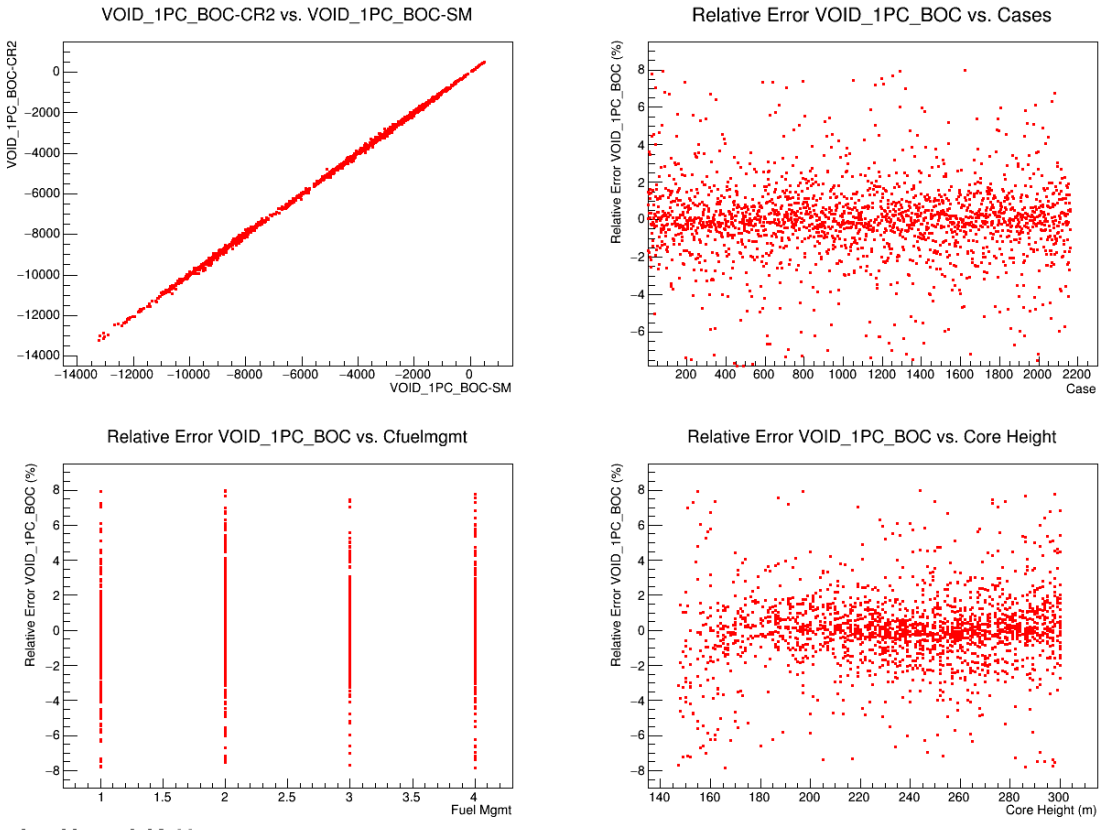

Figure F. 7 : HCSMR Core void coefficient (VOID_1PC_BOC) surrogate functions accuracy check

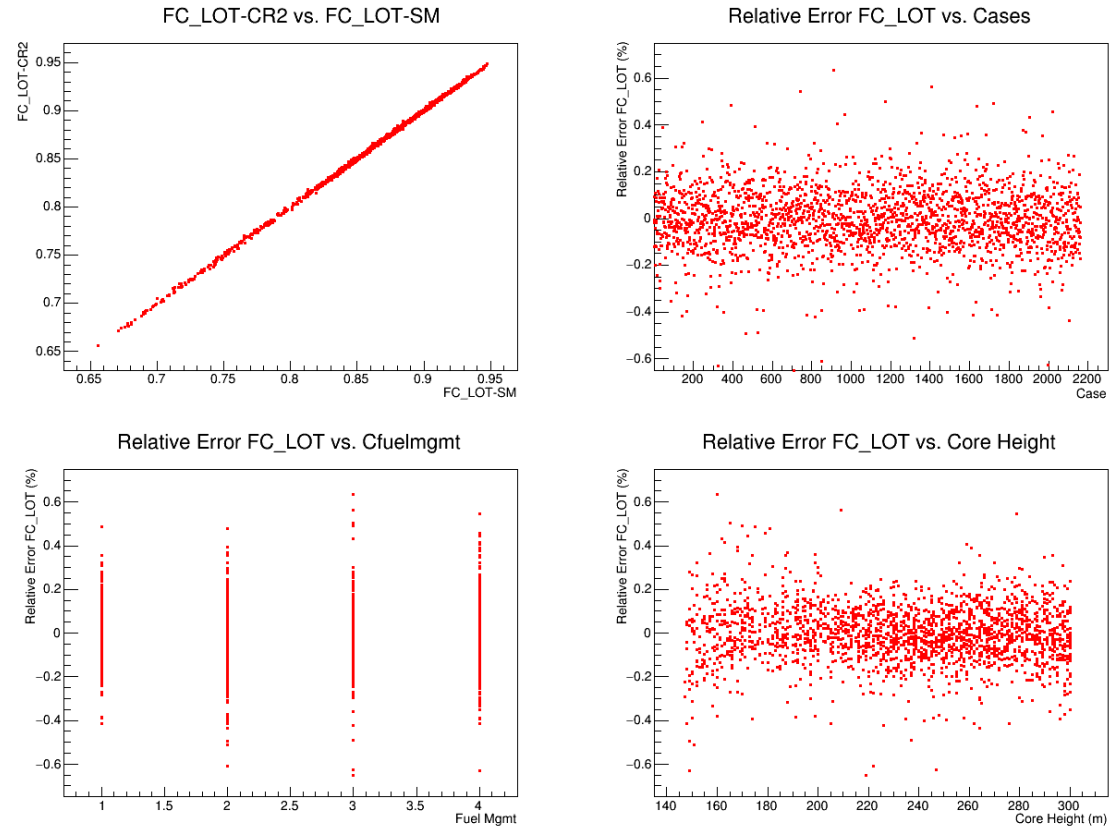

Figure F. 8 : HCSMR Core Conversion Factor (FC_LOT) surrogate functions accuracy check

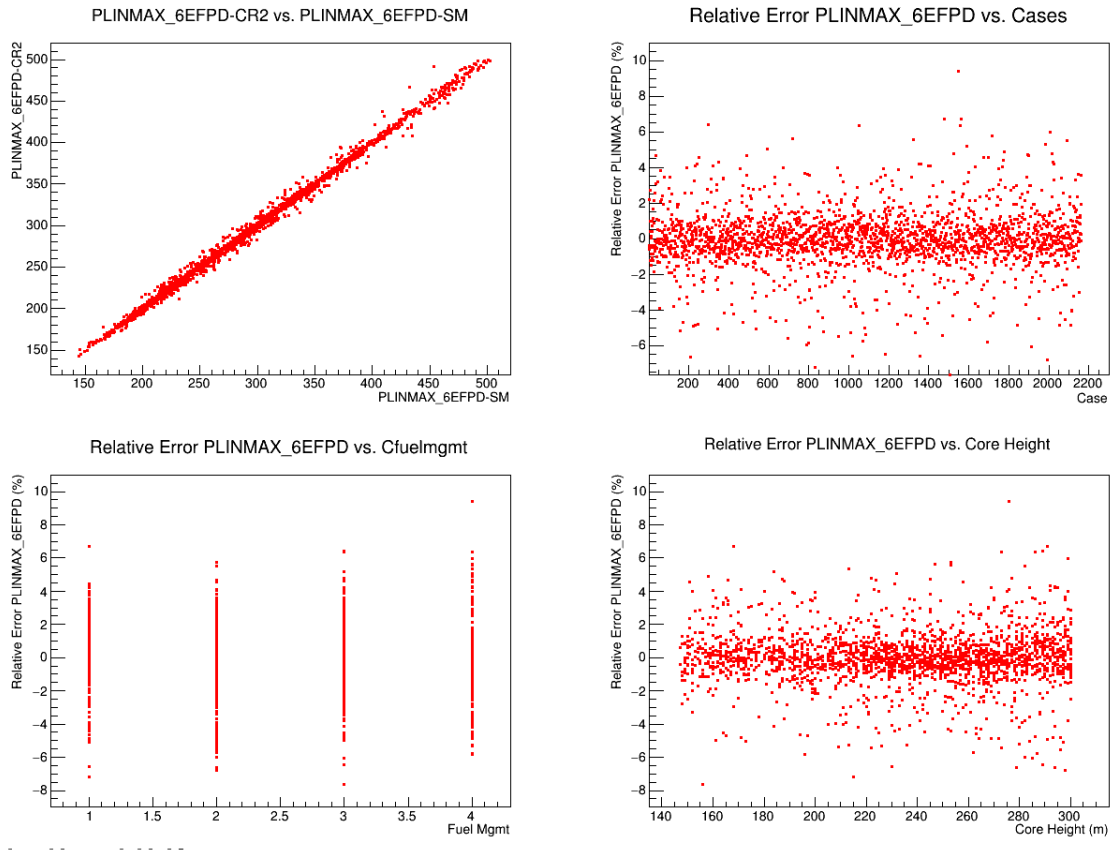

Figure F. 9 : HCSMR Core Linear Power (PLINMAX_6EFPD) surrogate functions accuracy check

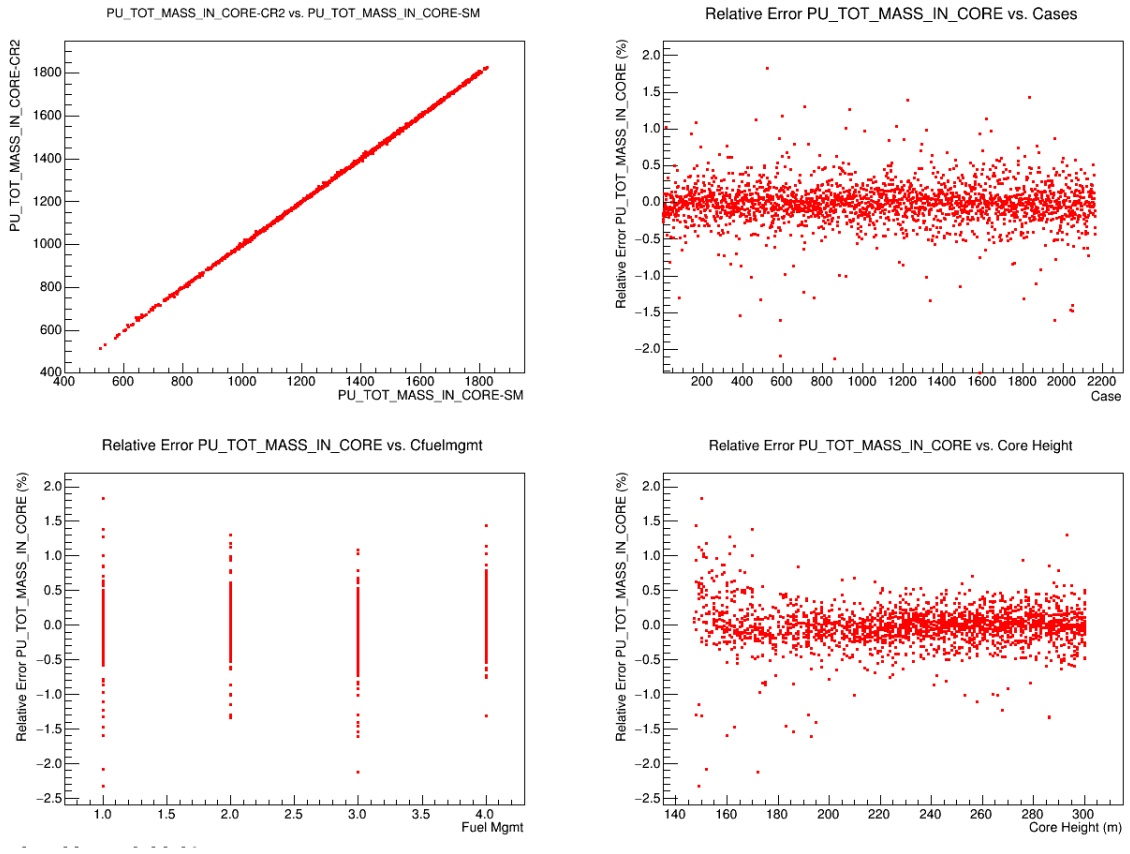

Figure F. 10 : HCSMR Core Plutonium Mass (PU_TOT_MASS_IN_CORE) surrogate functions accuracy check

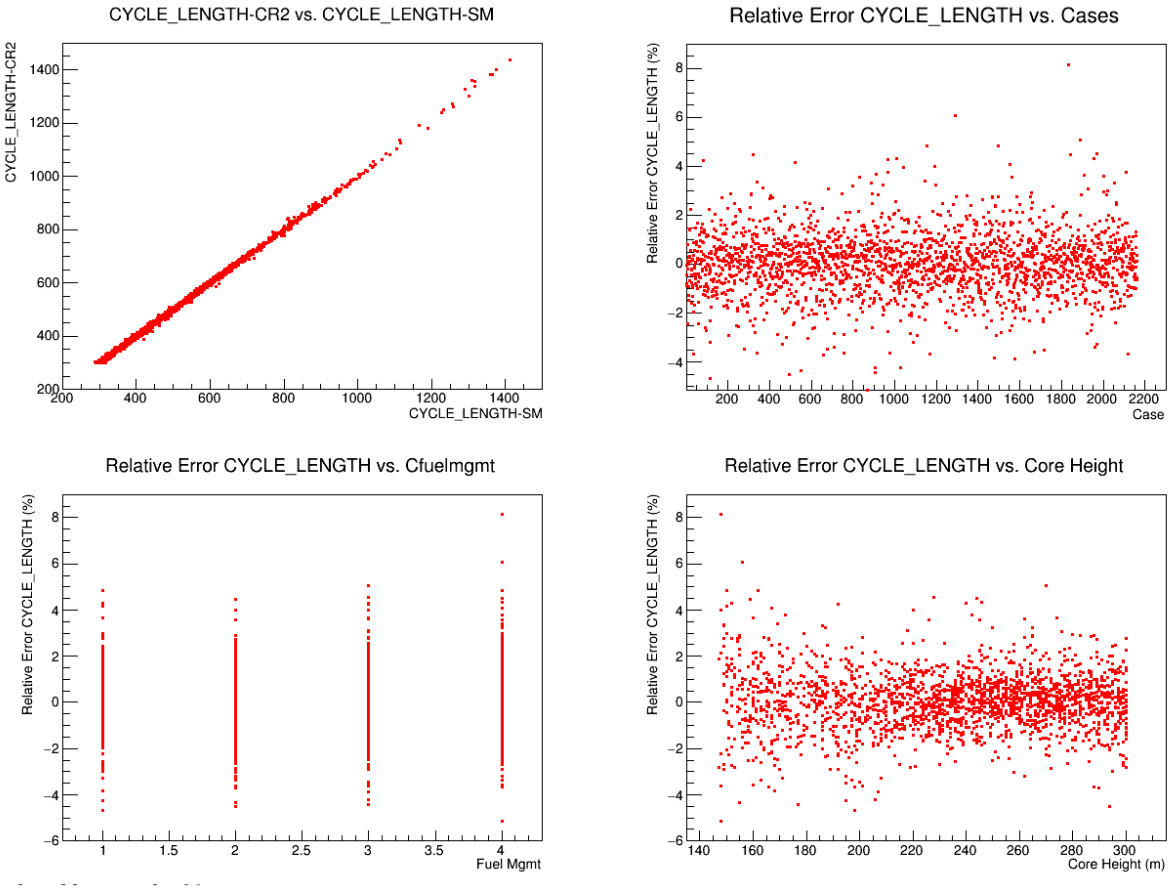

Figure F. 11 : HCSMR Core Cycle Length (CYCLE_LENGTH) surrogate functions accuracy check

ANNEX G : OPTIMIZATION RESULTS

G. 1. ZON FUEL ASSEMBLIES

G. 1. 1 ZON.15 FUEL ASSEMBLY

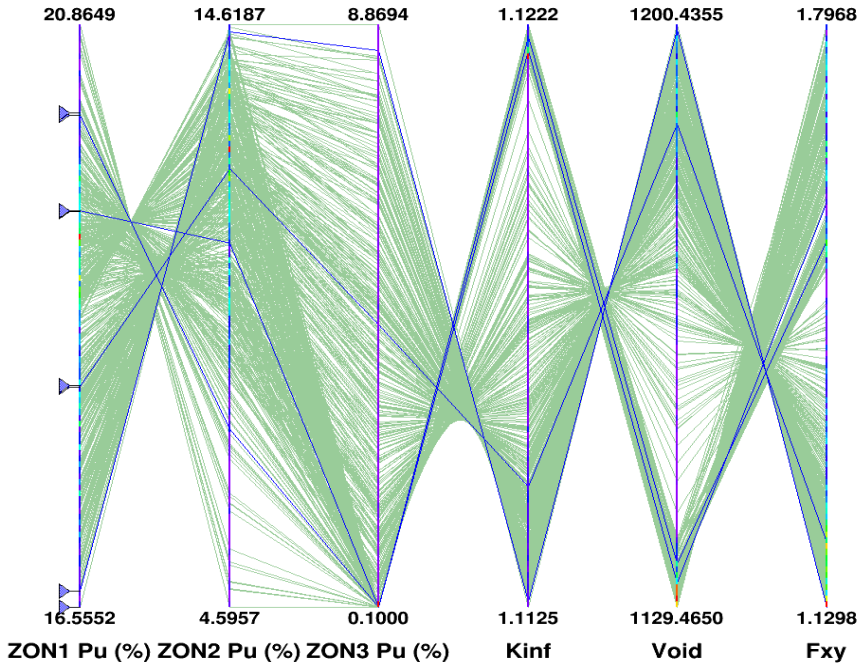

Figure G. 1 : HCSMR ZON.15 genetic algorithms optimization results

G. 1. 2 ZON.17 FUEL ASSEMBLY

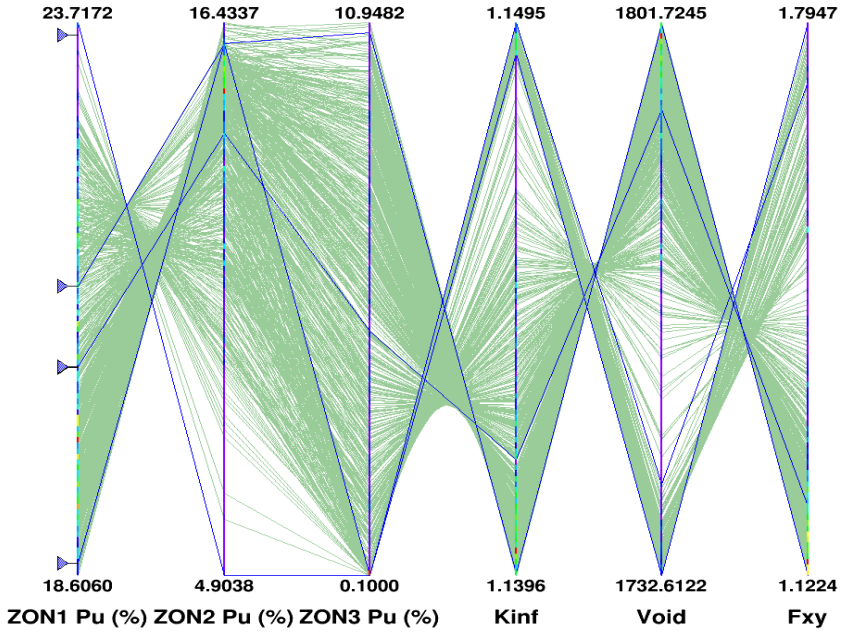

Figure G. 2 : HCSMR ZON.17 genetic algorithms optimization results

G. 1. 3 ZON.19 FUEL ASSEMBLY

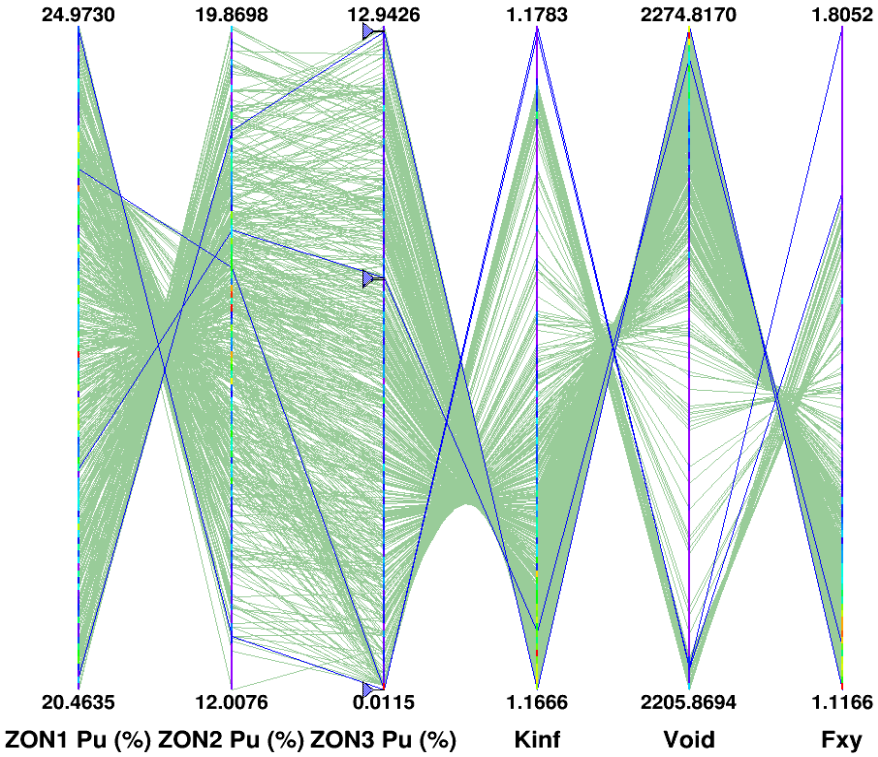

Figure G. 3 : HCSMR ZON.19 genetic algorithms optimization results

G. 1. 4 ZON.21 FUEL ASSEMBLY

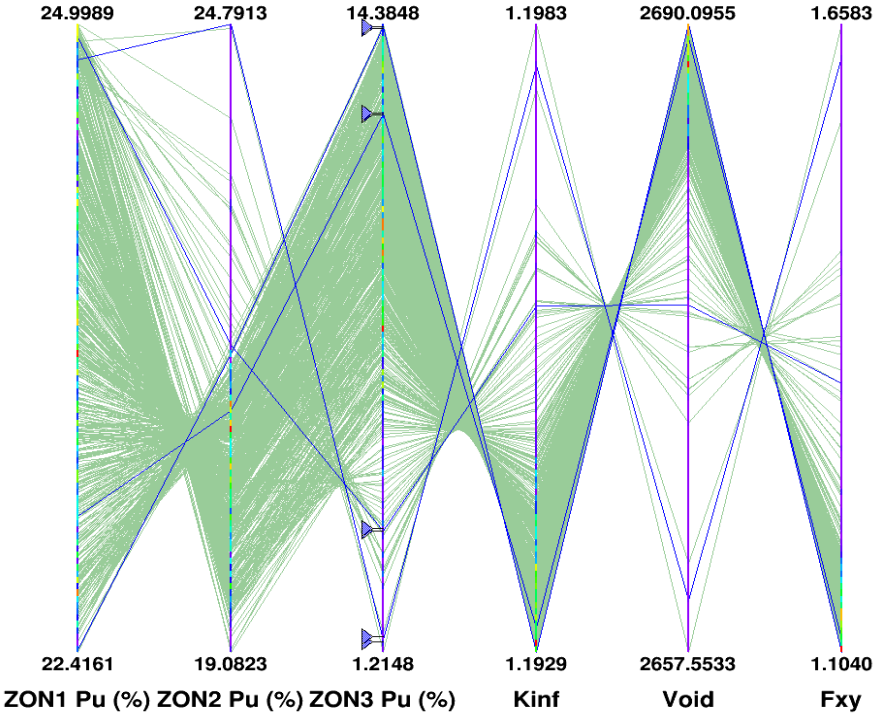

Figure G. 4 : HCSMR ZON.21 genetic algorithms optimization results

G. 2. HCSMR CORE

G. 2. 1 WITHOUT DESIGN CONSTRAINTS

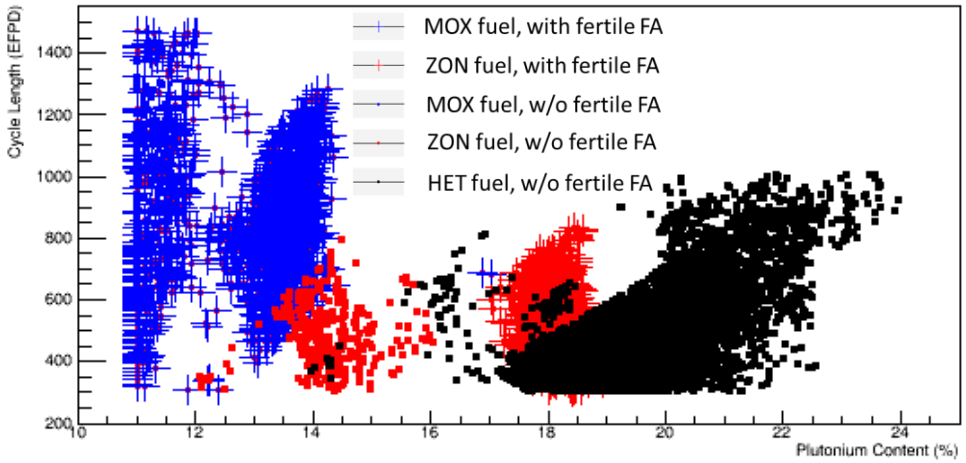

Figure G. 5 : Core Optimization Outcomes Cycle Length vs. Plutonium Content

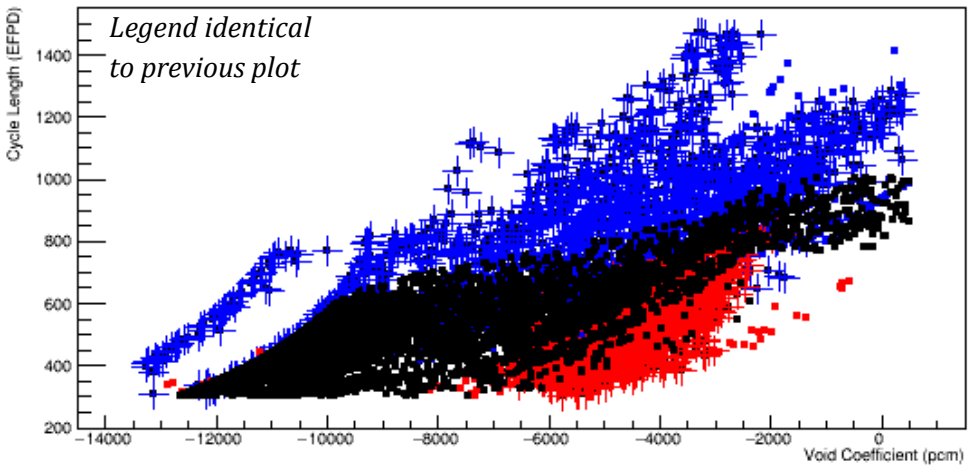

Figure G. 6 : Core Optimization Outcomes Cycle Length vs. Void Coefficient

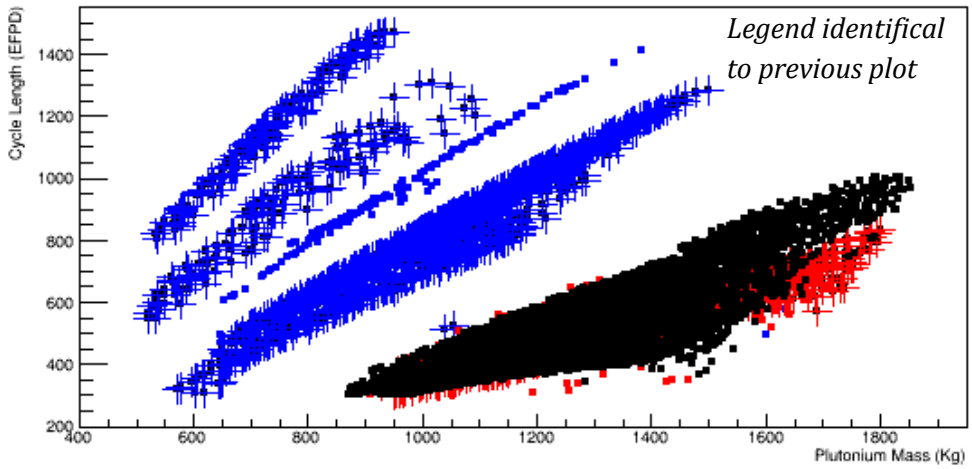

Figure G. 7 : Core Optimization Outcomes Cycle Length vs. Plutonium Mass

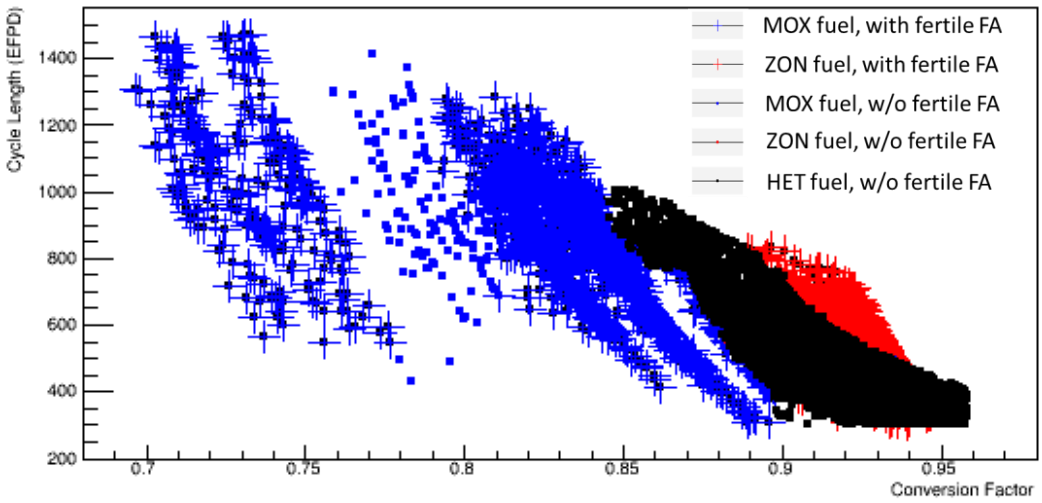

Figure G. 8 : Core Optimization Outcomes Cycle Length vs. Conversion Factor

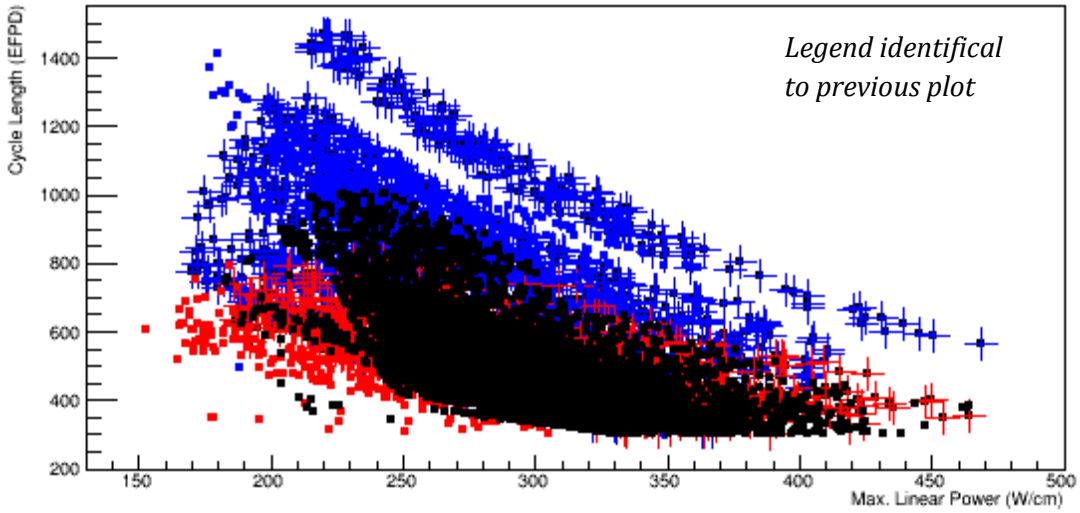

Figure G. 9 : Core Optimization Outcomes Cycle Length vs. Maximum Linear Power

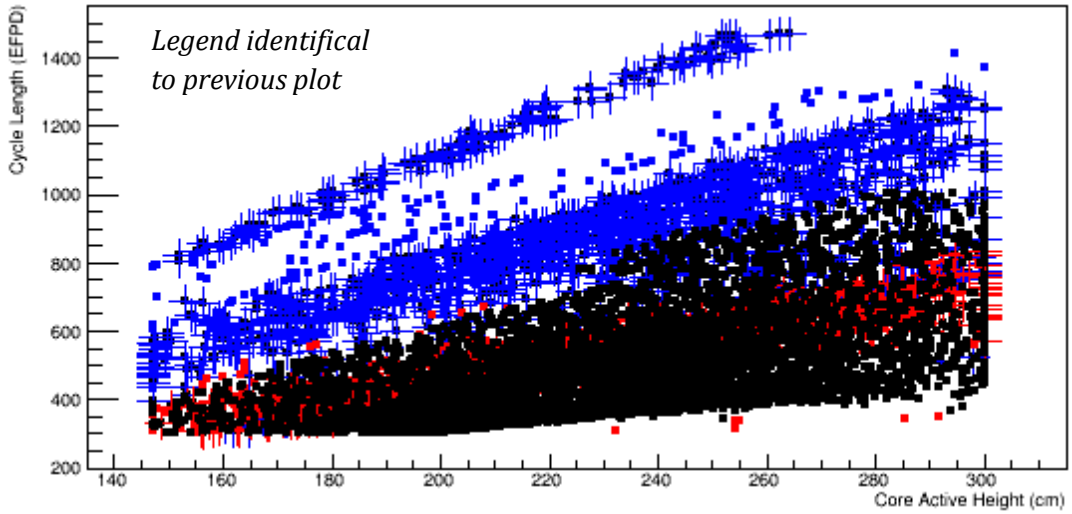

Figure G. 10 : Core Optimization Outcomes Cycle Length vs. Core Active Height

G. 2. 2 WITH DESIGN CONSTRAINTS

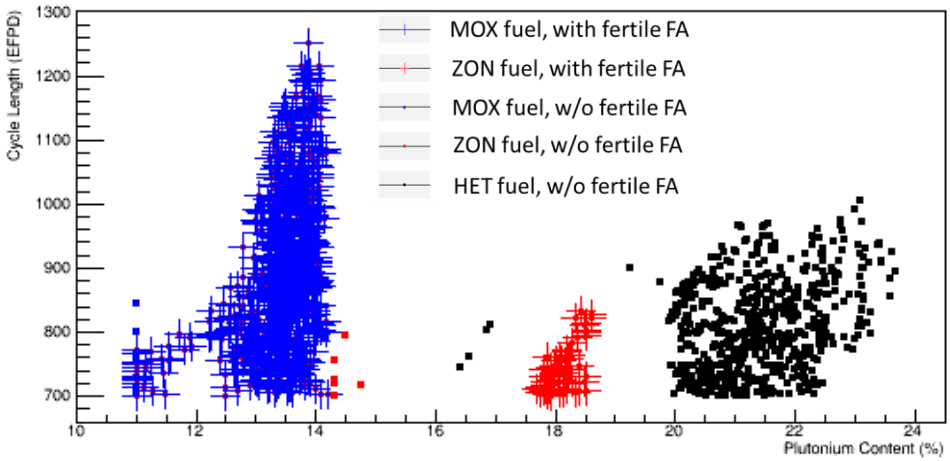

Figure G. 11 : Core Optimization with Constraints Outcomes Cycle Length vs. Plutonium Content

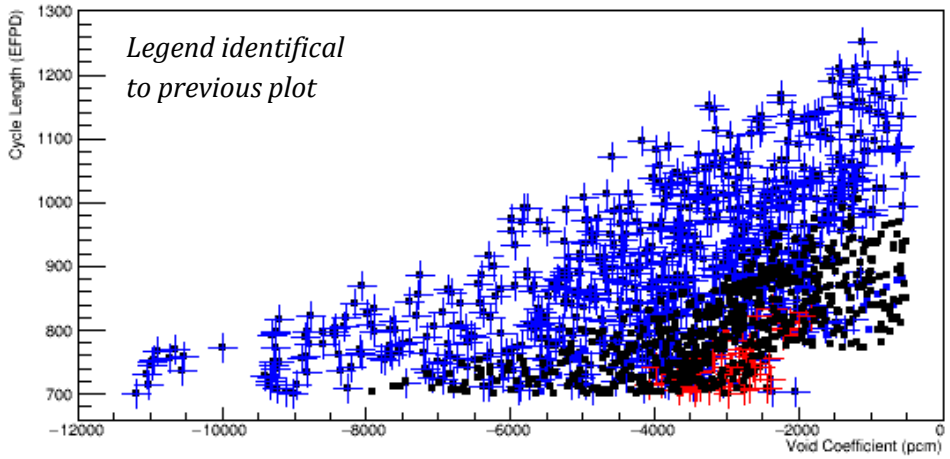

Figure G. 12 : Core Optimization with Constraints Outcomes Cycle Length vs. Void Coefficient

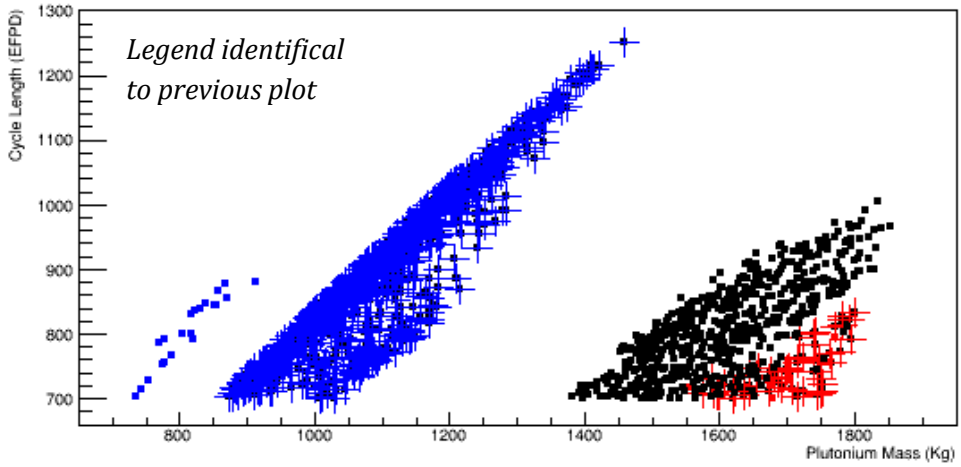

Figure G. 13 : Core Optimization with Constraints Outcomes Cycle Length vs. Plutonium Mass

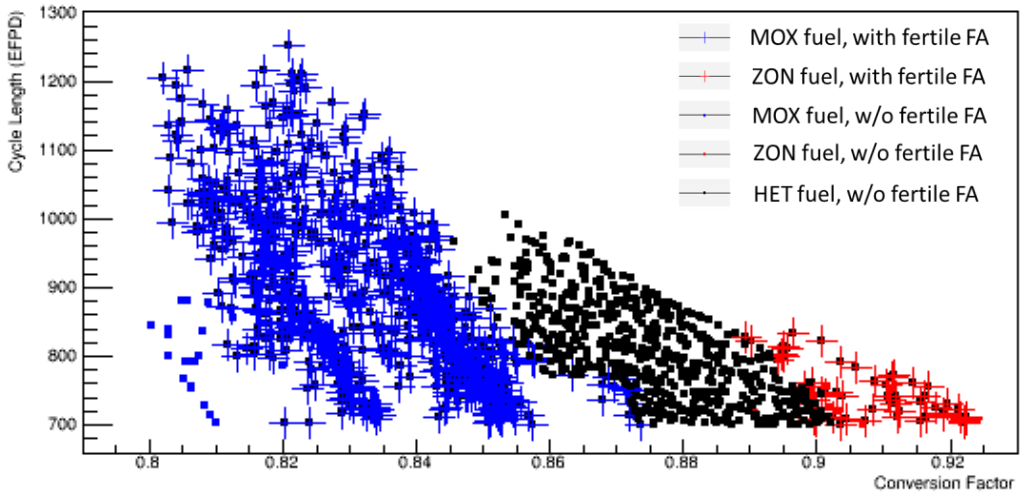

Figure G. 14 : Core Optimization with Constraints Outcomes Cycle Length vs. Conversion Factor

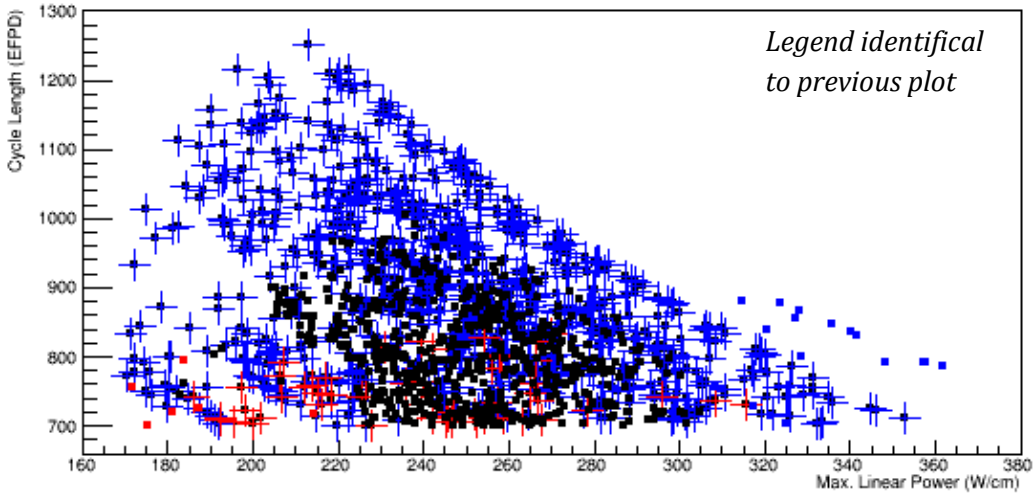

Figure G. 15 : Core Optimization with Constraints Outcomes Cycle Length vs. maximum Linear Power

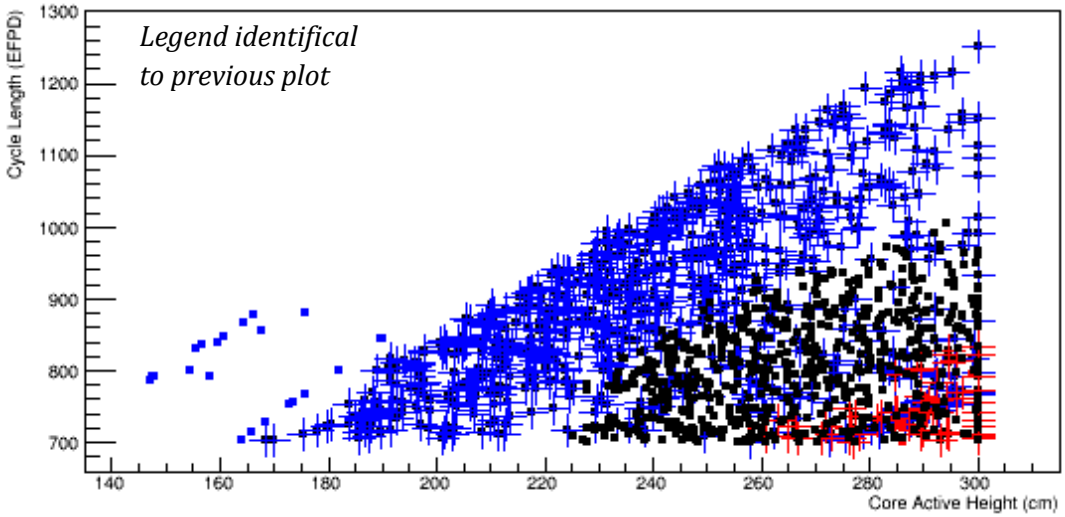

Figure G. 16 : Core Optimization with Constraints Outcomes Cycle Length vs. Core Active Height

ANNEX H : HCSMR HET FA PREDEFINED PATTERNS

To support the optimization of the HET FA predefined patterns are used. Those patterns are introduced in Figure H. 1 to Figure H. 6.

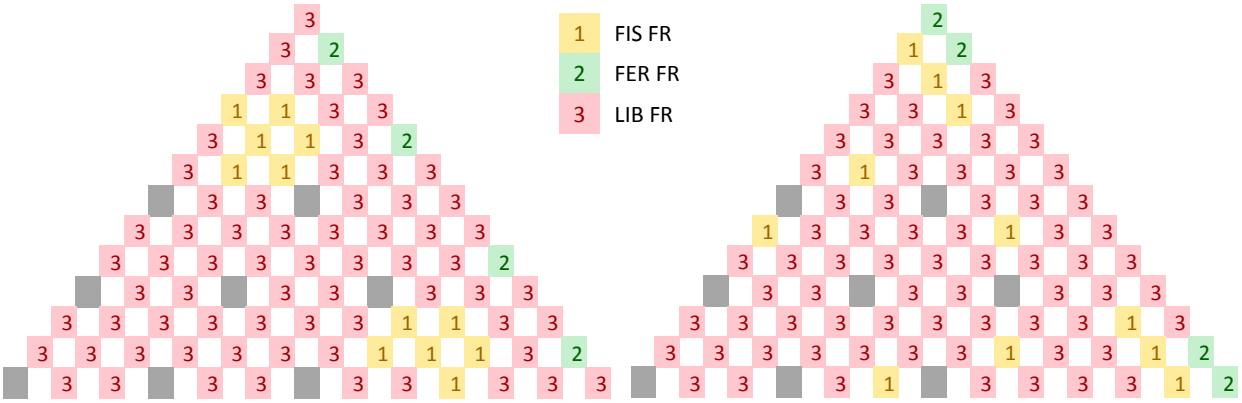

Figure H. 1 : HET FA predefined patterns A (left) and B (right)

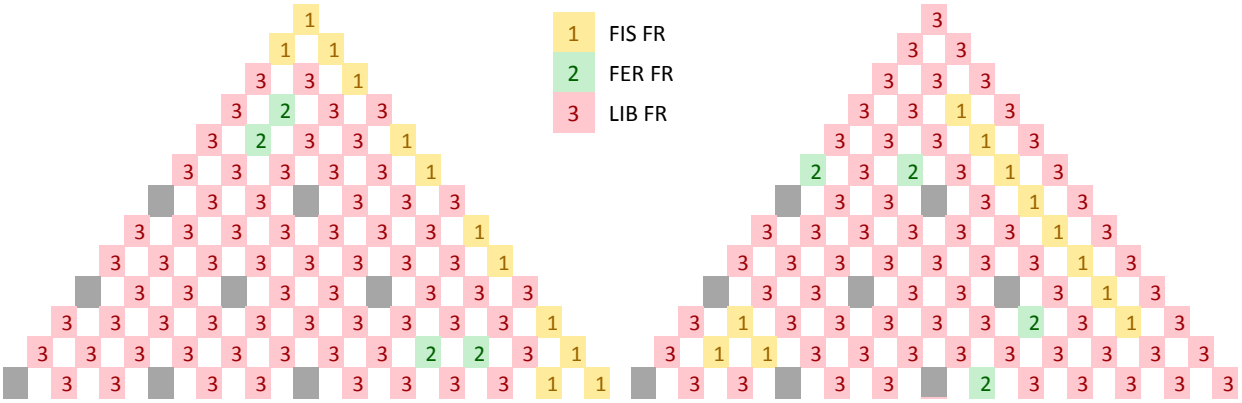

Figure H. 2 : HET FA predefined patterns C (left) and D (right)

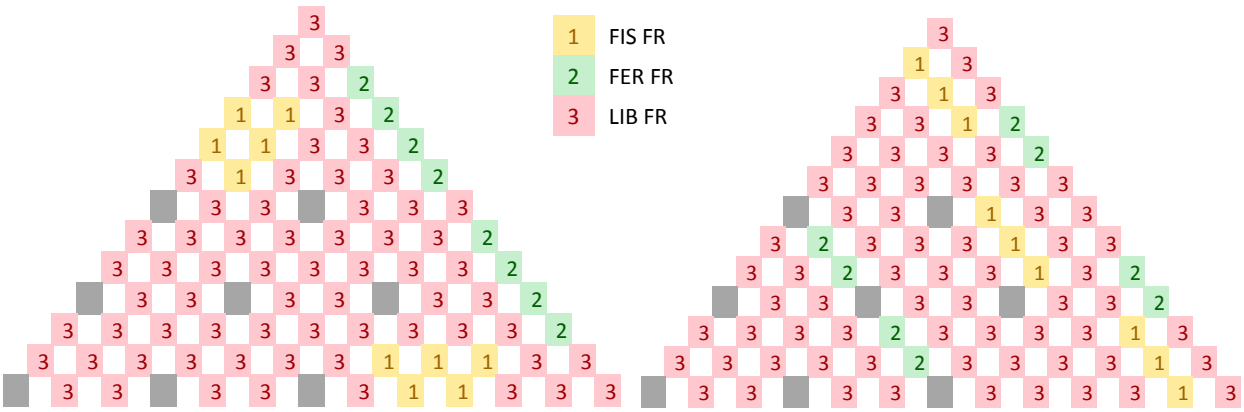

Figure H. 3 : HET FA predefined patterns E (left) and F (right)

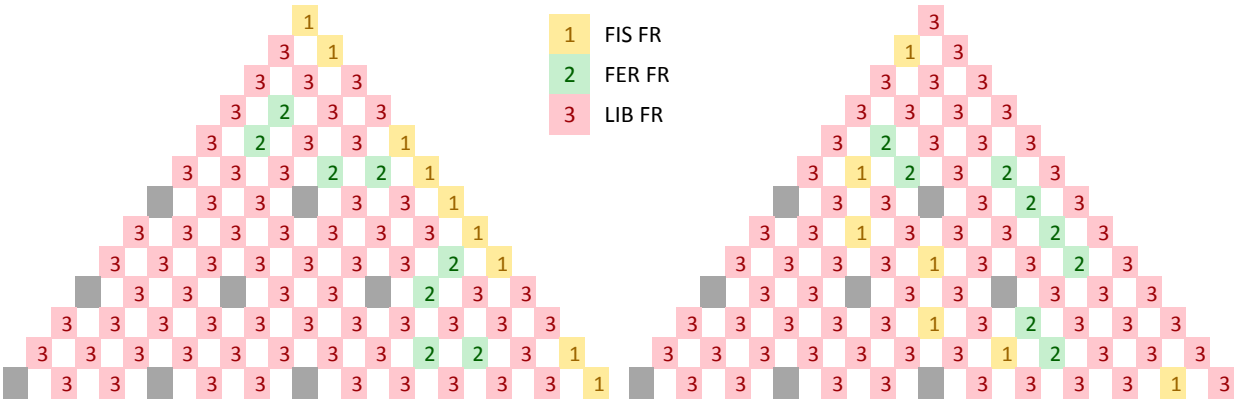

Figure H. 4 : HET FA predefined patterns G (left) and H (right)

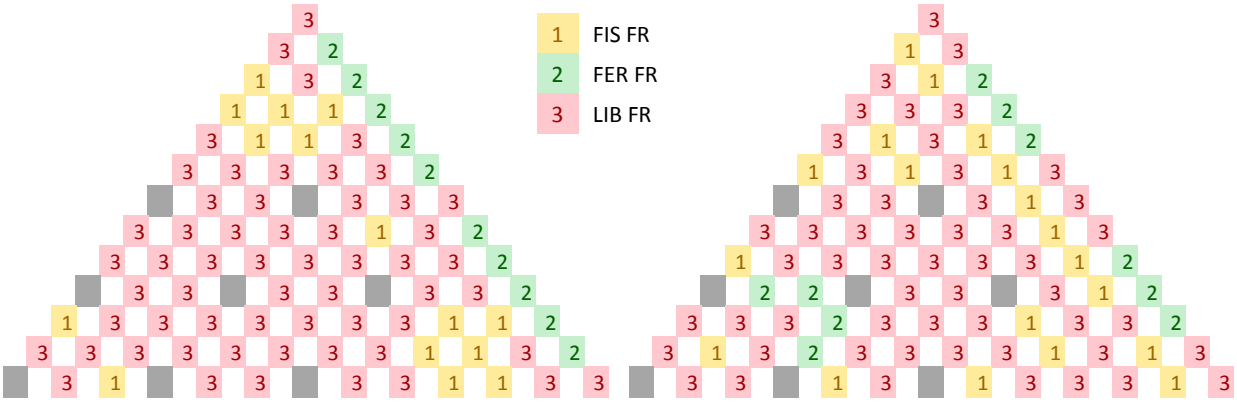

Figure H. 5 : HET FA predefined patterns I (left) and J (right)

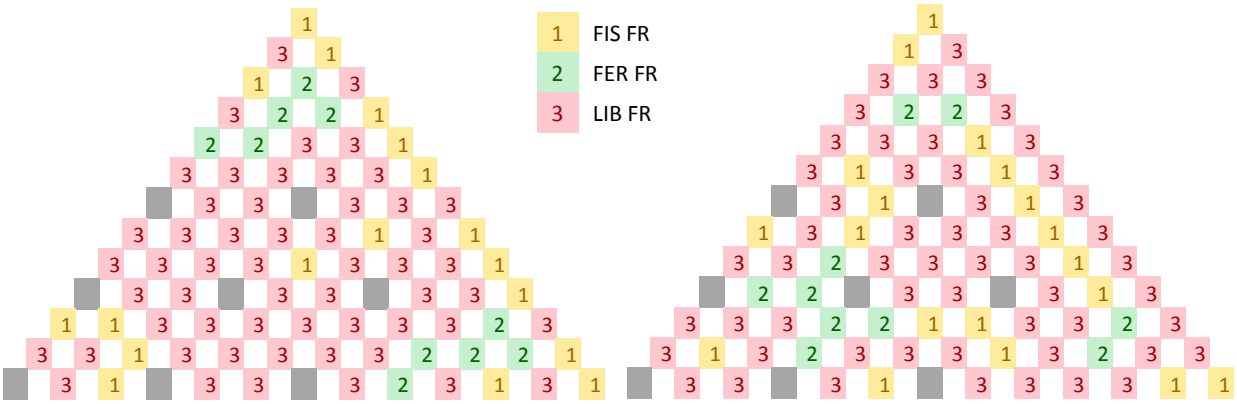

Figure H. 6 : HET FA predefined patterns K (left) and L (right)

ANNEX I : HCSMR LOADING PATTERNS

The loading patterns are given in Figure I. 1 to Figure I. 8 hereafter. In the loading patterns "M" fuel assembly are MOX, ZON or HET fuel assemblies whereas "F" are fertile fuel assemblies. In reloading schemes maps the coordinates of the FA origin is given. "|" means it is a fresh FA.

J. 1. "1/4" FUEL MANAGEMENT

	5	6	7	8	9	10	11	12	13	14	15	16
E					M4							
F				M1		M2		M1		M0		M3
G			M2		M2		M0		M3		M2	
H		M3		M1		M3		M0		M0		
J	M1		M2		M0		M1		M3			

	5	6	7	8	9	10	11	12	13	14	15	16
E					M4							
F				M1		M2		F3		M0		M3
G			M2		F1		M0		M3		M2	
H		F0		M1		M3		F2		M0		
J	M1		M2		M0		M1		M3			

Figure I. 1 : Loading patterns "1/4" FM for cores (a) without fertile FA and (b) core with fertile FA

	5	6	7	8	9	10	11	12	13	14	15	16
E					J13							
F				F14		J11		H14		|		G07
G			F12		J05		|		J07		F08	
H		G15		J09		F10		|				
J	H12		H08		|		G11		G09			

	5	6	7	8	9	10	11	12	13	14	15	16
E					J13							
F				F14		J11		H12		|		G07
G			J05		H06		|		J07		F08	
H		|		J09		F10		G09		|		
J	H14		H08		|		G11		G15			

Figure I. 2 : Reloading schemes "1/4" FM for cores (a) without fertile FA and (b) core with fertile FA

J. 2. "1/3" FUEL MANAGEMENT – LP1

	5	6	7	8	9	10	11	12	13	14	15	16
E					M3							
F				M1		M2		M1		M0		M1
G			M2		M1		M0		M1		M2	
H		M0		M1		M2		M0		M0		
J	M1		M2		M0		M0		M2			

	5	6	7	8	9	10	11	12	13	14	15	16
E					F3							
F				M1		M0		F1		M0		M2
G			M1		F1		M2		M0		M2	
H		F0		M0		M0		F0		M1		
J	M2		M1		F2		M1		M2			

Figure I. 3 : Loading patterns "1/3 - 1" FM for cores (a) without fertile FA and (b) core with fertile FA

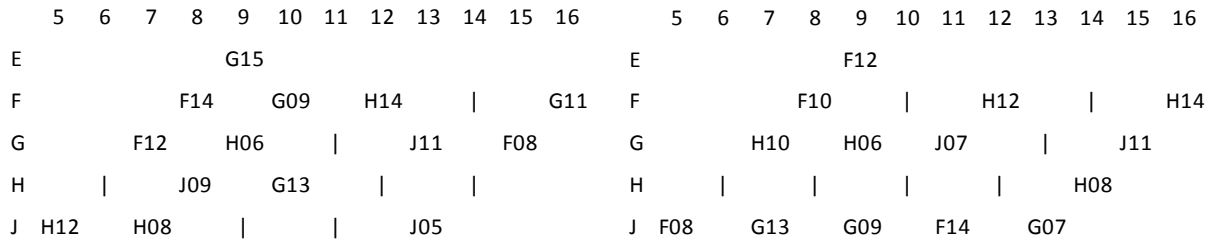

Figure I. 4 : Reloading schemes “1/3 - 1” FM for cores (a) without fertile FA and (b) core with fertile FA

J. 3. “1/3” FUEL MANAGEMENT – LP2

Figure I. 5 : Loading patterns “1/3 - 2” FM for cores (a) without fertile FA and (b) core with fertile FA

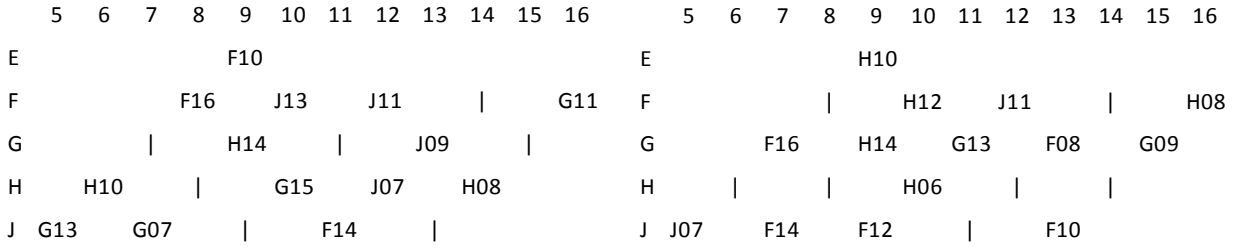

Figure I. 6 : Reloading schemes “1/3 - 2” FM for cores (a) without fertile FA and (b) core with fertile FA

I. 4. “1/2” FUEL MANAGEMENT

	5	6	7	8	9	10	11	12	13	14	15	16
E					M2							
F				M1		M1		M0		M1		M0
G			M1		M0		M1		M0		M0	
H		M0		M1		M0		M1		M1		
J	M1		M0		M0		M1		M0			

	5	6	7	8	9	10	11	12	13	14	15	16
E					M2							
F				M0		F0		M1		F1		M0
G			M1		M1		M1		M0		M0	
H		M0		F1		M0		F0		M1		
J	M1		M0		M0		M1		M1			

Figure I. 7 : Loading patterns “1/2” FM for cores (a) without fertile FA and (b) core with fertile FA

	5	6	7	8	9	10	11	12	13	14	15	16
E					H14							
F				H06		J13			J09			
G			J07				F16					
H				G15				F12		H10		
J	G09						G13					

	5	6	7	8	9	10	11	12	13	14	15	16
E					H14							
F							J07		F10			
G				J09		F16		H06				
H					H12				H10			
J	F08						G13		G15			

Figure I. 8 : Reloading schemes “1/2” FM for cores (a) without fertile FA and (b) core with fertile FA

ANNEX J : NATURAL URANIUM EQUIVALENT NEEDS

The HCSMR core ambitions to reduce the natural uranium needs by better utilizing natural resources. High conversion factor cores loaded with MOX fuel and multi fuel reprocessing supports this objective. Quantifying the natural uranium needs for high conversion core requires several assumptions as several parameters must be considered:

- The fuel management strategy: one-through or reload of partially irradiated fuel assemblies;
- The reprocessing process efficiency;
- The enrichment process characteristics for cases with enriched uranium fuel mixed with plutonium fuel and in particular the tails ^{235}U content (set at 0.25% ^{235}U);
- And of course the fuel cycle length and conversion factor.

This annex aims at describing the process and assumptions considered to evaluate HCSMR cores' natural uranium requirements. It is based on equilibrium cycle evaluations.

J. 1. PLUTONIUM CONSUMPTION

The conversion factor considering plutonium isotopes only $CF^{Pu} = \frac{Plutonium\ fissile\ mass_{final}}{Plutonium\ fissile\ mass_{initial}}$ quantifies the utilization of plutonium fissile isotopes. It is evaluated between the first irradiation of a fuel assembly and its final discharge.

$$Conso^{Pu} = (1 - CF^{Pu}) * FFratio * Plutonium\ Mass_{In\ core}^{Total} * F_{reprocessing} \quad \text{(J. 1)}$$

The equation J.1 gives the plutonium fissile consumption integrated over a fuel assembly total irradiation period and normalized to the core fresh plutonium requirement; with *FFratio* the ratio in core of fresh fuel assemblies loaded at each cycle and $F_{reprocessing}$ a factor added to consider the losses of fissile material during the reprocessing process, mostly due to ^{241}Pu decay. For the HCSMR core the following values are considered:

FFratio = 15/61, 21/61 and 30/61 respectively for the HCSMR 1/4, 1.3 and 1/2 Fuel Management.

$F_{reprocessing} = 1.05$; 5% losses are considered.

$Conso^{Pu}$ corresponds to the additional plutonium needs for each HCSMR cycle. It is a simplified and conservative evaluation based on fissile plutonium isotopes assessment. The initial plutonium fissile vector of 56% is between 54 and 55 % at FA discharge, depending on the core characteristics. The associated losses in energy potential are included in $Conso^{Pu}$ via CF^{Pu}.

The plutonium consumption can be normalized to the power generation as in J. 2:

$$Conso^{Pu}[kg.TWhe^{-1}] = \frac{N*Conso^{Pu}}{N*Cycle\ Length*24*Power*10^{-6}} \quad \text{(J. 2)}$$

with N the fuel management fractioning (N = 2 or 3 or 4 for the HCSMR core) and *Power* of 200 MWe.

The additional plutonium mass required at each cycle can be translated to various natural uranium needs. It depends on the plutonium origin as well as economic and political considerations. Translating the plutonium mass in natural uranium mass equals giving a value to plutonium. It is not the objective of this work to address this aspect. Hence several options are considered in this work via the following factors:

1 kg Pu = 10^0, 10^1, 10^3, 10^5, 10^6 kg Unat.

$Conso^{Pu}$ only considers the consumption of plutonium. Depleted uranium and enriched uranium are also part of HCSMR fuel. Their equivalence in natural uranium needs is introduced hereafter.

J. 2. DEPLETED URANIUM CONSUMPTION

MOX fuel contains mostly depleted uranium together with plutonium isotopes. In addition, some fuel assemblies considered for HCSMR cores are only containing depleted uranium: the fertile fuel assemblies. Three aspects mostly impact the evolution of depleted uranium. The total mass of uranium decreases between the first irradiation and FA discharge. With the epithermal neutron spectrum, some uranium isotopes are capturing neutrons to form ^{239}Pu, while some are fissioned. The content of ^{235}U, although already small at first (0.25%), decreases along irradiation. Last but not least, fission products and transuranic are formed, such as ^{236}U, limiting the energetic potential for depleted uranium reprocessing.

In an absolute perspective of natural resources efficiency, the depleted uranium could be reprocessed and re-used. However, an industrial view limits the interest of this approach: it would be costly on the one hand. On the other hand depleted uranium resources are largely available and will remain available in the future as long as enriched uranium fuel is fabricated.

Therefore for the HCSMR core studies, depleted uranium fuel material is considered without uranium reprocessing. This is a conservative approach with regards to the consumption of uranium for HCSMR cores. Considering depleted uranium as tails of standard uranium enrichment (5 %), the reference $\frac{natural\ Uranium_{mass}}{depleted\ Uranium_{mass}^{initial}} = 1.1$ is set. The associated natural uranium needs are evaluated with regards to the reload batch size.

J. 3. ENRICHED URANIUM CONSUMPTION

Some HCSMR FAs are loaded with MOX fuel containing uranium matrix enriched in ^{235}U isotopes. Those isotopes are consumed via fission during irradiation but the fuel discharged still contains ^{235}U isotopes. For those isotopes multi-reprocessing is considered for HCSMR cores.

The natural uranium needs for MOX fuel assemblies containing enriched uranium are evaluated as:

$$U_{Nat}^{mass} = \frac{e_{initial}^{235U} - e_{tails}}{e_{discharge}^{235U} - e_{tails}} * U_{discharge}^{mass} * (1 + l) + \left(U_{initial}^{mass} - U_{discharge}^{mass}\right) * \frac{e_{initial}^{235U} - e_{tails}}{e_{Nat}^{235U} - e_{tails}} \qquad \text{(J. 3)}$$

with:

- $e_{initial}^{235_U}$: 5 or 10% (HCSMR optimization boundary conditions);
- e_{tails}: 0.25%;
- $e_{Nat}^{235_U}$: 0.72%;
- $U_{initial}^{mass}$: total uranium mass of one fresh batch of fuel assemblies at beginning of irradiation;
- $U_{discharge}^{mass}$: total uranium mass of one discharged batch of fuel assemblies;
- l: factor introduced to account for apparition of uranium isotopes capturing neutrons (236U) and reducing the efficiency of reprocessed uranium. l is set to 10%: the natural uranium needs are increased by 10% to account for the limited efficiency. This is supported by the literature [138] and remains conservative.

For HCSMR cores containing fertile fuel assemblies the process described above is only applied to MOX fuel assemblies. The approach introduced in the previous paragraphs for depleted uranium is applied to fertile fuel assemblies. To establish the total natural uranium needs of a HCSMR core the equivalent needs from three categories are added: plutonium, depleted uranium, and enriched uranium. The total natural uranium need is eventually normalized to the electric power generated. This enables a comparison with natural consumption of standard PWR and SMR, considering the conservative assumptions introduced here.